

BOLU ABANT IZZET BAYSAL UNIVERSITY
THE GRADUATE SCHOOL OF NATURAL AND APPLIED
SCIENCES



PREPARATION AND CHARACTERIZATION OF SOME SIDE
CHAIN LIQUID CRYSTALLINE POLYMER GRAFT
COPOLYMERS OF HIGH DENSIT POLYETHYLENE AND
ISOTACTIC POLYPROPYLENE

DOCTOR OF PHILOSOPHY

BEHİYE ÖZTÜRK ŞEN

BOLU, JUNE 2018

BOLU ABANT IZZET BAYSAL UNIVERSITY
THE GRADUATE SCHOOL OF NATURAL AND APPLIED
SCIENCES
DEPARTMENT OF CHEMISTRY



PREPARATION AND CHARACTERIZATION OF SOME SIDE
CHAIN LIQUID CRYSTALLINE POLYMER GRAFT
COPOLYMERS OF HIGH DENSITY POLYETHYLENE AND
ISOTACTIC POLYPROPYLENE

DOCTOR OF PHILOSOPHY

BEHİYE ÖZTÜRK ŞEN

BOLU, JUNE 2018

APPROVAL OF THE THESIS

PREPARATION AND CHARACTERIZATION OF SOME SIDE CHAIN LIQUID CRYSTALLINE POLYMER GRAFT COPOLYMERS OF HIGH DENSITY POLYETHYLENE AND ISOTACTIC POLYPROPYLENE submitted by Behiye ÖZTÜRK ŞEN in partial fulfillment of the requirements for the degree of Doctor of Philosophy in Department of Chemistry, The Graduate School of Natural and Applied Sciences of ABANT IZZET BAYSAL UNIVERSITY in 22/06/2018 by

Examining Committee Members

Signature

Supervisor
Assoc. Prof. Dr. Sedat ÇETİN
Abant Izzet Baysal University



Member
Prof. Dr. Teoman TİNÇER
ODTU



Member
Prof. Dr. Zeki ÖKTEM
Kırıkkale University



Member
Prof. Dr. Özdemir ÖZARSLAN
Abant Izzet Baysal University

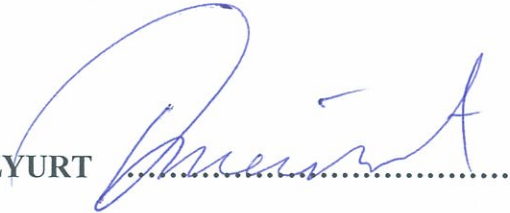


Member
Prof. Dr. Uğur YAŞI
Marmara University



June 22, 2018

Doç. Dr. Ömer ÖZYURT

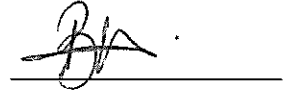


Director of Graduate School of Natural and Applied Sciences

DECLARATION

I hereby declare that all information in this document has been obtained and presented in accordance with academic rules and ethical conduct. I also declare that, as required by these rules and conduct, I have fully cited and referenced all material and results that are not original to this work.

Behiye ÖZTÜRK ŞEN



To my husband

DECLARATION

I hereby declare that all information in this document has been obtained and presented in accordance with academic rules and ethical conduct. I also declare that, as required by these rules and conduct, I have fully cited and referenced all material and results that are not original to this work.

Behiye ÖZTÜRK ŞEN

ABSTRACT

PREPARATION AND CHARACTERIZATION OF SOME SIDE CHAIN LIQUID CRYSTALLINE POLYMER GRAFT COPOLYMERS OF HIGH DENSITY POLYETHYLENE AND ISOTACTIC POLYPROPYLENE

PHD THESIS

BEHİYE ÖZTÜRK ŞEN

BOLU ABANT İZZET BAYSAL UNIVERSITY GRADUATE SCHOOL OF NATURAL AND APPLIED SCIENCES

DEPARTMENT OF CHEMISTRY

(SUPERVISOR: Assoc. Prof. Dr. SEDAT ÇETİN)

BOLU, JUNE 2018

The monomers, p-benzophenoneoxycarbonylphenyl acrylate (BPOCPA) and p-benzophenoneoxycarbonylphenyl methacrylate (BPOCPMA) were synthesized by the reaction of p-acryloyloxybenzoyl chloride (ABC) and p-methacryloyloxybenzoyl chloride (MBC) with p-hydroxybenzophenone, respectively, in xylene in the presence of pyridine. ABC and MBC were prepared by refluxing p-acryloyloxybenzoic acid and p-methacryloyloxybenzoic acid, formerly prepared by reaction of corresponding acid chlorides with p-hydroxybenzoic acid in alkaline medium, in thionyl chloride. The graft copolymerization of BPOCPMA onto high density polyethylene (HDPE) and of BPOCPA and BPOCPMA onto isotactic polypropylene (IPP) were carried out via bulk polymerization method by using dicumyl peroxide initiator in vacuum. The variation of grafting with the mixing ratio of the monomer (BPOCPA or BPOCPMA) and the matrix polymer (HDPE or IPP) in the reaction mixtures was investigated with six different monomer/matrix polymer ratios. While the content of graft units in the products consistently increased with the percentage of the monomers in the reaction mixtures, the percent graftings reached the maximum values at relatively lower monomer concentrations, which were followed by dramatic decreases.

The grafted products were characterized by FTIR, DSC, WAX, PALS, SEM and mechanical testing. Noteworthy and significant increases were recorded in the crystalline melting temperatures and percent crystallinities of matrix polymers.

The graft copolymerization of BPOCPMA gave rise to significant enlargements in the lateral dimensions of unit cells (*a* and *b* parameters) of the orthorhombic structure of HDPE, in consistence with the graft content. A constant expansion in *c* parameter, the unit cell axis parallel with the chain axis of HDPE molecular segments, however, was recorded in all products. The grafting also resulted in increases in the particle size of HDPE crystals.

The lateral dimensions of the monoclinic unit cell of IPP matrix were also found to be considerably affected by poly(BPOCPA) and poly(BPOCPMA) content in the products. Both *a* and *b* parameters increased significantly at low

percentages of the graft units. The effect was more prominent in the dimension a . At relatively high contents, the grafting led to decreases in dimensions. The parameter c decreased in all products in consistence with the content.

The graft copolymerization onto HDPE, while leading to relatively smaller increase in the free volume size at low percentage of poly(BPOCPMA), resulted in reduced volume with the increase of the content in the products. Moreover, the grafting resulted in dramatic decreases in the free volume fractions with the percentage, especially in the copolymers.

The graft copolymerization onto HDPE resulted in improvements in the mechanical properties of the products, especially in tensile strength and modulus. The improvements were observed to be accompanied by reductions in free volume size and fraction. On the other hand, while the graft copolymerization of BPOCPA onto IPP lead to some improvements in the mechanical properties of the products at low percentages of poly(BPOCPA). The graft copolymerization of BPOCPMA gave rise to diminishes in all tensile and impact behaviors in consistence with the content of poly(BPOCPMA). Both grafting imparted brittleness, increasing consistently with the contents to the material.

SEM analysis of tensile and impact fractured surface of poly(BPOCPMA)-g-HDPE, poly(BPOCPA)-g-IPP and poly(BPOCPMA)-g-IPP products revealed that the structures of the products were completely homogeneous. No phase separation was recorded at all. The products exhibited brittle nature with some ductility.

KEYWORDS: High Density Polyethylene, Isotactic Polypropylene, Graft Copolymerization, Unit Cell, Free Volume Size, Free Volume Fraction

ÖZET

**YÜKSEK YOĞUNLUKLU POLİETİLENİN VE İZOTAKTİK
POLİPROPİLENİN BAZI YAN ZİNCİR SIVI KRİSTAL POLİMER AŞI
KOPOLİMERLERİNİN HAZIRLANMASI VE KARAKTERİZASYONU
DOKTORA TEZİ
BEHİYE ÖZTÜRK ŞEN
BOLU ABANT İZZET BAYSAL ÜNİVERSİTESİ
FEN BİLİMLERİ ENSTİTÜSÜ
KİMYA ANABİLİM DALI
(TEZ DANIŞMANI: Doç.Dr.SEDAT ÇETİN)**

BOLU, HAZİRAN - 2018

p-Benzofenonoksikarbonilfenil akrilat (BPOCPA) ve p-benzofenonoksikarbonilfenil metakrilat (BPOCPMA) monomerleri piridin içeren ksilen çözeltisinde akrililoksibenzoil klorür (ABC) ve p-metakrililoksibenzoil klorürün (MBC) p-hidroksibenzofenon (HBP) ile tepkimesiyle elde edilmiştir. ABC ve MBC ise, asit klorürlerinin p-hidroksibenzoik asit ile tepkimesiyle hazırlanan p-akrililoksibenzoik asit ve p-metakrililoksibenzoik asidin tiyonil klorür içerisinde geri soğutucu altında kaynatılmasıyla elde edilmiştir. BPOCPMA'nın yüksek yoğunluk polietilen (YYPE) üzerine ve BPOCPA ve BPOCPMA'nın izotaktik polipropilen (IPP) üzerine aşırı kopolimerleşmesi dikünil peroksit başlatıcısı kullanılarak vakum altında kütle polimerleşmesiyle gerçekleştirilmiştir. Aşılama miktarının tepkime ortamındaki monomer (BPOCPA ya da BPOCPMA) derişimi ile deęişimi 6 farklı monomer/matris polimer (YYPE ya da IPP) oranında çalışılmıştır. Aşılama miktarı tepkime ortamındaki monomer derişimi ile artarken, yüzde aşılama ise nisbeten düşük monomer derişimlerinde maksimuma ulaştıktan sonra hızlı bir şekilde azalmıştır.

Aşırı ürünler FTIR, DSC, WAX, PALS, SEM ve mekanik test yöntemleriyle karakterize edilmiştir. Matris polimerlerin kristal erime sıcaklıklarında ve kristal yüzdelerinde kaydadeğer ve anlamlı artışlar gözlenmiştir.

BPOCPMA'nın aşırı kopolimerleşmesi YYPE'nin ortorombik kristal yapısındaki birim hücrelerin yanal boyutlarında (*a* ve *b* parametreleri) aşırı miktarı ile orantılı önemli genişlemelere neden olmuştur. YYPE zincirleri ile paralel boyutta (*c* parametresinde) tüm ürünlerde sabit genişleme kaydedilmiştir. Aşılama aynı zamanda YYPE kristallerinde büyümeye neden olmuştur.

IPP'nin monoklinik birim hücre boyutlarının da ürünlerde poli(BPOCPA) ve poli(BPOCPMA) derişiminden etkilendięi gözlenmiştir. *a* ve *b* parametrelerinin her ikisi de düşük aşırı yüzdelerinde artmış, nisbeten yüksek derişimlerde ise azalmıştır. *c* parametresi ise tüm ürünlerde aşırı içerięi ile orantılı olarak azalmıştır.

BPOCPMA'nın YYPE üzerine aşırı kopolimerleşmesi, düşük aşırı derişimlerinde serbest hacimde nisbeten küçük artışlara neden olurken yüksek derişimlerde ise daralmalara neden olmuştur. Serbest hacim fraksiyonu ise aşırı

yüzdesi ile orantılı olarak tüm ürünlerde, özellikle kopolimerlerde azalmıştır.

BPOCPMA'nın YYPE üzerine aş1 kopolimerleşmesi, ürünlerin mekanik davranışlarında, özellikle gerilim direnci ve modül değerlerinde, önemli iyileşmelere neden olmuştur. Ürünlerin mekanik özelliklerindeki bu gelişmelerin serbest hacmindeki daralmalarla birlikte gerçekleştiği gözlenmiştir. Diğer yandan, BPOCPA'nın IPP üzerine aş1 kopolimerleşmesi düşük aş1 derişimlerinde mekanik özelliklerde bazı iyileşmelere neden olurken, poli(BPOCPMA)-aş1-IPP ürünlerinin gerilim direnci ve darbe dayanımı ise aş1 miktarı ile orantılı olarak gerilemiştir. Her iki aşılama da malzemede aş1 miktarı ile artan kırılma davranışa neden olmuştur.

Poli(BPOCPMA)-aş1-YYPE, poli(BPOCPA)-aş1-IPP ve poli(BPOCPMA)-aş1-IPP ürünlerinin gerilim ve çarpma etkisiyle kırılmış olan yüzeyleri SEM ile analiz edilmiş ve ürünlerin tamamen homojen yapıda olduğu gözlenmiştir. Ürünlerde herhangi bir faz ayrımı kaydedilmemiştir. Ürünlerde düşük aş1 derişimlerinde sünek davranış ile birlikte, aş1 içeriği ile artan kırılma yapı gözlenmiştir.

ANAHTAR KELİMELER: Yüksek Yoğunluklu Polietilen, İzotaktik Polipropilen, Aş1 Kopolimerleşmesi, Birim Hücre, Serbest Hacim, Serbest Hacim Fraksiyonu.

TABLE OF CONTENTS

	<u>Page</u>
ABSTRACT	v
ÖZET.....	vii
TABLE OF CONTENTS.....	ix
LIST OF FIGURES	xii
LIST OF TABLES	xvii
LIST OF ABBREVIATIONS AND SYMBOLS	xix
1.INTRODUCTION.....	1
1.1 Polyethylene	1
1.2 Polypropylene.....	2
1.3 Liquid Crystalline Polymers (LCPs).....	4
1.4 Combining Thermoplastic with LCP's	7
1.5 Reinforcement of PE and PP with LCP's	9
1.6 Mechanical Properties of Polymers	13
1.7 Literature Survey For PE	14
1.8 Free Volume	18
1.9 Positron Property	19
1.10 Positron Generation	20
1.11 Positron Sources	20
1.12 Positronium	21
1.13 Positron Annihilation Lifetime Spectroscopy (PALS)	22
1.14 Lifetime Analysis	23
1.15 Lifetime Measurements in Polyethylene.....	24
1.16 The Tao-Eldrup Model	24
1.17 Factors Affecting Positronium Formation	26
1.18 PALS Literature Survey.....	28
2. AIM AND SCOPE OF THE STUDY	35
3. MATERIALS AND METHODS	36
3.1 Chemicals and Materials Used	36
3.1.1 Solvents and Reagents	36
3.1.2 Preparation of Powder High Density Polyethylene and Isotactic Polypropylene.....	36
3.2 Synthesis of the Monomers	37
3.2.1 Synthesis of p-Benzophenoneoxycarbonylphenyl Acrylate.....	37
3.2.1.1 Preparation of p-Acryloyloxybenzoic Acid	37
3.2.1.2 Preparation of p-Acryloyloxybenzoyl Chloride	37
3.2.1.3 Synthesis of p-Benzophenoneoxycarbonylphenyl Acrylate ...	38
3.2.2 Synthesis of p-Benzophenoneoxycarbonylphenyl Methacrylate	39

3.2.2.1	Preparation of p-Methacryloyloxybenzoic Acid	39
3.2.2.2	Preparation of p-Methacryloyloxybenzoyl Chloride	39
3.2.2.3	Synthesis of p-Benzophenoneoxycarbonylphenyl Methacrylate.....	39
3.3	Polymerization of the Monomers	40
3.4	Graft Copolymerization of the Monomers	40
3.5	Characterizations and Instruments.....	41
3.5.1	Fourier Transform Infrared Spectroscopy (FTIR)	41
3.5.2	Nuclear Magnetic Resonance (NMR) Analysis	41
3.5.3	Differential Scanning Calorimetry Analysis.....	42
3.5.4	X-Ray Diffraction (XRD).....	42
3.5.5	Tensile and Impact Properties.....	42
3.5.6	Fracture Surface Analysis (SEM)	43
3.5.7	Positron Annihilation Lifetime Spectroscopy (PALS).....	43
4.	RESULTS AND DISCUSSIONS	44
4.1	Characterizations of IPP, HDPE, BPOCPA, BPOCPMA	44
4.1.1	FTIR and DSC Characterization of IPP	44
4.1.2	FTIR and DSC Characterization of HDPE	45
4.1.3	FTIR, ¹ H-NMR and DSC Characterization of BPOCPA	47
4.1.4	DSC and FTIR Characterization of poly(BPOCPA).....	49
4.1.5	FTIR, ¹ H-NMR and DSC Characterization of BPOCPMA.....	51
4.1.6	DSC and FTIR Characterization of poly(BPOCPMA)	53
4.2	Graft Copolymerization of BPOCPMA onto HDPE	55
4.2.1	FTIR Characterization of the Products.....	57
4.2.2	DSC and XRD Characterization of the Products	59
4.2.3	PALS Analysis of The Products	70
4.2.4	Mechanical Properties of HDPE Copolymers and Coproducts ...	80
4.3	Graft Copolymerization of BPOCPA and BPOCPMA onto IPP	89
4.3.1	FTIR Characterization of the Products.....	94
4.3.2	DSC and X-Ray Characterization of The Products.....	97
4.3.2.1	Melting and Crystallization Behavior of Poly(BPOCPA)-g-IPP Copolymers and The Coproducts.....	98
4.3.2.2	Melting and Crystallization Behavior of Poly(BPOCPMA)-g-IPP Copolymers and The Coproducts.....	104
4.3.2.3	Microstructural Behavior of Poly(BPOCPA)-g-IPP Copolymers and The Coproducts.....	109
4.3.2.4	Microstructural Behavior of Poly(BPOCPMA)-g-IPP Copolymers and The Coproducts.....	115
4.3.3	Mechanical Properties of The Products.....	121
4.3.3.1	Mechanical Behavior of Poly(BPOCPA)-g-IPP Copolymers and The Coproducts	121
4.3.3.2	Mechanical Behavior of Poly(BPOCPMA)-g-IPP Copolymers and The Coproducts.....	127
4.4	SEM Analysis of The Polymers	131
4.4.1	SEM Analysis of Poly(BPOCPMA)-g-HDPE Copolymers and The Coproducts	132
4.4.2	SEM Analysis of Poly(BPOCPA)-g-IPP, Poly(BPOCPMA)-g-IPP Copolymers and The Coproducts	137
5.	CONCLUSIONS	152

6. REFERENCES.....	156
7. APPENDICES.....	167
8. CURRICULUM VITAE.....	168



LIST OF FIGURES

	<u>Page</u>
Figure 1.1. The effect of temperature on the modification reactions of iPP-radicals	3
Figure 1.2. Types of liquid crystalline polymers containing rigid mesogenic units	6
Figure 1.3. a) Hole volume (black ellipsoids) concept, and b) respective volumes	19
Figure 1.4. Decay of sodium 22 source.....	21
Figure 1.5. Scheme of <i>o</i> -Ps pick-off annihilation, <i>p</i> -Ps and direct annihilation.....	22
Figure 1.6. Tao-Eldrup model representation.....	25
Figure 1.7. Possible reactions in Ps formation in the presence of polar groups (PG= Polar Groups).....	27
Figure 3.1. The reaction of acryloyl chloride with HBA to produce ABA.....	37
Figure 3.2. Synthesis reaction of p-acryloyloxybenzoyl chloride (ABC).....	38
Figure 3.3. Synthesis reaction of benzophenoneoxycarbonylphenyl acrylate	38
Figure 3.4. The reaction of methacryloyl chloride with HBA to produce MBA.....	39
Figure 3.5. Synthesis reaction of p-methacryloyloxybenzoyl chloride	39
Figure 3.6. Synthesis reaction of p-benzophenoneoxycarbonylphenyl methacrylate	40
Figure 4.1. FTIR spectrum of IPP.....	44
Figure 4.2. DSC thermogram of IPP.....	45
Figure 4.3. FTIR spectrum of HDPE	46
Figure 4.4. DSC thermogram of HDPE	46
Figure 4.5. FTIR spectrum of BPOCPA	47
Figure 4.6. H-NMR spectrum of BPOCPA.....	48
Figure 4.7. DSC thermogram of BPOCPA	49
Figure 4.8. FTIR spectrum of poly(BPOCPA).....	50
Figure 4.9. DSC thermogram of poly(BPOCPA)	50
Figure 4.10. FTIR spectrum of BPOCPMA.....	51
Figure 4.11. H-NMR spectrum of BPOCPMA	52
Figure 4.12. DSC thermogram of BPOCPMA	53
Figure 4.13. FTIR spectrum of poly(BPOCPMA)	54
Figure 4.14. DSC thermogram of poly(BPOCPMA).....	54
Figure 4.15. The variation of poly(BPOCPMA) content in the products with BPOCPMA percentage in the reaction mixture	56
Figure 4.16. The variation of percent grafting of poly(BPOCPMA) with the percentage of BPOCPMA in reaction mixture.....	57
Figure 4.17. FTIR spectra of the copolymers involving a) 6.7%, and b) 21% poly(BPOCPMA)	58
Figure 4.18. FTIR spectra of the coproducts involving a) 7.3%, and b) 26.7% poly(BPOCPMA)	58
Figure 4.19. The DSC thermograms, of HDPE sample processed with 2% DCP (130.69°C), of the coproducts with 12.7% poly(BPOCPMA) (134.51°C), 25.1% poly(BPOCPMA) (130.81°C) and of the copolymers with 6.7% poly(BPOCPMA) (133.00°C), 21% poly(BPOCPMA) (130.26°C)	60

Figure 4.20. The variation of HDPE melting temperature with poly(BPOCPMA) content in the products	61
Figure 4.21. The variation of crystallinity in HDPE matrix with poly(BPOCPMA) content in the products	62
Figure 4.22. The XRD pattern of pure HDPE	63
Figure 4.23. The XRD patterns of some copolymers (with 6.7, 11.8 and 21.0% poly(BPOCPMA)) and coproducts (with 3.8, 12.7, 25.1% poly(BPOCPMA))	64
Figure 4.24.a and b. The variations of the unit cell parameters <i>a</i> (a) and <i>b</i> (b) with poly(BPOCPMA) content, calculated from the X-ray diffraction patterns (using the reflections (110), (200) and (211)).....	67
Figure 4.24.c and d. The variations of the unit cell parameters <i>c</i> (c), and the unit cell basal area <i>ab</i> (d) with poly(BPOCPMA) content, calculated from the X-ray diffraction patterns (using the reflections (110), (200) and (211))	68
Figure 4.25. The variation of crystal size (grain size) with poly(BPOCPMA) content.....	70
Figure 4.26. The variation of the direct annihilation lifetime of the positrons, the intermediate-lived component (τ_2) with poly(BPOCPMA) content in the products	72
Figure 4.27. The variation of the ortho-positronium lifetime (τ_3) with poly(BPOCPMA) contents in the products.....	76
Figure 4.28. The variation of the free volume hole sizes (A^3) with poly(BPOCPMA) contents in the products.....	77
Figure 4.29. The variation of the intensity I_3 with poly(BPOCPMA) content in the products	78
Figure 4.30. The variation of the free volume fraction with poly(BPOCPMA) content in the products	78
Figure 4.31. The variation of intensities I_1 and I_2 with poly(BPOCPMA) content in the products	79
Figure 4.32. Stress-strain curves of, a) the graft copolymers with 3.8, 6.7, 10.7, 11.8, 18.6 and 21.1% poly(BPOCPMA) and b) HDPE and of the coproducts with 3.8, 7.3, 12.7, 19.2, 25.1 and 26.7% poly(BPOCPMA)	82
Figure 4.33. The variation of ultimate tensile strength of the products with poly(BPOCPMA) content	84
Figure 4.34. The variation of Young's modulus of the products with poly(BPOCPMA) content	84
Figure 4.35. The variation of poly(BPOCPA) content in the products with the BPOCPA percentage in the reaction mixture.....	91
Figure 4.36. The variation of poly(BPOCPMA) content in the products with the BPOCPMA percentage in the reaction mixture	91
Figure 4.37. The variation of percent grafting of poly(BPOCPA) with the percentage of BPOCPA in the reaction mixture	92
Figure 4.38. The variation of percent grafting of poly(BPOCPMA) with the percentage of BPOCPMA in the reaction mixture	92
Figure 4.39. The variation of poly(BPOCPA) content in the copolymers with the concentration of DCP in the reaction mixture.....	94
Figure 4.40. FTIR spectra of the copolymers with a) 6.2% poly(BPOCPA), and b) 10.6% poly(BPOCPA).....	95

Figure 4.41. FTIR spectra of the coproducts with a) 7.3% poly(BPOCPA), and b) 39% poly(BPOCPA).....	95
Figure 4.42. FTIR spectra of the copolymers with a) 5.1% poly(BPOCPMA), and b) 10.3% poly(BPOCPMA)	96
Figure 4.43. FTIR spectra of the coproducts with a) 9.5% poly(BPOCPMA), and b) 37.8% poly(BPOCPMA)	96
Figure 4.44. The XRD pattern of pure IPP.....	97
Figure 4.45. The DSC thermograms, obtained with a heating rate of 10°C/min under N ₂ atmosphere, of the poly(BPOCPA)-g-IPP copolymers with a) 3.8% poly(BPOCPA), b) 6.2% poly(BPOCPA), c) 7.6% poly(BPOCPA), d) 9.6% poly(BPOCPA), e) 10.9% poly(BPOCPA), and f) 10.6% poly(BPOCPA).....	98
Figure 4.46. The DSC thermograms, obtained with a heating rate of 10°C/min under N ₂ atmosphere, of the coproducts with a) 4.0% poly(BPOCPA), b) 7.3% poly(BPOCPA), c) 12.3% poly(BPOCPA), d) 17.4% poly(BPOCPA), e) 28.4% poly(BPOCPA), and f) 39.0% poly(BPOCPA).....	99
Figure 4.47. DSC thermograms, obtained with a heating rate of 10°C/min under N ₂ atmosphere, of the poly(BPOCPA)-g-IPP copolymers produced by using the initiator a) 1% DCP, b) 3% DCP, and c) 4% DCP	101
Figure 4.48. The variation of percent crystallinity with poly(BPOCPA) content in a) copolymers, and b) coproducts.....	104
Figure 4.49. The DSC thermograms, obtained with a heating rate of 10°C/min under N ₂ atmosphere, of the poly(BPOCPMA)-g-IPP copolymers with a) 3.3% poly(BPOCPMA), b) 5.1% poly(BPOCPMA), c) 6.6% poly(BPOCPMA), d) 7.3% poly(BPOCPMA), e) 8.9% poly(BPOCPMA), and f) 10.3% poly(BPOCPMA).....	105
Figure 4.50. The DSC thermograms, obtained with a heating rate of 10°C/min under N ₂ atmosphere, of the coproducts with a) 4.6% poly(BPOCPMA), b) 9.5% poly(BPOCPMA), c) 14.0% poly(BPOCPMA), d) 18.8% poly(BPOCPMA), e) 27.9% poly(BPOCPMA), and f) 37.8% poly(BPOCPMA).....	106
Figure 4.51. The variation of percent crystallinity with poly(BPOCPMA) content in a) copolymers, and b) coproducts.....	108
Figure 4.52. The XRD patterns of poly(BPOCPA)-g-IPP copolymers	110
Figure 4.53. The XRD patterns of poly(BPOCPA)-g-IPP coproducts	110
Figure 4.54. The variations of the unit cell parameters (<i>a,b,c</i>) in IPP matrix with poly(BPOCPA) content, calculated from the X-ray diffraction patterns by using 110, 040 and 041 reflections	113
Figure 4.55. The variation of crystal size in IPP matrix with poly(BPOCPA) content in the products.....	114
Figure 4.56. The XRD patterns of poly(BPOCPMA)-g-IPP copolymers.....	115
Figure 4.57. The XRD patterns of poly(BPOCPMA)-g-IPP coproducts.....	116
Figure 4.58. The variations of the unit cell parameters (<i>a,b,c</i>) in IPP matrix with poly(BPOCPMA) content, calculated from the X-ray diffraction patterns by using 110, 040 and 041 reflections	119
Figure 4.59. The variation of crystal size in IPP matrix with poly(BPOCPMA) content in the products.....	120
Figure 4.60. Stress-strain curves of poly(BPOCPA)-g-IPP copolymers	122
Figure 4.61. Stress-strain curves of poly(BPOCPA)-g-IPP coproducts	122

Figure 4.62. The variation of a) ultimate strength, b) Young's modulus and c) impact strength of the coproducts with poly(BPOCPA) content .	125
Figure 4.63. Stress-strain curves of poly(BPOCPMA)-g-IPP copolymers	128
Figure 4.64. Stress-strain curves of poly(BPOCPMA)-g-IPP coproducts	128
Figure 4.65. The variation of a) ultimate strength, b) Young's modulus and c) impact strength of the products with poly(BPOCPMA) content .	130
Figure 4.66. SEM micrograph of tensile fractured surface of the coproduct with 3.8% poly(BPOCPMA)-g-HDPE	133
Figure 4.67. SEM micrograph of tensile fractured surface of the copolymer with 6.7% poly(BPOCPMA)-g-HDPE	133
Figure 4.68. SEM micrograph of tensile fractured surface of the copolymer with 10.7% poly(BPOCPMA)-g-HDPE	134
Figure 4.69. SEM micrograph of tensile fractured surface of the coproduct with 12.7% poly(BPOCPMA)-g-HDPE	134
Figure 4.70. SEM micrograph of tensile fractured surface of the coproduct with 25.1% poly(BPOCPMA)-g-HDPE	135
Figure 4.71. SEM micrograph of tensile fractured surface of the copolymer with 18.6% poly(BPOCPMA)-g-HDPE	135
Figure 4.72. SEM micrograph of tensile fractured surface of the copolymer with 21.0% poly(BPOCPMA)	136
Figure 4.73. SEM micrograph of tensile fractured surface of the coproduct with 26.7% poly(BPOCPMA)-g-HDPE	136
Figure 4.74. SEM micrograph of impact fractured surface of the coproduct with 26.7% poly(BPOCPMA)-g-HDPE	137
Figure 4.75. SEM micrograph of tensile fractured surface of the copolymer with 3.8% poly(BPOCPA)-g-IPP	138
Figure 4.76. SEM micrograph of tensile fractured surface of the copolymer with 7.6% poly(BPOCPA)-g-IPP	138
Figure 4.77. SEM micrograph of tensile fractured surface of the copolymer with 9.6% poly(BPOCPA)-g-IPP	139
Figure 4.78. SEM micrograph of tensile fractured surface of the coproduct with 12.3% poly(BPOCPA)-g-IPP	139
Figure 4.79. SEM micrograph of tensile fractured surface of the copolymer with 10.9% poly(BPOCPA)-g-IPP	140
Figure 4.80. SEM micrograph of tensile fractured surface of the coproduct with 28.4% poly(BPOCPA)-g-IPP	140
Figure 4.81. SEM micrograph of tensile fractured surface of the coproduct with 39.0% poly(BPOCPA)-g-IPP	141
Figure 4.82. SEM micrograph of impact fractured surface of the copolymer with 7.6% poly(BPOCPA)-g-IPP	142
Figure 4.83. SEM micrograph of impact fractured surface of the copolymer with 10.9% poly(BPOCPA)-g-IPP	142
Figure 4.84. SEM micrograph of impact fractured surface of the coproduct with 4.0% poly(BPOCPA)-g-IPP	143
Figure 4.85. SEM micrograph of impact fractured surface of the coproduct with 12.3% poly(BPOCPA)-g-IPP	143
Figure 4.86. SEM micrograph of impact fractured surface of the coproduct with 39.0% poly(BPOCPA)-g-IPP	144
Figure 4.87. SEM micrograph of tensile fractured surface of the copolymer with 5.1% poly(BPOCPMA)-g-IPP	145

Figure 4.88. SEM micrograph of tensile fractured surface of the copolymer with 6.6% poly(BPOCPMA)-g-IPP	145
Figure 4.89. SEM micrograph of tensile fractured surface of the copolymer with 8.9% poly(BPOCPMA)-g-IPP	146
Figure 4.90. SEM micrograph of tensile fractured surface of the copolymer with 10.3% poly(BPOCPMA)-g-IPP	146
Figure 4.91. SEM micrograph of tensile fractured surface of the coproduct with 14.0% poly(BPOCPMA)-g-IPP	147
Figure 4.92. SEM micrograph of tensile fractured surface of the coproduct with 18.8% poly(BPOCPMA)-g-IPP	147
Figure 4.93. SEM micrograph of tensile fractured surface of the coproduct with 27.9% poly(BPOCPMA)-g-IPP	148
Figure 4.94. SEM micrograph of tensile fractured surface of the coproduct with 37.8% poly(BPOCPMA)-g-IPP	148
Figure 4.95. SEM micrograph of impact fractured surface of the copolymer with 5.1% poly(BPOCPMA)-g-IPP	149
Figure 4.96. SEM micrograph of impact fractured surface of the coproduct with 9.5% poly(BPOCPMA)-g-IPP	150
Figure 4.97. SEM micrograph of impact fractured surface of the copolymer with 10.3% poly(BPOCPMA)-g-IPP	150
Figure 4.98. SEM micrograph of impact fractured surface of the coproduct with 27.9% poly(BPOCPMA)	151

LIST OF TABLES

	<u>Page</u>
Table 4.1. The dependence of poly(BPOCPMA) content in the products on the BPOCPMA percentage in the reaction mixture	56
Table 4.2. DSC results with poly(BPOCPMA) percentages in the copolymers (The crystalline melting temperatures, T_m , enthalpy of fusions, ΔH_m and the percent crystallinities, $X_c(\%)$).....	60
Table 4.3. DSC results with poly(BPOCPMA) percentages in the coproducts (The crystalline melting temperatures, T_m , enthalpy of fusions, ΔH_m and the percent crystallinities, $X_c(\%)$)	61
Table 4.4. The dependence of the unit cell parameters <i>a</i> , <i>b</i> and <i>c</i> , and crystal size in HDPE matrix on poly(BPOCPMA) content in copolymers.....	64
Table 4.5. The dependence of the unit cell parameters <i>a</i> , <i>b</i> and <i>c</i> , and crystal size in HDPE matrix on poly(BPOCPMA) content in coproduct.....	65
Table 4.6. The dependence of the lifetimes and the intensities of the positrons, the radii of the free volume hole, the free volume hole size and the free volume fraction of the copolymers on poly(BPOCPMA) content.....	73
Table 4.7. The dependence of the lifetimes and the intensities of the positrons, the radii of the free volume hole, the free volume hole size and the free volume fraction of the coproducts on poly(BPOCPMA) content.....	74
Table 4.8. Ultimate tensile strength and Young's modulus of the copolymers with poly(BPOCPMA) content.....	83
Table 4.9. Ultimate tensile strength and Young's modulus of the coproducts with poly(BPOCPMA) content.....	83
Table 4.10. Impact strength of the products with % poly(BPOCPMA) content..	88
Table 4.11. The dependence of poly(BPOCPA) content in the products on the BPOCPA percentage in the reaction mixture.....	90
Table 4.12. The dependence of poly(BPOCPMA) content in the products on the BPOCPMA percentage in the reaction mixture	90
Table 4.13. The dependence of poly(BPOCPA) content in the copolymers on the initiator concentration.....	93
Table 4.14. DSC results with poly(BPOCPA) percentages in the copolymers (The crystalline melting temperatures, T_m , enthalpy of fusions, ΔH_m and the percent crystallinities, $X_c(\%)$).....	103
Table 4.15. DSC results with poly(BPOCPA) percentages in the coproducts (The crystalline melting temperatures, T_m , enthalpy of fusions, ΔH_m and the percent crystallinities, $X_c(\%)$).....	103
Table 4.16. DSC results with poly(BPOCPMA) percentages in the copolymers (The crystalline melting temperatures, T_m , enthalpy of fusions, ΔH_m and the percent crystallinities, $X_c(\%)$)	107
Table 4.17. DSC results with poly(BPOCPMA) percentages in the coproducts(The crystalline melting temperatures, T_m , enthalpy of fusions, ΔH_m , and the percent crystallinities, $X_c(\%)$).....	107
Table 4.18. The dependence of the unit cell parameters <i>a</i> , <i>b</i> and <i>c</i> , and crystal size in IPP matrix on poly(BPOCPA) content in copolymers.....	112

Table 4.19. The dependence of the unit cell parameters <i>a</i> , <i>b</i> and <i>c</i> , and crystal size in IPP matrix on poly(BPOCPA) content in coproducts.....	112
Table 4.20. The dependence of the unit cell parameters <i>a</i> , <i>b</i> and <i>c</i> , and crystal size in IPP matrix on poly(BPOCPMA) content in copolymers.....	117
Table 4.21. The dependence of the unit cell parameters <i>a</i> , <i>b</i> and <i>c</i> , and crystal size in IPP matrix on poly(BPOCPMA) content in coproducts.....	118
Table 4.22. Ultimate tensile strength, Young's Modulus and impact strength of the poly(BPOCPA)-g-IPP copolymers with poly(BPOCPA) content.....	124
Table 4.23. Ultimate tensile strength, Young's Modulus and impact strength of the poly(BPOCPA)-g-IPP coproducts with poly(BPOCPA) content.....	124
Table 4.24. Ultimate tensile strength, Young's Modulus and impact strength of the poly(BPOCPMA)-g-IPP coproducts with poly(BPOCPMA) content.....	129
Table 4.25. Ultimate tensile strength, Young's Modulus and impact strength of the poly(BPOCPMA)-g-IPP coproducts with poly(BPOCPMA) content.....	129

LIST OF ABBREVIATIONS AND SYMBOLS

PE	: Polyethylene
HDPE	: High Density Polyethylene
PP	: Polypropylene
IPP	: Isotactic Polypropylene
MAH	: Maleic Anhydride
LCP	: Liquid Crystalline Polymer
LC	: Liquid Crystalline
TLCP	: Thermotropic Liquid Crystalline Polymer
TP	: Thermoplastic
PA6	: Polyamide 6
UHMWPE	: Ultra High Molecular Weight Polyethylene
PE-g-MAH	: Maleic Anhydride Grafted Polyethylene
PP/LCP	: Polypropylene/Liquid Crystalline Polymer
PE/LCP	: Polyethylene/Liquid Crystalline Polymer
TP/LCP	: Thermoplastic/Liquid Crystalline Polymer
MAP	: Maleic Anhydride-Grafted Polypropylene
PEA	: Polyesteramide
LDPE	: Low Density Polyethylene
HMMPE	: High Molecular Weight Polyethylene
RODRUN LC5000	: Thermotropic Liquid Crystalline Polymer containing- <i>p</i> -Hydroxy Benzoic Acid and Polyethylene Terephthalate
PET	: Polyethylene Terephthalate
HBA	: <i>p</i> -Hydroxy Benzoic Acid
VECTRA A950	: Thermotropic Liquid Crystalline Polymer containing- <i>p</i> -Hydroxy Benzoic Acid and 2,6-Hydroxynaphthoic Acid
VECTRA B950	: Thermotropic Liquid Crystalline Polymer containing- <i>p</i> -Hydroxy Benzoic Acid, Aminophenol and Terephthalic Acid
LC3000	: Thermotropic Liquid Crystalline Polymer containing- <i>p</i> -Hydroxy Benzoic Acid, and Poly (Ethylene Terephthalic Acid)
EGMA	: Ethylene-Glycidyl-Methacrylate
CNF	: Carbon Nanofiber
DSC	: Differential Scanning Calorimetry

GNP	: Graphene Nanoplatelet
MWCNT	: Multi-walled Carbon Nanotube
MMMIM	: Multi-Melt-Multi-Injection Molding
PBI	: Polybenzimidazole
V_f	: Free Volume
V_{occ}	: Occupied Volume
V_w	: Van der Waals Volume
V	: Total Volume
h or f	: Free Volume Fraction
y	: Occupied Fraction
e^+	: Positron
PALS	: Positron Annihilation Lifetime Spectroscopy
Ps	: Positronium
PET	: Positron Emission Tomography
SPM	: Scanning Positron Microscopy
TPM	: Transmission Positron Microscopy
ACAR	: Angular Correction of Annihilation Radiation
PAES	: Positron-Annihilation Induced Auger Electron Spectroscopy
CDB	: Coincidence Doppler Broadening
SPL	: Slow Positron Beam
<i>p-Ps</i>	: Para Positronium
<i>o-Ps</i>	: Ortho Positronium
τ	: Mean Lifetime
λ	: Annihilation Rate
I	: Intensity
I_1	: Para Positronium Intensity
I_2	: Free Positron Intensity
I_3	: Ortho Positronium Intensity
I_4	: Ortho Positronium Intensity in crystalline region
R	: Free Volume Hole Radius
τ_1	: Para Positronium Lifetime
τ_2	: Free Positron Lifetime
τ_3	: Ortho Positronium Lifetime
τ_4	: Ortho Positronium Lifetime in crystalline region

RT	: Room Temperature
T_g	: Glass Transition Temperature
SBR	: Styrene Butadiene Rubber
PPN	: Isotactic Polypropylene with 55% Crystallinity
PPHC	: Isotactic Polypropylene with High Crystallinity 66%
PP-N	: Normal Polypropylene, which is 55% Crystallinity
PP-HC	: Polypropylene High Crystallinity, which is 66% crystallinity)
PC	: Polycarbonate
HBP	: 4-Hydroxybenzophenone
HBA	: p-Hydroxybenzophenone
BPOCPA	: p-Benzophenoneoxycarbonylphenyl Acrylate
BPOCPMA	: p-Benzophenoneoxycarbonylphenyl Methacrylate
DCP	: Dicumyl Peroxide
PETKIM	: Turkish Petrochemical Industry
ABA	: p-Acryloyloxybenzoic Acid
ABC	: p-Acryloyloxybenzoyl Chloride
FT-IR	: Fourier Transform Infrared Spectroscopy
H-NMR	: Hydrogen Nuclear Magnetic Resonance
SEM	: Scanning Electron Microscope
DMSO	: Dimethylsulfoxide
DMF	: Dimethylformamide
Poly(BPOCPA)-g-IPP:	Poly (p-Benzophenoneoxycarbonylphenyl Acrylate) Grafted Isotactic Polypropylene
Poly(BPOCPMA)-g-IPP:	Poly(p-Benzophenoneoxycarbonylphenyl Methacrylate) Grafted Isotactic Polypropylene
MBC	: p-Methacryloyloxybenzoyl Chloride
Poly(BPOCPA):	Poly (p-Benzophenoneoxycarbonylphenyl Acrylate)
Poly(BPOCPMA):	Poly (p-Benzophenoneoxycarbonylphenyl Methacrylate)
TMS	: Tetramethyl Silane
Poly(BPOCPMA)-g-PE:	Poly(p-Benzophenoneoxycarbonylphenyl Methacrylate) Grafted High Density Polyethylene
X_c	: Percentage Crystallinity
ΔH_m	: Heat of Fusion/Enthalpy of Fusion
FWHM	: Full Width at Half Maximum

- d** : Crystal Thickness
- θ_B** : Bragg Angle
- B_s** : Half Width of Standard Material
- B_m** : The sign of the difference between the angles at FWHM of the peak
- T_g** : Glass Transition Temperature



ACKNOWLEDGEMENTS

First of all, I wish to express my deepest gratitude to my supervisor Assoc. Prof. Dr. Sedat ÇETİN for his guidance, advice, criticism, encouragements and insight throughout the research.

I would also like to endless thank Prof. Dr. Uğur YAŞI for PALS analysis, calculations and discussion of free volume behavior and also his suggestions and comments. Also, I would like to thank Prof. Dr. Cumali TAV and Murat Yavuz YENER for PALS analysis in Positronium Laboratory of Physics Department, Marmara University. Furthermore, thanks to Assoc. Prof. Dr. Ayşe YUMAK YAŞI and Serap KALKAN for their help and hospitality during nearly one year in Faculty of Arts and Sciences of Marmara University.

I am very grateful to Prof. Dr. Teoman TİNÇER for giving me a chance for mechanical analysis in METU. Also, thanks to Osman YASLITAŞ for his technical support.

I would like to express my endless thanks to all my lab mates, Lecturer Uğur SOYKAN and my colleagues in Abant İzzet Baysal University.

I would like to extend special thanks to Res. Assists. Ayşen ÇETİN, Tuğba METİN, Gülgez Gökçe YILDIZ and Gülderen TOKMAK for their endless support and for making my graduate study enjoyable and full of friendship and also, they are my family in BOLU and never forget all of them.

In addition, I wish to thank Nevin SOYLU for SEM analysis, Metin ALKAN for glassware and technical support and Emine DEMİRTÜRK and Dr. Fırat KARABOĞA for XRD analysis.

I would like to thank to my PhD exam committee members.

I would like to extend my deepest thanks to School of Pharmacy at Altınbaş University for supporting me to complete my PhD in Chemistry Department, AIBU.

My deepest thanks to my husband, Sunay ŐEN. Because he waited for me approximately 5 years to gather and every week, he had a journey from Istanbul to Bolu and I wish to thank to my father, my mother, father in law and mother in law, my sister for their support, encouragement and patience.

This study was supported by the AIBU research fund, Grant No: BAP-2010.03.03.372.



1.INTRODUCTION

Polyolefins are widely used commercial thermoplastics in polymer industry due to extensive abundance of the monomers, relatively superior processability and a numerous applications in several industries owing to their physical and mechanical properties (Abedi et al., 2014). Despite the viable success of polyolefins, on the other hand, modification of polyolefins has been area of interest as a route to superior property products. Various methods of functionalization have been employed to alter their chemical and physical properties (Bunescu et al., 2017).

Polypropylene and polyethylene are commonly used polyolefins and some of the properties of these polyolefins can be improved with modifications and thus their applications are increased. Graft polymerization such as grafting of unsaturated monomers onto polyolefin and grafting of specific monomers (chemically induced, photochemically induced, high energy radiation-induced etc.), blending, incorporation of fillers and fibers are some of the polymer modification techniques. Among these techniques, graft copolymerization has a strong interest. Because not only most of the original properties of polymer are conserved but also some desirable properties are introduced to the material without changing inherent architecture of the polymer. Thus available market expands for applications. Grafting improves compatibility, stability and adhesion of the polymer matrix and hence leads to some modified properties of polymer. For example, the compatibility with other polar polymers can be improved by introducing polar groups and effective interfacial agents to polyolefins (Chung, 2002).

1.1 Polyethylene

Polyethylene (PE) is one of the major commercial thermoplastic polymers. There are different types of commercial polyethylene depending on its density and branching. Various types of polyethylene exhibit a wide range of physical properties, and so it is employed in a diverse range of applications such as in biomedical applications due to low cost, regular chain structure, unusual electrical properties,

excellent chemical inertness, and ease of processing (AlMaadeed et al., 2013). It can be adapted to many end uses by controlling molecular weight, molecular weight distribution, branching characteristics, and by manipulating processing variables (Peacock, 2000).

High density polyethylene (HDPE) is one of the semi-crystalline polyethylene and owing to good processability, non-toxicity, ease of recycling, biocompatibility and good chemical resistance, commonly used. However, the limited mechanical properties such as environmental stress cracking resistance and low toughness restrict its use in various commercial applications for certain purposes (Faiz et al., 2016). So, it's important topic, how to improve the mechanical properties of HDPE (Hu et al., 2012).

By forming composites, its properties such as stiffness and rigidity may be improved (Liu et al., 2015). In recent years, to enhance these properties, various natural (kenaf, sisal jute, henequen etc.) and synthetic fibers (carbon, aramid, Kevlar, glass) are used as modifiers to increase its application for commercial composites (Faiz et al., 2016).

1.2 Polypropylene

Polypropylene (PP), thermoplastic polymer is used in different applications such as plastic parts, packaging, textiles, automotive components and laboratory equipments etc. owing to the ease of availability and low cost (Yılmaz, 2011). There are different types of polypropylene based on tacticity and one of them is a semi-crystalline isotactic propylene (IPP) and mostly used polypropylene because of its ordered structure and higher melting point and crystallinity compared to syndiotactic and atactic polypropylene. However, poor hydrophilicity, lack of reactive sites and sensitivity to photo-oxidation restrict its application in some areas. In order to improve these properties, chemical modification techniques such as copolymerization of propylene with polar monomers, grafting, blending, reinforcement of PP with fibers are necessary without affecting the nature of polypropylene (Srinivasa et al., 1996).

For the modification of polypropylene in the solid state, it is required to abstract hydrogen atom from the main chain which possesses *tert-C* atoms and hence e-beam radiation at low temperatures or the decomposition of peroxides techniques are used to abstract the hydrogen atoms (Ratzsch et al., 2002). Radical transfer or oxyradicals, which are made up of the thermal decomposition of organic peroxides initiate the abstraction of hydrogen and then, these radicals can abstract hydrogen from PP (Ratzsch et al., 2002) and this polypropylene can be modified with different polymers and use in different applications.

Modification of IPP through grafting expands its application. But, suitable polymerization temperature must be chosen for grafting owing to radical-reactions between 80 and 150°C. From 140°C to 180°C, branching and cross-linking are predominant and the degradation reaction is dominant above 180°C (Ratzsch et al., 2002). The effect of temperature on the modification reactions of IPP radicals is figured out in Figure 1.1.

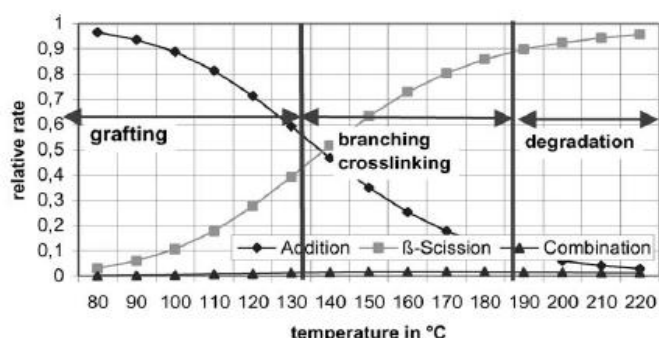


Figure 1.1. The effect of temperature on the modification reactions of iPP-radicals

Functionalization of PP with various reagents, such as sulfuric acid, phosphoric acid, iminodiacetic acid, sodium sulfite, amines and hydroxylamine, grafting of glycidyl methacrylate, acrylic acid and acrylamide onto PP are example to the modification of PP. In recent years, grafting of maleic anhydride (MAH) on polyolefin has great attention (Ecevit, 2012).

1.3 Liquid Crystalline Polymers (LCPs)

Liquid crystalline polymers (LCPs) are composed of rigid and rod-like molecules which form well-ordered structures. The organized structure results in anisotropic behavior in the material. The smaller groups responsible for forming anisotropic property and thus for forming liquid crystal phase are called mesogens. Two types of LCPs, depending on the type of the incorporation of the mesogenic groups into polymer chain, have come into use. *LC (liquid crystalline) main chain polymers* involve the mesogenic groups composed of segments from the backbone of the polymer, while *LC side chain polymers* are formed by the incorporation of the mesogenic units as side groups to the backbone. *LC main chain polymers* and *LC side chain polymers* exhibit rather different properties due to their basic structural differences. *LC main chain polymers* find uses as high strength fibers and self-reinforcing plastics, whereas *LC side chain polymers* are often used in optical applications (Mayer et al., 2002).

LC polymers that form liquid crystalline structure in solution are termed *lyotropic LCPs*. Those that form liquid crystalline organization upon heating are called *thermotropic LCPs* (TLCP) (Calundann, 1980-1981). The application of *thermotropic LCP* is more common with respect to *lyotropic LCP*. While *lyotropic LCP* is fabricated only in films or fibers, *thermotropic LCP* is fabricated in conventional processes, such as injection molding (Yoon et al., 1992).

The organized structure of LCPs leads to significantly increased crystalline melting temperature comparing to the chain-folded semi-crystalline polymers. In addition, high state of organization and orientation in these polymers may give rise to extremely high modulus and high strength (Collyer, 1989). Therefore, LCPs are known as high performance engineering materials due to better mechanical and thermal properties (Donald et al., 1992; Sun et al., 1989).

The main factor that affects the properties of a LCP is its orientability in the fluid state and distribution in the solid state (Kenig, 1987). In order to utilize and control the LCP's properties, it is so important to comprehend the processing conditions-orientation relationship. The effect of processing conditions on the properties of polymer liquid crystals was reviewed by Lewis and Fellers (Lewis et

al., 1988). Elongational flow was pointed out to be very effective in advance of orientation in different polymers studied.

High melting temperature of LCPs, however, leads to poor melt processability. A number of works have been carried out to modify the structures and properties of LCPs thus to attain more practical conditions for ease of processability (Elsmer et al., 1985). Incorporation of nonlinear links (Chang et al., 2002), frustrated chain packing (Tokita et al., 1998) and insertion of flexible spacers, which separate the mesogenic units along the backbone of polymer (Zheng et al., 1999) are some of the approaches to reduce the transition temperatures of LCPs, and hence to improve the processability of LCPs. At the same time, the chemical periodicity of LCP repeating units is preserved (Chen et al., 2005) in the processes.

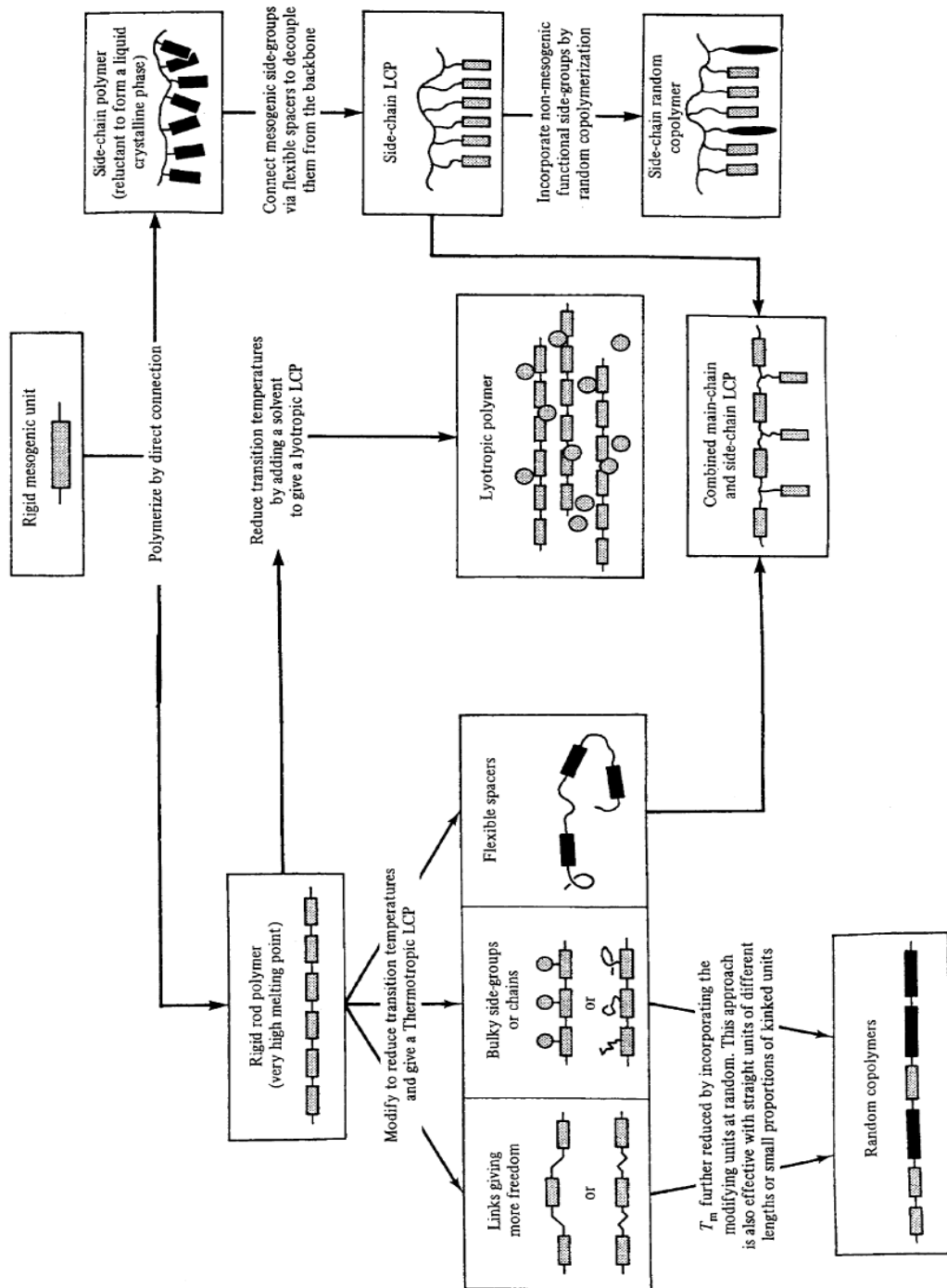


Figure 1.2. Types of liquid crystalline polymers containing rigid mesogenic units

1.4 Combining Thermoplastic with LCP's

Polymeric materials generally possess lower moduli and strength in comparison with metals or ceramics (Grala et al., 2015). There have been common efforts to improve the poor physical properties of polymers for commodity purposes. Therefore, polymer reinforcement has been a growing and important topic for researchers. Some of the poor properties of the polymeric materials such as low strength, stiffness and thermal properties can be improved by blending of two polymers or by forming composites to which reinforcement agents are added (Liu et al., 2015).

A new approach, widely used is polymer blending, which combines two polymers for the production of better performance materials. Performance of polymer blends are based on the properties of individual polymer and miscibility of polymers. Among the different types of polymer blends, thermoplastic (TP) and thermotropic liquid-crystalline polymer blends are attractive and these types of blends have been prepared since 1980s. Because;

- The TLCPs may act as a viscosity reduction agent of polymer matrix at nematic phase for engineering thermoplastic polymer and thus lead to improvement in processability
- At optimum processing conditions, the TLCP deforms into elongated fibrils and reinforce the thermoplastic matrix (Souza et al., 1996).

Reinforcement effect of LCPs on the properties of thermoplastics depends on several factors. These are:

- ✓ The mechanical properties of virgin LCP,
- ✓ The concentration and dispersion of LCP,
- ✓ The effect of the flow field on orientation,
- ✓ Processing temperature,
- ✓ Miscibility of the components (O'Donnell et al., 1995).

The mechanical properties of these blends are higher compared to thermoplastic polymer owing to LCPs stiff molecular backbone and orientation of

LCPs. For example, the modulus of injection-moulded LCP is between 4 and 20 GPa and strengths are between 139 and 213 MPa, whereas the modulus of thermoplastic resins are between 1 and 4 GPa and the strengths are between 20 to 60 MPa. As a result, at appropriate processing conditions, LCPs reinforce thermoplastics by forming LCPs fibrils and hence fibre-reinforced composites can be obtained due to fibrillar morphology (O'Donnell and Baird, 1995).

LCP-reinforced thermoplastic polymers are defined *in-situ composites* and often used due to their lower viscosity and easier processability compared to neat LCPs (Lee et al., 2003). The morphology of *in situ composites* prepared by different methods such as injection molding, film extrusion and compression molding is important to obtain fibrillar morphology and this leads to better mechanical properties. In some cases, however, phase separation is observed due to incompatible nature of these polymers and this leads to lower mechanical properties. In attempt to reduce phase separation between thermoplastic/LCP blends, *compatibilizers*, which can be a copolymer composed of two blocks that resemble to polymers in blend and have specific interaction with polymers or a functionalization with one of the polymer, are used (O'Donnell and Baird, 1995) and also these compatibilizers reduce the viscosity of polymer and interfacial energy and improve the processability and interfacial adhesion of polymers in blend (Hatui et al., 2012). Therefore, the impact strength and the toughness of the thermoplastic matrix can be enhanced by compatibilization. One of the compatibilizer was functionalized polypropylene and used for TLCP/PP blends (Bose et al., 2010). On the other hand, without compatibilizer, poor adhesion, large phase sizes and lower mechanical properties would be observed.

However, in some cases, it is not necessary to use compatibilizer based on the morphology of blends, and lower modulus of some LCPs can be improved by polyamide-6 (PA6) without compatibilizers. Jang and Kim reported that injection-molded PA/LCP blends had better mechanical properties compared to LCP owing to the well-oriented fibrillar structure and enhancement in interfacial adhesion between PA matrix and LCP (Jang et al., 1994). It was revealed that, when more flexible LCP molecules are synthesized, compatibilization between PA matrix and LCP may

increase and lead to higher modulus and strength in blend without compatibilizers (Shin et al., 1990).

Another factor causing the changes in the properties of polymer blend is flow field type and leads to the orientation of LCPs. The deformation of the LCP phase in polymer blends exists in uniaxial extension flow by leading to fibrillar morphology and hence gives rise to reinforcement in the polymer matrix and higher mechanical properties. Moreover, for enhanced mechanical properties, it is necessary to obtain solidified fibrils before occurring interfacial instabilities such as break-up of the fibres into droplets and relaxation (O'Donnell and Baird, 1995).

The other factor affecting the properties of polymer blend is the processing temperature. Normally, the processing temperatures of LCPs are above 300°C, whereas the processing temperatures of thermoplastics are below this temperature and so it is necessary to choose adequate processing temperature for improved blend properties. For processing of blends, however, higher temperatures compared to the melting point of the LCPs are required and hence in this case, lead to lower mechanical properties (O'Donnell and Baird, 1995). Although the differences in temperatures, at appreciated temperature, fibrous morphology can be observed at TP/LCP blends and results in enhanced mechanical properties.

1.5 Reinforcement of PE and PP with LCP's

In recent year, PP and PE have been reinforced with various LCPs by using different techniques such as injection molding and extrusion. PE/LCP and PP/LCP blends have been studied and the thermal, mechanical and other properties of these blends have been investigated.

Zhou and Yan researched the tribological and mechanical behavior of ultra high molecular weight polyethylene (UHMWPE)-liquid crystalline polymer composite, which has 60% *hydroxynaphthalic acid*, 20% *aminophenol* and 20% *terephthalic acid* as LCP and also investigated the effect of PE-g-MAH (maleic anhydride grafted high density polyethylene) as a compatibilizer on the composite properties and compression molding was applied to prepare different contents of LCP and PE-g-MAH composites. Within the experimental results, the increment in

PE-g-MAH content and existence of LCP gave rise to decrease in the melting temperature and the crystallinity of UHMWPE because of the interaction in the amorphous region, and hence lower T_m in the composites. On the other hand, the higher LCP content and existence of PE-g-MAH in blends led to improvement in the tensile strength and modulus of composites owing to reinforcing effect of LCP, but the higher PE-g-MAH content led to decrease in the tensile properties because of structural inhomogeneity of blend and weakened interfacial bonding (Zhou et al., 2004).

Menon et al. prepared the polyesteramide (PEA), thermotropic liquid crystalline polymer and low density polyethylene (LDPE) blend and investigated the mechanical, thermal and processability characteristic of blend. It was observed that the higher PEA content resulted in higher tensile strength and modulus of the blends due to increase in tensile stiffness. The improvement in highly oriented and thin LCP fibrils is considered essential for better mechanical properties. In addition, in the presence of PEA, enhancement in the thermal stability of LDPE was observed due to aromatic content of PEA. It can be concluded that thermotropic liquid crystalline polymer led to enhancement in the physicomechanical properties and some of the processability characteristics of blends (Menon et al., 2000).

Tang et al. studied the viscosity reduction effect of TLCP (a copolyester composed of mol fraction of 35% *sebacic acid*, 30% *p-hydroxybenzoic acid* and 35% *hydroquinone*) on the viscosity properties of polyethylene. When 2.0 wt% TLCP was added into HDPE, approximately, 93% viscosity reduction was observed. Also, 1.0 wt% TLCP was added into high molecular weight polyethylene (HMMPE, TR570) and gave rise to decrease in bulk viscosity about 95.0% at 190°C and at this temperature, nematic phase structure was observed (Tang et al., 2010).

Whitehouse et al. investigated the effect of thermotropic liquid crystalline polymer on the viscosity reduction properties and thermal behavior of HDPE matrix. In their study, TLCP, which was a copolyester of *hydroxybenzoic acid*, *hydroquinone* and *sebacic acid* was blended with HDPE and the variation of TLCP content on the properties of HDPE was researched. Within experimental results, the increment in TLCP content led to decrease in the heat of fusion and the melting temperature due to the crystal growth inhibition of TLCP and resulted in lower crystal-size. In

addition, the rheological properties of pure HDPE and blends were investigated to determine the viscosity reducing properties of TLCP (Souza and Baird, 1996; Whitehouse et al., 1997).

Saengsuwan et al. studied the morphology, rheology and tensile properties of PP and TLCP composites. **Rodrun LC5000**, composed of 80% *p*-hydroxy benzoic acid (HBA) and 20% polyethylene terephthalate (PET) was used as TLCP and composites were prepared in a twin-screw extruder. According to experimental results, the higher LCP content in composites gave rise to the higher young's modulus, whereas the lower tensile strength. It can be concluded that the improvement in molecular orientation, the higher number of the elongated fibers and fiber aspect ratio led to increase in young's modulus and enhanced the mechanical properties of PP (Saengsuwan et al., 2003).

Lee et al. studied the mechanical properties of thermotropic liquid crystalline polymer, which has 20% polyethylene terephthalate (PET) and 80% *p*-hydroxy benzoic acid (HBA)/ polypropylene hybrid nanocomposites and silica particles were used as filler and this nanofiller could enhance the fibrillation of *in-situ* LCP/PP composites. Nanocomposites having different contents of filler were melt-blended in a twin-screw extruder. The variation in filler content gave rise to changes in young's modulus, tensile strength, stress-strain properties of composites. According to results, young's modulus of the composites increased at higher filler content. It can be concluded that rigid silica filler could render the matrix stiff and hence reinforce. As a result of stress-strain behavior, the addition of LCP and filler led to decrease in strain values, whereas increase in stress values. It can be concluded that PP was reinforced with LCP in the presence of filler (Lee et al., 2003).

Donnell and Baird studied the influence of maleic anhydride-g-polypropylene (MAP) on the mechanical and morphological behavior of PP/LCP blends and the effect of MAP content on these properties were evaluated. In the study, three different types of LCPs were used. These were **Vectra A950**, which contains 27% *mol* hydroxyl naphthoic acid and 73% *mol* hydroxy benzoic acid, **Vectra B950**, which has 60% *mol* hydroxy benzoic acid, 20% *mol* aminophenol and 20% *mol* terephthalic acid and **LC3000**, which has 40% *mol* poly (ethylene terephthalic acid) and 60% hydroxy benzoic acid. **Vectra A950** and **Vectra B950** were copolyester and

LC3000 was poly (ester amide) and maleic anhydride-g-polypropylene was used as a compatibilizer owing to molecular chain with polar groups in order to enhance the interfacial bonding between nonpolar PP and polar LCPs and improve the dispersion. Therefore, MAP is one of the most common compatibilizer which increases interfacial adhesion between different polymers (Zhou and Yan, 2004). According to mechanical results, higher MAP content in the blends gave rise to higher tensile strength among three different types of PP/LCPs blends and PP/*Vectra A950* had the highest tensile strength among them. Also, the increments in MAP concentration led to increase in tensile modulus, but the tensile modulus of blends decreased after 20% MAP concentration. In addition, stress-strain curves of blends were researched at higher MAP concentration. At 50% MAP content, both *Vectra B950* and *Vectra A950* blend had a transition from a ductile to a brittle failure. Moreover, compatibilized PP/LCP blend possessed fibrillar morphology and enhanced mechanical properties compared to uncompatibilized PP/LCP blend. It can be concluded that compatibilizer creates better adhesion, by reducing interfacial tension and improvement in matrix with more fibrillar structure (O'Donnell and Baird, 1995).

Chio et al. investigated the mechanical and thermal behavior of PP/LCP blends in the presence and the absence of a compatibilizer, ethylene-glycidyl methacrylate copolymer (EGMA). *Vectra A900* was used as TLCP. Uncompatibilized PP/LCP was immiscible and incompatible blend. In the presence of EGMA, these properties of blends were improved. EGMA has polyethylene segment and epoxy functional group to react with PP and carbonyl group in LCP, respectively. According to experimental results, uncompatibilized blends had higher crystallinity compared to compatibilized blends. It can be concluded that, EGMA-g-LCP inhibits PP crystallization and hence the PP crystallinities of the compatibilized PP/LCP blends were lower compared to uncompatibilized blends and in the compatibilized blend, compatibilizer may cause a reduction in the crystallinity of PP. In addition, the impact strength of compatibilized PP/LCP were higher than uncompatibilized, but lower tensile modulus due to lower crystallinity of blends compared to PP and increment in adhesion of the compatibilized blends were observed (Chiou et al., 1996).

1.6 Mechanical Properties of Polymers

There are some terms to define the mechanical properties of polymers. These terms, their meanings and factors that affect these mechanical properties of polymers and their results are given below:

A stress versus strain curve characterizes the tensile strength properties of the materials. Initially, it is linear owing to reversible elastic deformation and the slope of this curve is equal to the modulus of elasticity. The maximum stress is called as “**yield stress**”. After yield stress, irreversible plastic deformation is observed. The slope of this curve will decrease and the slope will be negative. This means that the material fractures and called as failure (Cassidy et al., 2016).

In linear polymers, Strobl et al. fit the stress-strain and determined the true stress-strain properties of polymers by using video-controlled device and put forward a general visco-elastic model, where two linear regions terminated and called as “**double yielding points**”, whereas the third critical point was attributed to “**onset of fibrillation**” and the last point was due to chain disentanglements and attributed to “**initiation of cracking**” (Dong et al., 2014).

Another term is “**hardness**” and defined as a resistance of material to plastic deformation and Rockwell hardness number gives information about the hardness of materials (Cassidy et al., 2016).

There are different factors affecting the mechanical properties of polymer. For example, in semi-crystalline polymers, their blends or composites, the crystalline structure is significantly important factor to obtain better mechanical properties (Feng et al., 2014). Furthermore, the molecular packing morphology such as crystallization morphology, which includes the crystalline and amorphous phases and also intermediate phase observed in semi-crystalline polymer like polypropylene (PP), polyethylene (PE), and polyethylene terephthalate (PET), etc and the orientation of chains affect the mechanical properties of polymers. Moreover, in micro-injected polymers, holding pressure and mold temperature are important in the crystallization morphology. For instance, in the macro injection molding, the higher mold temperature can lead to the bigger spherulite size in the core, resulting in

enhanced mechanical properties. Also, enhanced E-modulus may be obtained at higher mold temperature. Both thermal history and flow history, which increase the nucleation density speed-up the crystallization process and promote the orientation (Lin et al., 2013). Therefore, the optimum processing conditions must be determined to obtain high performance materials.

Another factor that affects the mechanical behavior of polymer blend is miscibility. Miscible and immiscible blends have different phase morphology and these morphologies lead to changes in mechanical properties. Multiphase morphology is observed in immiscible blends and hence leads to more complicated mechanical behavior compared to miscible ones (Faker et al., 2008).

1.7 Literature Survey For PE

In recent years, different types of HDPE blend and composites have been prepared and different properties such as mechanical, thermal and morphological have been researched.

Xu et al. investigated the influence of carbon nanofiber on the tribological, mechanical behavior and biocompatibility of HDPE. In order to determine these properties, two different contents of carbon nanofibers (CNFs) (0.5 wt% and 3 wt%) and 2.8 nm and 46 nm silane coating thicknesses were used to improve the interfacial bonding between HDPE and CNFs. According to experimental results, strain at fracture, ultimate stress and young modulus of nanocomposites were higher compared to neat HDPE. It can be concluded that the surface areas per unit volume of CNFs was more and this gave rise to better load transfer to the nanofibers and the increment in young modulus. In addition, the increase in ultimate stress may be due to restriction in the mobility of polymer chains. The thicker silane coating increased the interfacial bonding more significantly owing to the physical entanglement of the polymer chains and at the initial plastic deformation near the yield point, the polymer chains were less mobile (Xu et al., 2015).

Pokharel et al. studied the mechanical and morphological properties of graphene nanoplatelets (GNPs)/HDPE nanocomposites and the effect of titanate as a coupling agent, which linkage chemically between GNPs and HDPE and improve the

adhesion between GNPs and HDPE, on the properties of GNPs/HDPE nanocomposites. In the research, solution dispersion method was used to prepare composites and different contents of GNPs (2, 5, 10 wt%) composites with same content titanate and without titanate were prepared. The mechanical properties of virgin HDPE and composites were determined. According to these results; titanate treated samples had enhanced mechanical properties (higher young's modulus and tensile strength) compared to untreated samples. The increment in GNPs content gave rise to increment in young's modulus and it can be concluded that the plasticizing effect of titanate was insignificant at higher GNPs content because of large improvement in modulus, but elongation at break and the tensile strength of composites decreased after 2 wt% GNP because of matrix defect and agglomeration of graphene dominated. In order to determine the thermal and crystallinity behavior of composites, differential scanning calorimetry (DSC) analysis was applied. As a result, the melting temperatures of composites were approximately close to the melting point of virgin HDPE (130°C), but 2 wt% the melting temperature of treated composite was 131.2°C and the highest crystallinity among the treated and untreated composites. With respect to experimental results, there was a positive interaction between HDPE and GNPs, but at higher GNP content, crystallinity decreased owing to filler agglomeration and imperfection of crystallinity. Generally, in the presence of nanomaterials, smaller crystalline domains are formed and the overall crystallinity reduce at higher filler content (Pokharel et al., 2015).

Liu et al. researched the microcrystalline and mechanical properties of HDPE/nanofiller composites. In order to investigate these properties, carbon nanofillers at different size and morphology were used as a reinforcement reagent and HDPE as a matrix material. These nanofillers were carbon nanofiber (CNF) and graphite nanoplatelet (GNP). Different composites (HDPE/CNF-GNP and HDPE/CNF), at different strain rates were prepared. At dynamic and static, compression and tension tests were applied. According to experimental results, the increase in strain rate gave rise to increase in the tensile strength and the compression strength of both composites and all composites had higher tensile strength compared to virgin HDPE, but the compression strength of composites were higher than tensile strength. It can be concluded that, tensile strengths were more sensitive to defects under tension loadings. But, the tensile strength of HDPE/CNF-GNP composites

were higher than HDPE/CNF because of enhanced load bearing capacity. Also, as a result of microstructure characterization, HDPE had some voids and these may cause lower tensile strength and the increment in strain rate resulted in the decrease in fibrous structure. At higher strain rates, deformability is reduced. Owing to reduced ductility, the sensitivity to defects is more under tension compared to in compression (Liu et al., 2015).

Xiang et al. investigated the influence of multi-walled carbon nanotube (MWCNT) on the electrical, structural and mechanical properties of HDPE. In their research, different contents of MWCNT (2, 4, 8% wt) were used to prepare composites at two different process, blown film extrusion and compression molding. With respect to thermal analysis results (DSC), at blown film extrusion process, the crystallinity and crystallization temperature of pure HDPE and its composites did not change, yet the melting temperature of blown film extruded samples were lower compared to compression molding samples. Moreover, the variation in stress and strain at break (%) and modulus were determined and the modulus's were lower than neat HDPE. Also, the modulus's of compression molded composites increased at higher MWCNT content. The stress and strain at break of the composite films increased by increasing blow up ratio because of the break up of MWCNT agglomerates (Xiang et al., 2015).

Lu et al. researched the mechanical behavior of polyethylene composites, which included different contents of nylon-66 nanofibers (up to 0.65% wt nanofibers) and samples were prepared by electronspun method and these nanofibers are mechanically strong owing to the oriented macromolecular chains. In the study, the reinforcement and toughen effect of nanofiber were investigated. The tensile strength, tensile modulus, strain at break, toughness of composites increased by increasing nanofiber content and it can be concluded that reinforcement composites were obtained with electronspun method. Moreover, the crystallinity of composites was investigated and the increase in nanofiber content of composite led to increment in crystallinity and hence resulted in improvement mechanical properties (Lu et al., 2015).

Feng et al. investigated the mechanical, rheological and thermal properties of HDPE/polyamide 6 (PA) *in situ* microfibrillar composites. To prepare PA6/HDPE

blend, which was ratio of 10:90, a single-screw extruder was used and this blend was molded with multi-melt multi-injection molding (MMMIM), which has two injection units. Within the differential scanning analysis, the melting temperatures of HDPE and PA6 were 115.5°C and 116.55°C, respectively and also PA6/HDPE blend had higher crystallinity. It was obtained that PA6 microfibrillar could serve as an effective heterogeneous nucleation agent for neat HDPE. In order to explain detail crystalline structure like orientation and crystalline morphologies, SEM images of etched blend, by dissolving in strong acid was taken. In etched process, PA6 fibrils dissolved, there were only spindle – like voids left and highly oriented crystals were observed at SEM microphotographs. It can be concluded that PA6 microfibrillar gave rise to oriented crystals and also it was important in the improvement molecular orientation of HDPE matrix. According to mechanical results, the stress-strain behavior and tensile properties of neat HDPE and blend were determined and young modulus and the tensile strength of blend were higher compared to neat HDPE, whereas elongation at break was lower due to poor elongation of blend. On the other hand, HDPE had large elongation at break, resulted in necking and ductile fracture mode. In conclusion, PA6 gave rise to increase mechanical properties of HDPE by improving molecular orientation (Feng et al., 2014).

Faiz et al. researched the reinforcement effect of polybenzimidazole fiber (PBI) on the thermal, morphological, mechanical and viscoelastic properties of HDPE. A twin screw extruder was used for the preparation of HDPE/PBI composites. As a consequence of DSC analysis, the melting temperatures of composites didn't change so much, but the crystallinities of composites decreased by increasing fiber content and were lower than virgin HDPE because of amorphous properties of PBI and its interaction with HDPE retards the nucleating effect that means amorphous PBI obstruct the crystal growth and hence reducing crystallinity. According to mechanical results, the increment in PBI content led to increment in tensile strength, flexural strength and modulus, strain at break. It can be concluded that the restricted motion of polymer chains resulted in increase in modulus owing to strong interaction between matrix and the fibers. Also, the enhancement in mechanical behavior can be attributed to the stiff nature of the PBI fillers and the flexural modulus indicates that more flexible (bending and buckling) composite was obtained than neat HDPE (Faiz et al., 2016).

1.8 Free Volume

Free volume, V_f is defined as empty microscopic space that exists between molecules. In another definition, free volume equals the total volume V (cm^3/g) subtracted by the specific occupied volume by atoms or molecules, V_{occ} . If this specific occupied volume is called as van der Waals volume V_w , which is the space occupied by a molecule and this is not penetrable to other molecules, V_f is known as total free volume (Yang Y, 2011).

$$V_f = V - V_{occ}$$

V_w can be calculated with Bondi's method. For calculation, it is necessary to know the size, the bond length and the angles of each atom in a molecule. Therefore, Van Krevelen compiled tables can be used for the contribution of many common polymer groups to V_w (Yang Y, 2011).

Free volume theory has been proposed to explain micro-structural changes in polymers because many chemical and physical properties of polymers are associated with their free volume. Free volume influences the substance properties such as viscosity, mobility, structure relaxation, physical aging, molecular transport, permeability etc. (Yang Y, 2011). According to experimental studies, it was found that the decrease or increase in the size and number of free volume in polymers resulted in micro-structural changes and cross-linking or chain-scission affected the size and the number of free volume (Kumar et al., 2008). Moreover, the mobility of polymer chains was correlated with the amount and size of free volume. By determining the free volume, information about the polymer chain movements can be obtained (Qi N et al., 2015).

Free volume, however is different for amorphous and crystal material. In crystal materials, it is known as interstitial volume, whereas in amorphous materials, excess free volume is observed because of structural disorders. Also, these local free volumes are known as "*holes*" (Yang Y, 2011).

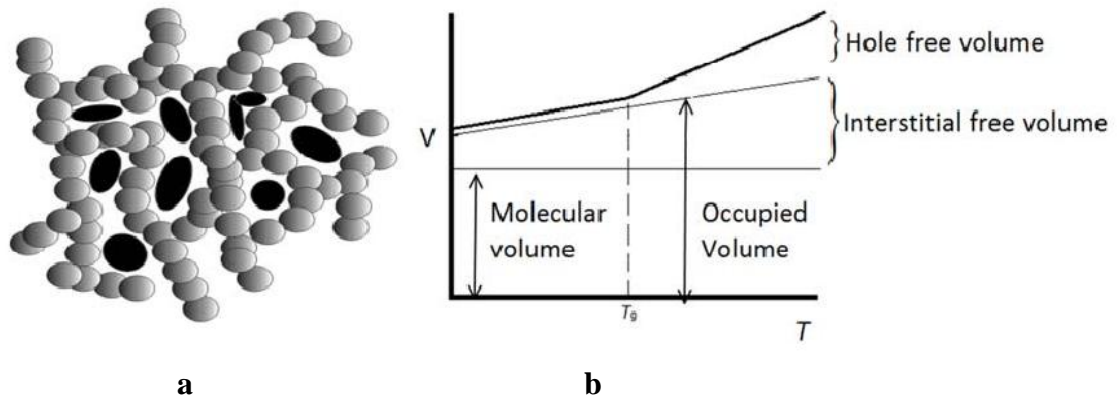


Figure 1.3. a) Hole volume (black ellipsoids) concept, and b) respective volumes

There are different terms to explain the free volume properties. One of them is hole or free volume fraction and denoted as h or f and formula is given below:

$$f = V_f / V$$

The other parameter is the occupied fraction and represented as y and given below:

$$y = 1 - f$$

1.9 Positron Property

Positron (e^+) was discovered in 1932 by Carl D Anderson. In physics, the discovery of positron is a great event due to the first evidence for the existence of antimatter. The positron is the anti-particle of the electron and its physical properties resemble the electron (rest mass corresponding to 511 keV, spin: 1/2) except for charge (+1 electron charge) (Yang Y, 2011).

There are some different methods, where positron is used such as **PET** (Positron Emission Tomography), **SPM** (Scanning Positron Microscopy), **TPM** (Transmission Positron Microscopy), **ACAR** (Angular Correction of Annihilation Radiation), Positron Diffraction Technique, **PAES** (Positron-annihilation induced Auger Electron Spectroscopy), **CDB** (Coincidence Doppler Broadening) and **SPL** (Slow Positron Beam) and **PALS** (Positron Annihilation Lifetime Spectroscopy).

1.10 Positron Generation

When positron is compared to electron, it is difficult to find stable positron due to the shorter lifetime of positron and fewer in nature. There are mainly two ways to generate positron. One of them is *pair production* and the other is *radioactive decay*.

Pair Production: When a photon reaches energy exceeding twice the rest mass of electron (1.022 MeV), it can produce an electron and a positron. This is defined as “*pair production*” (Yang Y, 2011).

Radioactive Decay: Positron is ejected from positron source by using different positron source such as ^{22}Na (Yang Y, 2011) and entered into polymer. Later, thermalization and diffusion processes occur (Yang Y, 2011).

➤ **Thermalization:** When high energetic positrons are injected into material or polymer, they create excess electrons and these electrons can annihilate with free positrons to form positronium (Hirade, 2003).

➤ **Diffusion:** After thermalization, positron travels without annihilating or falls into a localized state. This process is called “**diffusion**”.

1.11 Positron Sources

There are different types of positron sources such as ^{68}Ge , ^{58}Co , ^{64}Cu , ^{44}Ti , ^{21}Na and ^{22}Na , but ^{22}Na is generally used due to economic, proper half-lifetime and emitting gamma signal.

^{22}Na is artificially obtained from NaCl and it has the highest kinetic energy due to β^+ and the half-life of sodium 22 is 2.602 years. After one of the protons in ^{22}Na emits a positron and becomes a neutron, the ^{22}Na transforms to excited state of ^{22}Ne and decay scheme of sodium 22 is given in Figure 1.4 (Yang Y, 2011).

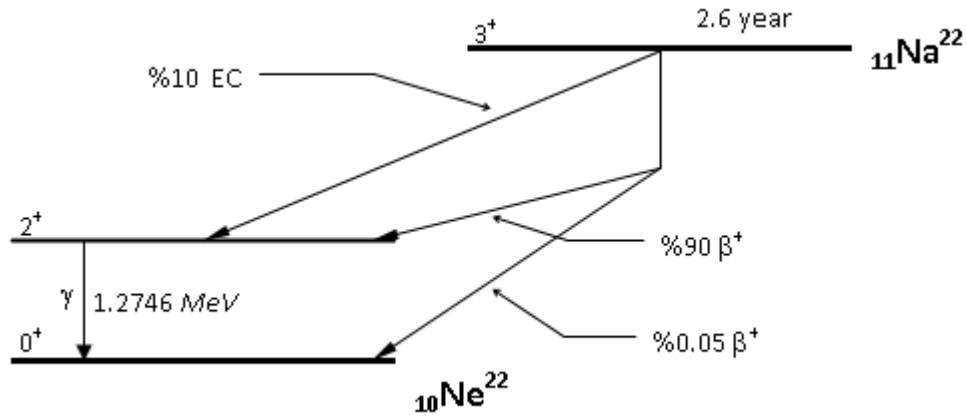


Figure 1.4. Decay of sodium 22 source

1.12 Positronium

Positron ejected from the positron source annihilates with an electron directly or forms an intermediate state between positron and electron ($e^+ \dots e^-$) and this form is defined as “**positronium**” atom (**Ps**). (Yang Y, 2011). Two different types of Ps form; one of them is *para-positronium* (*p-Ps*) ($\uparrow\downarrow$) (the spins of the electron and positron are antiparallel and called as opposite spin direction, denoted 1S_0) and the other is *ortho-positronium* (*o-Ps*) ($\uparrow\uparrow$) (the spins of the positron and electron are parallel and called as same spin direction, denoted 3S_1) (Mostafa et al., 2009). Furthermore, the spin angular momentum of *p-Ps* is zero, whereas the spin angular momentum of *o-Ps* is unit. In vacuum, the self-annihilation lifetime of *p-Ps* is 124 ps and for *o-Ps* is 142 ns.

o-Ps is formed in the free volume sites of polymer and there are electrons around, and hence the positron in *o-Ps* annihilates with another electron of opposite spin in nanoseconds and emit two photons rather than three. This process is defined as “**pick-off annihilation**”(Mostafa et al., 2009). Also, in polymers, Ps can be formed in free volume holes of polymer or lower electron density areas and it has been proposed that it is an important indicator for the detection of free volumes in polymers (Mostafa et al., 2009).

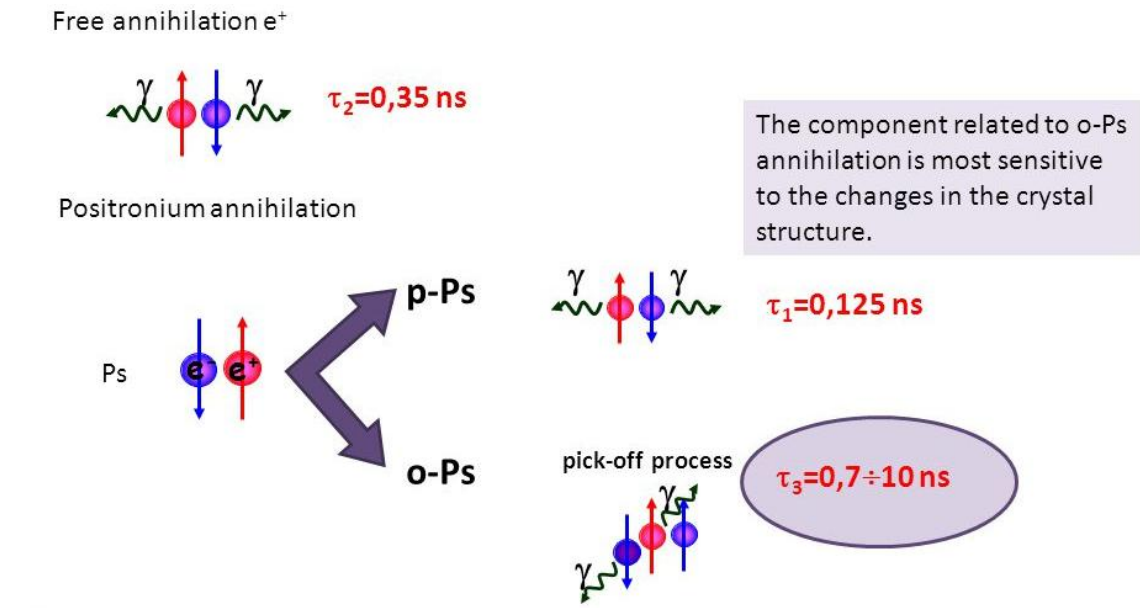


Figure 1.5. Scheme of *o*-Ps pick-off annihilation, *p*-Ps and direct annihilation

1.13 Positron Annihilation Lifetime Spectroscopy (PALS)

“**Positron annihilation lifetime spectroscopy**” (PALS) is one of the most important techniques for the determination of local free volume and micro structural characterization (Yu et al., 2006).

The principle of this technique depends on the generation and annihilation of the “positrons” and these positively charged positrons reside and decay by forming positronium in low electron density region (Djourelou et al., 2003). With respect to free volume theories, *o*-Ps particles exist in a free-volume region. The increase in the size of void results in lower positron sensitivity, but higher Ps sensitivity in lower charge density region and hence it is suitable probe for the determination of free volume in polymers due to Ps localization in the free volume holes and amorphous region (Dai et al., 2003; Terlemezyan et al., 2008).

In PALS measurement, generally ^{22}Na radioactive source is used to generate positrons and ejects a 1.28 MeV photon, as a start signal and then the positron annihilates with an electron and 511 keV is emitted and this is stop signal. The time differences between start and stop signal equals to the annihilation lifetime of positrons and PALS measures this time differences (Yang Y, 2011).

1.14 Lifetime Analysis

The mean lifetime (τ), is the reciprocal of the annihilation rate (λ) of positrons and this lifetime is correlated with electron density around the molecule and hence the mean lifetime of positron can give information about free volume. The higher τ results in the higher free volume in material (Yang Y, 2011).

There are three lifetime components with mean lifetimes and intensities (I). These are:

para-Ps (**p-Ps**, channel 1), (τ_1 or τ_{p-Ps}) (*para-positronium lifetime*)

positrons which don't form Ps (e^+ , channel 2) (τ_2 or τ_{free}) (*free positron lifetime*)

ortho-Ps (**o-Ps**, channel 3) (τ_3 or τ_{o-Ps}) (*ortho positronium lifetime*)

τ_1, τ_2 and τ_3 values in polymeric materials are given below:

$$\tau_{p-ps} = \frac{1}{\frac{\eta}{\tau_{p-ps}^0} + \frac{1}{\tau_{po}}}, \tau_{p-ps}^0 = 125 \text{ ps}$$

$$\tau_{free} = \tau_p \approx 350 \text{ to } 500 \text{ ps}$$

$$\tau_{o-Ps} = \frac{1}{\frac{\eta}{\tau_{o-Ps}^0} + \frac{1}{\tau_{po}}} \approx 1 \text{ to } 4 \text{ ns}$$

$$I_{free} = 1 - (I_{p-Ps} + I_{o-Ps})$$

In polymers, **p-Ps** lifetime is not affected in polymer nature and it equals to 0.125 ns in vacuum, however, **o-Ps** lifetime is sensitive to the free volume and by using **o-Ps** lifetime, the free volume properties of polymers can be obtained. Ps is generally occurred in the lower electron density and if the electron density in polymer is higher, positrons are annihilated directly instead of positronium formation.

1.15 Lifetime Measurements in Polyethylene

Generally, three lifetime components are observed in polymers. Due to semi-crystalline properties of HDPE, four lifetime components can be deduced if a good statistic is possible (Suzuki et al., 1996).

With respect to PALS analysis, the lifetime spectrum of polyethylene is resolved into the three lifetime components. The shortest-lived component is the *para positronium* lifetime (τ_1) about 125 ps with the intensity, I_1 . An intermediate-lived component is the free positron lifetime (τ_2) about 650-800 ps with the intensity, I_2 and this is due to trapped positrons and/or trapped positronium. The longest-lived component is the *ortho-positronium* lifetime (τ_3) about 2.5 ns with the intensity, I_3 and this is owing to pick-off annihilation (Brusa et al., 1995). Furthermore, I_3 and τ_3 are correlated with the number of free volume and the size of free volume, respectively (Hsieh et al., 2000).

1.16 The Tao-Eldrup Model

The relation between the pick-off annihilation lifetime and free volume hole radius " R " was given Tao and calibrated by Eldrup et al. (Eldrup et al., 1981) later Nakanishi et al. (Nakanishi et al., 1990). Also, this relation is known as Tao-Eldrup model and given in equation (1). With respect to Tao-Eldrup model, Ps wave function occupies the ground state in the infinite potential and overlaps with bulk in the range between R and $R + \Delta R$ (Yang Y, 2011).

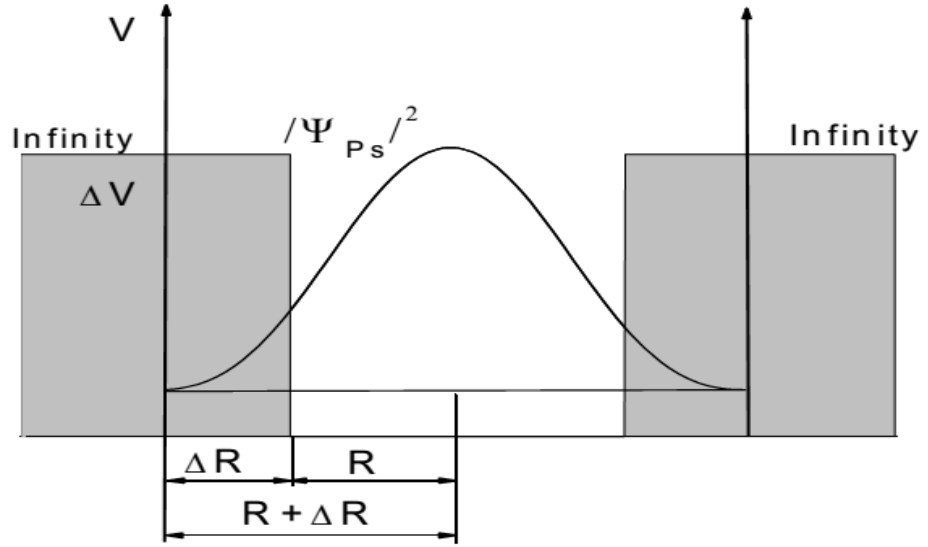


Figure 1.6. Tao-Eldrup model representation

$$\tau_3(ns) = \frac{1}{2} \left(1 - \frac{R}{R_0} + \frac{1}{2\pi} \sin \frac{2\pi R}{R_0} \right)^{-1} \quad (1)$$

where $R_0 = R + \delta R$ with $\delta R = 0.1656nm$ which is the thickness of the homogeneous electron layer that constitutes the wall of the hole and τ_3 is in nanoseconds, and R is in angstroms (Nakanishi et al., 1988).

By using calculated free volume hole radius in Equation (1), free volume is calculated in formula given below by assuming spherical free volume

$$V_f = \frac{4}{3} \pi R^3 \quad (2)$$

1.17 Factors Affecting Positronium Formation

Many factors affect the positronium formation. These are;

- ✓ Low temperature,
- ✓ Positron-source intensity,
- ✓ γ - irradiation (radiation effect),
- ✓ Positron mobility,
- ✓ Positron irradiation effect,
- ✓ The crystallinity of polymers,
- ✓ Formation of free radicals,
- ✓ Chemical functional groups,
- ✓ Polymer structures,
- ✓ Electron affinity,
- ✓ Inhibition effect of carbonyl groups

The effect of positron source on Ps formation has been investigated and it was revealed that positron source possesses a radiation effect upon different measuring times and this gives rise to the changes in lifetime results. I_3 decreases at higher measuring time and this decrease depends on polymer type. For illustrate, a large decrease in I_3 was observed for PP owing to free radicals formed by positron irradiation. It can be concluded that the effect of positron irradiation on positron formation can be correlated with the free radicals. According to some researches, I_3 and τ_3 decrease in the presence of the free radicals. However, the decrease in I_3 is related to not only the free radicals, but also structural changes (Suzuki et al., 1995).

Moreover, the influence of γ -irradiation on Ps formation has been researched and it is found that I_3 decreases in γ -irradiated polymers, which have higher crystallinity like HDPE. Because free radicals are formed upon γ - irradiation and these free radicals behave as an efficient electron scavengers, and hence causes to decrease in I_3 (Suzuki et al., 1995).

On the other hand, the effect of measurement time on *o*-Ps formation at low temperature and room temperature (RT) has been investigated and it was found that at low temperatures, especially lower than 150K, the increment in measurement time

led to the higher I_3 at semi-crystalline and amorphous polymers (Kindl et al., 1987; Reiter et al., 1990; Suzuki et al., 1996; Uedono et al., 1997; Wang CL et al., 1998). The increment in I_3 is due to trapped electrons, created by the positron radiation (Reiter and Kindle, 1990; Suzuki et al., 1996; Uedono et al., 1997). But, at room temperature, the higher measurement time for some polymers like polyethylene and polypropylene resulted in the lower I_3 . The decrement is because of γ -irradiation effect of positron source. Also, at room temperature, free radicals like alkyl and allyl radicals are observed and thus these free radicals catch the positrons, leading to lower I_3 (Hirade et al., 2001).

Ps formation in polypropylene was researched and it was found that chemical degradation in the amorphous phase of polypropylene may inhibit Ps formation and thus leads to decrease in I_3 (Badia et al., 1999).

The effect of carbonyl group on Ps formation was investigated and Ps formation decreased due to carbonyl groups and conjugated oxygen. Because these groups are electron scavenger and may restrict Ps formation leading to decrease in I_3 (Badia and Duplatre, 1999; Shantarovich et al., 2003). Moreover, different type of reactions occur at Ps formation in the presence of polar group and these reactions are given below (Qi CZ et al., 2000).

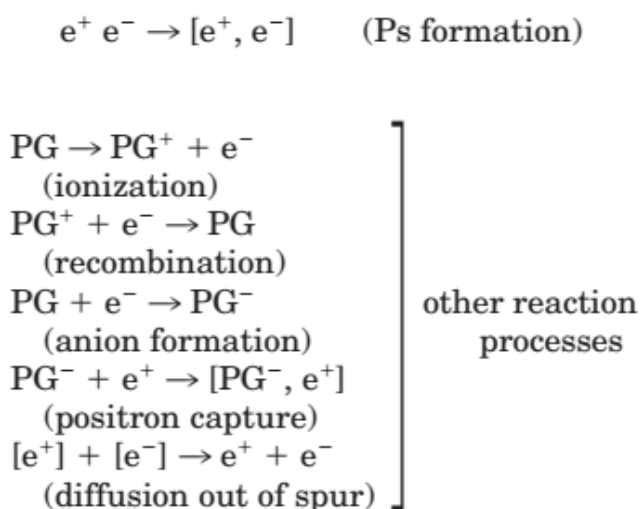


Figure 1.7. Possible reactions in Ps formation in the presence of polar groups (PG= Polar Groups)

1.18 PALS Literature Survey

In recent years, PALS has been used for the detection of free volume properties of different polymer, polymer blends and the free volume results of polymers have been explained below:

Nahid and counterparts studied the effect of trapped electrons on the positronium formation of high density polyethylene, which has 70-80% crystallinity below glass transition temperatures (20K, 40K, 60K, 80K, 120K, 150K and 200K). According to experimental results, I_3 at 20K was higher compared to I_3 at 200K and with increasing temperature, I_3 decreased. In addition, the variation in I_3 was studied at different irradiation times at this temperature range. By increasing irradiation time, higher I_3 was obtained owing to higher inter-track trapped electrons. It can be concluded that at lower temperatures, these trapped electrons are localized and they can react with positrons (Nahid et al., 2011).

Mostafa et al. investigated the free volume properties and glass transition temperature (T_g) of low density polyethylene (LDPE), which is 60% crystallinity and density is 0.94 g/cm³; high density polyethylene (HDPE), which is 87% crystallinity and density is 0.95 g/cm³; styrene butadiene rubber (SBR) and their blends, which are LDPE/SBR (50/50) and HDPE/SBR (50/50) via PALS in the temperature range between 100-300K. Free volume-hole distribution of neat LDPE, HDPE and their blends were investigated. According to experimental results, free volume size distribution of blends was between pure components. Pure SBR had larger free volume distribution than LDPE owing to three electrons in benzene rings, resulting in more spaces and increment in free volume. However, the free volume size distribution of HDPE was lower compared to LDPE because of higher crystallinity. Because the higher crystallinity of HDPE resulted in Ps inhibition leading to smaller free volume (Mostafa et al., 2009). Moreover, the variation in τ_3 was investigated at different temperature and T_g of blends and pure components were determined. For 50/50 LDPE/SBR and 50/50 HDPE/SBR blend and pure components, τ_3 increased between 100K and 300K owing to the thermal expansion of free volumes at higher temperatures. Also, T_g was determined from lifetime-temperature curves. At higher SBR content, T_g of LDPE and HDPE blends increased and one T_g was obtained for every blend. This refers that these blends are miscible. Below T_g , the side-chain

motion starts and the motion is on a single chain segment resulting in rotation of small parts of the molecules. Above T_g , the long chain segments and molecules are associated with the motion and hence rubbery matrix becomes and higher free volume obtains (Mostafa et al., 2009). *o-Ps* intensity, I_3 of pure polymers, their blends and the changes in I_3 were determined at different temperatures. Below T_g , with increasing temperature, *o-Ps* intensity, I_3 of LDPE, LDPE/SBR, HDPE, HDPE/SBR were increased owing to spur reaction model. With respect to this model, at lower temperature, electrons generated in polymers by γ - irradiation are localized in shallow traps. Above T_g , the higher temperature led to the lower I_3 due to disappearance of localized electrons. Also, trapping positron gave rise to decrease in intensity. Because, positrons forming Ps may be captured at these traps and I_3 decreases.

Hirade and Kumada investigated the effect of γ -irradiation on the positronium formation of high density polyethylene. According to their study, the higher irradiation dose led to the lower positronium intensity (Hirade and Kumada, 2001). It can be concluded that chemical changes such as a carbonyl group (Suzuki T et al., 1993) and free radicals (Suzuki et al., 1995) created by positron irradiation affect Ps formation (Mogensen, 1974).

Suzuki and counterparts investigated the influence of temperature and positron source intensities on the positronium formation of high density polyethylene, which has 59% crystallinity, determined from X-Ray analysis, and melting temperature is 407K. In order to investigate source effect, four different intensities (0.7 MBq, 1.1 MBq, 1.6 MBq and 3.7 MBq) of positron source were used to irradiate at 50K. In addition, γ -ray irradiation was applied at 50K and τ_3 , I_3 were determined between 50 and 300K for unirradiated PE. According to experimental results for unirradiated sample, at low temperatures near glass transition temperature, I_3 was higher than I_3 at 300K due to the trapping electrons and the decrease in molecular motion at low temperatures. Also, at higher temperatures than 150K, I_3 started to decrease because of local mode relaxation. As obtained from the experimental results, positronium formation is based on temperature. However, at higher temperatures, τ_3 increased. In addition, with increasing positron source intensity, τ_3 , *o-Ps* lifetime of unirradiated PE increased and it can be concluded that

with increasing irradiation doses, trapped electrons increased and maximum trapped electrons were obtained at 3.7 MBq. When PE was irradiated with different γ -ray irradiation, *o*-Ps intensity and lifetime changed with irradiation. For unirradiated, 1 MGy and 2 MGy irradiated samples, *o*-Ps lifetime and intensity were investigated and it was found that at higher irradiation dose, *o*-Ps lifetime and intensity of unirradiated sample was higher compared to irradiated samples. It can be concluded that upon irradiation, radicals are formed and eliminate trapped electrons and thus leads to the decrease in lifetime and intensity (Suzuki et al., 2000).

Badia and Duplatre studied the effect of gamma irradiation and electron beam on *o*-Ps intensity I_3 and lifetime τ_3 of high density polyethylene via PALS. Experimentally, the lifetime spectra were analyzed into four lifetime components and the variations in crystalline and amorphous parts were determined. In order to determine these changes, 80 kGy.s⁻¹ electron irradiation and 26x10⁻³ kGy.s⁻¹ gamma irradiation were used and carried out at 291K, for fluences up to 300 kGy. No changes were observed in lifetimes. However, I_3 decreased rapidly with fluence, up to 8 kGy and later remained constant up to 300 kGy. In addition, I_4 decreased up to about 5 kGy. It can be concluded that, cross-linking formed in amorphous or crystalline phases and caused to decrease in I_3 and I_4 and hence, Ps formation decreased. Moreover, the free volume radiuses of crystalline and amorphous phase were determined and founded as 0.182 nm for crystalline phase, 0.333 nm for amorphous phase (Badia and Duplatre, 1999).

Hirade and counterparts applied Co-60 γ -radiation for high density polyethylene and amorphous poly(methyl methacrylate) and investigated the changes at I_3 at lower temperatures. As a result, trapped electrons increased the formation of Ps at lower temperatures. Because molecular motions were restricted at lower temperatures and irradiation gave rise to increase the trapped electrons, thus I_3 increased and the increase in *o*-Ps intensity of poly(methyl methacrylate) were higher than polyethylene. It was concluded that the positrons in amorphous polymers diffused easier compared to positrons in crystalline polymers due to regular shape of crystalline polymers. Thus, especially at low temperature, positrons had higher localization probability in amorphous polymers (Hirade et al., 2000).

Brusa and his counterparts studied the positron mobility of polyethylene between 60K and 400K. All lifetime spectra were analyzed into three lifetime components. I_1 and I_3 changed by applying an electric field, while I_1 , I_3 and τ_3 changed with the sample temperature (Brusa et al., 1995). It can be concluded that free volume changed due to semi-crystalline nature of polyethylene and the internal structure was dominant in the crystalline segments, whereas, lamellar crystals were dominant in the folded chains and disordered amorphous regions and defects in the crystalline region led to higher free volume.

Suzuki et al. researched the radiation effect on positronium formation in different types of polyethylene (Tekmilon, 90% crystallinity; HDPE, 64% crystallinity; LDPE, 34% crystallinity) and polypropylene (58% crystallinity). The samples were irradiated with γ -ray at room temperature and the variation in positronium formation with the elapsed time was examined for pristine HDPE, 1 MGy γ -irradiated PE and annealed of this sample. With regard to results, *o-Ps* intensity, I_3 of 1 MGy γ -irradiated PE was lower than pristine HDPE because of the effect of free radicals on positronium formation in irradiated sample, whereas annealed sample had higher *o-Ps* intensity, I_3 than pristine. Because free radicals were eliminated and the crystallinity of annealed sample was lower than pristine and increased the amount of the amorphous part, which has more trapping sites of electrons. In addition, the effect of irradiation time and irradiation dose on *o-Ps* formation was investigated for polypropylene. According to results, at same irradiation time, *o-Ps* intensity of irradiated polypropylene was lower than non-irradiated polypropylene owing to free radicals, which are electron scavengers and act as the inhibitor of Ps formation (Suzuki et al., 2001).

Kobayashi et al. investigated the effect of electric field on the lifetime parameters of gamma irradiated and unirradiated polypropylene and polyethylene via positron annihilation lifetime spectroscopy. Two different polyethylene (low density polyethylene (LDPE), which is 34% crystallinity and high density polyethylene (HDPE), which is 66% crystallinity) and two different polypropylene (normal polypropylene (PP-N), which is 55% crystallinity and polypropylene high crystallinity (PP-HC), which is 66% crystallinity) were used and irradiation dose changed from 0.13 kGy to 1300 kGy and electric field was between 0 and 48 kV/cm.

With respect to experimental results, I_3 of both irradiated PP and irradiated PE decreased at higher irradiation dose. At low irradiation dose, I_3 values decreased sharply due to spur reaction model and polypropylene was more sensitive to irradiation compared to polyethylene due to reaction between positrons and trapped electrons. Also, the decrease in I_3 was owing to free radicals formed during irradiation. It can be revealed that, the reduction in *o-Ps* intensity was attributed to not only free radicals, but also polymer structure and free volume (Duplatre et al., 1990). In addition, the intensities, I_3 of these irradiated samples and unirradiated samples were decreased at higher electric field. It was found that the decrease in unirradiated samples was higher compared to irradiated ones (Kobayashi Y. et al., 1997).

Suzuki and counterparts researched the positron irradiation effect on polypropylenes, which are isotactic polypropylene (55% crystallinity, PPN) and polypropylene with high crystallinity (66% crystallinity, PPHC) also polyethylenes which are ultra high molecular weight polyethylene (54% crystallinity, UHMWPE), low density polyethylene (34% crystallinity, LDPE) and high density polyethylene (66% crystallinity, HDPE) via PALS. Positron irradiation effect was examined in vacuum and air at 300K, also γ - irradiation effect was investigated. According to experimental results, with increasing positron irradiation time, the decrease in I_3 increased and the decrease in I_3 in polypropylene samples were higher compared to polyethylene. But, *o-Ps* lifetime didn't change so much and it can be concluded that the hole sizes remain were constant (Suzuki et al., 1995). Four lifetime components for polypropylene were determined and *o-Ps* intensity in amorphous and crystalline region were investigated. According to experimental results, τ_3 and τ_4 were constant, but the decrease in I_4 was higher than I_3 . The decrease in I_3 was due to the increment in free radicals in the crystalline region. From the experimental results, positron irradiation affected *o-Ps* intensity, formed in amorphous region and main chain scissions may create methyl groups, by inhibiting Ps formation. On the other hand, the decrease in I_3 of polyethylene was lower than polypropylene because different radiation effect was observed in polyethylene and polypropylene, resulting in changes in I_3 . Also, the higher decrease in *o-Ps* intensity of polypropylene was due to methyl groups created by scission and hence results in the thermal activation and Ps inhibition (Levay et al., 1989; P, 1990; Suzuki T et al., 1993; Zhang Z et al.,

1991). Moreover, the difference in *o*-Ps intensity in vacuo and air irradiation may be due to carbonyl group effect and radiation-induced oxidation. In addition, γ -irradiation affected the *o*-Ps intensity, I_3 of polypropylene and polyethylene (Suzuki T et al., 1993).

Hsieh et al. researched the rheology, free volume and miscibility properties of thermotropic liquid crystalline polyester/polycarbonate blends by using PALS. In their study, *Vectra A950*, a thermotropic liquid crystalline polymer (TLCP) was blended with polycarbonate (PC). I_3 , τ_3 and the free volume of pure PC, pure *Vectra A950* and blends including different contents of *Vectra A950* (10, 20, 30, 50, 75%) were evaluated. According to analysis, *Vectra A950* was lower free volume in comparison to PC owing to the limited flexibility of TLCP molecules, greater chain rigidity and slit-like free volume in TLCPs instead of spherical. In addition, by increasing *Vectra A950* content, I_3 , τ_3 and free volume of blends decreased. The increase in *Vectra A950* content gave rise to positive deviation in *o*-Ps intensity, I_3 and this means until 30% *Vectra A* content, blend is immiscible, while at 50% and greater than this *Vectra A950* content, negative deviation was observed in *o*-Ps intensity, I_3 and this means that these blends are partially miscible. It can be concluded that positive deviation in I_3 was observed in immiscible blends and resulted in free volume cavities (larger τ_3) and create new cavities were formed between different phases owing to the repulsion of different molecular chains. However, a negative deviation was observed in miscible TP/TP blends and leads to lower free volume owing to intermolecular interactions (Hsieh et al., 2000). Moreover, the free volume density and the free volume fraction of blends as a function of *Vectra A950* content and pure components were investigated. The increment in *Vectra A950* content caused to increase in the free volume density, whereas it caused to decrease in the free volume fraction.

According to some papers, τ_3 shortens and I_3 reduces owing to the free radicals. However, the effect of γ ray irradiation on I_3 and τ_3 cannot be associated with not only free radicals but also the structural changes (Suzuki et al., 1995). Suzuki investigated the effect of γ ray irradiation on I_3 and τ_3 , at 373K. According to the study, the radical concentration reduced at 373K, but, I_3 didn't change. Therefore, this indicates that non-correlation between the radical concentration and I_3

at this temperature (Suzuki T et al., 1992). Upon γ irradiation, various factors affect Ps formation such as crystallinity, cross-linking, carbonyl groups and free radicals (Kobayashi Y. et al., 1997; Suzuki et al., 2001).



2. AIM AND SCOPE OF THE STUDY

The objective of this study is to graft copolymerize the monomer p-benzophenoneoxycarbonylphenyl methacrylate onto both high density polyethylene and isotactic polypropylene and the monomer p-benzophenoneoxycarbonylphenyl acrylate onto isotactic polypropylene. The homopolymers of the monomers were reported to exhibit mesomorphic behavior. That is, the macromolecules exist as associated in an ordered fashion with a high state of orientation at molecular level. By the presumed mesomorphic properties of the polymers, the improvements in the properties of high density polyethylene and isotactic polypropylene were mainly aimed by the graft copolymerizations. It was also intended to improve processability of the materials with a better dispersion of the reinforcing liquid crystalline polymer phase in the grafted products. It was planned to investigate the effect of the graft copolymerizations on the thermal, mechanical, morphological and microstructural behavior of the materials. It was also planned to unfold and to clarify the effect of microstructural behavior, that is, free volume characteristics on the properties especially mechanical behaviors of the products.

3. MATERIALS AND METHODS

3.1 Chemicals and Materials Used

3.1.1 Solvents and Reagents

Dimethyl formamide, dimethyl sulfoxide, acetone, dioxane, methanol and xylene (Merck A.G.) and ethanol (technical grade) were used without any purification.

Acryloyl chloride, p-hydroxybenzoic acid and thionyl chloride (Merck A.G.), methacryloyl chloride and 4-hydroxybenzophenone (Alfa Aesar A.G.) were the main chemicals for the preparation of the monomers, p-benzophenoneoxycarbonylphenyl acrylate and p-benzophenoneoxycarbonylphenyl methacrylate and used without any purification. Dicumyl peroxide (DCP) (Merck A.G.), the initiator used in the polymerizations was received.

3.1.2 Preparation of Powder High Density Polyethylene and Isotactic Polypropylene

High density polyethylene (HDPE), coded as S 0464 and isotactic polypropylene (IPP), coded as MH 418 were supplied by Turkish Petrochemical Industry (PETKIM).

The polymer (HDPE or IPP) granules were dissolved in boiling xylene (138-139°C) and precipitated by adding ethanol. The precipitates were collected by filtering, dried at 40°C in vacuum and ground by cooling in liquid nitrogen. The obtained HDPE and IPP powders were used in the graft copolymerization experiments.

3.2 Synthesis of the Monomers

3.2.1 Synthesis of p-Benzophenoneoxycarbonylphenyl Acrylate

3.2.1.1 Preparation of p-Acryloyloxybenzoic Acid

p-Acryloyloxybenzoic acid, ABA used in the synthesis of the monomer, p-benzophenoneoxycarbonylphenyl acrylate was prepared by condensation reaction of acryloyl chloride with p-hydroxybenzoic acid in alkaline medium, Figure 3.1, as described by Soykan U (Soykan, 2013). In a typical procedure, 34.5 g (0.25 mol) p-hydroxybenzoic acid was dissolved in a solution of 20 g (0.5 mol) NaOH in 250 mL of distilled water in a flask equipped with a magnetic stirrer. After cooling the solution to 0-5°C in an ice bath, 21.5 mL (0.25 mol) of acryloyl chloride was added dropwise by stirring simultaneously. The stirring was continued at 0-5°C for 1 h and then at room temperature for another 1 h. The product, ABA was precipitated by adding diluted and cooled HCl solution, filtered and washed with water. The obtained ABA was then purified by repeated recrystallizations from acetone. The yield was 75%, in good agreement with the literature (Soykan, 2013).

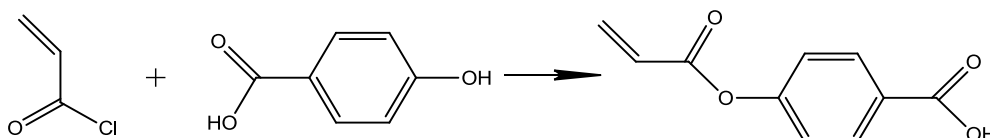


Figure 3.1. The reaction of acryloyl chloride with HBA to produce ABA

3.2.1.2 Preparation of p-Acryloyloxybenzoyl Chloride

p-Acryloyloxybenzoyl chloride, ABC was prepared by refluxing ABA, synthesized previously, in thionyl chloride in the presence of trace amount of dimethyl formamide as described by Soykan U (Soykan, 2013), Figure 3.2. Typically, 50.0 g of ABA was refluxed with 500 mL of thionyl chloride containing a few drops of dimethylformamide for 8 hours. The excess thionyl chloride was removed by vacuum distillation. The product was purified by repeated recrystallizations from dichloromethane by lowering the solubility with the addition of hexane until turbidity. The yield was 98 wt%.

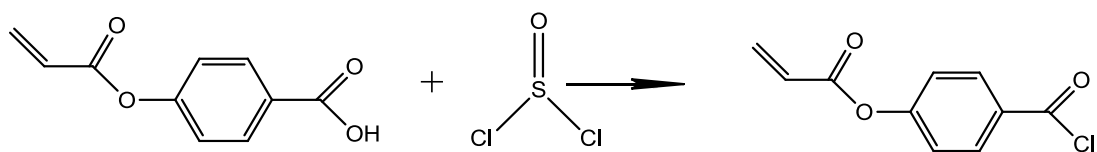


Figure 3.2. Synthesis reaction of p-acryloyloxybenzoyl chloride (ABC)

3.2.1.3 Synthesis of p-Benzophenoneoxycarbonylphenyl Acrylate

The monomer p-benzophenoneoxycarbonylphenyl acrylate, BPOCPA was synthesized by condensation reaction of p-acryloyloxybenzoyl chloride with p-hydroxybenzophenone in the presence of pyridine, Figure 3.3. Typically, 24.4 g ABC (0.116 mol) and 23.0 g (0.116 mol) HBP were dissolved in 250 mL of xylene. The solution was stirred about 30 minutes at room temperature, and a pale yellow mixture was obtained. 9.4 mL (0.116 mol) of pyridine was added to the mixture in a slow manner, one mL per hour, by stirring simultaneously. The stirring was continued about 72 hours at room temperature. In order to separate dark brown residue formed during the reaction from the white product (the monomer), the mixture was heated, and the resulted solution was separated from the residue by decantation. The product, BPOCPA was obtained by cooling the solution, and purified by repeated recrystallizations from xylene. The yield was 60%.

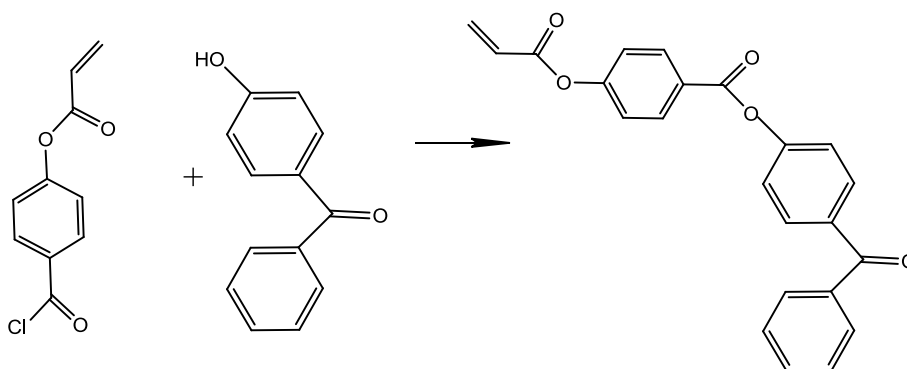


Figure 3.3. Synthesis reaction of benzophenoneoxycarbonylphenyl acrylate

3.2.2 Synthesis of p-Benzophenoneoxycarbonylphenyl Methacrylate

3.2.2.1 Preparation of p-Methacryloyloxybenzoic Acid

p-Methacryloyloxybenzoic acid, MBA required in the synthesis of p-benzophenoneoxycarbonylphenyl methacrylate was prepared by condensation reaction of methacryloyl chloride with p-hydroxybenzoic acid in alkaline medium as in the preparation of ABA with the same procedure and the same amounts, Figure 3.4.

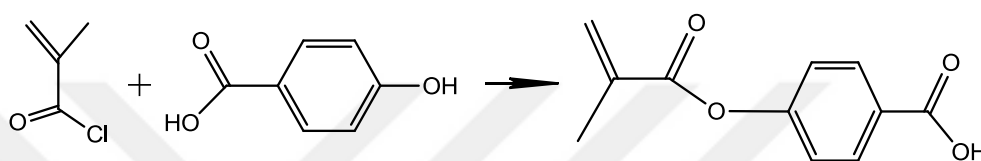


Figure 3.4. The reaction of methacryloyl chloride with HBA to produce MBA

3.2.2.2 Preparation of p-Methacryloyloxybenzoyl Chloride

p-Methacryloyloxybenzoyl chloride, MBC was prepared by refluxing MBA, formerly prepared, in thionyl chloride in the presence of trace amount of dimethyl formamide as was carried out in the preparation of ABC, Figure 3.5.

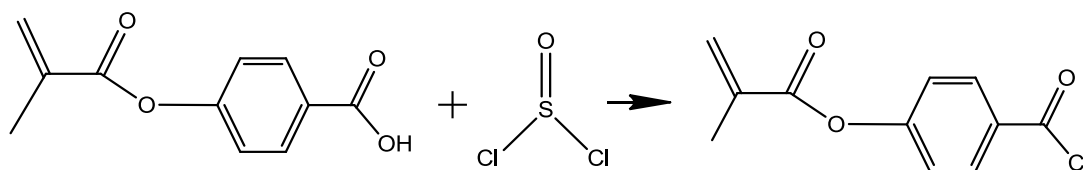


Figure 3.5. Synthesis reaction of p-methacryloyloxybenzoyl chloride

3.2.2.3 Synthesis of p-Benzophenoneoxycarbonylphenyl Methacrylate

The monomer p-benzophenoneoxycarbonylphenyl methacrylate, BPOCPMA was synthesized by condensation reaction of MBC with p-hydroxybenzophenone by stirring the equimolar solution of the reactants in xylene containing pyridine for 3-4 days, Figure 3.6. The product, BPOCPMA was purified by repeated recrystallizations from xylene. The yield was 57%.

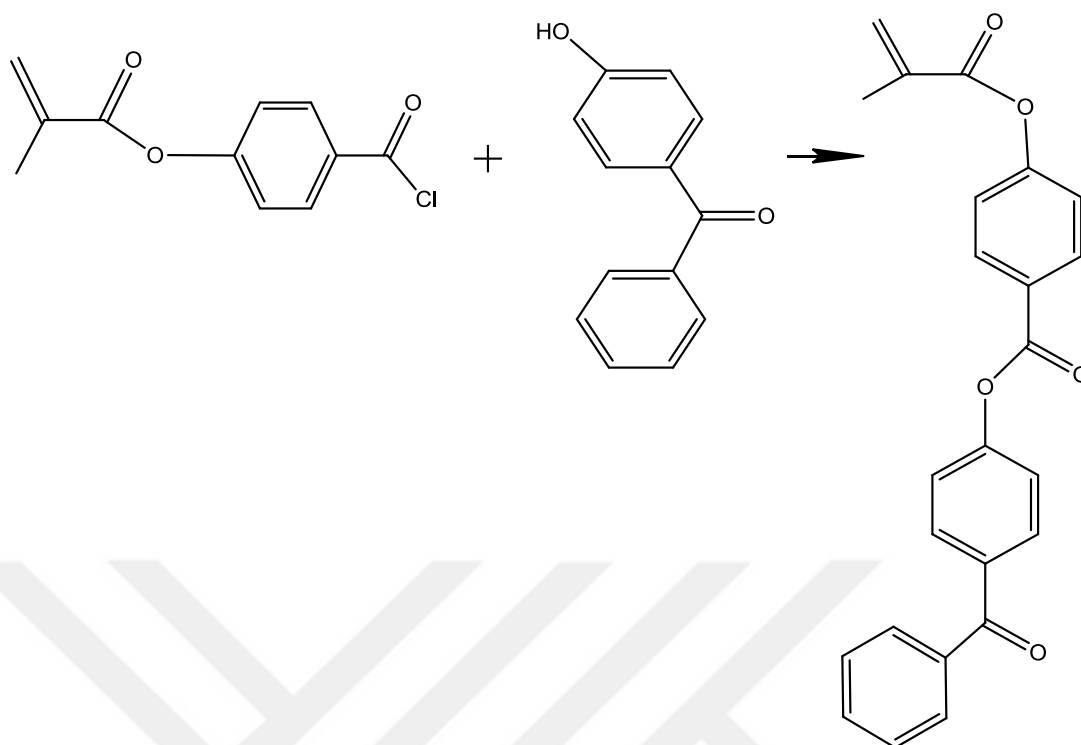


Figure 3.6. Synthesis reaction of p-benzophenoneoxycarbonylphenyl methacrylate

3.3 Polymerization of the Monomers

Both the monomers, BPOCPA and BPOCPMA were polymerized by bulk melt polymerization. Mixture of monomer (BPOCPA or BPOCPMA) and dicumyl peroxide (3% with respect to weight of monomer) was heated to 140°C in vacuum keeping the temperature constant for 1 h. The product (poly(BPOCPA) or poly(BPOCPMA)) was washed with acetone and then DMSO to remove residual monomer and byproducts formed during the polymerization, and dried at 40°C in vacuum. Yield was about 95% in both polymerizations.

3.4 Graft Copolymerization of the Monomers

The graft copolymerization of BPOCPMA onto HDPE and of both monomers BPOCPA and BPOCPMA onto IPP were carried out by means of bulk polymerization method. Typically, the polymer in powder form (HDPE or IPP), the monomer (BPOCPA or BPOCPMA) and the initiator DCP were mixed in desired

ratios in a mortar with extensive hand grinding, and the mixture then was transformed into reaction tube. The tube was evacuated, sealed and heated up to desired temperature keeping the temperature constant for a certain period of reaction time. At the end of the reaction time, the tube was cooled at room temperature and crack-opened. The product was washed firstly with acetone to remove monomer residual and then with DMSO to remove low molecular weight products and byproducts formed during the polymerization. Finally, the grafted polymer was rewashed with acetone several times to ensure the removal of DMSO, and dried at 40°C in vacuum. The obtained product, named as coproduct, was consist of the polymer with grafted units and the homopolymer molecules since the homopolymer molecules, poly(BPOCPA) and poly(BPOCPMA), forming during the reaction but not grafted onto the matrix polymer were not soluble in DMSO. Moreover, to remove the homopolymer molecules from the products and thus to obtain the products, named as copolymers, and also to determine the extent of grafting, some products were also washed with hot DMF, since the homopolymer molecules were soluble in hot DMF.

3.5 Characterizations and Instruments

3.5.1 Fourier Transform Infrared Spectroscopy (FTIR)

The intermediate products in the synthesis of the monomers BPOCPA and BPOCPMA, the polymers HDPE, IPP, poly(BPOCPA) and poly(BPOCPMA) and the graft products were characterized by using a Shimadzu 8400 S FTIR spectrophotometer. FTIR spectra of the samples, from 4000 to 400 cm^{-1} , were obtained from KBr pellets prepared with approximately 2 mg sample and 100 mg spectroscopic grade KBr.

3.5.2 Nuclear Magnetic Resonance (NMR) Analysis

ABA, MBA, BPOCPA and BPOCPMA were also characterized by using a Bruker-Spectrospin Avance DPX 400 Ultra-shield ^1H -NMR spectrometer with a frequency of 400 MHz in dimethyl sulfoxide- d_6 . Tetramethylsilane (TMS) was used as an internal reference.

3.5.3 Differential Scanning Calorimetry Analysis

Shimadzu DSC 60 Differential Scanning Calorimeter was used for DSC analysis of the intermediate products, the monomers and of the graft products. The analyses of the samples varying between 2-5 mg were carried out under N₂ atmosphere with a heating rate of 10°/min. Crystalline melting temperatures (T_m) and heat of fusion values (ΔH_m) were determined from the obtained thermograms.

3.5.4 X-Ray Diffraction (XRD)

Microstructural properties of the products were investigated by a Rigaku Multiflex X-ray diffractometer. The X-Ray data were collected with the Cu-K_α radiation (λ=1.54 Å for Cu). The XRD patterns were obtained from 10° to 60° for HDPE and from 10° to 40° for IPP. The patterns were collected with the step size of 0.02° in air at room temperature.

3.5.5 Tensile and Impact Properties

Tensile properties of HDPE, IPP and of the graft products were determined by a LLYOD LR5K Mechanical Tester with the speed of elongation, 50 mm/min at room temperature. The test samples with a gauge dimension of 50 mm (length) x 7.6 mm (width) x 2 mm (thickness) were prepared by micro-injection moulding with Daga Instruments Microinjector at 220°C with 8 bar injecting pressure. The tensile strengths and moduli were directly obtained from the stress-strain curves by the provided software of the instrument. Minimum four samples were tested for each composition.

The impact behavior of the test samples were studied by Coesfeld Material Test Pendulum Impact Tester at room temperature. The test samples were prepared as were for tensile tests but with thickness of 1 mm and width of 7 mm. The test results were given as an average of at least four samples for each composition.

3.5.6 Fracture Surface Analysis (SEM)

The morphological observations of fractured surfaces were conducted with JEOL 6390-LV Scanning Electron Microscope at 20 kV and 3 nm resolution power. To improve the conductivity, all samples were gold coated before the analysis.

3.5.7 Positron Annihilation Lifetime Spectroscopy (PALS)

Free volume properties of virgin HDPE, the copolymers and the coproducts involving HDPE were studied by using PALS technique. For this purpose, fast-fast conventional coincidence system has been employed measuring the elapsed time between the β^+ emission of ^{22}Na source, characterized by a 1.274 MeV photon as a birth signal of positron, and the annihilation gamma emission of 0.511 MeV as a dead signal.

The ^{22}Na source was prepared by depositing and evaporating about 20 μCi of $^{22}\text{NaCl}$ aqueous sandwiched between two pieces of sample with 0.5x0.5 cm² and 1 mm thickness. All lifetime spectra were resolved with the RESOLUTION (Kirkegaard et al., 1981) and PATHFIT (Kirkegaard et al., 1981) programs to determine lifetimes and intensities with the system resolution. A resolution of the system was about 528 ps (FWHM) and 5 million counts were collected in each lifetime spectrum and output files of all products were given in Appendices. The measurements were carried out at room temperature.

The lifetimes of positrons for virgin HDPE, the copolymers and the coproducts were measured and all lifetime spectra were analyzed into three lifetime components. The shortest-lived component, τ_1 with an intensity I_1 , associated with the annihilation of *para-positronium* (*p-Ps*), the intermediate-lived component, τ_2 with an intensity I_2 , attributed to the direct annihilation of positrons, and the longest-lived component as *ortho-positronium* (*o-Ps*), τ_3 with an intensity I_3 , associated with pick off annihilation, were obtained from the lifetime spectra. These analyzed parameters were calculated using τ_1 fixed at 125 ps, assumed as independent of free volume.

4. RESULTS AND DISCUSSIONS

4.1 Characterizations of IPP, HDPE, BPOCPA, BPOCPMA

4.1.1 FTIR and DSC Characterization of IPP

FTIR spectrum of isotactic polypropylene (IPP) was given in Figure 4.1. The spectrum indicated the absorption bands of stretching vibrations of CH₃ group at 2953 and 2870 cm⁻¹ and those of CH₂ group at 2922 and 2839 cm⁻¹. The absorption bands due to bending vibrations of the groups were observed at 1377 and 1460 cm⁻¹, respectively.

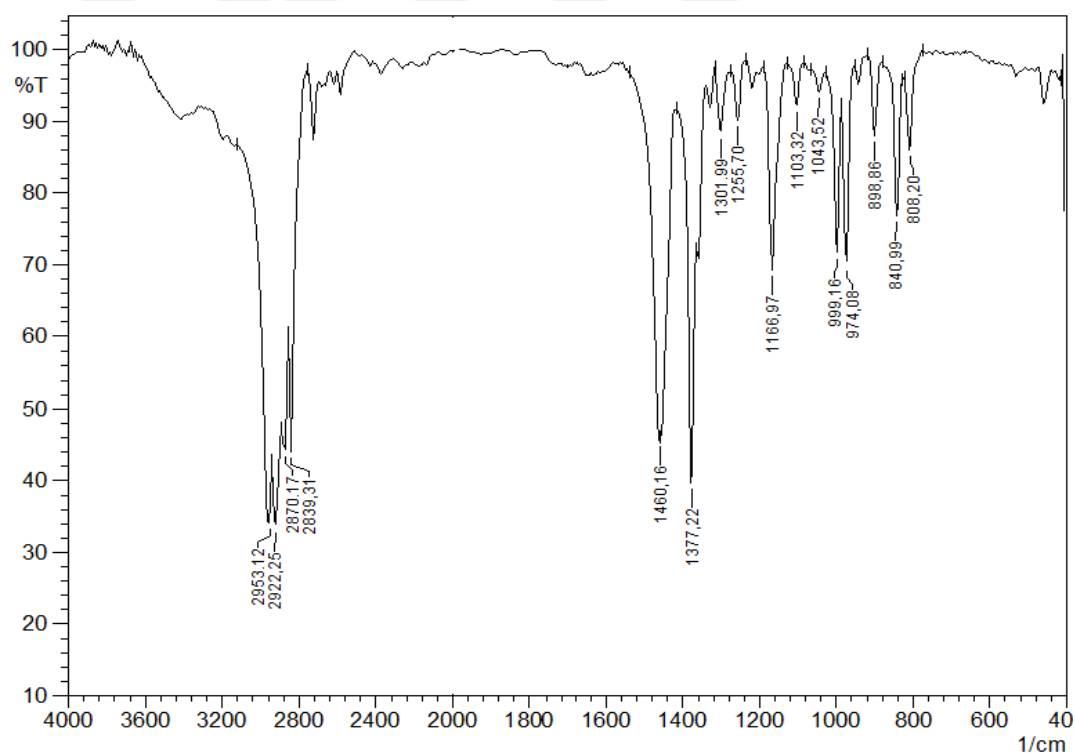


Figure 4.1. FTIR spectrum of IPP

The crystalline melting temperature of IPP was 164.06°C on record by DSC with heating rate of 10°C/min in nitrogen atmosphere, Figure 4.2.

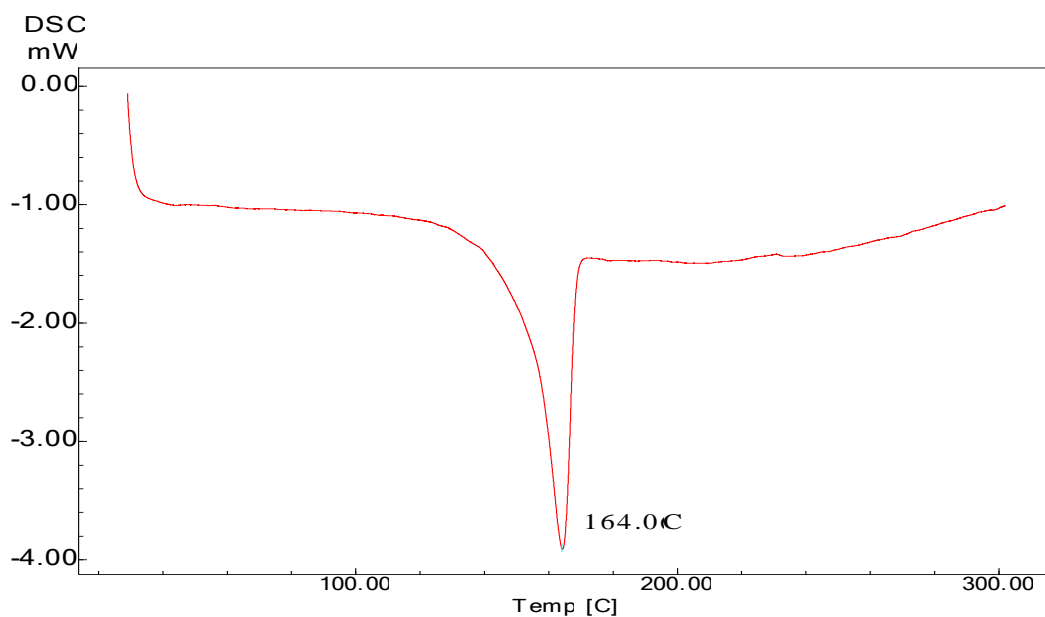


Figure 4.2. DSC thermogram of IPP

4.1.2 FTIR and DSC Characterization of HDPE

FTIR spectrum of high density polyethylene (HDPE), Figure 4.3, indicated the absorption bands of stretching vibrations of CH₂ group at 2918 and 2848 cm⁻¹, and the bands at 1558 and 1469 cm⁻¹ due to the bending vibrations of the group. The band observed at 721 cm⁻¹ was assigned to C-C bending vibrations.

The crystalline melting temperature of HDPE was found 130.22°C by DSC with heating rate of 10°C/min in N₂ atmosphere, Figure 4.4.

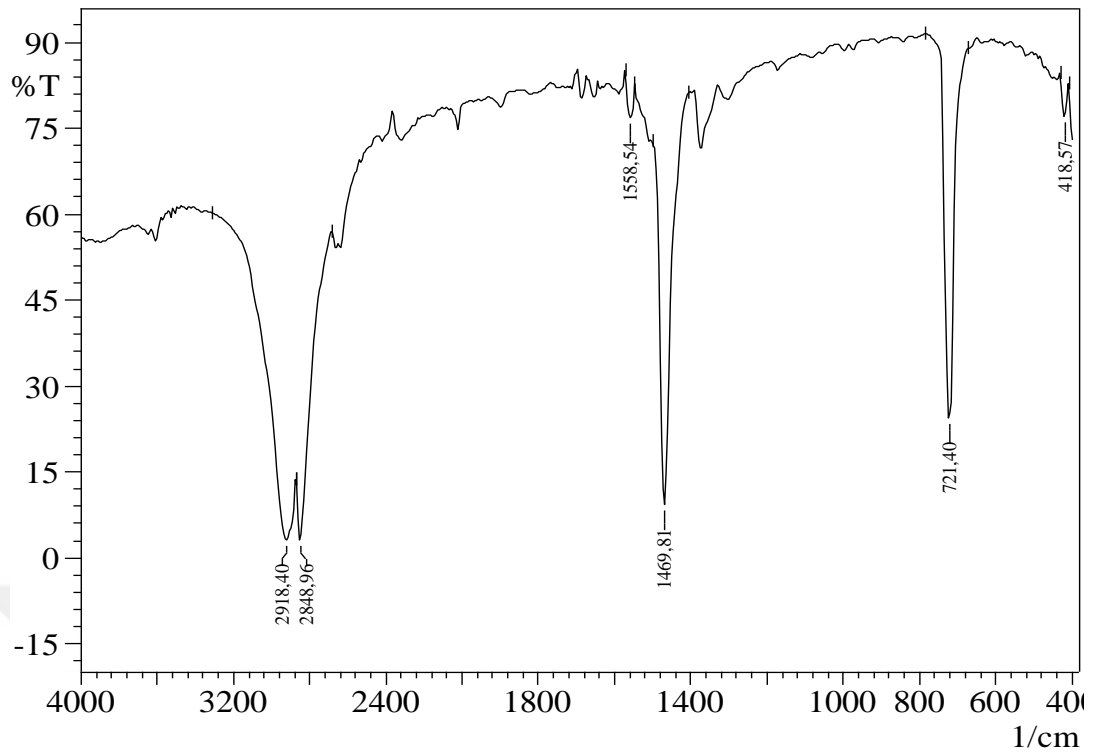


Figure 4.3. FTIR spectrum of HDPE

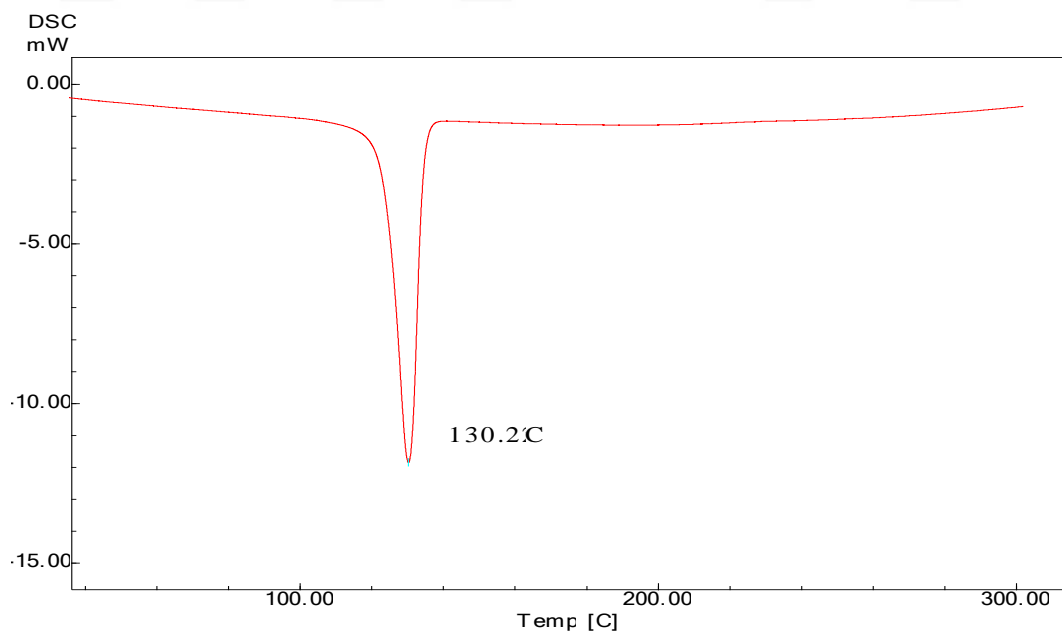


Figure 4.4. DSC thermogram of HDPE

4.1.3 FTIR, ¹H-NMR and DSC Characterization of BPOCPA

FTIR spectrum of BPOCPA, Figure 4.5, indicated C=O stretching vibrations of ester groups at 1741 and 1734 cm⁻¹. The strong band at 1649 cm⁻¹ was assigned to C=O stretching vibration of the benzophenone group. The aromatic C=C stretching vibrations were observed at 1599 and 1504 cm⁻¹. The strong bands at 1205 and 1276 cm⁻¹ were assigned to ester C-O-C stretching vibrations. The bands between 1000 and 1200 cm⁻¹ were attributed to monosubstituted aromatic C-H bending vibrations. The bands between 974 and 927 cm⁻¹ are corresponding to vinylic C-H out-of-plane bending vibrations.

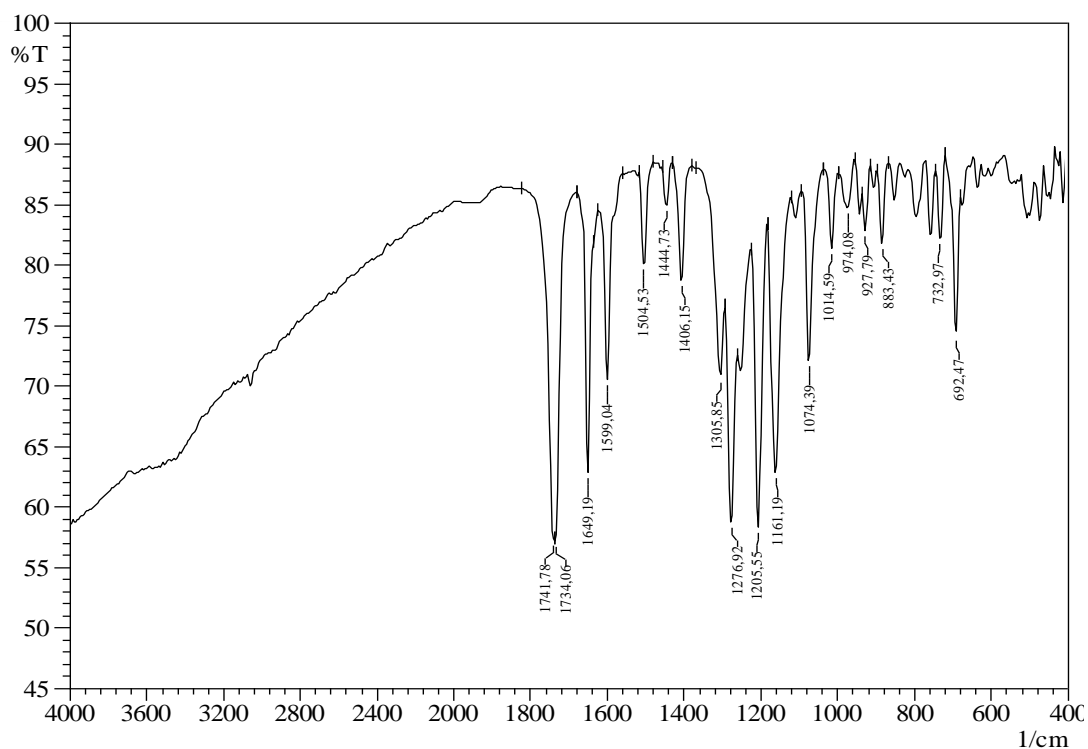
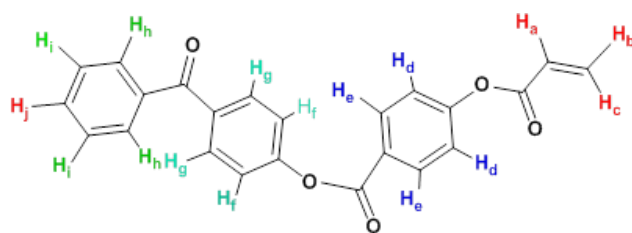


Figure 4.5. FTIR spectrum of BPOCPA

The schematic representation of BPOCPA was given in scheme 1 with proton assignments, and ¹H-NMR spectrum of the molecule was presented in Figure 4.6. The spectrum indicated a doublet at δ 6.1 and a quartet at δ 6.45 corresponding to H_b and H_a protons of the vinylic group. The doublet observed at δ 6.6 is due to H_a-H_c trans coupling of the group. The doublets at δ 7.45, 7.50, 7.76, 7.86 and 8.21 are corresponding to H_d, H_f, H_e, H_g, H_h protons and are due to single O-coupling of the C₆H₄-groups. The triplets at δ 7.57 and 7.68 are assigned to H_j and H_i protons.



Scheme 1. Schematic representation of BPOCPA with proton assignments

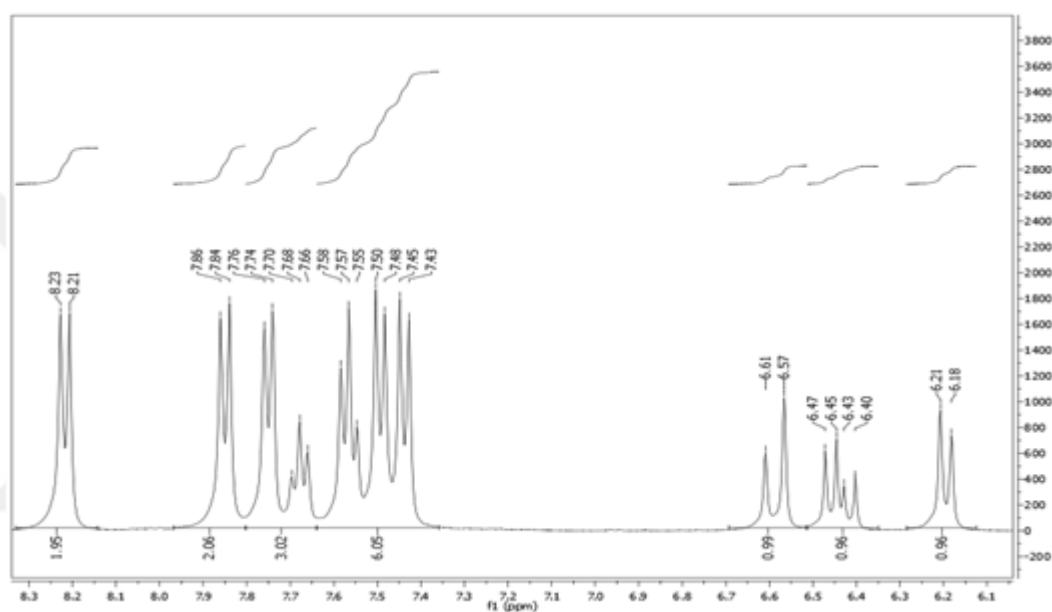


Figure 4.6. H-NMR spectrum of BPOCPA

Melting temperature of BPOCPA was 130.56°C, determined by DSC with heating rate of 10°C/min in N₂ atmosphere, Figure 4.7.

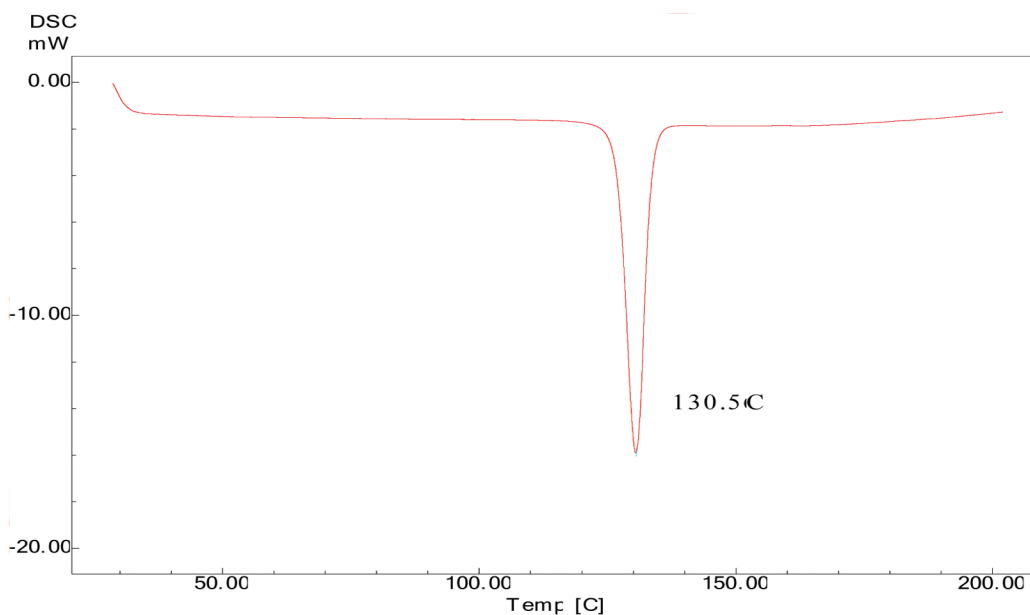


Figure 4.7. DSC thermogram of BPOCPA

4.1.4 DSC and FTIR Characterization of poly(BPOCPA)

FTIR spectrum of homopolymer poly(BPOCPA), Figure 4.8, showed an absorption band at 1741 cm^{-1} corresponding to C=O stretching vibrations of the ester groups. The strong band at 1653 cm^{-1} was due to C=O stretching vibrations of the benzophenone group. Aromatic C=C stretching vibrations were observed at 1502 and 1597 cm^{-1} . The strong bands at 1197 and 1271 cm^{-1} were due to esteric C-O-C stretching vibrations. The bands seen between 1000 and 1200 cm^{-1} were attributed to monosubstituted aromatic C-H bending vibrations. Some of the bands attributed to vinylic C-H out-of-plane bending vibrations disappeared in the spectrum of poly(BPOCPA). This result confirmed the polymerization of BPOCPA through the vinylic group.

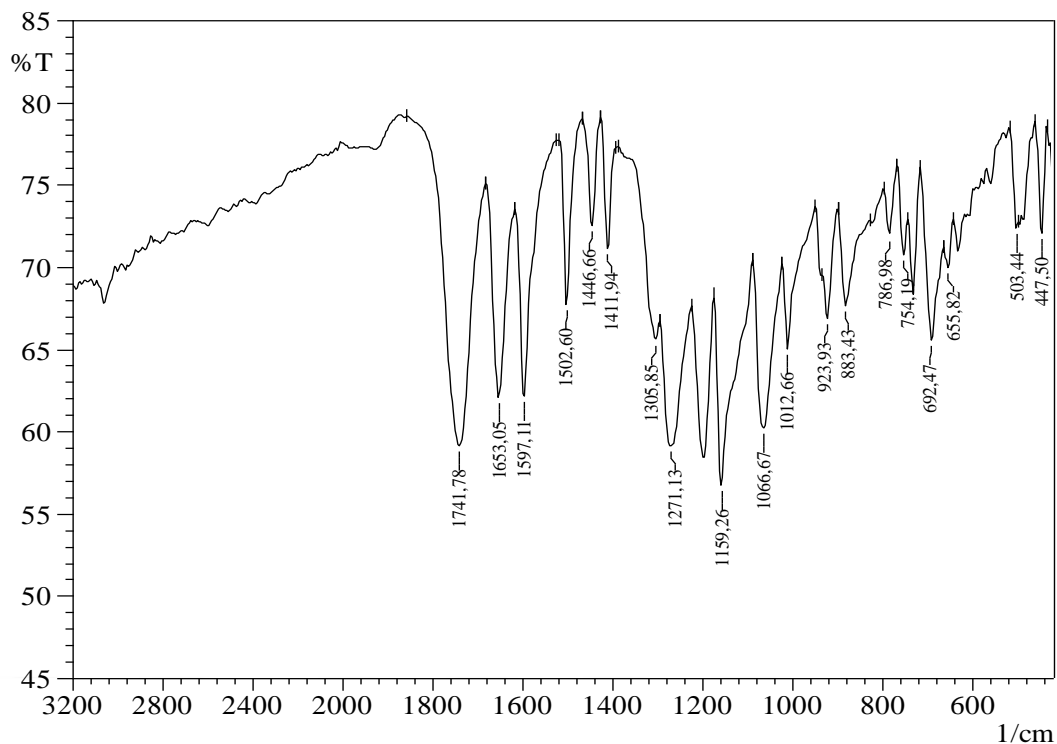


Figure 4.8. FTIR spectrum of poly(BPOCPA)

DSC analysis carried out with a heating rate of 10°C/min in N₂ atmosphere exhibited two endotherms, at 198.58°C and 231.08°C, Figure 4.9. The former may be attributed to liquid crystal-isotropization, in relation to the study reported by Sainath et al. (Sainath et al., 2000). The latter was assigned to melting of crystalline domains.

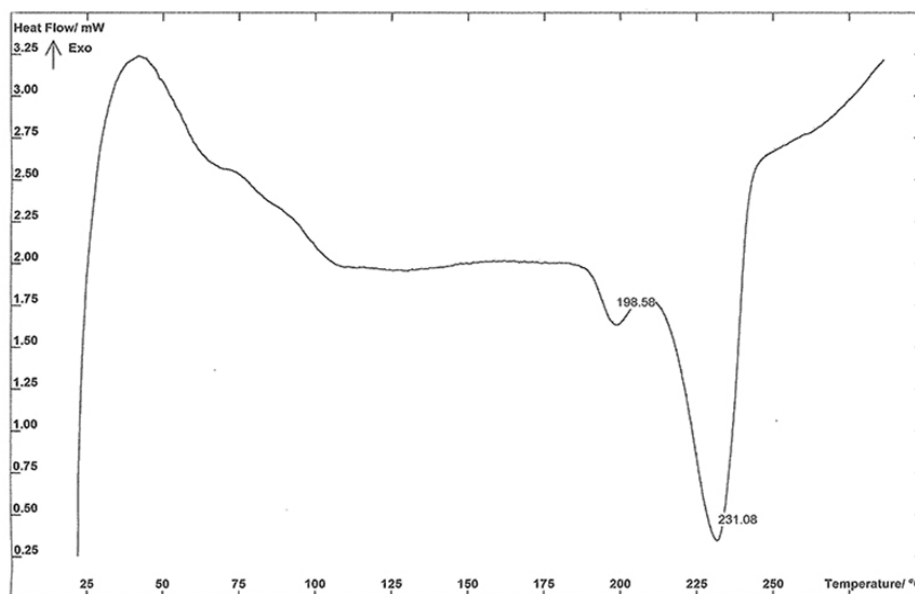


Figure 4.9. DSC thermogram of poly(BPOCPA)

4.1.5 FTIR, ¹H-NMR and DSC Characterization of BPOCPMA

FTIR spectrum of BPOCPMA, Figure 4.10, showed weak absorption peak at about 2980 cm⁻¹, characteristic C-H stretching vibrations of methyl group. The strong bands at 1747 and 1736 cm⁻¹ were assigned to C=O stretching vibrations of the ester groups. The absorption bands due to C=C stretching vibrations of aromatic groups were observed at 1597 and 1504 cm⁻¹. The bands recorded at 1259 and 1198 cm⁻¹ were attributed to C-O-C stretching vibrations. The moderate bands between 941, 925 and 893 cm⁻¹ were corresponding to the vinylic C-H out of plane bending vibrations.

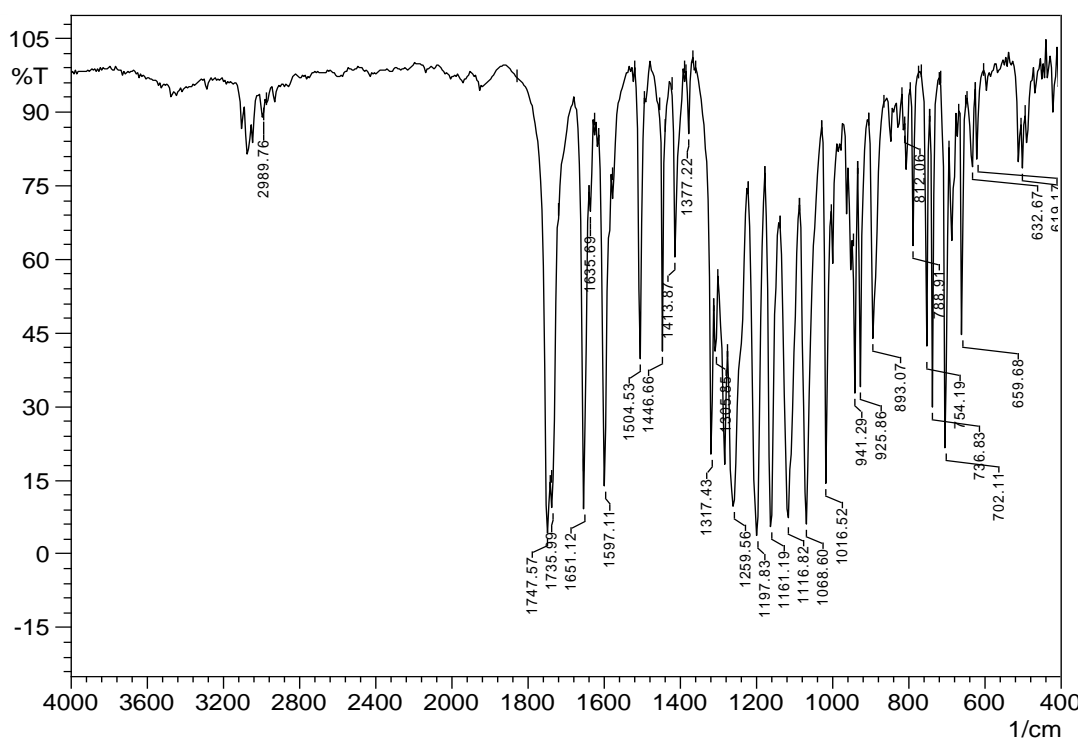
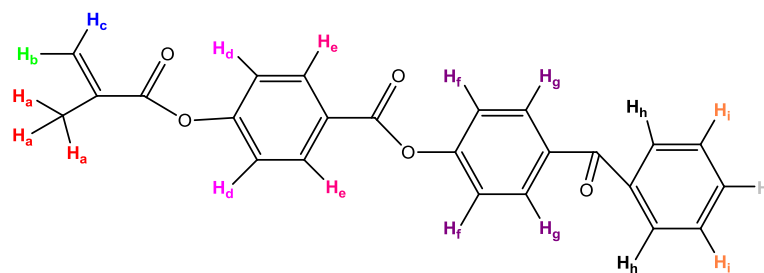


Figure 4.10. FTIR spectrum of BPOCPMA

The schematic structure of BPOCPMA was shown in scheme 2 with proton assignments, and ¹H-NMR spectrum of the molecule was presented in Figure 4.11. The singlets at δ 5.97 and 6.35 are attributed to H_b and H_c protons of the vinylic group and one quartet at δ 2.04 is corresponding to H_a. The doublets observed at δ 7.45, 7.78, 7.53, 7.88 and 8.25 are H_d, H_e, H_f, H_g, H_h protons. The triplets at δ 7.61 and 7.73 are due to H_j and H_i protons.



Scheme 2. Schematic representation of BPOCPMA with proton assignments

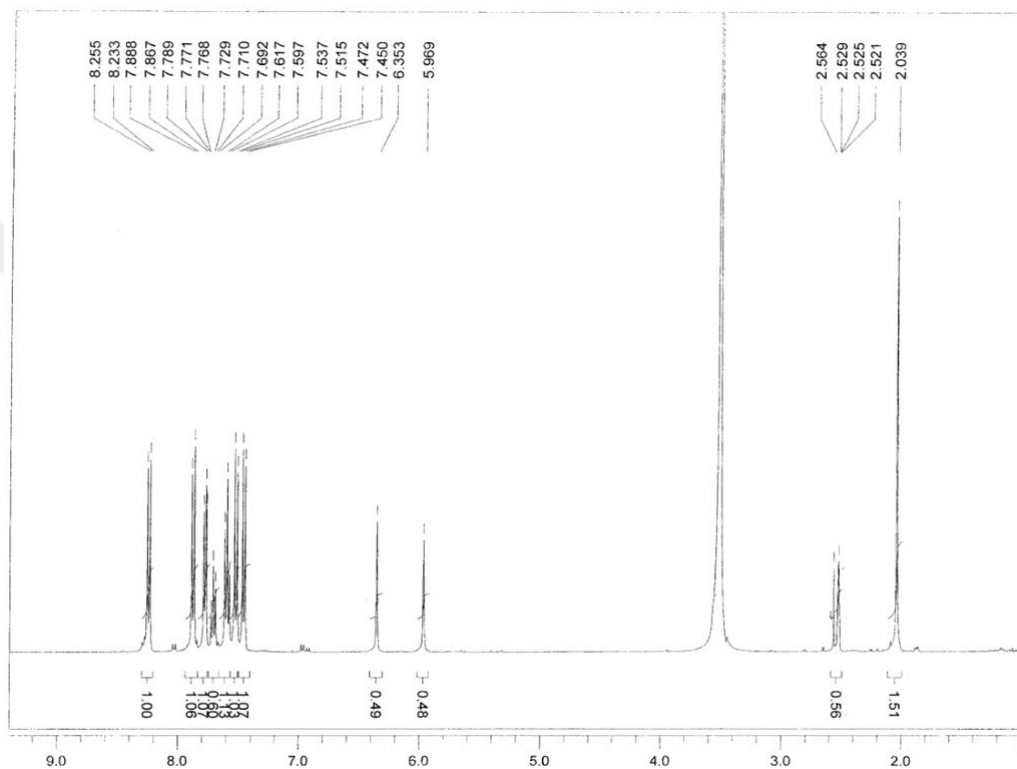


Figure 4.11. H-NMR spectrum of BPOCPMA

DSC melting point of BPOCPMA was 130.13°C, determined with heating rate of 10°C/min in N₂ atmosphere, Figure 4.12.

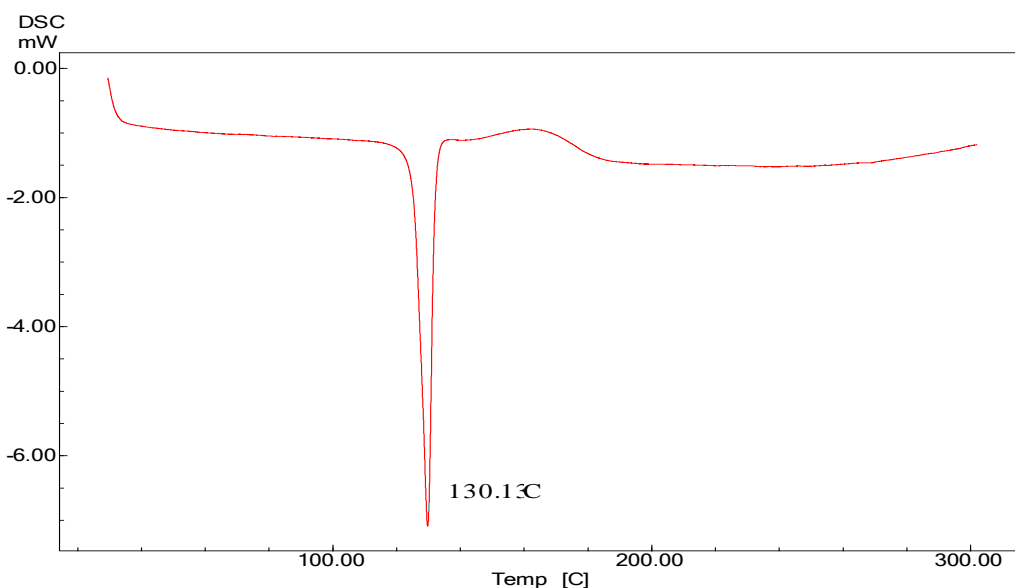


Figure 4.12. DSC thermogram of BPOCPMA

4.1.6 DSC and FTIR Characterization of poly(BPOCPMA)

FTIR spectrum of the homopolymer poly(BPOCPMA), Figure 4.13, displayed a strong band at 1741 cm^{-1} due to C=O stretching vibrations of the ester groups. The absorption band ascribed to C=O stretching vibrations of benzophenone group was observed at 1657 cm^{-1} . The absorption bands due to C=C stretching vibrations of aromatic groups were recorded at 1599 and 1502 cm^{-1} . The bands at 1263 and 1199 cm^{-1} were attributed to C-O-C stretching vibrations. Some of the bands observed in the spectrum of the monomer BPOCPMA due to vinylic C-H out-of-plane bending vibrations between 950 and 800 disappeared in the spectrum of poly(BPOCPMA). This result verified the polymerization of BPOCPMA through the vinylic group.

An amorphous character was observed in the DSC analysis of the homopolymer poly(BPOCPMA) carried out with $10^\circ\text{C}/\text{min}$ in N_2 atmosphere, Figure 4.14. Although it was reported to melt at 121°C (Sainath et al., 2000), there was not any heat flow indicating any endothermic or exothermic behavior in the studied temperature range.

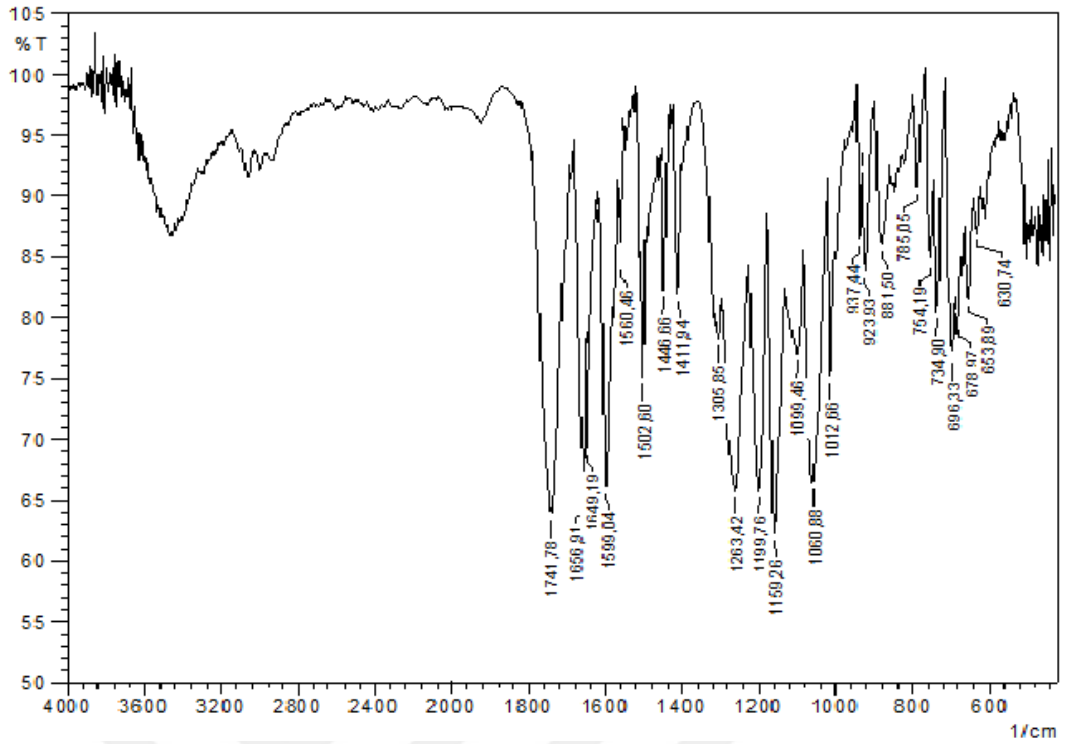


Figure 4.13. FTIR spectrum of poly(BPOCPMA)

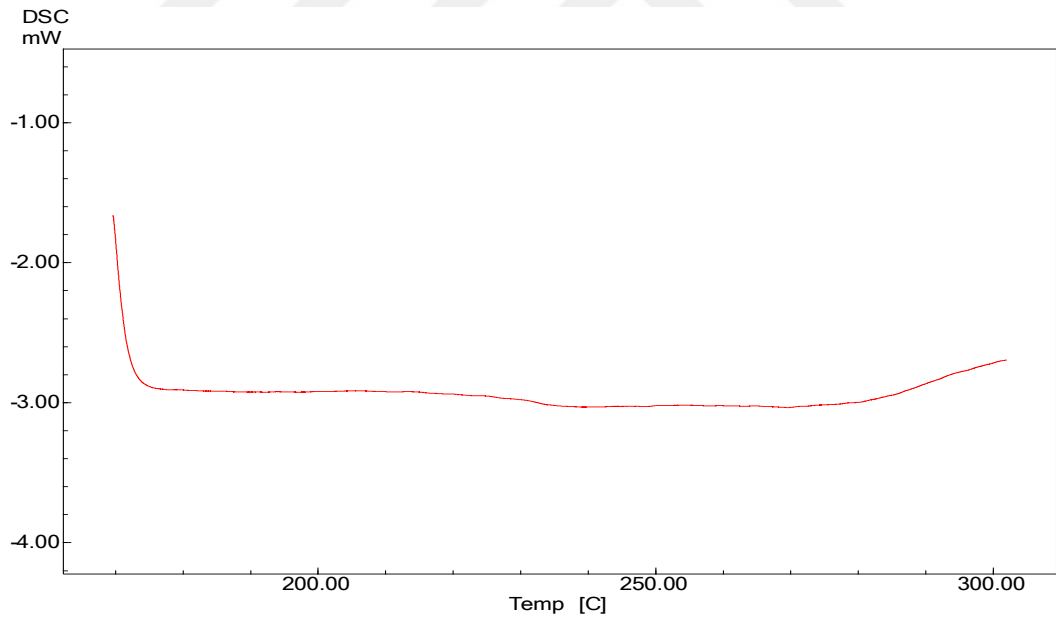


Figure 4.14. DSC thermogram of poly(BPOCPMA)

4.2 Graft Copolymerization of BPOCPMA onto HDPE

Thermally initiated graft copolymerization of BPOCPMA onto HDPE was studied at 140°C, the temperature greater than melting point of both HDPE and BPOCPMA (Both are melting at about 130°C) for 40 minutes. Variation of grafting with the mixing ratio of the monomer and HDPE in the reaction mixtures was investigated with six different monomer/HDPE ratios. The content of poly(BPOCPMA) in the products as graft units in the copolymers, and as both the graft units and the homopolymer molecules in the coproducts was determined gravimetrically. The percentage of poly(BPOCPMA) in the products of both classes, and percent grafting were presented in Table 4.1, and the variation of poly(BPOCPMA) content with monomer percentage in the reaction mixture were drawn in Figure 4.15. The content of the products consistently increased with the percentage of BPOCPMA in the reaction mixture. 21.0% poly(BPOCPMA) was obtained with 40% BPOCPMA in the copolymers. The percent grafting, on the other hand, reached to the maximum value 75.3% at 15% BPOCPMA, which was followed by a dramatic decrease to 49.1% grafting at 40% BPOCPMA, Figure 4.16. By considering the results, it can be stated that the grafting took place via the radicals forming on HDPE chains rather than the reactions between propagating poly(BPOCPMA) radicals and HDPE chains, presumably due to steric hindrance. Consistently, at lower monomer thus initiator (2% of weight of BPOCPMA) concentrations radicals presumably formed on HDPE chains in the majority due to the high probability of direct reactions between HDPE chains and the radicals of the initiator. Thus, high percentages of grafting, with the maximum 75.3% at 15% BPOCPMA, were obtained. The rise in the extent of grafting with the BPOCPMA percentage presumably resulted from the propagation of poly(BPOCPMA) units grafted onto HDPE chains, leading to high content of grafted poly(BPOCPMA).

Table 4.1. The dependence of poly(BPOCPMA) content in the products on the BPOCPMA percentage in the reaction mixture

% BPOCPMA in reaction mixture	5%	10%	15%	20%	30%	40%
% Poly(BPOCPMA) in the copolymers	3.8	6.7	10.7	11.8	18.6	21.0
% Poly(BPOCPMA) in the coproducts	3.8	7.3	12.7	19.2	25.1	26.7
% Grafting	69.4	69.5	75.3	64.5	51.3	49.1

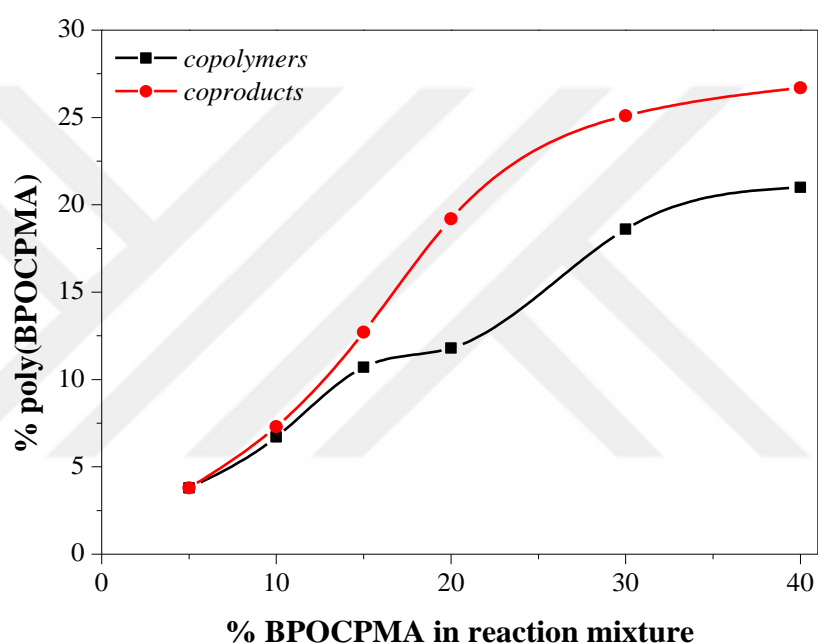


Figure 4.15. The variation of poly(BPOCPMA) content in the products with BPOCPMA percentage in the reaction mixture

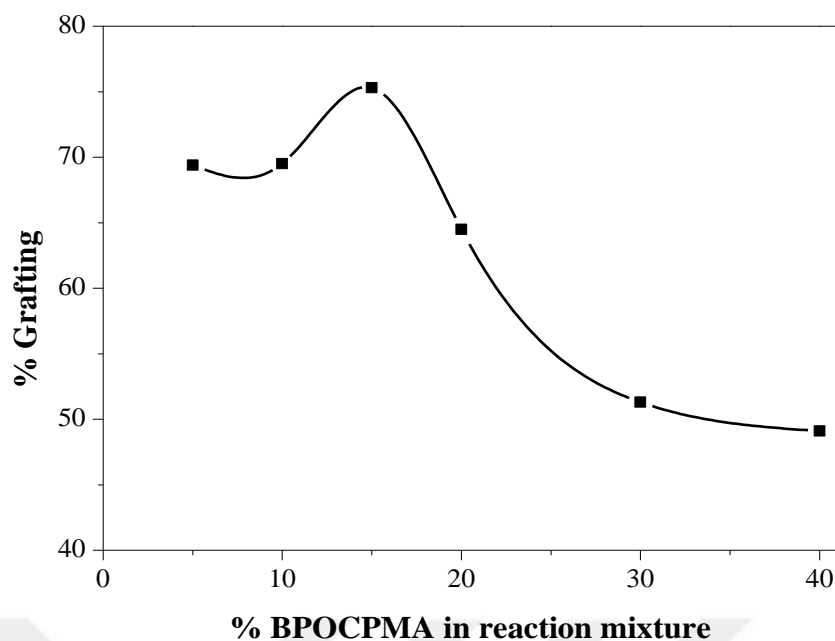


Figure 4.16. The variation of percent grafting of poly(BPOCPMA) with the percentage of BPOCPMA in reaction mixture

4.2.1 FTIR Characterization of the Products

FTIR spectra of the copolymers involving 6.7% and 21.0% poly(BPOCPMA), Figure 4.17, and of the coproducts with 7.3% and 26.7% poly(BPOCPMA), Figure 4.18, displayed strong bands between 1743 cm^{-1} and 1740 cm^{-1} owing to C=O stretching vibrations of the ester groups of poly(BPOCPMA) units. The absorption bands observed between 1662 cm^{-1} and 1653 cm^{-1} were attributed to C=O stretching vibrations of the benzophenone group. The bands seen at $1265\text{-}1263$ and 1201 cm^{-1} were corresponding to C-O-C ester stretching vibrations. The strong bands at 2918 and 2848 cm^{-1} were assigned to CH_2 stretching vibrations of HDPE chains. The bands at 1469 cm^{-1} and 717 cm^{-1} were due to the CH_2 and C-C bending vibrations, respectively. The increase in the content of poly(BPOCPMA) in the products led to stronger bands at $1743\text{-}1739$, $1665\text{-}1654$, $1265\text{-}1263$, and 1201 cm^{-1} , the characteristic bands of the graft unit.

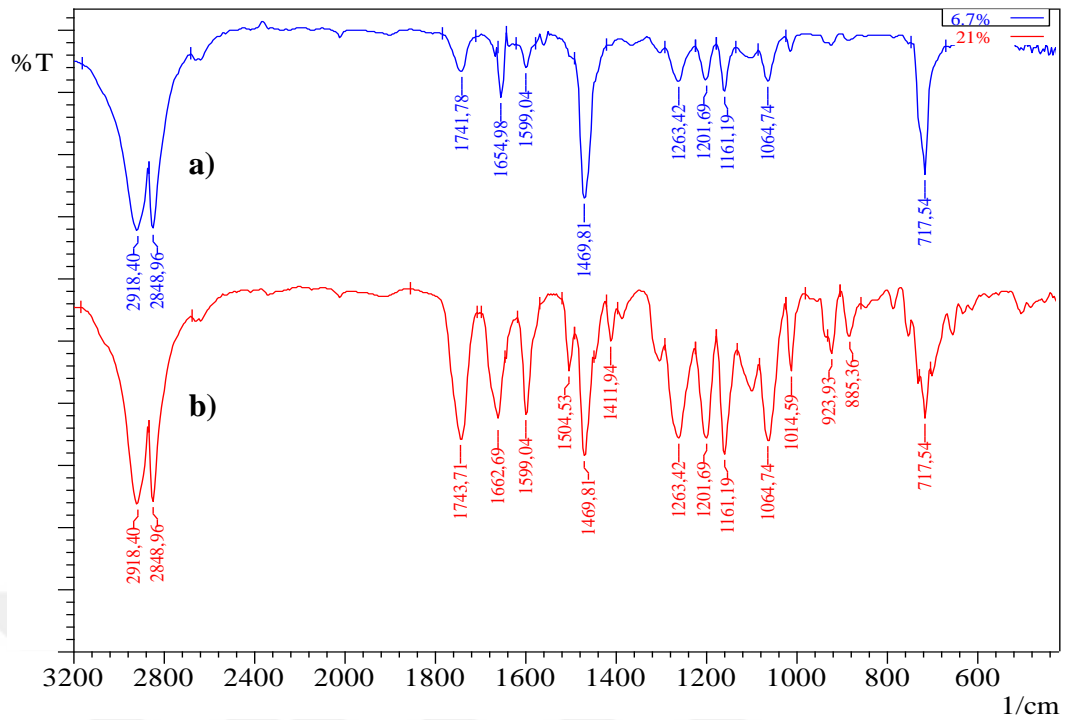


Figure 4.17. FTIR spectra of the copolymers involving a) 6.7%, and b) 21% poly(BPOCPMA)

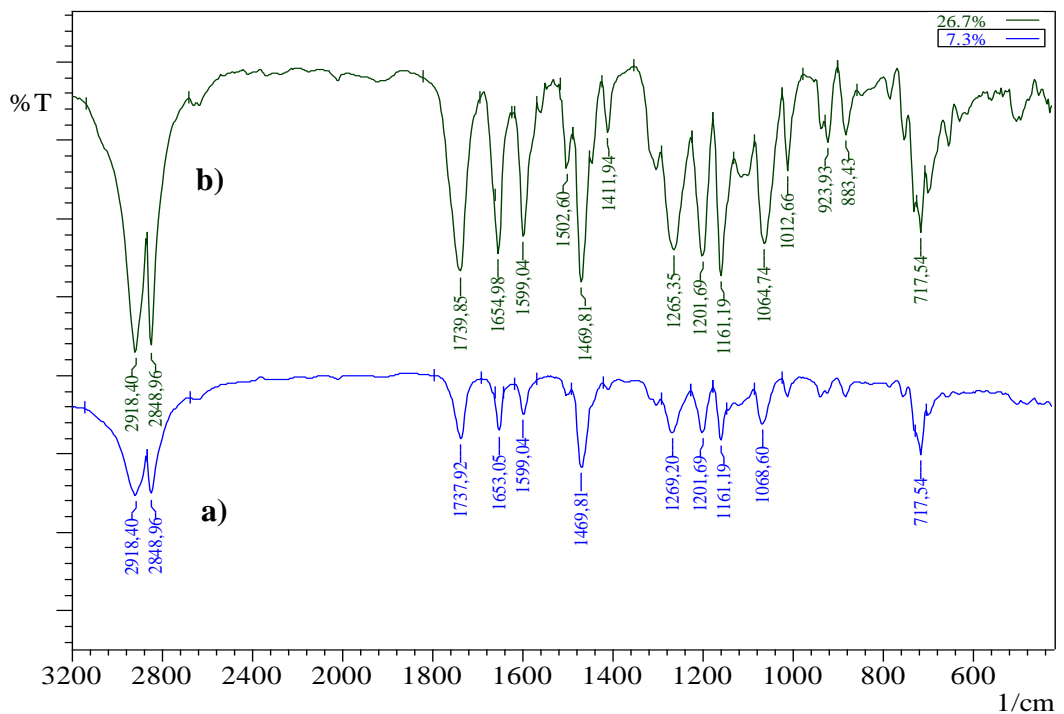


Figure 4.18. FTIR spectra of the copolymers involving a) 7.3%, and b) 26.7% poly(BPOCPMA)

4.2.2 DSC and XRD Characterization of the Products

The effect of the graft copolymerization of BPOCPMA onto HDPE on the thermal behavior of the products was comprehensively investigated by DSC. Any endotherm attributable to the crystalline melting of poly(BPOCPMA) units was not detected in the thermograms of the products as neither was for poly(BPOCPMA) homopolymer, Figure 4.19, although the polymer was announced to melt at 121°C (Sainath et al., 2000). On the other hand, significant and comparable increases were recorded in the melting temperature of HDPE in both classes of the products, Figure 4.20 and Table 2 and 3. They were, however, more consistent with the graft content in the copolymers, while more scattering and irregular melting temperatures were seen in the coproducts, that is, when the copolymers contained the homopolymer molecules. The highest values, 134.07°C and 134.51°C were detected in both classes with similar contents, with 11.8% poly(BPOCPMA) in the copolymers and with 12.7% content in the coproducts, respectively. The temperatures then had a decreasing trend at higher percentages. In order to unfold the effect of the graft copolymerization on the thermal behavior of the material, a HDPE sample and a mixture of HDPE and DCP (2% with respect to weight of PE) were annealed at 140°C for 1 hour in vacuum, as in graft copolymerization experiments. The melting temperatures of both samples were observed to remain almost unchanged at about 130°C (the same as virgin PE).

The crystallinity in HDPE matrix of the products decreased initially with the content of poly(BPOCPMA), Figure 4.21, and diminished to 43.8% crystallinity with 10.7% poly(BPOCPMA). The grafted poly(BPOCPMA) units at low percentages probably had an hindering effect in the arrangement of HDPE chains in crystalline domains. The crystallinity then increased with the content, but to the values comparable with pure HDPE. The polar interactions between the side groups of grafted poly(BPOCPMA) units, becoming more effective as the content increases, presumably led to the further growths in the crystallinities.

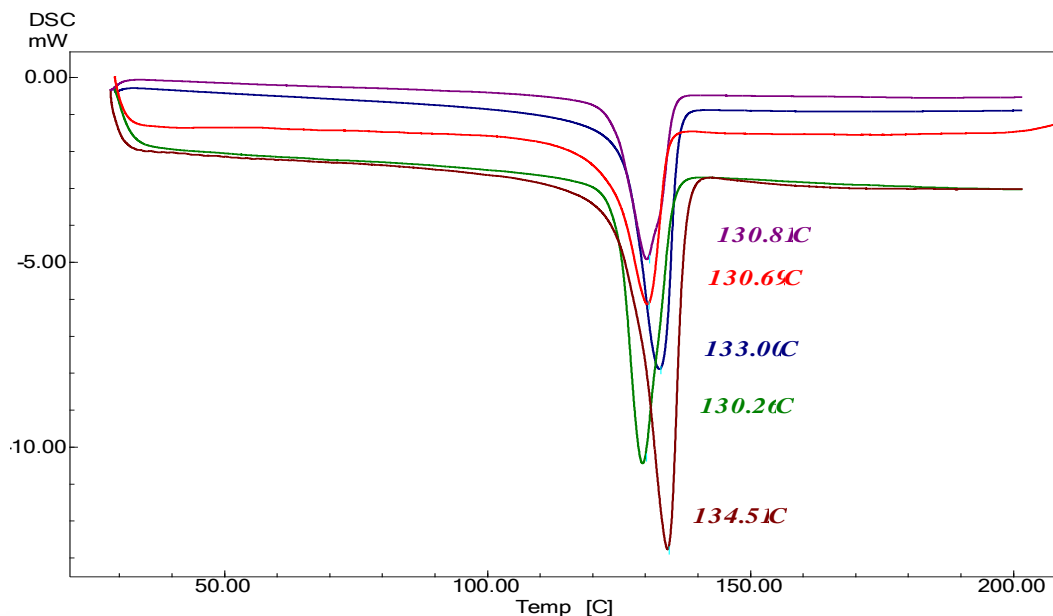


Figure 4.19. The DSC thermograms, of HDPE sample processed with 2% DCP (130.69°C), of the coproducts with 12.7% poly(BPOCPMA) (134.51°C), 25.1% poly(BPOCPMA) (130.81°C) and of the copolymers with 6.7% poly(BPOCPMA) (133.00°C), 21% poly(BPOCPMA) (130.26°C)

Table 4.2. DSC results with poly(BPOCPMA) percentages in the copolymers (The crystalline melting temperatures, T_m , enthalpy of fusions, ΔH_m and the percent crystallinities, X_c (%))

Sample	T_m (°C)	ΔH_m (J/g)	X_c (%)
Neat HDPE	130.22	203.029	70.010
3.8% poly(BPOCPMA)	132.25	134.606	46.416
6.7% poly(BPOCPMA)	133.00	142.120	49.007
10.7% poly(BPOCPMA)	133.82	126.930	43.769
11.8% poly(BPOCPMA)	134.07	132.121	45.559
18.6% poly(BPOCPMA)	131.00	129.830	44.769
21.0% poly(BPOCPMA)	130.26	161.579	55.717

Table 4.3. DSC results with poly(BPOCPMA) percentages in the coproducts (The crystalline melting temperatures, T_m , enthalpy of fusions, ΔH_m and the percent crystallinities, X_c (%))

Sample	T_m (°C)	ΔH_m (J/g)	X_c (%)
Neat HDPE	130.22	203.029	70.010
3.8% poly(BPOCPMA)	131.58	191.620	66.076
7.3% poly(BPOCPMA)	132.37	143.356	49.433
12.7% poly(BPOCPMA)	134.51	143.521	49.490
19.2% poly(BPOCPMA)	132.88	173.269	59.748
25.1% poly(BPOCPMA)	130.81	166.404	57.036
26.7% poly(BPOCPMA)	130.71	138.716	47.833

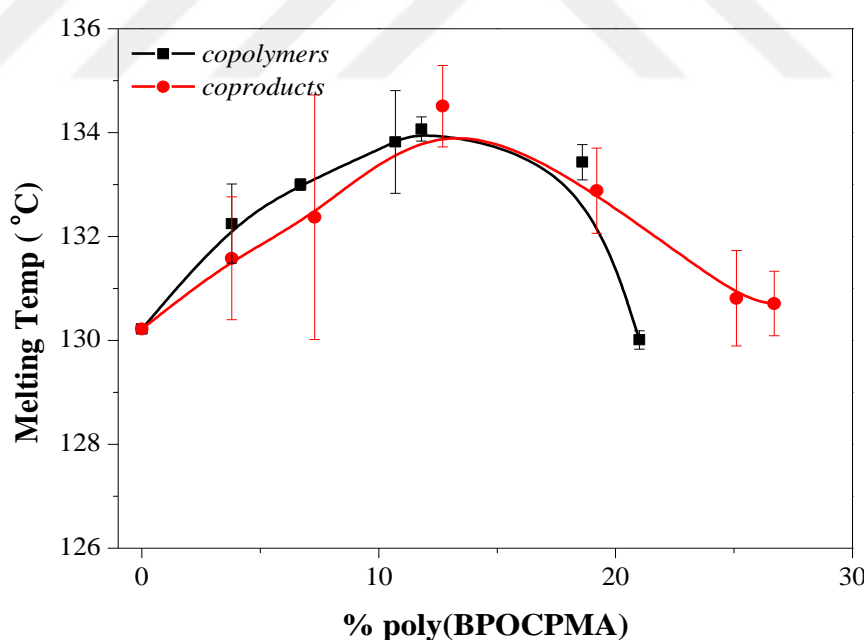


Figure 4.20. The variation of HDPE melting temperature with poly(BPOCPMA) content in the products

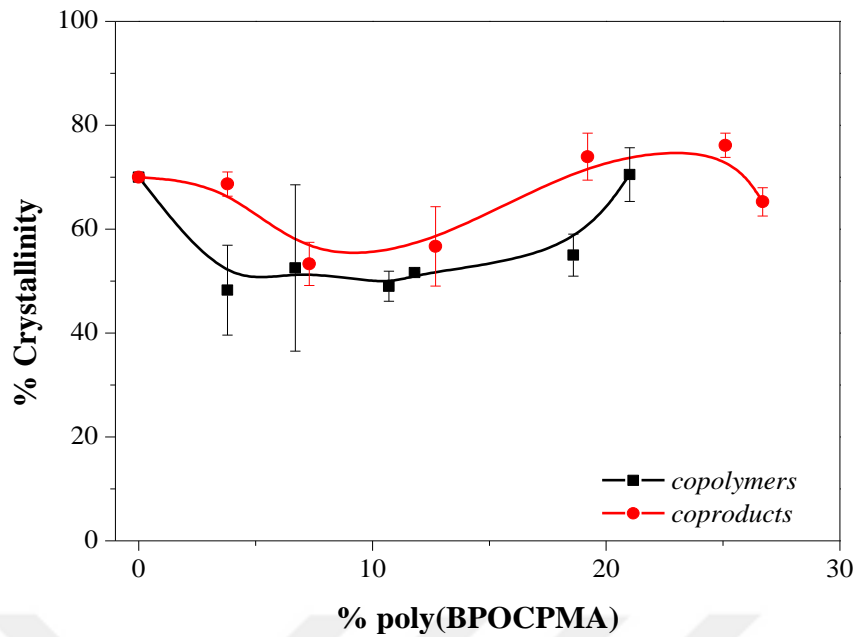


Figure 4.21. The variation of crystallinity in HDPE matrix with poly(BPOCPMA) content in the products

In order to bring out the effect of the graft copolymerization on the microstructural properties of the HDPE matrix, the products were also analyzed by XRD. The crystal parameters were calculated on the basis of a least square method using (hkl) planes and d values. The unit cell size of crystal domains of the products was estimated from the XRD patterns by using the formula;

$$d = 0.941 \lambda / B \cos\theta_B$$

where d is the crystal thickness, λ denotes the wavelength of the XRD source, B is the full width at half maximum (FWHM) of the Bragg peak, and θ_B is the Bragg angle. Here, B is defined as;

$$B^2 = B_m^2 - B_s^2$$

where B_s shows the half width of the standard material and B_m is the sign of the difference between the angles at FWHM of the peak.

The crystalline lattice behavior of pure HDPE with Bragg's angle (2θ) varying from 10° to 60° can be seen in Figure 4.22 from the X-ray diffraction pattern. In Figure 4.22, pure polyethylene showed two characteristic peaks at $2\theta=21.5^\circ$ and $2\theta=23.9^\circ$, which are assigned to the 110 and 200 reflections of the Bunn

orthorhombic subcell. These values agree well with the values reported as 21.3° and 23.5° for polyethylene by Josie et al (Joshi et al., 2006).

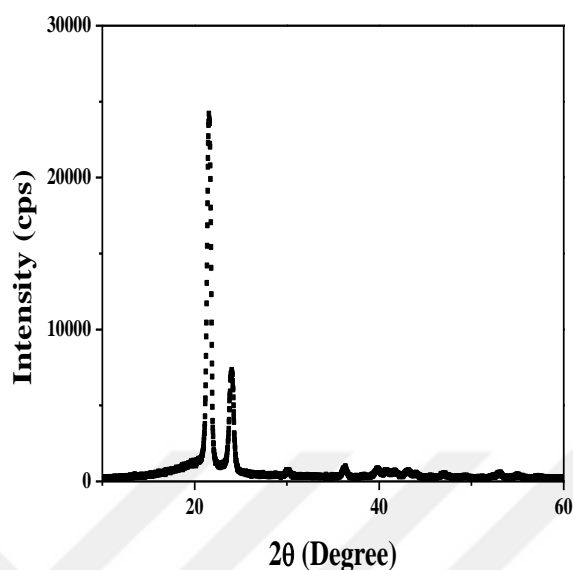


Figure 4.22. The XRD pattern of pure HDPE

The XRD analyses showed that the microstructure, the crystalline characteristic of HDPE matrix of the products has been conserved throughout the graft copolymerizations. This was revealed by the patterns typical of orthorhombic polyethylenes, indicating the crystalline packing of HDPE chains merely in orthorhombic unit cell as seen in Figure 4.23. The lateral dimensions of the unit cell, however, were found to be considerably affected by poly(BPOCPMA) content. Significant increases in the unit cell parameters were observed in both classes of the products. The dependence of the unit cell parameters and *ab* basal area on the content of poly(BPOCPMA) in the products were given in Table 4.4 and 4.5 in detail, and their variations were drawn in Figure 4.24.a, b, c and d.

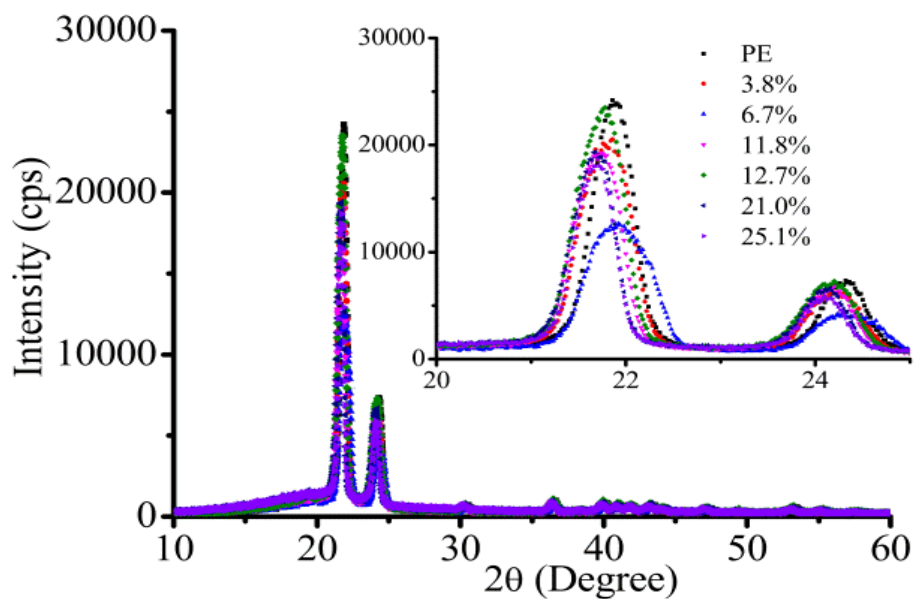


Figure 4.23. The XRD patterns of some copolymers (with 6.7, 11.8 and 21.0% poly(BPOCPMA)) and coproducts (with 3.8, 12.7, 25.1% poly(BPOCPMA))

Table 4.4. The dependence of the unit cell parameters *a*, *b* and *c*, and crystal size in HDPE matrix on poly(BPOCPMA) content in copolymers

Sample	<i>a</i> (Å)	<i>b</i> (Å)	<i>c</i> (Å)	Crystallite size (nm)
Neat HDPE	7.34	4.91	2.54	16.40
3.8% poly(BPOCPMA)	7.36	4.91	2.55	17.08
6.7% poly(BPOCPMA)	7.36	4.91	2.55	18.21
10.7% poly(BPOCPMA)	7.36	4.91	2.55	20.33
11.8% poly(BPOCPMA)	7.38	4.92	2.55	21.37
18.6% poly(BPOCPMA)	7.38	4.92	2.55	21.43
21.0% poly(BPOCPMA)	7.38	4.92	2.55	22.65

Table 4.5. The dependence of the unit cell parameters *a*, *b* and *c*, and crystal size in HDPE matrix on poly(BPOCPMA) content in coproduct

Sample	<i>a</i> (Å)	<i>b</i> (Å)	<i>c</i> (Å)	Crystallite size (nm)
Neat HDPE	7.34	4.91	2.54	16.40
3.8% poly(BPOCPMA)	7.38	4.92	2.55	21.50
7.3% poly(BPOCPMA)	7.39	4.93	2.55	23.15
12.7% poly(BPOCPMA)	7.39	4.93	2.55	23.86
19.2% poly(BPOCPMA)	7.39	4.93	2.55	23.51
25.1% poly(BPOCPMA)	7.40	4.95	2.55	28.67
26.7% poly(BPOCPMA)	7.40	4.94	2.55	24.11

The increase in the parameter *a* was expressively stepwise in the copolymers, Figure 4.24.a. About 0.27% increase was seen with graft content in the range of 3.8-10.7%, while the expansions concentrated around 0.54% increase, twice the former rise, in the interval of 11.8-21.0%. The parameter *b*, on the other hand, after a stationary value in the initial graft percentages, 3.8-10.7%, identical to that of virgin HDPE, had a 0.20% enlargement throughout the content of 11.8-21.0%, Figure 4.24.b. The expansions in the unit cell dimensions were also evidently revealed from the shifts of the reflections toward left in the patterns, Figure 4.23. The HDPE chains in the unit cells were probably forced apart laterally by the polar graft units, thus giving rise to expansions in the lateral dimensions. Seemingly, this effect was more prominent in the dimension *a*. The similar commentaries were announced for the expanded unit cells of oriented (Howard et al., 1989) and branched polyethylene, in relation to the type, distribution and content of the branches (Baker et al., 2001a; Baker et al., 2001b). In these reports, the expansions were explained on the basis of the included branches in the crystalline regions compelling the chains to laterally enlarged unit cell dimensions. Additionally, the possibility of branch rejection was also announced for the structural changes (Baker and Windle, 2001b). Apparently, at initial percentages of about 3.8% poly(BPOCPMA), the graft units were effective enough to led to 0.27% increase in dimension *a* by a force exerted laterally on the HDPE chains by the units. Further inclusion of the graft units until about 10.7%,

however, did not contribute to the expansion, and the parameter a remained almost unchanged. A further increase in the content than 10.7% until 21.0% poly(BPOCPMA) resulted in another 0.27% enlargement with 0.54% expansion overall. The spatial arrangement and orientation of the graft units in the products and their relative effects in coercing HDPE chains apart laterally are believed to result in the dissimilar enlargement behavior in the parameters and the stepwise behavior in the former parameter. On the other hand, the c parameter, the unit cell axis parallel with the chain axis of HDPE molecular segments (Peacock, 2000) was found to increase by about 0.39%, identically in all products, Figure 4.24.c. The lateral expansions in a and b dimensions and the corresponding widenings in the ab basal area, Figure 4.24.d, have presumably resulted in the identical extension in the c axis parallel with HDPE chains.

In the coproducts, the inclusion of the homopolymer poly(BPOCPMA) molecules besides those present as grafted units gave rise to further expansions in the unit cell dimensions of a and b , and the relative enlargements in ab basal area. The dependence of the parameters and the basal area on the content of poly(BPOCPMA) were also depicted in Figure 24.a, b, c and d. The initial increase in the parameter a with the content was followed by a stationary value, almost 0.68% greater compared to virgin HDPE and abiding along with the percentages 7.3-19.2%. The parameter then proceeded with further rise with the content and reached an 0.81% enlarged dimension in the inclusion of 25.1-26.7% poly(BPOCPMA), Figure 24.a. The similar trend was also observed in the parameter b which stayed almost constant but at the level with 0.41% enlargement throughout the percentages of 7.3-19.2%. This stationary behavior was then accompanied with further expansion with the content, and about 0.81% expanded b parameter was seen with 25.1% poly(BPOCPMA), Figure 24.b. These results, the additional expansions in lateral dimensions of the unit cell with the inclusion of the homopolymer in the coproducts were found to be explained by the strong interactions between the polar groups of grafted and ungrafted poly(BPOCPMA) molecules. The adhesive forces between the polar groups of the grafted units and the homopolymer molecules had presumably an additional effect, as mentioned above, in enlargements of the lateral dimensions. On the other hand, the same expansion, 0.39%, was recorded in the parameter c in all coproducts, as identically observed in the copolymers, Figure 24.c. The additional

increases in lateral dimensions in the coproducts had no effect on the expansions in the axis (c) of the unit cells, parallel with the axis of HDPE chains.

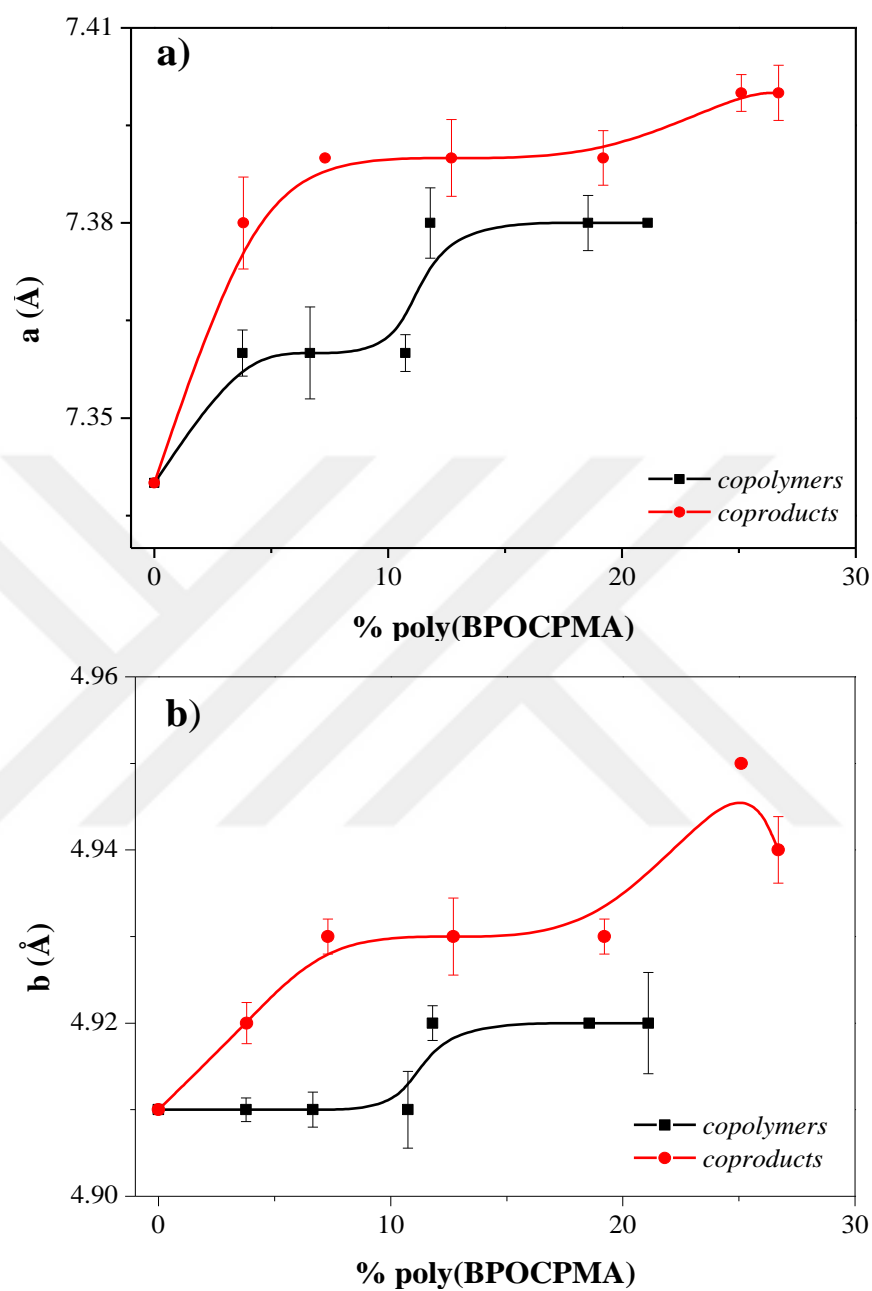


Figure 4.24.a and b. The variations of the unit cell parameters a (a) and b (b) with poly(BPOCPMA) content, calculated from the X-ray diffraction patterns (using the reflections (110), (200) and (211)).

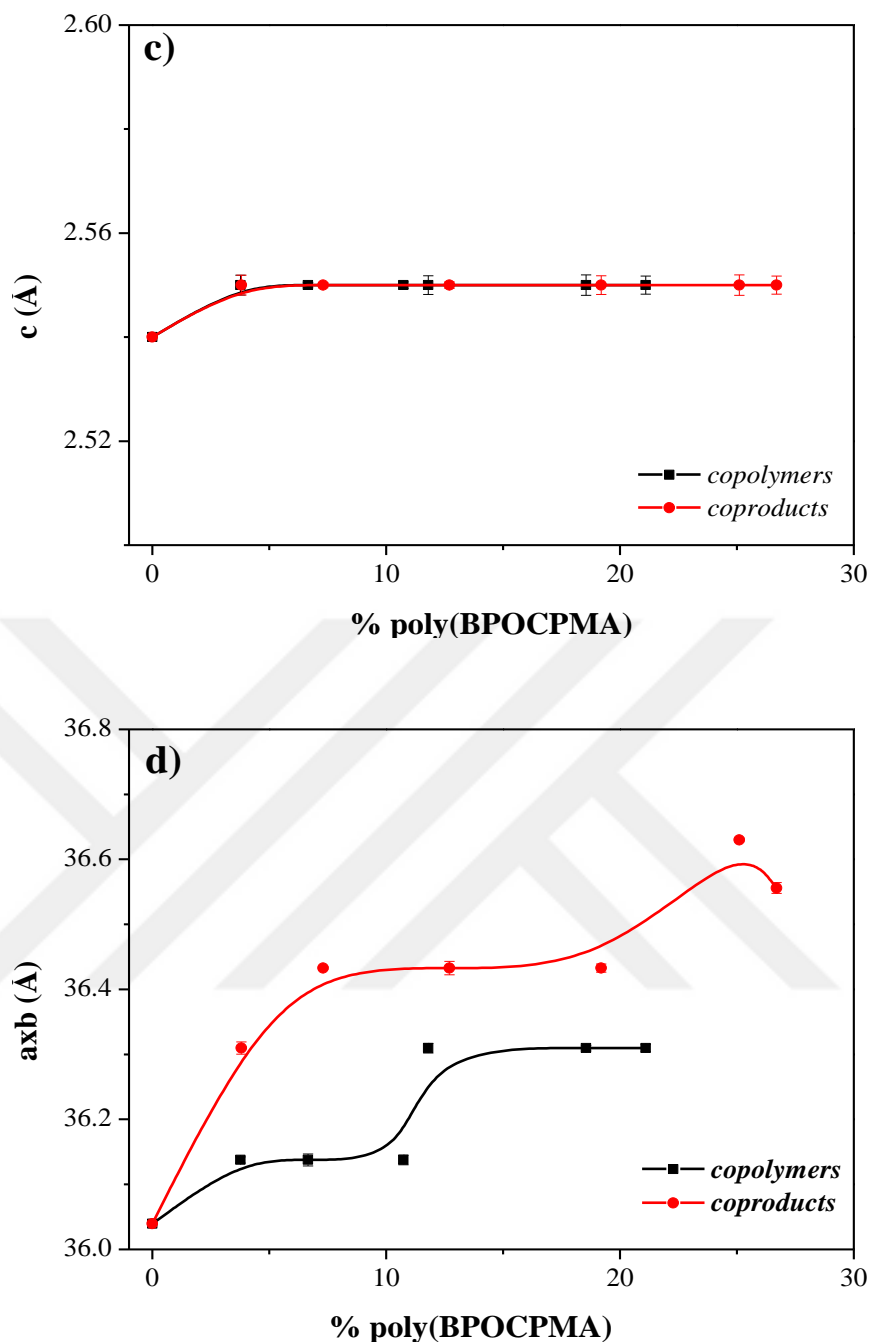


Figure 4.24.c and d. The variations of the unit cell parameters c (**c**), and the unit cell basal area ab (**d**) with poly(BPOCPMA) content, calculated from the X-ray diffraction patterns (using the reflections (110), (200) and (211))

The consistent increases in the melting temperature of HDPE in both classes of the products with the content up to about 12%, Figure 4.20, are believed to result from the advances in the ordered packing of HDPE chains in the crystallites due to the constitution of side chain LCP poly(BPOCPMA) molecules as graft units. Poly(BPOCPMA) chains with mesogenic side groups were reported to exhibit glassy

nematic arrangement (Sainath et al., 2000). With the potential of forming such regularly organized structure, poly(BPOCPMA) molecules present as graft units in the products might have dynamically conducted to a better ordering and orientation of HDPE chains during crystallizations. Furthermore, the glassy nematic structured poly(BPOCPMA) units (Sainath et al., 2000) might also have acted as nucleating agents, and thus led to more ordered arrangement and packing of the chains in the crystalline regions. Because, a better array and promoted arrangement can be potentially expected in the crystal when it originates from a center with a more ordered structure. Moreover, the HDPE chains with greater mobility in the larger *ab* basal area of the unit cells might have further assistance in their advanced orderings and alignments. These advances in the microstructures thus resulted in the increased melting temperatures from about 130°C to the maximum values around 134°C achieved at about 12% poly(BPOCPMA) in both classes of the products. The decrease trend in the melting points at further contents, however, can be explained by a relative loss in the promoted ordering of the chains. That is, the graft units at higher percentages than a significant value, 12-13%, might have started to lose their assisting function in the ordered and oriented packing of the HDPE chains, probably owing to large occupations by the units in between them and to relatively strong interactions between the polar groups of the units. This restrain can be conditionally expected to be more effective and prominent with the increase of the content. The outcome was eventually observed as the decrease trend in the melting temperatures after the maximum values.

The similar trend seen in the expansions of the lateral dimensions and thus of *ab* basal area was also observed in the variation of the particle size (HDPE crystals) with the content of poly(BPOCPMA) in both classes of the products, Figure 4.25. In a similar manner recorded in the basal areas, crystal size initially increased with the content in both classes. The increases were followed by a stationary behavior with 41-43% expanded size in the coproducts with the content of 7.3-19.2%, and with about 30% enlargement in the copolymers with the inclusion of 11.8-18.6%. The sizes then had further rise with the percentage content. The similarity observed between the content dependence of the *ab* basal area and the particle size revealed that as the basal area of the unit cells got enlarged, the size of the crystals increased. This was found to be simply explained by further growth of the crystals on a larger

basal area of the unit cells. That is, the expansions in the lateral dimensions of the unit cells have seemingly resulted in the extended growth of the crystals with the dimensional enlargements. Moreover, the glassy nematic structured poly(BPOCPMA) units (Howard and Crist, 1989) acting as nucleating agents during crystallizations might have additionally contributed to the promoted growth of the crystals. Because, it can be rationally expected that the growth of the crystals propagates to larger sizes when it originates from more ordered structures.

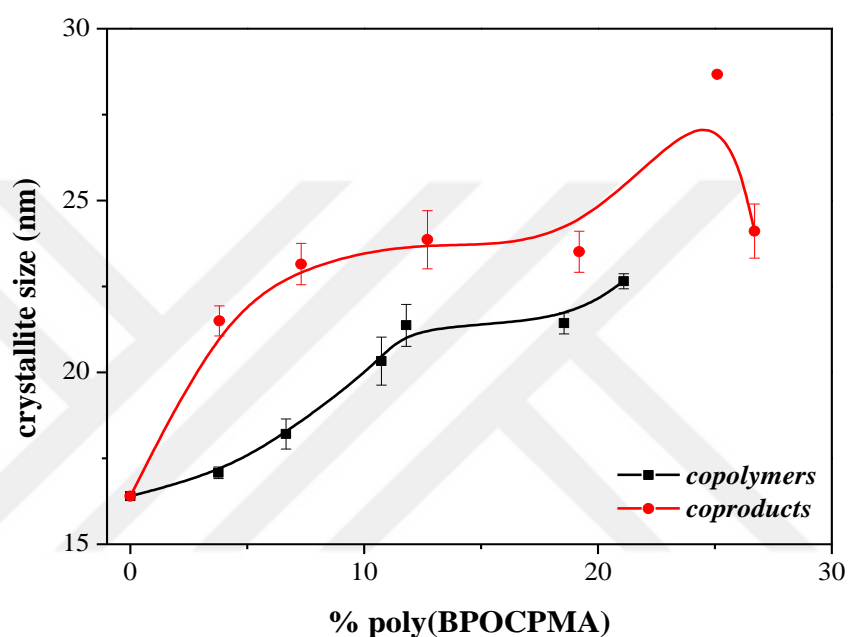


Figure 4.25. The variation of crystal size (grain size) with poly(BPOCPMA) content

4.2.3 PALS Analysis of The Products

Many chemical and physical properties of polymers depend on their free volume. The material properties such as viscosity, permeability, mobility, structure relaxation, physical aging and molecular transport etc are all affected by free volume (Yand Y, 2011). Therefore, HDPE and the products were also analyzed by Positron Annihilation Lifetime Spectroscopy in Marmara Positronium Laboratory (MARPOS) in Physics Department at Marmara University in order to unfold the effect of the graft copolymerization on the free volume properties of the HDPE matrix and the products.

The lifetimes of positrons for neat HDPE, the copolymers and the coproducts were measured and all the lifetime spectra were analyzed into three lifetime components. The shortest-lived component, τ_1 with an intensity I_1 , associated with the annihilation of *para-positronium* (*p-Ps*), the intermediate-lived component, τ_2 with an intensity I_2 , attributed to the direct annihilation of positrons, and the longest-lived component as *ortho-positronium* (*o-Ps*), τ_3 with an intensity I_3 , associated with pick off annihilation, were obtained from the lifetime spectra. These analyzed parameters were calculated using τ_1 fixed at 125 ps, assumed as independent of free volume.

In the free volume model, τ_3 is related to the free volume hole radius, R (free volume radius, R), whilst I_3 is related to the number of holes. Thus, the volume of a hole increases with increasing τ_3 and the number of holes increases with increasing intensity, I_3 (Mostafa et al., 2009).

The free volume hole radius (R) may be calculated by using *o-Ps* lifetime (τ_3) and by the semi-empirical approximation given by (Eldrup et al., 1981) with the assumption of the holes being spherical:

$$\tau_3(ns) = \frac{1}{2} \left(1 - \frac{R}{R_0} + \frac{1}{2\pi} \sin \frac{2\pi R}{R_0} \right)^{-1} \quad (1)$$

where $R_0 = R + \delta R$ with $\delta R = 0.1656 \text{ nm}$, the thickness of the homogeneous electron layer that constitutes the wall of the hole (Nakanishi and Jean, 1990). The free volume hole size (V_f) can be calculated by

$$V_f = \frac{4}{3} \pi R^3 \quad (2)$$

and the free volume fraction (f) proposed by Kobayashi et al. can be stated as

$$f_v = AI_3 V_f(\tau_3) \quad (3)$$

where A is a proportionality coefficient; that is taken as 0.0018 (Kobayashi Y et al., 1989).

The dependence of the lifetimes and the intensities of the positrons measured in the analyses, the radii of the free volume hole, the free volume hole size and the free volume fraction of the copolymers and coproducts calculated by using the equations 1, 2 and 3 on poly(BPOCPMA) contents were presented in Table 4.6 and 4.7, respectively.

The variation of the intermediate-lived component (τ_2) with poly(BPOCPMA) content in the products were given in Figure 4.26. It can be stated that the direct annihilation lifetime of the positrons, the intermediate-lived component (τ_2), has almost unchanged in the copolymers. It was 0.409 ± 0.002 ns, analogous with pure HDPE throughout the compositions. In the coproducts, however, an increase was observed in the lifetime at lower poly(BPOCPMA) contents. 0.421 ± 0.002 ns, the maximum lifetime with 2.9% increase with respect to that of HDPE, was recorded with 3.8% poly(BPOCPMA). The maximum was then followed by slight decrease trend, consistent with the content. The lowest lifetime, 0.404 ± 0.002 ns was recorded with 26.7% poly(BPOCPMA), the highest content among the coproducts.

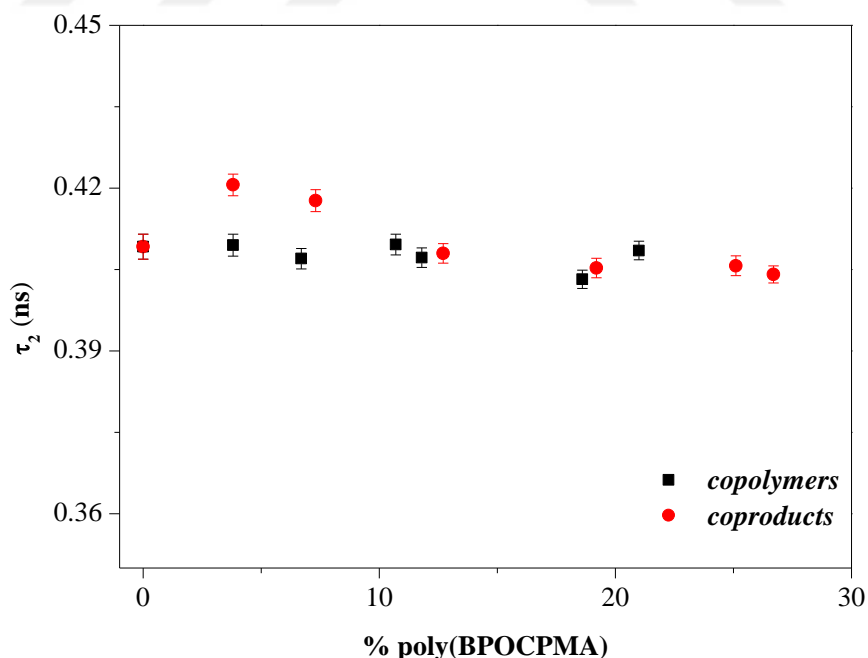


Figure 4.26. The variation of the direct annihilation lifetime of the positrons, the intermediate-lived component (τ_2) with poly(BPOCPMA) content in the products

Table 4.6. The dependence of the lifetimes and the intensities of the positrons, the radii of the free volume hole, the free volume hole size and the free volume fraction of the copolymers on poly(BPOCPMA) content

Percentage Content (%)	Neat HDPE	3.8	6.7	10.7	11.8	18.6	21
τ_2 (ns)	0.409±0.002	0.410±0.002	0.407±0.002	0.410±0.002	0.407±0.002	0.403±0.002	0.409±0.002
τ_3 (ns)	2.282±0.009	2.296±0.010	2.272±0.010	2.263±0.010	2.239±0.010	2.222±0.010	2.222±0.010
I_1 (%)	31.19±0.34	27.64±0.35	26.49±0.36	26.02±0.35	24.80±0.36	23.62±0.38	24.30±0.36
I_2 (%)	45.56±0.30	51.57±0.31	53.50±0.32	54.89±0.32	57.52±0.33	59.41±0.34	60.03±0.33
I_3 (%)	23.24±0.08	20.79±0.08	20.01±0.08	19.10±0.08	17.68±0.08	16.96±0.07	15.68±0.07
R (Å)	3.094±0.006	3.105±0.006	3.085±0.006	3.078±0.006	3.058±0.007	3.043±0.007	3.043±0.007
v_f (Å ³)	124.1±0.7	125.4±0.7	123.0±0.7	122.2±0.8	119.8±0.8	118.1±0.8	118.1±0.8
f_v (%)	5.19±0.04	4.69±0.05	4.43±0.04	4.20±0.04	3.81±0.04	3.61±0.04	3.33±0.04

Table 4.7. The dependence of the lifetimes and the intensities of the positrons, the radii of the free volume hole, the free volume hole size and the free volume fraction of the coproducts on poly(BPOCPMA) content

Percentage Content (%)	Neat HDPE	3.8	7.3	12.7	19.2	25.1	26.7
τ_2 (ns)	0.409±0.002	0.421±0.002	0.418±0.002	0.408±0.002	0.405±0.002	0.406±0.002	0.404±0.002
τ_3 (ns)	2.28±0.01	2.33±0.01	2.33±0.01	2.28±0.010	2.28±0.010	2.27±0.010	2.23±0.011
I_1 (%)	31.19±0.34	29.36±0.32	28.68±0.32	26.23±0.35	25.90±0.35	26.71±0.35	25.60±0.36
I_2 (%)	45.56±0.30	50.37±0.28	51.62±0.29	54.98±0.31	55.62±0.32	55.61±0.31	59.28±0.32
I_3 (%)	23.24±0.08	20.27±0.08	19.70±0.08	18.79±0.08	18.48±0.07	17.68±0.07	15.11±0.07
R (Å)	3.094±0.006	3.134±0.006	3.133±0.006	3.090±0.007	3.091±0.007	3.086±0.007	3.049±0.007
ν_f (Å ³)	124.1±0.7	129.0±0.8	128.8±0.8	123.6±0.8	123.7±0.8	123.0±0.8	118.8±0.9
f_v (%)	5.19±0.04	4.71±0.05	4.57±0.05	4.18±0.04	4.12±0.04	3.92±0.04	3.23±0.04

The *ortho-positronium* lifetime (τ_3), the longest-lived component and associated with pick off annihilation, is proportional to the free volumes in the materials. The dependence of the lifetimes and the calculated free volume sizes on the poly(BPOCPMA) contents of the products were presented in Figure 4.27 and 4.28, respectively. The coproducts, in general, had the higher lifetime τ_3 values relatively comparing to the copolymers at the corresponding poly(BPOCPMA) contents, Figure 4.27, which shows relatively larger free volumes in the coproducts, Figure 4.28. The presence of poly(BPOCPMA) homopolymer molecules led to larger holes in the amorphous region of the coproducts throughout the compositions. Seemingly, the ungrafted homopolymer molecules played a preventing role from compact packing of the chains in the matrix of the products. Internally, the lifetime τ_3 initially increased with the content in the coproducts, Figure 4.27. 2.33 ± 0.01 ns (2.2% raise) was measured at 3.8% and 7.3% poly(BPOCPMA). This increase in the τ_3 value reveals an about 3.8% enlargement in the free volume with $129.0 \pm 0.8 \text{ \AA}^3$ value at the corresponding contents, Figure 4.28 and Table 4.7. The neat HDPE has the hole size of $124.1 \pm 0.7 \text{ \AA}^3$ at the prevailing conditions. The lifetime τ_3 then reduced to a plateau value 2.28 ± 0.01 ns recorded within 12.7%-25.1% poly(BPOCPMA), the same as observed for unprocessed HDPE. Thus the coproduct samples with those contents have the free volume hole sizes identical to that of pure HDPE. A further increase in the content gave rise to further decrease in the lifetime with 2.23 ± 0.01 ns at 26.7% poly(BPOCPMA), which demonstrates a moreover reduction in the free volume, almost 4.3% decrease with $118.8 \pm 0.9 \text{ \AA}^3$ free volume hole size, with respect to pure HDPE .

In the copolymers, a slight increase in τ_3 value, 0.6% raise with 2.296 ± 0.010 ns at 3.8% poly(BPOCPMA), which illustrates about 1% enlargement in the free volume size was followed by a gradual reduce as the graft percentage increased, Figure 4.27. 2.222 ± 0.010 ns lifetime, almost 2.6% decrease comparing to unprocessed HDPE, was measured within 18.6% - 21.0% poly(BPOCPMA) involving samples. This decrease in the lifetime shows an about 4.8% reduction in the free volume size with $118.1 \pm 0.8 \text{ \AA}^3$ at those percentages, Table 4.6. Thus, the grafting, while leading to relatively smaller increase in the hole size at low percentage of poly(BPOCPMA) (3.8%), resulted in reduced free volume sizes with the increased contents, even smaller than that of neat HDPE, Figure 4.28. It seems

that relatively larger holes were formed in the material at low contents presumably due to larger openings between the chains brought about by the voluminous side groups of the poly(BPOCPMA) molecules that compel the chains laterally, thus prevent close packing. The weak interactions between polar side groups of the graft units and nonpolar HDPE chains might have an additional effect in reducing the compact packing. As the content increases, on the other hand, the interactions between the polar side groups, becoming more effective with content, probably led to more compact packing of the chains, which resulted in reduced free volumes in the material. Furthermore, the bulky side groups which give rise to the larger openings between the chains might have occupied the voids in majority with the increase of the content, owing to the preferred interactions between the polar groups and to the weak interactions between the polar units and nonpolar HDPE chains.

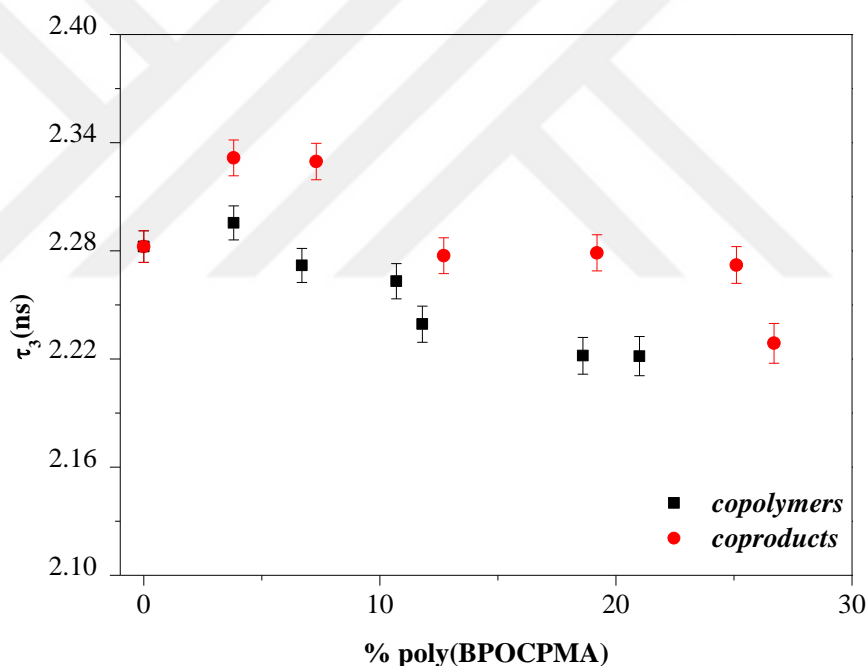


Figure 4.27. The variation of the ortho-positronium lifetime (τ_3) with poly(BPOCPMA) contents in the products

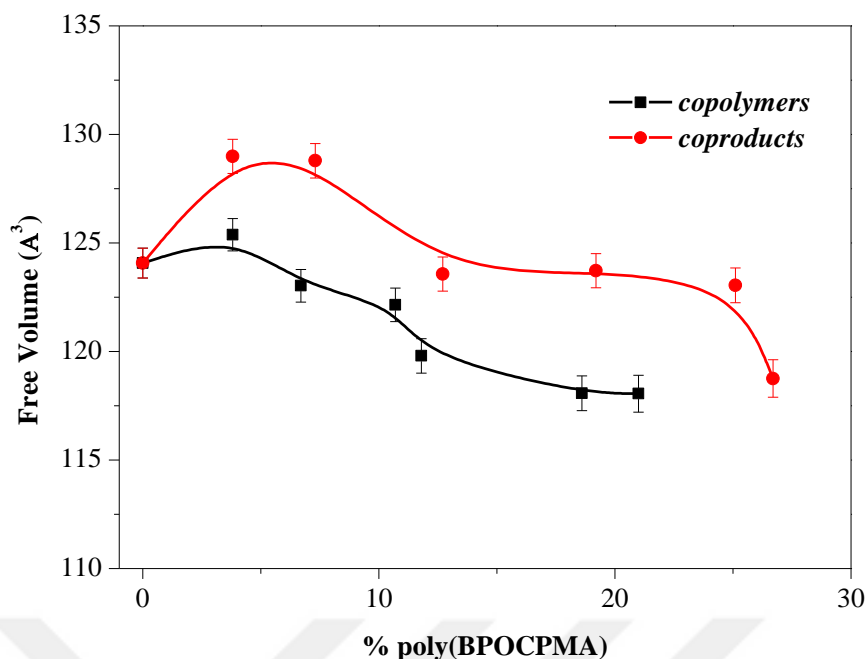


Figure 4.28. The variation of the free volume hole sizes (A^3) with poly(BPOCPMA) contents in the products

In the free volume model, the intensity I_3 is proportional with number of free volume holes, as mentioned above. The number of holes increases with increasing I_3 (Mostafa et al., 2009). The variations of the intensities I_3 , measured in the studies, with poly(BPOCPMA) percentage in the products were plotted in Figure 4.29. The intensities decreased with the percentage in both copolymers and coproducts, more consistently with the content in the former. At lower contents, up to about 10%, decrease trend was approximately similar in both classes of the products. At higher contents, however, the intensity lay about higher in the coproducts compared to copolymers, accordingly revealing the higher the number of free volume holes in coproducts. Thus, the poly(BPOCPMA) homopolymer molecules, besides leading to larger holes in the coproducts by playing a preventing role from compact packing of the chains, as mentioned above, gave rise additionally to the higher the number of the holes in the matrix.

The free volume fractions (f) of the products were calculated by using the equation 3, proposed by Kobayashi et al., (Kobayashi Y et al., 1989) and in which the free volume hole size and the intensity were evaluated together. The dependences of the fractions on poly(BPOCPMA) content were presented in Figure 4.30. The similar decrease trends observed in the intensities were also recorded in the fractions.

Hence, the grafting, while leading to small enlargements in the size of the free volumes at relatively lower percentages of poly(BPOCPMA), Figure 4.28, resulted in dramatic decreases in the free volume fractions with the content, especially in the copolymers. Presumably, the interactions between the polar side groups, becoming more effective with the content, probably led to more compact packing of the chains in the matrix, which results in the reduction of the free volume fraction. The presence of the homopolymer molecules, however, gave rise to a smaller decrease in the fraction, assumingly by playing a preventing role in the compact packing of the grafted HDPE chains in the coproducts.

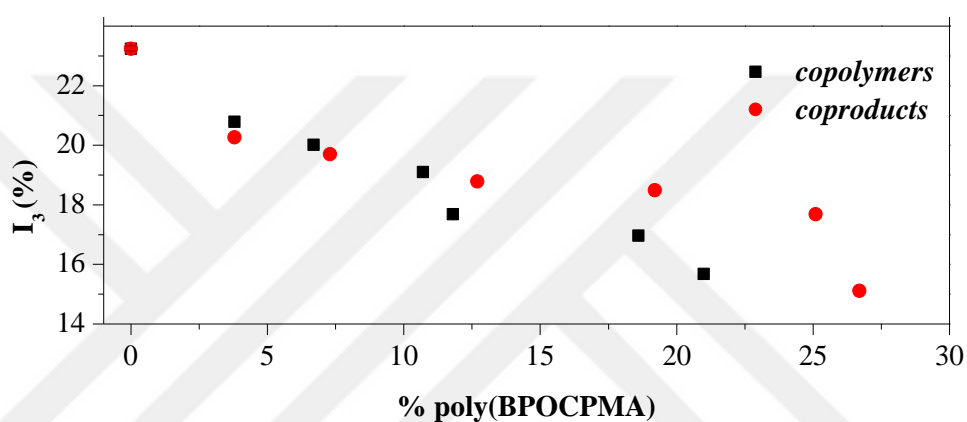


Figure 4.29. The variation of the intensity I_3 with poly(BPOCPMA) content in the products

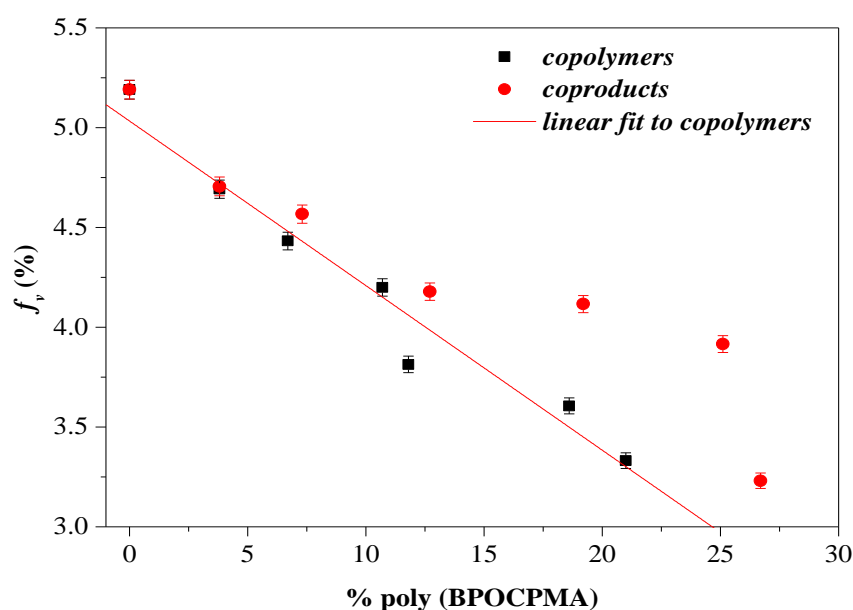


Figure 4.30. The variation of the free volume fraction with poly(BPOCPMA) content in the products

The dependence of the intensities I_1 and I_2 on poly(BPOCPMA) content in the products were plotted in Figure 4.31. In both coproducts and copolymers, while the intensity I_1 decreased almost linearly with the percentage of poly(BPOCPMA), the direct annihilation intensity, I_2 steadily increased with the content.

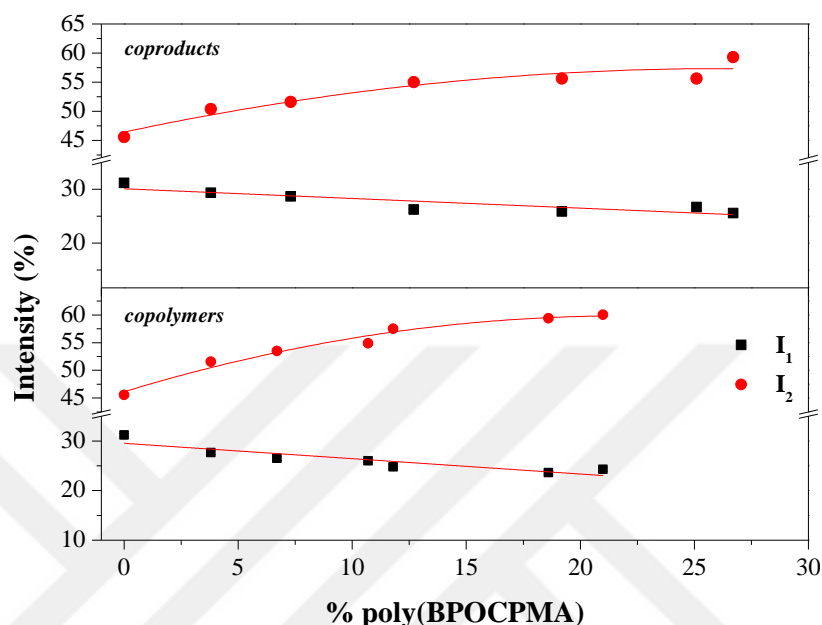


Figure 4.31. The variation of intensities I_1 and I_2 with poly(BPOCPMA) content in the products

Several factors such as crystallinity of polymers, positron mobility and chemical functional groups affect Ps formation in the materials. Carbonyl groups were reported to be the most efficient electron scavenger and Ps inhibitor among the functional groups in organic materials (Abbe et al., 1981); (Duplatre et al., 1985). The positively charged positrons reside and decay in low electron density region (Djourelou et al., 2003). In the products, the poly(BPOCPMA) graft units bear three carbonyl groups per each repeating unit (on the side groups) along the chains. Thus the increases in the poly(BPOCPMA) content in the products might have brought about lowering in electron density due to the electron scavenging role of the carbonyl groups. This effect might potentially lead to the higher direct annihilation thus to the increases in the intensity I_2 and the decreases in the intensity I_1 which arises from annihilation of *para-positronium*.

4.2.4 Mechanical Properties of HDPE Copolymers and Coproducts

The effect of poly(BPOCPMA), a side chain liquid crystalline polymer existing as grafted units in the copolymers and as both grafted and homopolymer molecules in the coproducts, on the mechanical behavior of the material was studied by analyzing the stress-strain and impact behavior of the products. The test samples in dumb-bell shape were prepared by micro-injection molding at 220°C. The processing was optimized at this fairly high temperature, comparing to the melting point of HDPE, due to high viscosity, that is the difficulties in flow behavior of the melts at lower temperatures. Poly(BPOCPMA) with rigid and polar side groups might have caused to a restriction in chain mobility in the products, leading to an increase in the viscosity of the melts during processing. Notwithstanding, the temperature is well below the starting point of decomposition (245-250°) (Sainath et al., 2000). On the other hand, remarkable improvements were achieved in the mechanical properties of the products, particularly, in ultimate tensile strength and modulus. But, percent elongation and yield stress were lost at high contents of poly(BPOCPMA), and brittleness dominated in the mechanical characters.

Typical stress-strain curves of the products from each class and of pure HDPE were illustrated in Figure 4.32.a and b. The extensive cold drawing observed in pure HDPE was not recorded in any of the products even at low contents of the graft units. At low percentages, the samples from both classes failed during strain softening. They exhibited ductile failure with neck formation. The presence of the homopolymer poly(BPOCPMA) molecules in the coproducts, however, has resulted in relatively longer elongations in the softening prior to failure. Apparently, while being observed roughly between 15% and 34% strain in the copolymers, the elongations were seen between about 15% and 46% strain in the coproducts. As mentioned above in the PALS analysis, the homopolymer molecules in the coproducts, besides leading to larger holes in the coproducts, gave rise additionally to the higher the number of the holes in the matrix. It seems that the larger free volumes and their greater fraction conducted to further flow of the molecules in the softening and thus to relatively extensive drawing to longer elongations in the tensile direction. A reduction in resistive frictional force in sliding of the molecules and thus a much easier slip of the chains over each other in the material, when the free holes

between them are larger and their fraction is greater, might account for the observed longer strains in the coproducts. In addition, the larger the free volume, the higher the conformational freedom the molecules have. This freedom might have assisted the chains in taking the required conformations to slide over each other, which resulted in the longer elongations in the tests. The longer elongations were also perceived as wide extensions in the fractographs of the coproduct samples. Some small extensions persisted even at high contents, recorded in SEM analysis of the fracture surfaces. At relatively higher percentages with respect to the extent of grafting results, on the other hand, brittle nature started to prevail in the behaviors. The samples involving about 18% poly(BPOCPMA) in the copolymers and 25% poly(BPOCPMA) in the coproducts failed at the beginning of plastic deformation, just before or at the yield point. At further respective contents, the products then exhibited brittle fracture in the tests. The ductility and brittleness in the samples were also revealed in SEM images. Conclusively, the material revealed a gradual transition from a viscoelastic behavior to a brittle nature with increasing graft content. Seemingly, for this changeover the contributions from two factors might be accounted. As revealed in PALS analysis, the grafting, while leading to small enlargements in the free volume sizes at relatively lower percentages of poly(BPOCPMA), Figure 4.28, resulted in dramatic decreases in the fractions of the volume with the content, especially in the copolymers. Mainly, the probable losses and restrictions in chain mobility, brought about by the decreases in the hole sizes and the fractions have presumably resulted in the brittleness in the samples in the tests. Furthermore, the rigid character of poly(BPOCPMA) molecules at room temperature [with T_g value of 72°C (Sainath et al., 2000)] stemming from its voluminous and rigid side groups with polar nature and thus restricting the plasticity behavior in the products have additionally led to the brittle character in the samples.

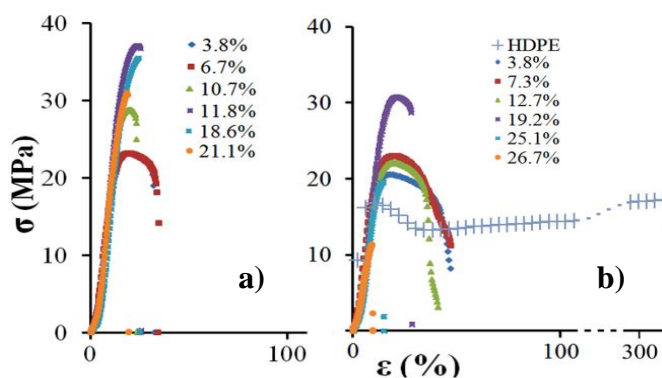


Figure 4.32. Stress-strain curves of, a) the graft copolymers with 3.8, 6.7, 10.7, 11.8, 18.6 and 21.1% poly(BPOCPMA) and b) HDPE and of the coproducts with 3.8, 7.3, 12.7, 19.2, 25.1 and 26.7% poly(BPOCPMA)

The results of the tensile strength measurements of the products were presented in Table 4.8 and 4.9, and drawn in Figure 4.33 and 4.34. The percentage decrease or increase in tensile strength and modulus in tables were given with respect to neat HDPE.

The strength increased initially with poly(BPOCPMA) content in both classes, but, with a better improvement in the copolymers. The maxima, 36.3 MPa (93% improvement compared to pure HDPE) and 31.8 MPa (69% improvement) were achieved with 11.8% poly(BPOCPMA) in the copolymers, and with 19.2% content in the coproducts, respectively. They were then followed by a slow decrease in the former and a relatively severe decline in the latter, Figure 4.33. Almost identical trends were also recorded in Young's modulus, determined on the same samples during the tests. 514 MPa (42% rise) and 479 MPa (32% rise) maximum values were noted at the same respective percentages at which the strength maxima were observed, Figure 4.34. In fact, the maxima in both copolymers and coproducts were achieved with about the same grafted contents. Because, the coproduct containing 19.2% poly(BPOCPMA), at which the maximum were seen, involves about 12% content as grafted units, and hence 7% as homopolymer molecules. The green dotted lines in Figure 4.33 and 4.34 show the variations drawn in this regard, that is, they were depicted by considering only the grafted poly(BPOCPMA) percentage in the coproducts.

Table 4.8. Ultimate tensile strength and Young's modulus of the copolymers with poly(BPOCPMA) content

Specimen	Ultimate Strength (MPa)	Young's Modulus (MPa)
Neat HDPE	18.78	362
3.8% poly(BPOCPMA)	24.69 (+31.47%)	387 (+6.76%)
6.7% poly(BPOCPMA)	26.27 (+39.88%)	433 (+19.58%)
10.7% poly(BPOCPMA)	29.39 (+56.50%)	471 (+30.12%)
11.8% poly(BPOCPMA)	36.30 (+93.29%)	514 (+41.99%)
18.6% poly(BPOCPMA)	33.56 (+78.65%)	455 (+25.79%)
21.0% poly(BPOCPMA)	32.99 (+75.67%)	436 (+20.50%)

Table 4.9. Ultimate tensile strength and Young's modulus of the coproducts with poly(BPOCPMA) content

Specimen	Ultimate Strength (MPa)	Young's Modulus (MPa)
Neat HDPE	18.78	362
3.8% poly(BPOCPMA)	20.65 (+9.96%)	371 (+2.34%)
7.3% poly(BPOCPMA)	21.22 (+12.99%)	369 (+1.99%)
12.7% poly(BPOCPMA)	21.65 (+15.28%)	373 (+2.97%)
19.2% poly(BPOCPMA)	31.77 (+69.17%)	479 (+32.39%)
25.1% poly(BPOCPMA)	19.28 (+2.66%)	402 (+10.94%)
26.7% poly(BPOCPMA)	10.69 (-43.08%)	260 (-28.27%)

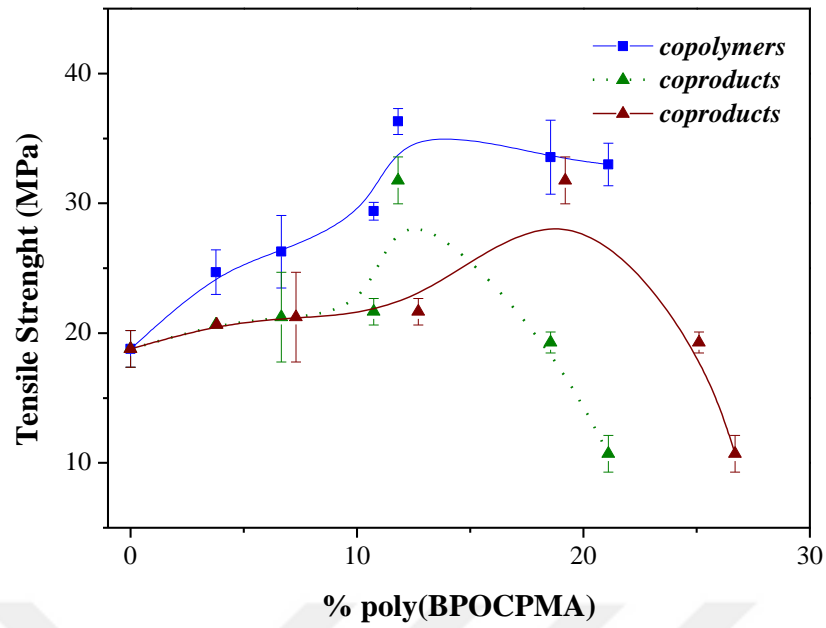


Figure 4.33. The variation of ultimate tensile strength of the products with poly(BPOCPMA) content

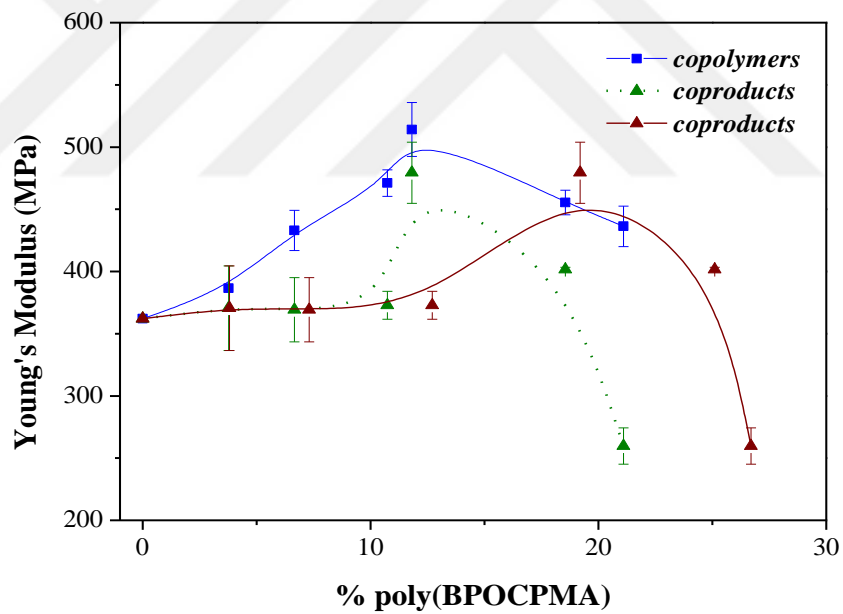


Figure 4.34. The variation of Young's modulus of the products with poly(BPOCPMA) content

Generally, mechanical property of a pure polymer and its free volume are dependent on the crystallinity (hard or soft segments) of the polymer, molecular entanglements, the existing dipole–dipole interactions and hydrogen bonding. Some other factors such as the restricted mobility of the polymer chains, crosslink density,

interfacial interaction, and glass transition also play role (Ponnamma et al., 2015). In a variety of polymer blend or composite studies, the free volume size (hole size) and the free volume fraction were announced to be anti-correlated with the modulus and the tensile strength; that is, the higher the free volume resulted in the lower the tensile strength and the modulus. The correlation between free volume and mechanical properties in natural rubber/multiwalled carbon nanotube composites was investigated by Ponnamma et al. At higher multiwalled carbon nanotube contents, the hindered interaction between the filler and the rubber matrix was reported to lead to higher free volume holes and low tensile strength (Ponnamma et al., 2015). El-Nashar et al. (El-Nashar et al., 2009) studied the relation between the macroscopic properties and the microstructure free-volume properties of acrylonitrile butadiene rubber, ethylene propylene diene rubber, and their blends by using Na bentonite, Ca bentonite and kaolin as fillers. It was declared that the reduction in the size and the fraction of free volume resulted in an improvement in the mechanical properties of the rubber. This behavior was explained by better homogenization introduced in the rubber on addition of fillers, which showed better mechanical and electrical properties. The reduction in the free volume size was attributed to the decrease in chain mobility on the filler surface in the presence of nanosized filler, since it was associated with the macromolecule mobility. The reduction in free volume in styrene butadiene rubber/montmorillonite composites, on the other hand, was reported to be correlated with enhanced interfacial interaction by Wang et al. (Wang YQ et al., 2004). Gomaa et al. studied the relation between free volume parameters such as τ_3 and I_3 and physical properties of polyethylene-nitrile rubber blend. The increase in tensile strength and hardness was found to be oppositely correlated with free volume parameters with the addition of nitrile rubber resulting in lower τ_3 and I_3 (Gomaa et al., 2003).

It seems that the mechanical behaviors of the products were largely governed by their free volume properties. Firstly, superior tensile behaviors were recorded in the products that have lower free volume size and fraction, that is, in copolymers comparing to coproducts, even in the case when the products have similar contents of poly(BPOCPMA). Moreover, a strong relation was observed between the free volume fraction and the tensile properties of the copolymers. The improvements in the tensile behaviors were firmly accompanied with the reductions in the free volume

fraction. Especially, it is very striking that, when the content increased from 10.7% to 11.8% poly(BPOCPMA) in the copolymers, the sharp increase in the tensile strength (from 29.9 MPa to 36.30 MPa) and the modulus (from 471 MPa to 514 MPa) were accompanied with the abrupt drop in the free volume fraction (from 4.20% to 3.81%), Table 4.6 and 4.8. At relatively high contents of poly(BPOCPMA), that are above about 12% in copolymers and about 19% in coproducts, however, the strength and modulus decreased with the reduction in the free volume fraction. A conceivable explanation for the observed free volume dependency of the mechanical behaviors lies on the assumptions that the resistive frictional force in sliding of the molecules over each other will be lower when the free holes between them are larger and their fractions are greater. Thus, a much easier slip of the chains would customarily be expected in the material. In addition, the larger the free volume, the higher the conformational freedom the molecules have. This freedom might have assisted the chains in taking the required conformations to slide over each other with less effort. Consequently, an increase in the resistive frictional force between the molecules and a lower conformational freedom arising from the decrease in size and fraction of the free holes, might have made the chains more resistive in sliding over each other. This effect, thus, might have made the material superiorly withstanding under load and more resistive against deformation. A remarkable support to this commentary was received in strain behaviors in the tensile tests. As mentioned above, longer strains were accompanied with greater free volume fraction. That is, the greater size and fraction in the free holes conducted to further flow of the molecules in the softening and thus to further elongations in the tensile direction.

In the improvements of the tensile behaviors mentioned above, the developments in the alignment and orientation of HDPE chains due to the constitution of side chain LCP poly(BPOCPMA) molecules as graft units might also play role. As discussed in the interpretation of the thermal behaviors, a promoted ordering and orientation of HDPE chains, conducted by poly(BPOCPMA) molecules with the potential of forming so regularly organized structure as glassy nematic arrangement (Sainath et al., 2000) might have given rise to advanced tensile behaviors as well to increased melting temperatures of crystalline domains of the HDPE matrix. These comments on the structural advances have also been supported by the fibrillar and oriented structures observed in SEM analysis of the fracture

surfaces. This was, in fact, what proposed at the beginning of this study. It is noteworthy, on the other hand, the microstructural variations, namely, the lateral expansions in the unit cell dimensions for the consequential improvements. The initial increase trends in the melting temperature and in the tensile behaviors were accompanied with the enlargements in the *a* and *b* unit cell parameters. Conveniently, the higher chain mobility in the larger *ab* basal area might have cooperated with cohesive forces of the polar graft units, played an efficient role in conducting to better arrangement of HDPE chains, and thus had an influential contribution to the achievement of the resulting improvements.

The presence of the homopolymer molecules in the coproducts, on the other hand, led to relatively lower improvements in the initiatory increase trends and to relatively sharp decreases after the maxima. The changes in free volume size and fraction might also have played a dominant role in the stationary behavior in the tensile strength of the coproducts, between 20.65 - 21.65 MPa and in the corresponding modulus, along with the percentages 3.8% - 12.7%. In accordance with the explanations given above, the strength might be expected to increase due to the reduction in the fraction of free volume with the content of poly(BPOCPMA). However, the size of the free volume enlarged at the corresponding contents in spite of the decreases in its fraction. Moreover, great enlargements were also recorded in the *ab* basal area of the HDPE unit cells. These enlargements, that are, the increases in the size of the free holes and the basal area of the unit cells normal to the chain axes in the HDPE matrix, thus, might have led to the stationary tensile behavior at the corresponding contents. In addition, a low tensile load capacity of poly(BPOCPMA) molecules might have contributed to both the decreases in the tensile behaviors after the maxima and the relatively lower advances in the properties of the coproducts. Because, a polymer composed of the chains with so large and rigid side groups is very difficult to exhibit appreciable withstanding under the load with respect to HDPE. Consequently, this might have made the material less prone to resist in tensile tests at high contents. With the same line of reasoning, the inclusion of the homopolymer molecules in the coproducts might have brought about relatively lower improvements in the properties comparing to the copolymers.

The impact behavior of the products was investigated by Izod impact test. The results of the tests were given in Table 4.10. In spite of the brittleness revealed in tensile tests at high contents, almost all the samples from the both classes were not broken in the tests, except for the coproduct with 26.7% poly(BPOCPMA). The improvements in the impact behavior were accompanied with the reductions in the free volume fraction. Furthermore, the improvements in alignments and orientations in the structure of the material owing to the constitution of such regularly organized poly(BPOCPMA) graft units might also contribute to the advances in the impact behavior of the samples. This was supported by the extensive fibrillar structure with ductile extensions at lower contents and the existence of small and thin fibrils even at high contents of poly(BPOCPMA), revealed in the impact fractographs. Conversely, poly(BPOCPMA) homopolymer molecules might additionally contribute to the brittleness of the products. Because, the homopolymer molecules with so rigid and large side groups and thus with a high T_g value (72°C) (Sainath et al., 2000) can conventionally be expected to exhibit a lower resistance to break. This brittleness in nature of the homopolymer, seemingly made a negative contribution to the impact behavior of the coproducts.

Table 4.10. Impact strength of the products with % poly(BPOCPMA) content

Copolymers	Impact strength (kJ/m²)	Coproducts	Impact strength (kJ/m²)
Neat HDPE	Not Broken	Neat HDPE	Not Broken
3.8% poly(BPOCPMA)	Not Broken	3.8% poly(BPOCPMA)	Not Broken
6.7% poly(BPOCPMA)	Not Broken	7.3% poly(BPOCPMA)	Not Broken
10.7% poly(BPOCPMA)	Not Broken	12.7% poly(BPOCPMA)	Not Broken
11.8% poly(BPOCPMA)	Not Broken	19.2% poly(BPOCPMA)	Not Broken
18.6% poly(BPOCPMA)	Not Broken	25.1% poly(BPOCPMA)	Not Broken
21.0% poly(BPOCPMA)	Not Broken	26.7% poly(BPOCPMA)	12.06

4.3 Graft Copolymerization of BPOCPA and BPOCPMA onto IPP

Thermally initiated graft copolymerization of BPOCPA and BPOCPMA onto IPP were studied at 160°C and for 50 minutes reaction time. Variation of grafting with the mixing ratio of the monomers and IPP in the reaction mixtures were investigated with six different monomer/IPP ratios. The contents of poly(BPOCPA) and poly(BPOCPMA) in the products were also determined gravimetrically, as were for the grafting products with HDPE. The dependence of poly(BPOCPA) and poly(BPOCPMA) contents in the graft copolymers and coproducts on the monomer concentrations in the reaction mixtures were presented in Table 4.11 and Table 4.12, respectively. The dependencies were drawn in Figure 4.35 and 4.36, and the variations in percent graftings in Figure 4.37 and 4.38, respectively.

In both product classes similar behavior was observed from the viewpoint of grafting extent. In the copolymers, at relatively lower monomer/IPP ratios, the extent of grafting increased with monomer concentration in the reaction mixture, and reached 9.6, 10.9 and 10.6% poly(BPOCPA), forming almost a plateau at about 10% poly(BPOCPA), with 20, 30 and 40% BPOCPA, respectively. In poly(BPOCPMA)-g-IPP copolymers, on the other hand, the increase in the amount of grafting at lower BPOCPMA/IPP ratios was maintained at higher concentrations of the monomer, but with relatively smaller increments. The contents, 7.3, 8.9 and 10.3% poly(BPOCPMA) were achieved with 20, 30 and 40% BPOCPMA, respectively. In the coproducts, however, the amount of both poly(BPOCPA) and poly(BPOCPMA) units present increased almost linearly with monomer concentrations in the reaction mixtures, Figure 4.35 and 4.36. That is, the polymerizations took place with high conversions. Nevertheless, the extents of grafting were not proportional with the conversions, and the percent grafting decreased with monomer concentrations in both classes, Figure 4.37 and 4.38. The maxima, 76.8% and 69.1% grafting, achieved with 5% both BPOCPA and BPOCPMA, respectively, were followed by dramatic decreases with monomer concentrations in both products. These results revealed that the grafting took place via the radicals forming on IPP chains in majority, rather than the reactions between propagating poly(BPOCPA) and poly(BPOCPMA) radicals and IPP chains. It seems that the higher probability of radical formation on IPP chains at relatively lower monomer concentrations essentially resulted in higher

grafting efficiencies on IPP chains. Steric hindrance created by crowded and polar side groups of poly(BPOCPA) and poly(BPOCPMA) units, on the other hand, are presumed to account for the observed decreases in the grafting yields.

Table 4.11. The dependence of poly(BPOCPA) content in the products on the BPOCPA percentage in the reaction mixture

% BPOCPA in reaction mixture	5%	10%	15%	20%	30%	40%
% Poly(BPOCPA) in the copolymers	3.8	6.2	7.6	9.6	10.9	10.6
% Total Poly(BPOCPA) in the coproducts	4.0	7.3	12.3	17.4	28.4	39.0
% Grafting	76.8	63.7	50.0	48.4	32.0	15.9

Table 4.12. The dependence of poly(BPOCPMA) content in the products on the BPOCPMA percentage in the reaction mixture

% BPOCPMA in reaction mixture	5%	10%	15%	20%	30%	40%
% Poly(BPOCPMA) in the copolymers	3.3	5.1	6.6	7.3	8.9	10.3
% Total Poly(BPOCPMA) in the coproducts	4.6	9.5	14.0	18.8	27.9	37.8
% Grafting	69.1	50.0	39.9	30.3	22.8	17.4

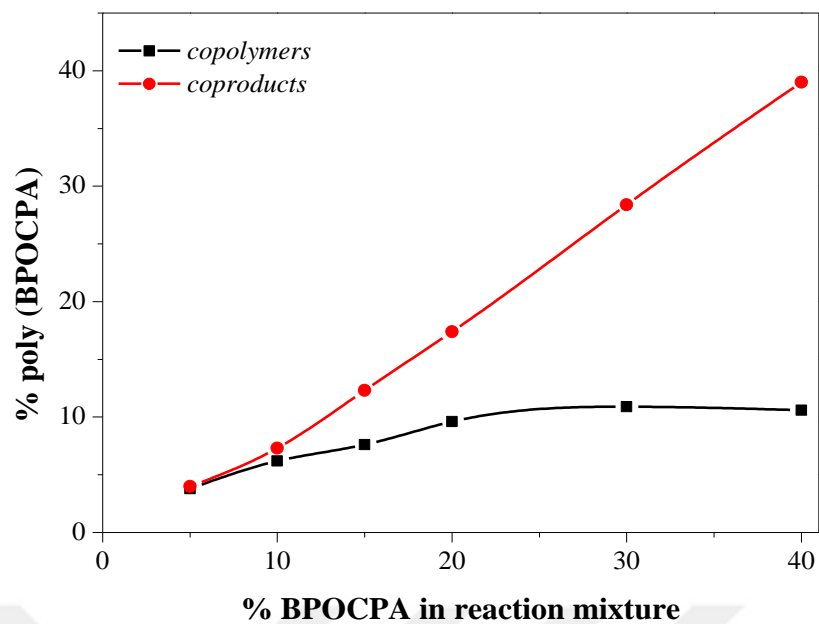


Figure 4.35. The variation of poly(BPOCPA) content in the products with the BPOCPA percentage in the reaction mixture

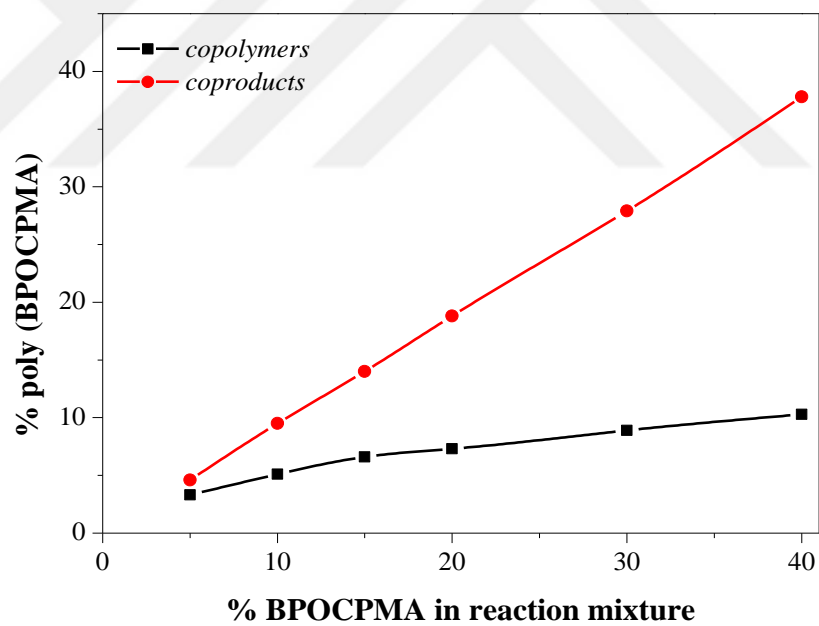


Figure 4.36. The variation of poly(BPOCPMA) content in the products with the BPOCPMA percentage in the reaction mixture

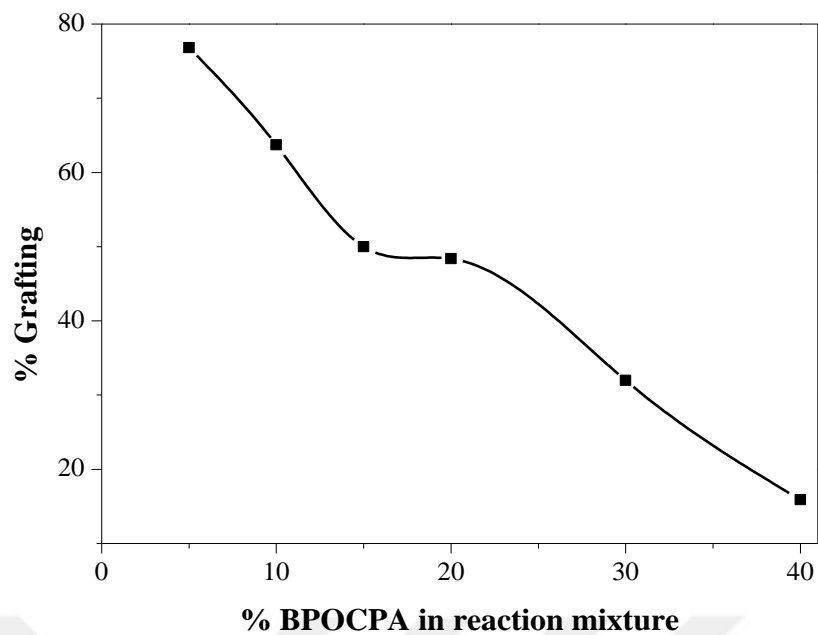


Figure 4.37. The variation of percent grafting of poly(BPOCPA) with the percentage of BPOCPA in the reaction mixture

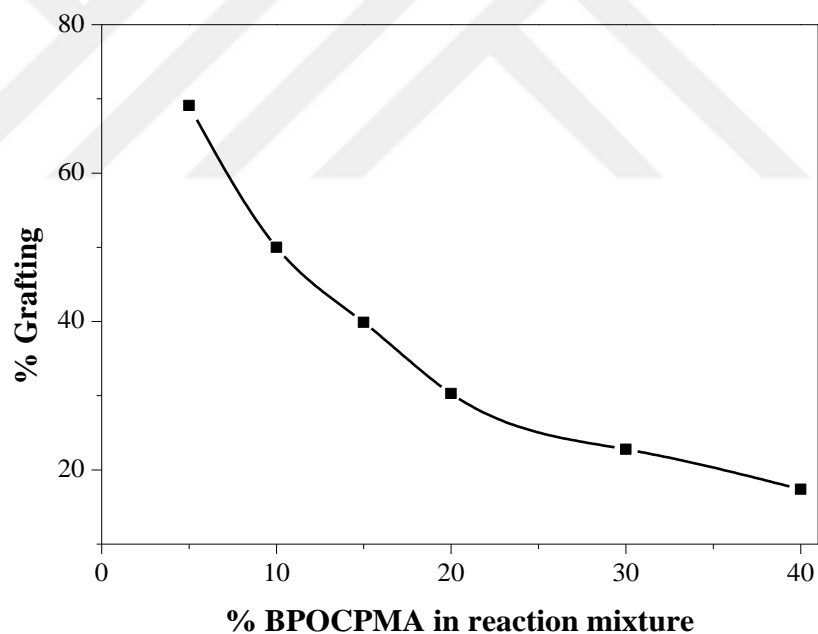


Figure 4.38. The variation of percent grafting of poly(BPOCPMA) with the percentage of BPOCPMA in the reaction mixture

The variation of grafting upon changing the initiator (dicumyl peroxide) concentration was also studied at 160°C for 50 minutes and for constant mixing ratio of BPOCPA in the reaction mixture, that is 30%. The dependence of poly(BPOCPA)

content in the copolymers on the initiator concentration is presented in Table 4.13, and drawn in Figure 4.39.

The gravimetric analyses of the products displayed that poly(BPOCPA) content in the copolymers decreased consistently with the increase of DCP percentage in the reaction mixture. Two major factors might lead to this decreasing trend of poly(BPOCPA) content. Firstly, recombination reactions between the macroradicals might be significant as concentration of DCP increased, which customarily resulted in the decreases in the efficiency of the initiator. Secondly, the proportion of the poly(BPOCPA) homopolymer formation instead of grafting might be raised due to higher concentration of the initiator.

Table 4.13. The dependence of poly(BPOCPA) content in the copolymers on the initiator concentration

% DCP in reaction mixture	1%	2%	3%	4%
% BPOCPA in reaction mixture	30%	30%	30%	30%
% Poly(BPOCPA) in the copolymers	11.6%	10.9%	10.7%	8.9%
% Grafting	38.5	32.0	27.5	22.8

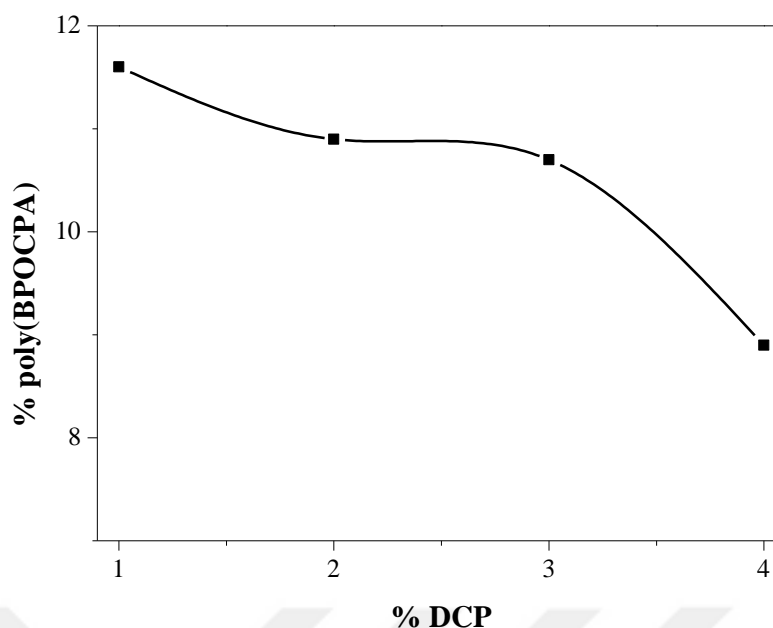


Figure 4.39. The variation of poly(BPOCPA) content in the copolymers with the concentration of DCP in the reaction mixture

4.3.1 FTIR Characterization of the Products

The graft copolymerization of the monomers BPOCPA and BPOCPMA onto IPP was confirmed by FTIR analysis. The characteristic absorption bands of poly(BPOCPA)-g-IPP and poly(BPOCPMA)-g-IPP, due to C=O stretching vibrations of the ester ($1747\text{-}1741\text{ cm}^{-1}$) and benzophenone groups ($1658\text{-}1653\text{ cm}^{-1}$), aromatic C=C stretching vibrations ($1600\text{-}1597\text{ cm}^{-1}$ and $1512\text{-}1502\text{ cm}^{-1}$), esteric C-O-C stretching vibrations ($1271\text{-}1262\text{ cm}^{-1}$ and $1203\text{-}1197\text{ cm}^{-1}$) and of the aliphatic groups due to IPP and main chain of poly(BPOCPA) and poly(BPOCPMA) units ($2958\text{-}2953\text{ cm}^{-1}$, $2924\text{-}2920\text{ cm}^{-1}$, $2877\text{-}2870\text{ cm}^{-1}$ and 2839 cm^{-1}) were also observed in the FTIR spectra of the products, Figure 4.40 - 4.43.

Because of insolubility of the products, poly(BPOCPA)-g-IPP and poly(BPOCPMA)-g-IPP in any solvent, NMR analysis could not be carried out.

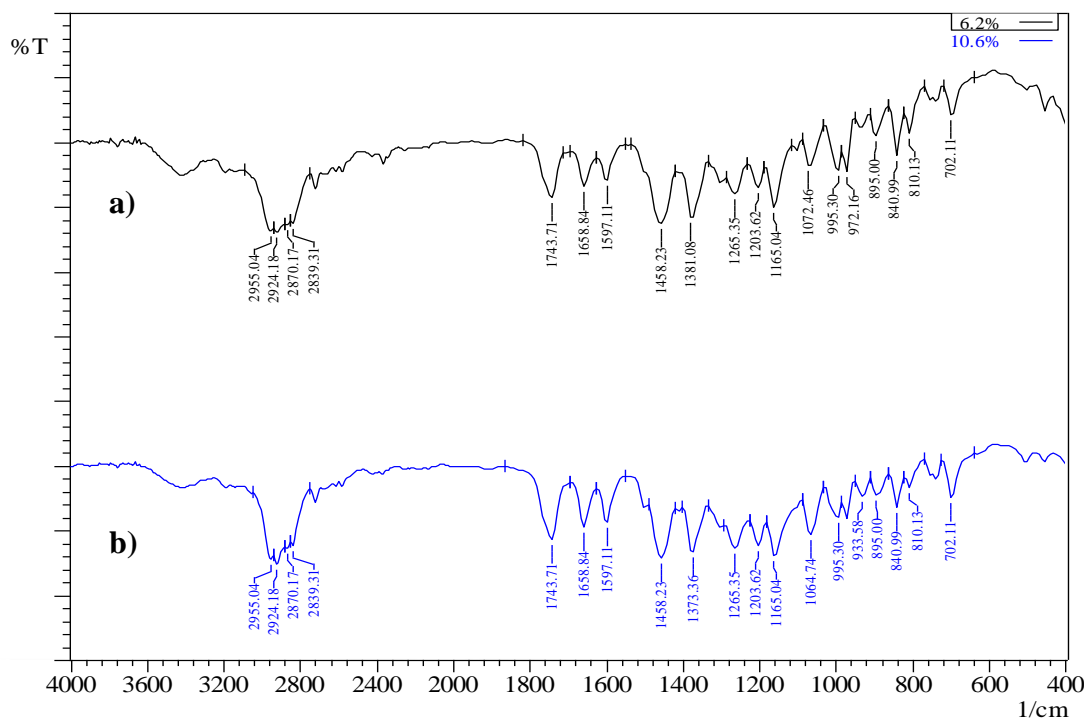


Figure 4.40. FTIR spectra of the copolymers with a) 6.2% poly(BPOCPA), and b) 10.6% poly(BPOCPA)

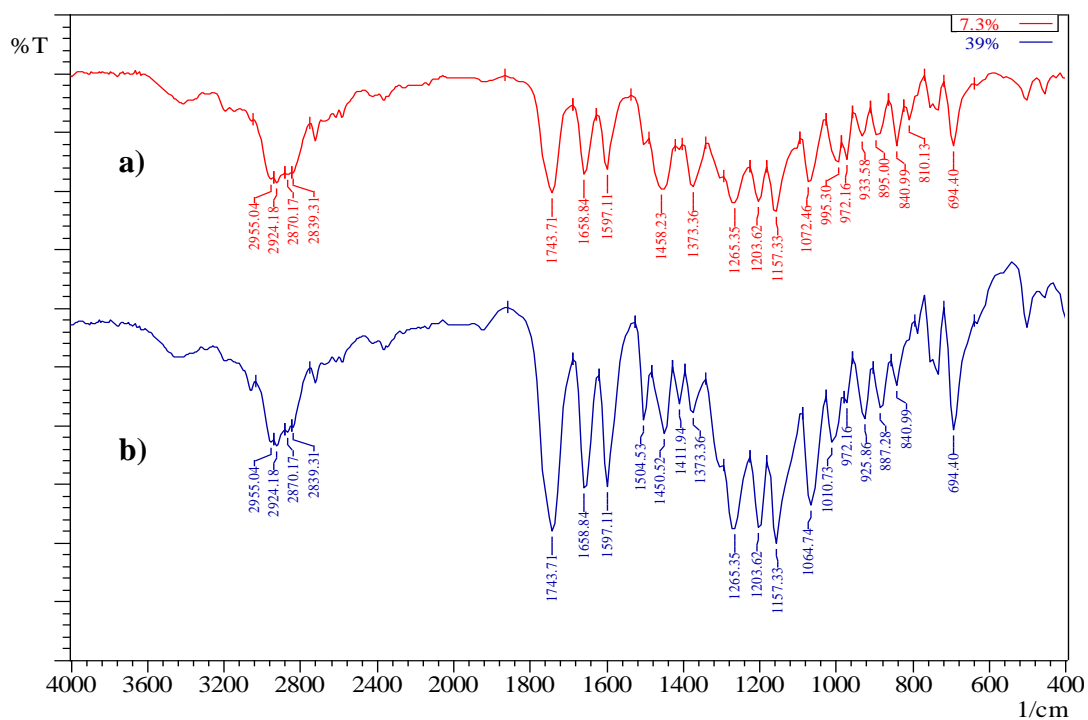


Figure 4.41. FTIR spectra of the coproducts with a) 7.3% poly(BPOCPA), and b) 39% poly(BPOCPA)

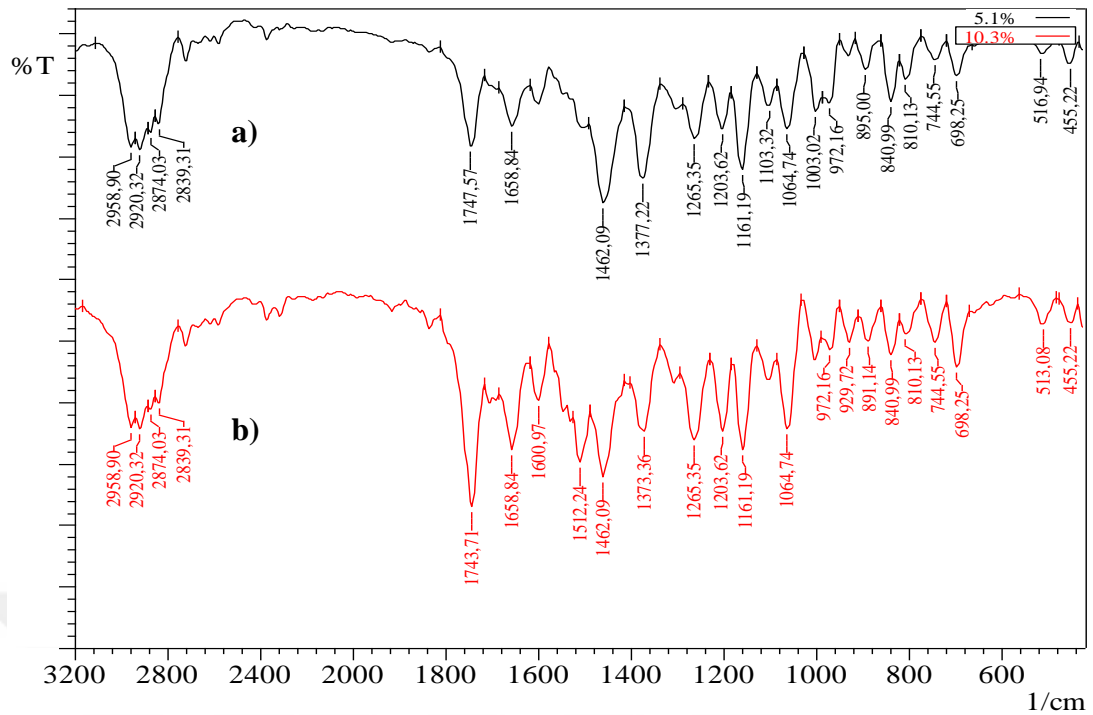


Figure 4.42. FTIR spectra of the copolymers with a) 5.1% poly(BPOCPMA), and b) 10.3% poly(BPOCPMA)

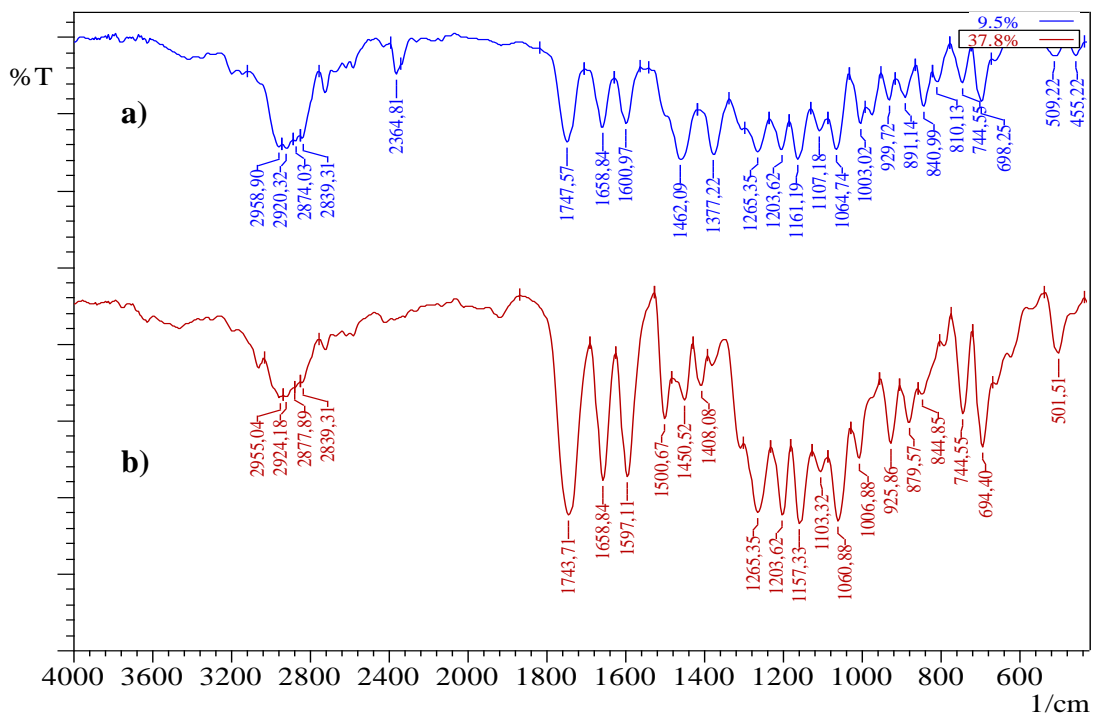


Figure 4.43. FTIR spectra of the coproducts with a) 9.5% poly(BPOCPMA), and b) 37.8% poly(BPOCPMA)

4.3.2 DSC and X-Ray Characterization of The Products

In order to find out the effect of graft copolymerization of BPOCPA and BPOCPMA onto IPP on the thermal and crystallization behavior of the coproducts and copolymers, the product samples were also analyzed by DSC and XRD. The DSC thermograms of the products were obtained under nitrogen atmosphere and with a heating rate of 10°C/min.

Isotactic polypropylene crystallizes in at least three different crystalline forms: α (monoclinic), β (hexagonal), and γ (triclinic). α form, arranged on monoclinic unit cell, is the most stable and conventional form, and can be easily obtained by crystallization from melt or solution (Cetin and Tinçer, 2007). The isotactic polypropylene used in the experiments was in the α form, verified by XRD experiments which displayed the reflections with the Bragg's angles (2θ) varying from 10° to 40°, characteristic of the form, Figure 4.44. The α crystal arrangement has been conserved in the products throughout the graft copolymerization experiments, verified by the X-ray diffraction studies (Section 4.3.3).

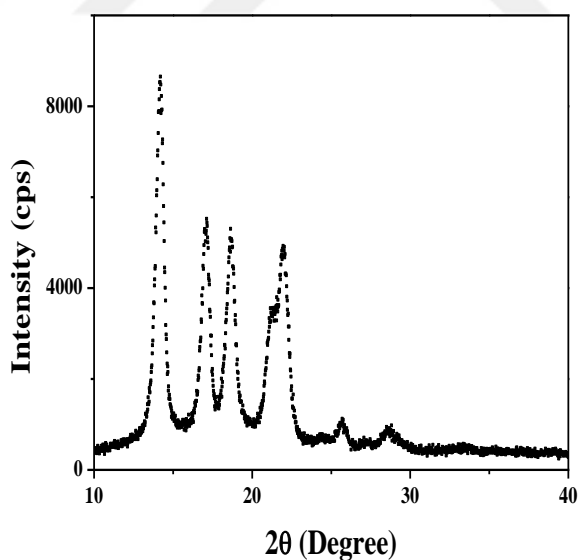


Figure 4.44. The XRD pattern of pure IPP

4.3.2.1 Melting and Crystallization Behavior of Poly(BPOCPA)-g-IPP Copolymers and The Coproducts

Any endotherm attributable to the crystalline melting of the graft poly(BPOCPA) units was not detected in the thermograms of the products. The melting temperature of the homopolymer was 231°C, determined in earlier measurement, Figure 4.9. On the other hand, the graft copolymerization resulted in the increases in the melting temperature of IPP, Figure 4.45 and 4.46, significantly and remarkably in some samples. It was observed between 164.9°C, recorded with the copolymer involving 7.6% poly(BPOCPA), and 169.5°C, measured with the coproduct comprising 39% poly(BPOCPA).

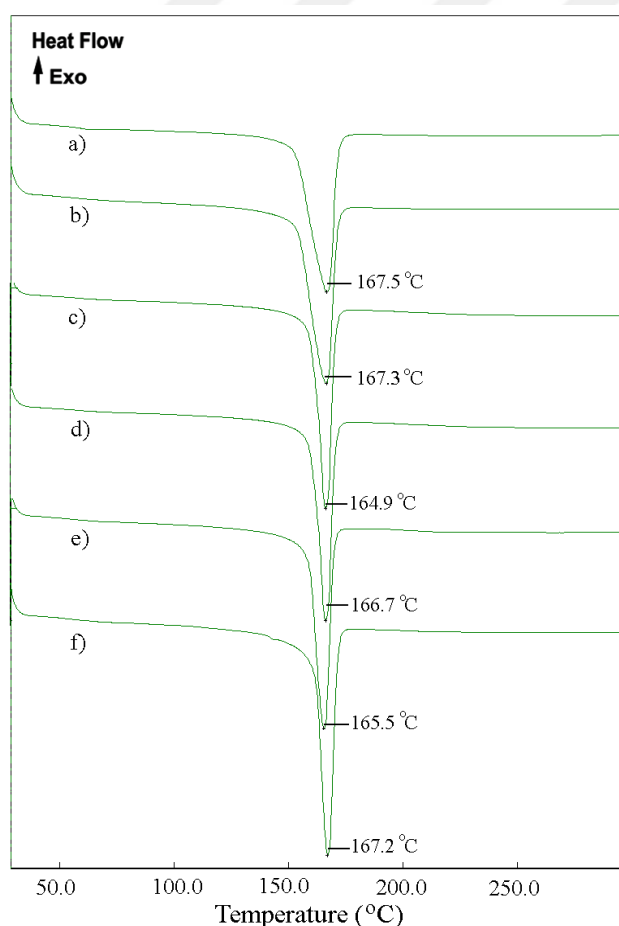


Figure 4.45. The DSC thermograms, obtained with a heating rate of 10°C/min under N₂ atmosphere, of the poly(BPOCPA)-g-IPP copolymers with a) 3.8% poly(BPOCPA), b) 6.2% poly(BPOCPA), c) 7.6% poly(BPOCPA), d) 9.6% poly(BPOCPA), e) 10.9% poly(BPOCPA), and f) 10.6% poly(BPOCPA)

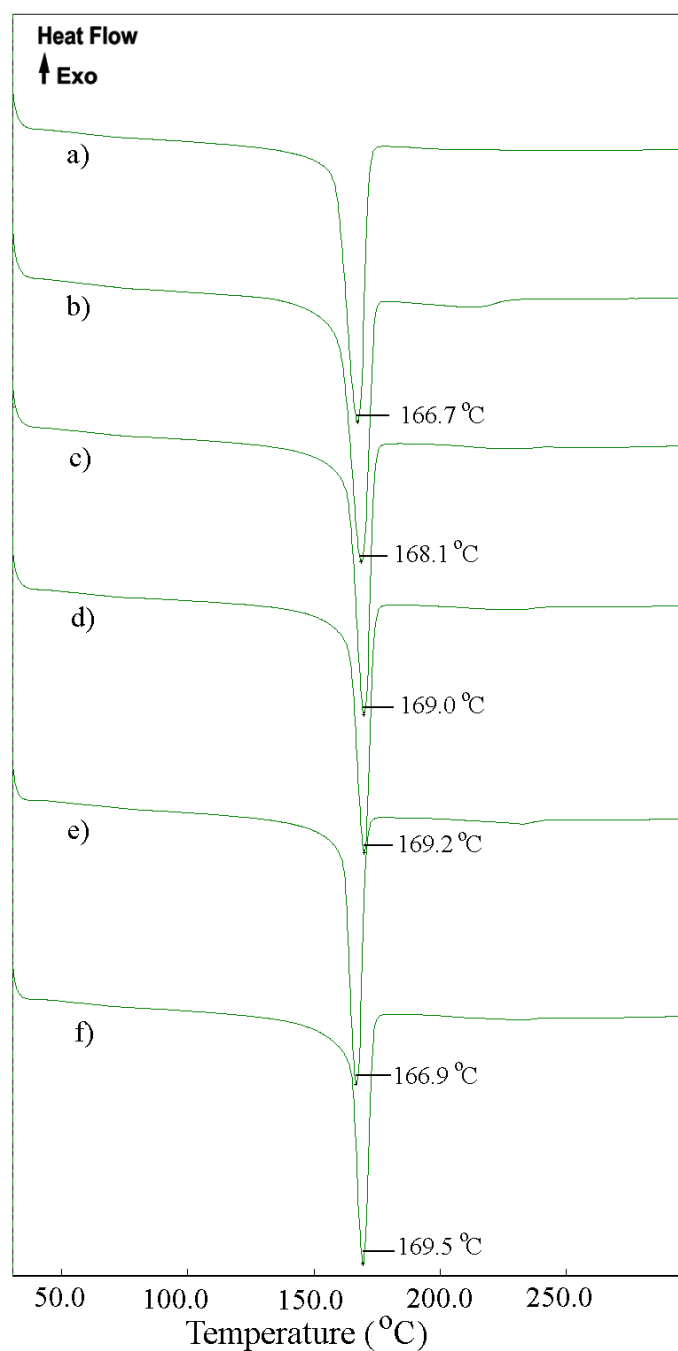


Figure 4.46. The DSC thermograms, obtained with a heating rate of 10°C/min under N₂ atmosphere, of the coproducts with a) 4.0% poly(BPOCPA), b) 7.3% poly(BPOCPA), c) 12.3% poly(BPOCPA), d) 17.4% poly(BPOCPA), e) 28.4% poly(BPOCPA), and f) 39.0% poly(BPOCPA)

In the melting behavior of the products presented above a combination of two opposing factors contributing simultaneously may be effective within the range of concentrations studied. The LCP phase stimulating a range of crystalline structures (heterogeneous phase nucleation) of different sizes and shapes of the IPP may lead to

the breakdown of the crystal structure of IPP and the consequent behavior in the melting temperature can be observed. The broadening of the softening range may possibly be due to a range of widely different sizes of the crystal structures, which increase by increasing proportions of LCP. Thus, it may be assumed that the effect of crystallinity in the ultimate blends remains almost identical to that of the virgin PP, which, in effect, might have compensated the high melting point of stereoregular isotactic PP (Mandal et al., 2003). Regarding this explanation, heterogeneous phase nucleation might occur due to grafting of the side chain LCPs, and different sizes of crystalline structures might be effective, leading to dispersed melting temperatures compared to IPP. Also, this heterogeneous nucleation might have given rise to changes in crystallinity of products. According to the crystallization theory, the process of crystallization takes place in two stages: nucleation of individual crystals and their subsequent growth. Each stage occurs at a characteristic rate and both the processes contribute to the overall rate of crystallization, considered as the mass of the crystalline material formed from the melt in unit time. The rate of the nucleation stage determines the number of nuclei which arise per unit mass per unit time, while the rate at which the crystal growth front progresses in units of velocity, accounts for growth. The faster the nucleation process, the higher will be the nucleation density and hence the average diameter of spherulites will become smaller. Nuclei smaller than the critical nucleus are continuously formed and disrupted in the melt, whereas those of critical dimensions are able to grow. Depending on the chemical composition of the nuclei, the nucleation may be homogeneous or heterogeneous. In the first case, the atoms which aggregate to form a nucleus arise from the polymer chains themselves, while an extraneous nucleating particle (like impurities, catalyst residues, chain end groups, etc.) act as a nucleus in the heterogeneous nucleation type. In order that foreign particles are able to act as nucleating agents, the interfacial energy between their surface and the polymer crystal must be very low (Avella et al., 1997).

DSC thermograms of the poly(BPOCPA)-g-IPP copolymers produced upon changing DCP concentration for constant mixing ratio of BPOCPA in the reaction mixture (30%) were shown below. While single melting endotherms were seen in the thermograms of the products obtained by using 2% DCP, as presented in Figures 4.45 and 4.46, and by using 1% DCP, Figure 4.47.a, double melting endotherms

were observed for the samples when initiator concentration was increased from 2% to 3-4% in the productions. The first melting peak, seen as shoulder, was at about 163°C, and the second at about 170°C, Figure 4.47.b and c.

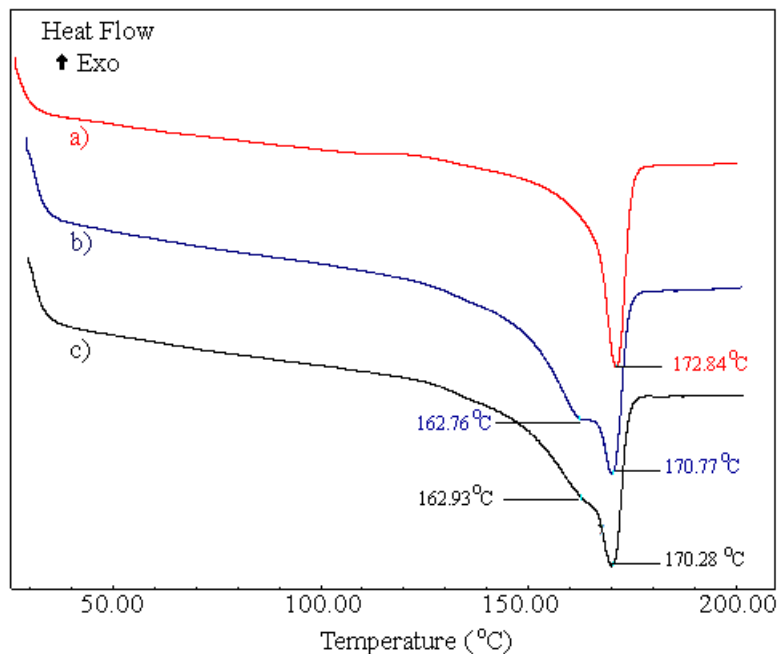


Figure 4.47. DSC thermograms, obtained with a heating rate of 10°C/min under N₂ atmosphere, of the poly(BPOCPA)-g-IPP copolymers produced by using the initiator a) 1% DCP, b) 3% DCP, and c) 4% DCP

The crystalline forms α , β and γ of polypropylene denote different crystallographic symmetries. All the forms are constituted from chains in a₃₁ helical conformation with a common repeat distance (approximately 6.5 Å), but differentiate in unit cell symmetry, structural disorder and inter-chain packaging. The α -form is arranged on a “monoclinic unit cell” and characterized by the changes in b-axis direct, of layers parallel to the ac-plane and composed of left handed (L) or right-handed (R) helices. The position of methyl groups in IPP are at down or up sides, and the changes in the position affect α -phase of polypropylene, leading to α_1 or α_2 modification. Two limiting structures were postulated for the α form: a disordered limiting structure (α_1) with the corresponding crystallographic symmetry being C2/c and an ordered limiting structure (α_2) having crystallographic symmetry being P2₁/c (Pae and Sauer, 1968; Guerra et al., 1984). Reported that isotactic polypropylene may exhibit two melting endotherms in DSC, even if the sample is composed of only

the α form (Guerra et al., 1984). The first peak of two melting endotherms observed at low heating rates on the samples of isotactic PP (α form) was attributed to the melting of crystals having a structure with α_1 modification and the second one was related to the melting of crystals with a structure nearer to α_2 modification (Guerra et al., 1984).

In the thermograms of the samples produced by using 3% and 4% DCP, Figure 4.47, the first peak observed as shoulder at about 163°C probably denotes the melting of the crystals with α_1 modification. The second peak recorded at about 170°C presumably represents the melting of the crystals with α_2 modification.

The percent crystallinities in the IPP matrices of the products were calculated by using the DSC thermograms and the equation given below:

$$X_c(\%) = \frac{\Delta H_f}{\Delta H_f^\circ} \times 100$$

In this equation; ΔH_f is heat of fusion of sample, ΔH_f° is heat of fusion of 100% crystalline IPP (209 J/g) (Costa et al., 2007). The measured crystalline melting temperatures of the products, the heat of fusion values and the calculated percent crystallinities were presented in Table 4.14 and 4.15, and the variations in percent crystallinity with poly(BPOCPA) content in both copolymers and coproducts were plotted in Figure 4.48.

The DSC analyses indicated that percent crystallinity in the IPP matrices increased with poly(BPOCPA) content in the copolymers at low percentages and reached the maximum 64.3% crystallinity (IPP used in the studies had 43.3% crystallinity) with the copolymer involving 9.6% poly(BPOCPA). The crystallinity then decreased at further contents. On the other hand, the presence of homopolymer molecules in the coproducts led to slightly smaller or comparable crystallinities in the products, except for the coproduct with 57% crystallinity and comprising 39% poly(BPOCPA). It could be hypothesized that the constitution of the reported side chain LCP poly(BPOCPA) molecules as graft units on IPP chains, with such regularly organized glassy nematic structure (Sainath et al., 2000) presumably led to the increases in the crystallinities at low contents up to 9.6% poly(BPOCPA). The regularly organized poly(BPOCPA) units might have acted as nucleating agents,

conducting to more ordered packing of IPP chains in crystallites and resulting in the high crystallinities. At relatively high contents, the extensive nucleating due to increases in the content of the graft units, which might impede the growth of the crystals, and polar interactions between the graft units probably prevented the increases in the crystallinities, which also account for the lower crystallinities in the coproducts.

Table 4.14. DSC results with poly(BPOCPA) percentages in the copolymers (The crystalline melting temperatures, T_m , enthalpy of fusions, ΔH_m and the percent crystallinities, X_c (%))

Sample	T_m (°C)	ΔH_m (J/g)	X_c (%)
Neat IPP	164.1	90.42	43.26
3.8% poly(BPOCPA)	167.5	102.00	48.79
6.2% poly(BPOCPA)	167.3	103.80	49.66
7.6% poly(BPOCPA)	164.9	114.40	54.73
9.6% poly(BPOCPA)	166.7	134.40	64.29
10.9% poly(BPOCPA)	165.5	92.60	44.31
10.6% poly(BPOCPA)	167.2	84.81	40.58

Table 4.15. DSC results with poly(BPOCPA) percentages in the coproducts (The crystalline melting temperatures, T_m , enthalpy of fusions, ΔH_m and the percent crystallinities, X_c (%))

Sample	T_m (°C)	ΔH_m (J/g)	X_c (%)
Neat IPP	164.1	90.42	43.26
4.0% poly(BPOCPA)	166.7	89.75	42.94
7.3% poly(BPOCPA)	168.1	85.35	40.84
12.3% poly(BPOCPA)	169.0	83.18	39.80
17.4% poly(BPOCPA)	169.2	92.60	44.31
28.4% poly(BPOCPA)	166.7	85.66	40.98
39.0% poly(BPOCPA)	169.5	119.10	56.97

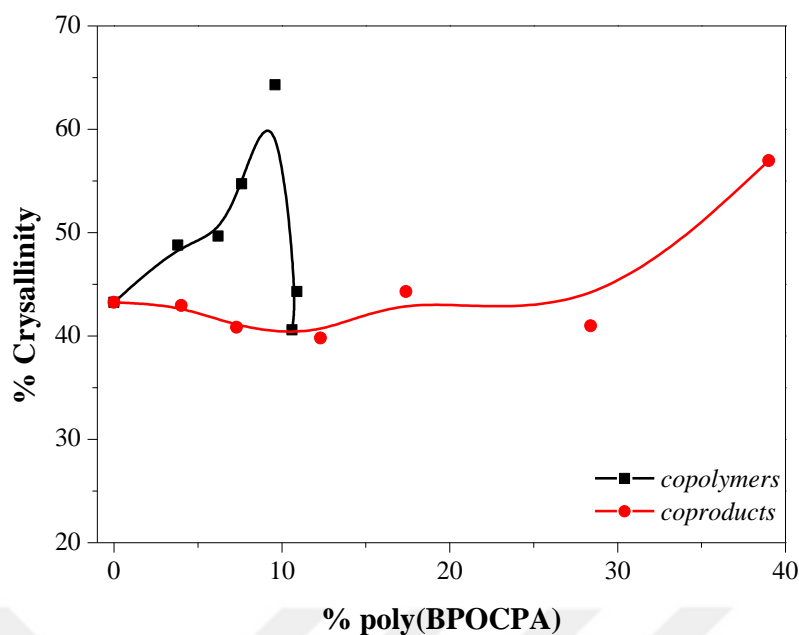


Figure 4.48. The variation of percent crystallinity with poly(BPOCPA) content in a) copolymers, and b) coproducts

4.3.2.2 Melting and Crystallization Behavior of Poly(BPOCPMA)-g-IPP Copolymers and The Coproducts

The effect of graft copolymerization of BPOCPMA on the thermal behavior of IPP was also analyzed by DSC. Any endothermic heat flow attributable to the crystalline melting of the graft poly(BPOCPMA) units was not seen in any of the thermogram of the products. In fact, completely amorphous behavior had been recorded in DSC analysis of the homopolymer poly(BPOCPMA) carried out in earlier measurements, Figure 4.14, although it was announced to melt at 121°C (Sainath et al., 2000). On the other hand, the crystalline melting temperature of IPP either remained almost unchanged or increased, considerably in some products, Figure 4.49-4.50. It was observed between 164.0°C and 169.4°C, recorded with the coproducts involving 4.6% and 37.8% poly(BPOCPMA), respectively.

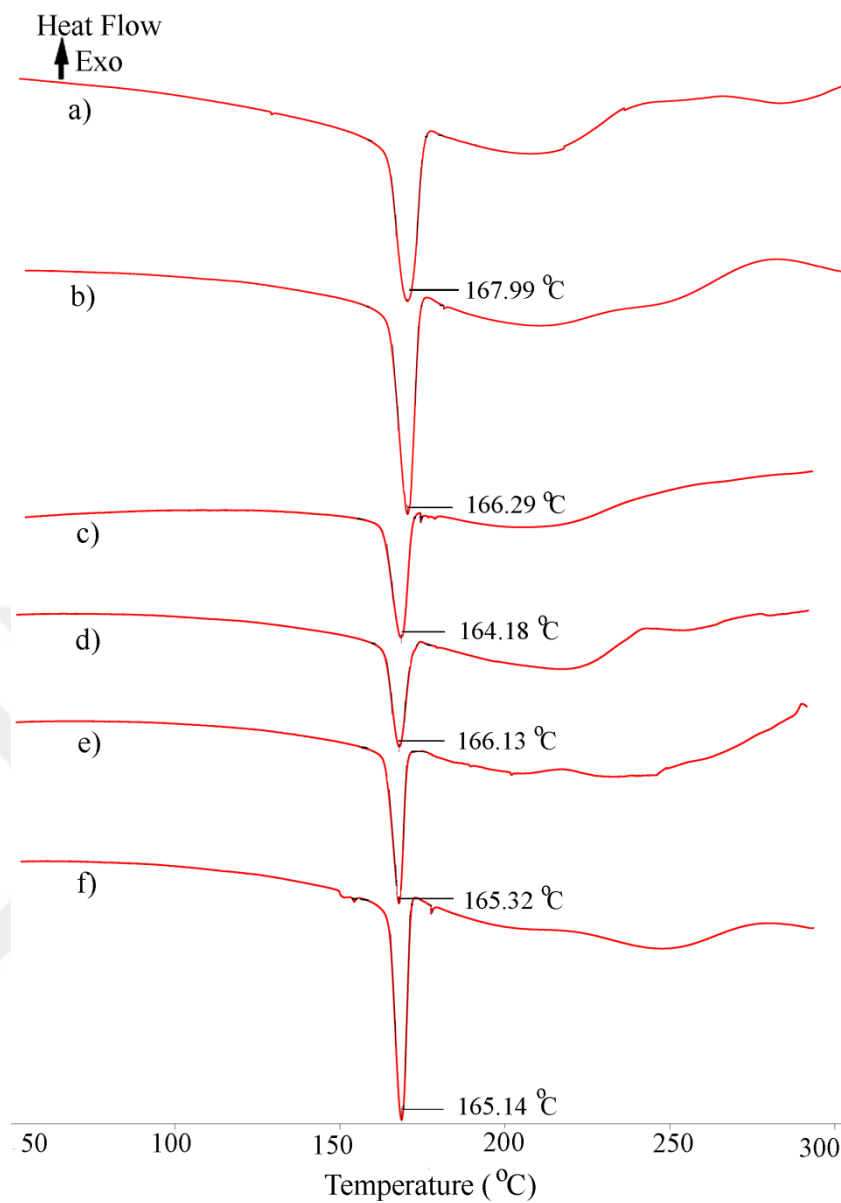


Figure 4.49. The DSC thermograms, obtained with a heating rate of 10°C/min under N₂ atmosphere, of the poly(BPOCPMA)-g-IPP copolymers with a) 3.3% poly(BPOCPMA), b) 5.1% poly(BPOCPMA), c) 6.6% poly(BPOCPMA), d) 7.3% poly(BPOCPMA), e) 8.9% poly(BPOCPMA), and f) 10.3% poly(BPOCPMA)

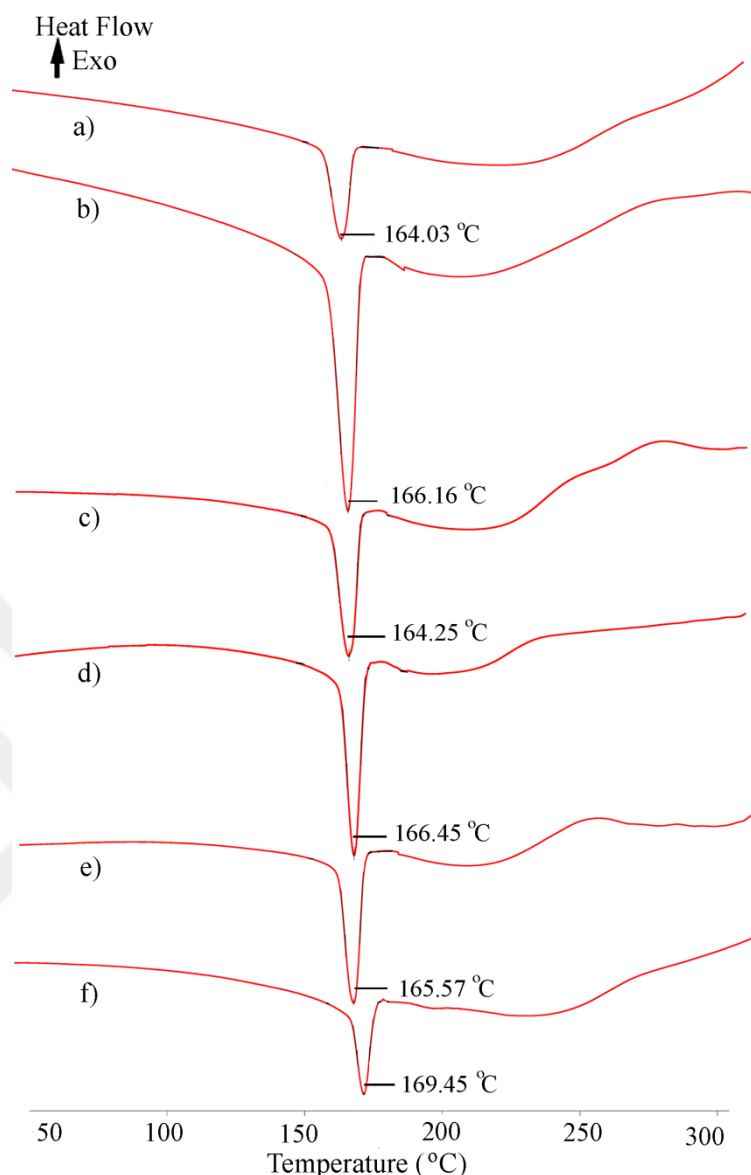


Figure 4.50. The DSC thermograms, obtained with a heating rate of 10°C/min under N₂ atmosphere, of the coproducts with a) 4.6% poly(BPOCPMA), b) 9.5% poly(BPOCPMA), c) 14.0% poly(BPOCPMA), d) 18.8% poly(BPOCPMA), e) 27.9% poly(BPOCPMA), and f) 37.8% poly(BPOCPMA)

The percent crystallinities in IPP matrices of the products were also calculated by using the DSC thermograms and the equation as were for the products involving poly(BPOCPA). The crystalline melting temperatures of the products, the heat of fusion values and the calculated percent crystallinities were presented in Table 4.16 and 4.17, and the variations in percent crystallinity with

poly(BPOCPMA) content in both copolymers and coproducts were plotted in Figure 4.51.

Table 4.16. DSC results with poly(BPOCPMA) percentages in the copolymers (The crystalline melting temperatures, T_m , enthalpy of fusions, ΔH_m and the percent crystallinities, X_c (%))

Sample	T_m (°C)	ΔH_m (J/g)	X_c (%)
Pure IPP	164.1	90.42	43.26
3.3% poly(BPOCPMA)	168.0	96.31	46.08
5.1% poly(BPOCPMA)	166.3	108.63	51.98
6.6% poly(BPOCPMA)	164.2	112.02	53.60
7.3% poly(BPOCPMA)	166.1	122.79	58.75
8.9% poly(BPOCPMA)	165.3	105.71	50.58
10.3% poly(BPOCPMA)	165.1	102.89	49.23

Table 4.17. DSC results with poly(BPOCPMA) percentages in the coproducts (The crystalline melting temperatures, T_m , enthalpy of fusions, ΔH_m , and the percent crystallinities, X_c (%))

Sample	T_m (°C)	ΔH_m (J/g)	X_c (%)
Pure IPP	164.1	90.42	43.26
4.6% poly(BPOCPMA)	164.0	67.76	32.42
9.5% poly(BPOCPMA)	166.2	117.77	56.35
14.0% poly(BPOCPMA)	164.3	114.12	54.60
18.8% poly(BPOCPMA)	166.4	119.45	57.15
27.9% poly(BPOCPMA)	165.6	113.40	54.26
37.8% poly(BPOCPMA)	169.4	74.50	35.65

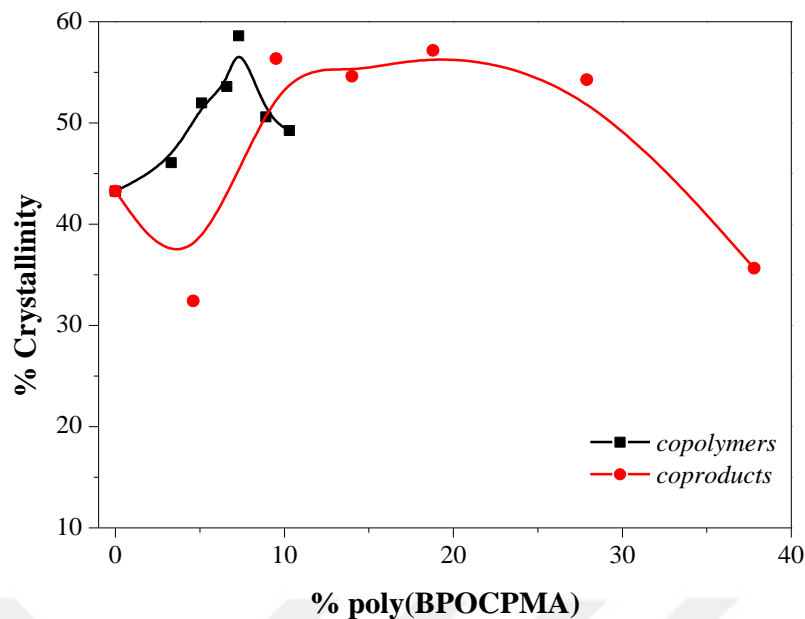


Figure 4.51. The variation of percent crystallinity with poly(BPOCPMA) content in a) copolymers, and b) coproducts

The DSC analyses indicated that percent crystallinity in the IPP matrices increased also with poly(BPOCPMA) content in the copolymers at low percentages, as was for poly(BPOCPA) copolymers, and reached the maximum 58.8% crystallinity with the copolymer involving 7.3% poly(BPOCPMA). The maximum was then followed by decreases at further contents, down to 49.2% crystallinity with 10.3% poly(BPOCPMA). The presence of poly(BPOCPMA) homopolymer molecules in the coproducts, on the other hand, brought about relatively lower crystallinities comparing to the copolymers. The maximum crystallinity, 57% seen at 18.8% poly(BPOCPMA), was followed by gradual decreases in consistence with the content, and the lowest crystallinity, 35.7%, was recorded with the coproduct involving 37.8% poly(BPOCPMA). The polar interactions between the side groups of grafted poly(BPOCPMA) molecules presumably gave rise to the increases in the crystallinities of the copolymers. The similar interactions between the side groups of the homopolymer molecules and the grafted units, however, seemingly resulted in the decreases in the crystallinities in the coproducts, which became more significant with the content.

4.3.2.3 Microstructural Behavior of Poly(BPOCPA)-g-IPP Copolymers and The Coproducts

In order to find out the effect of the graft copolymerization on the microstructural behavior of the IPP matrices, in conjunction with their thermal behaviors, the unit cell parameters of crystal domains of the products were also estimated from the XRD patterns, as were carried out for the HDPE products.

The isotactic polypropylene used in the graft copolymerization experiments was in the α form (monoclinic arrangement), verified by the XRD experiments. The X-ray diffraction pattern of pure polypropylene, Figure 4.44, displayed four characteristic peaks at 2θ of 14.14° , 17.12° , 18.6° and 21.84° , which are assigned to the 110, 040, 130 and 111 reflections of the monoclinic subcell. These values agree well with the values reported for isotactic polypropylene, which are indexed as $(110)_\alpha$, $(040)_\alpha$, $(130)_\alpha$, $(111)_\alpha$, $(041)_\alpha$, confirming the development of only α crystal in used IPP (Fereidoon et al., 2009; Yang BX et al., 2008). In monoclinic form, all the axes are different lengths. Two of them, a and c axes, meet at 90° , but the third one does not. For the form of polypropylene, unit cell parameters are assigned as $a = 6.6\text{\AA}$, $b = 20.8\text{\AA}$, $c = 6.5\text{\AA}$ (Edward et al., 1996; Turner-Jones et al., 1964). The X-ray diffraction studies indicated that the α crystal arrangement has also been conserved in the products throughout the graft copolymerization experiments. The diffraction patterns of the poly(BPOCPA)-g-IPP copolymers and of the coproducts, which displayed the reflections with the Bragg's angles (2θ) varying from 10° to 40° , characteristic of the form, were presented in Figure 4.52 and 4.53, respectively.

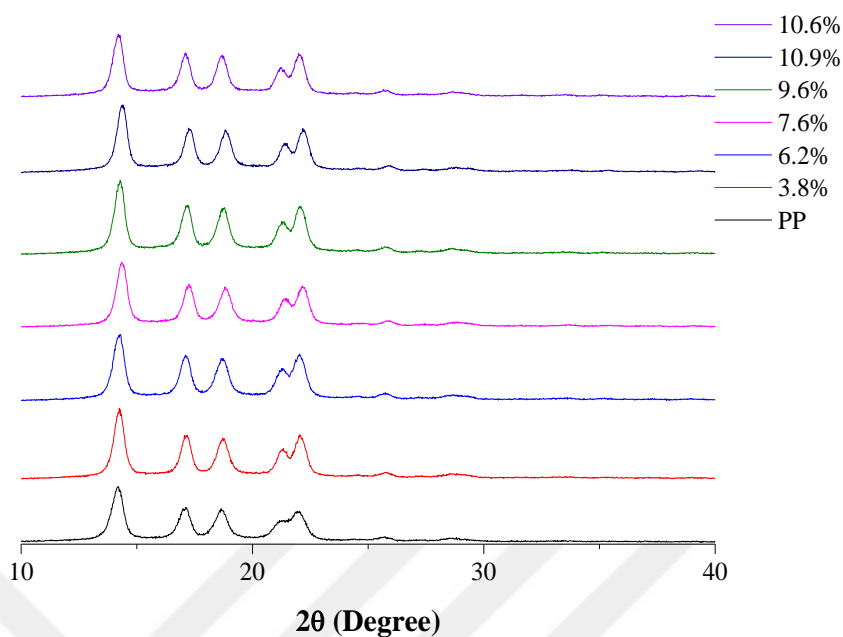


Figure 4.52. The XRD patterns of poly(BPOCPA)-g-IPP copolymers

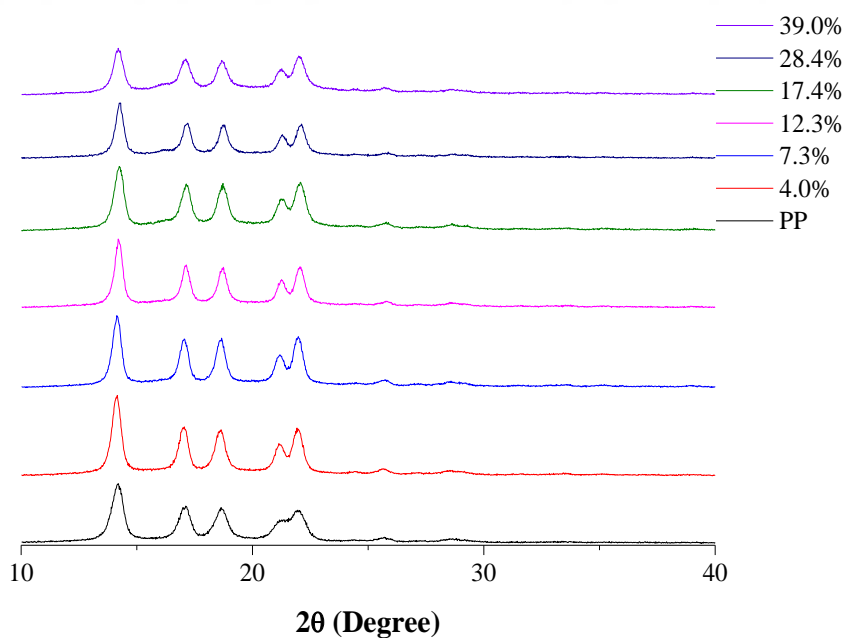


Figure 4.53. The XRD patterns of poly(BPOCPA)-g-IPP coproducts

The lateral dimensions of the monoclinic unit cell, on the other hand, were found to be considerably affected by poly(BPOCPA) content in the products. The

dependence of the unit cell parameters a , b and c , and the crystal sizes on the percentage of poly(BPOCPA) in the products were given in Table 4.18 and 4.19 and the variations in the parameters were drawn Figure 4.54 in detail. Firstly, it can be stated that the parameters a and b lay on the values higher in the coproducts comparing to the copolymers at all contents of poly(BPOCPA). Both parameters increased significantly at low percentages of poly(BPOCPA) in both classes of the products. The maximum 6.685 Å was achieved with 7.3% poly(BPOCPA) in the coproducts (0.80% rise comparing to virgin IPP). In the copolymers the maximum 6.674 Å was recorded with 6.2% poly(BPOCPA) (0.63% increase). The maxima were then followed by decreases with the content, gradually and slowly in coproducts, but sharply in the copolymers. In addition, in spite of the decreases in the parameter a after the maxima, it remained still higher in the coproducts comparing to virgin IPP except for the coproduct involving 39% poly(BPOCPA). In the copolymers, on the other hand, the decrease continued dramatically with the content, down to 6.565 Å seen at 10.9% poly(BPOCPA) (1.0% decrease). A similar behavior was also observed in the parameter b except for that, after the maximum 20.844 Å (0.46% rise), also recorded with 7.3% poly(BPOCPA), it remained almost stationary by forming a plateau at about 20.790 Å between 12.3% and 39.0% poly(BPOCPA) in the coproducts. It is assumed that the IPP chains in the unit cells were probably forced apart laterally by the polar graft units, thus giving rise to expansions in the lateral dimensions at low percentages of poly(BPOCPA). The weak interactions between polar side groups of the grafted units and nonpolar IPP chains might have an additional effect in the expansions at those low contents. Seemingly, this effect was more prominent in the dimension a . As the content of grafted units increased, on the other hand, the developed interactions between the polar side groups probably led to the decreases in lateral dimensions of the unit cells. The presence of the poly(BPOCPA) homopolymer molecules in the coproducts, however, resulted in the relatively lower contractions in the dimensions. Apparently, the interactions between the polar side groups of grafted and ungrafted poly(BPOCPA) molecules might play role in the lower contractions of the lateral dimensions comparing to the copolymers.

Table 4.18. The dependence of the unit cell parameters *a*, *b* and *c*, and crystal size in IPP matrix on poly(BPOCPA) content in copolymers

Sample	a (Å)	b (Å)	c (Å)	Crystal size (nm)
Virgin IPP	6.632	20.748	6.549	17.62
3.8% poly(BPOCPA)	6.638	20.741	6.509	20.45
6.2% poly(BPOCPA)	6.674	20.810	6.510	20.66
7.6% poly(BPOCPA)	6.615	20.706	6.492	22.45
9.6% poly(BPOCPA)	6.605	20.702	6.422	21.52
10.9% poly(BPOCPA)	6.565	20.572	6.401	19.60
10.6% poly(BPOCPA)	6.603	20.698	6.419	20.33

Table 4.19. The dependence of the unit cell parameters *a*, *b* and *c*, and crystal size in IPP matrix on poly(BPOCPA) content in coproducts

Sample	a (Å)	b (Å)	c (Å)	Crystal size (nm)
Virgin IPP	6.632	20.748	6.549	17.62
4.0% poly(BPOCPA)	6.666	20.800	6.447	22.90
7.3 % poly(BPOCPA)	6.685	20.844	6.443	23.77
12.3% poly(BPOCPA)	6.652	20.788	6.431	23.23
17.4% poly(BPOCPA)	6.645	20.792	6.424	21.62
28.4% poly(BPOCPA)	6.634	20.790	6.402	19.46
39.0% poly(BPOCPA)	6.624	20.780	6.393	18.61

The graft copolymerization resulted in the decreases in the parameter *c*, however, at all contents in both classes of the products, in consistence with the percentage, Figure 4.54. The voluminous and polar side groups of grafted poly(BPOCPA) units probably brought about in the decreases in the dimension of the unit cells.

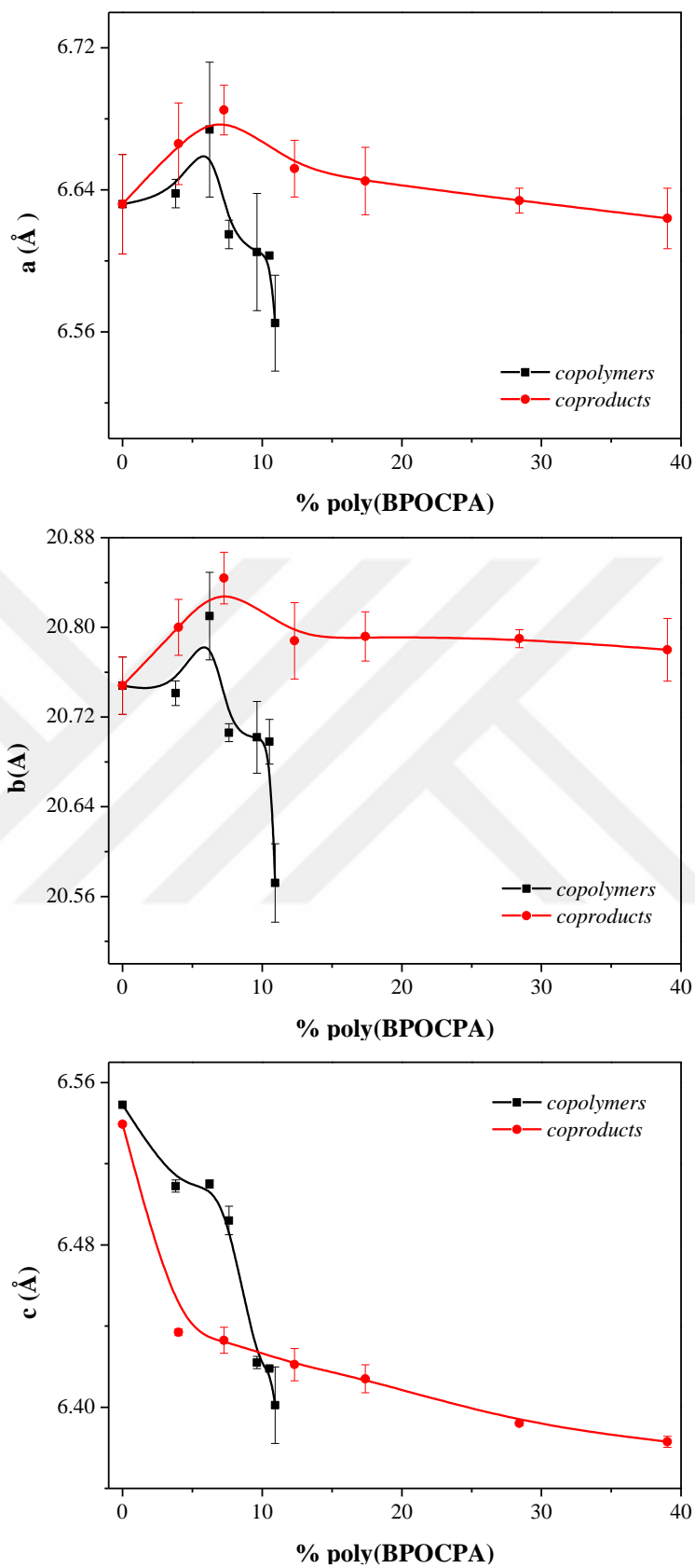


Figure 4.54. The variations of the unit cell parameters (a, b, c) in IPP matrix with poly(BPOCPA) content, calculated from the X-ray diffraction patterns by using 110, 040 and 041 reflections

The variation of crystal size (IPP crystals in the matrix) with poly(BPOCPA) content in the products were drawn in Figure 4.55. The crystal size increased initially with the percentage of poly(BPOCPA) in both classes of the products. The maximum size 23.77 nm (34.9% increase with respect to the crystal size of virgin IPP crystals) was recorded with 7.3% poly(BPOCPA) in the coproducts. In the copolymers, the maximum was 22.45 nm (27.4% increase), achieved with 7.6% poly(BPOCPA). The maxima were then followed by decreases with the content, gradually in the former, but sharply in the latter. Nevertheless, in spite of the decreases, the size lay on the values still higher comparing to the virgin IPP. It could be concluded that the poly(BPOCPA) units with regular structure (with the potential of forming the glassy nematic phase (Sainath et al., 2000) might have acted as nucleating agents and conducted to more ordered packing of IPP chains and thus to the promoted growth of the crystals. Because, larger sizes of the crystals can be rationally expected when they originate from more ordered initiatory structures. The decreases after the maxima might arise mainly from the extensive nucleation resulted from the increasing poly(BPOCPA) content, which may eventually give rise to a large number of IPP crystals but with a smaller size.

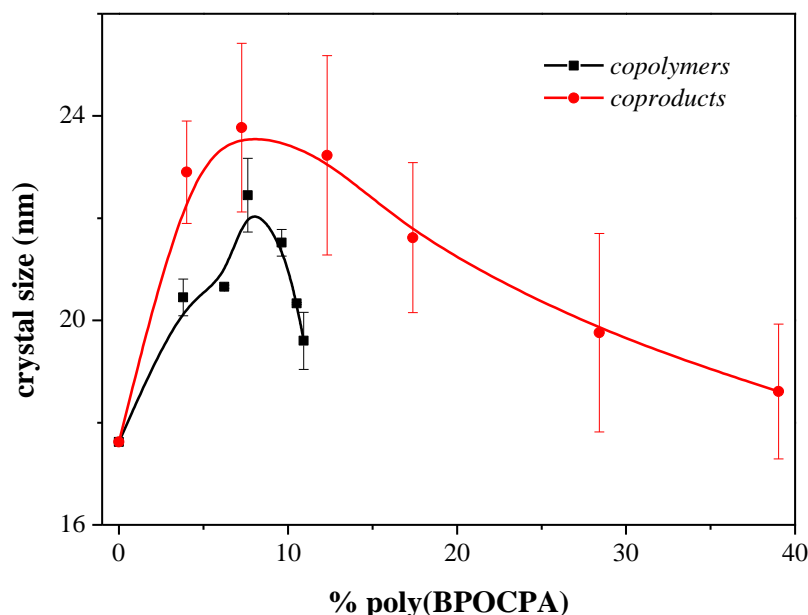


Figure 4.55. The variation of crystal size in IPP matrix with poly(BPOCPA) content in the products

4.3.2.4 Microstructural Behavior of Poly(BPOCPMA)-g-IPP Copolymers and The Coproducts

The effect of the graft copolymerization of BPOCPMA onto IPP on the microstructural behavior of the material was also investigated. The unit cell parameters of the crystal domains of the products were also estimated from the XRD patterns, as were previously studied in the products with poly(BPOCPA).

The X-ray diffraction studies indicated that the α crystal arrangement in IPP crystal domains has also been preserved throughout the graft copolymerization experiments. The diffraction patterns of the poly(BPOCPMA)-g-IPP copolymers and of the coproducts, which displayed the reflections with the Bragg's angles (2θ) varying from 10° to 40° were presented in Figure. 4.56 and 4.57, respectively.

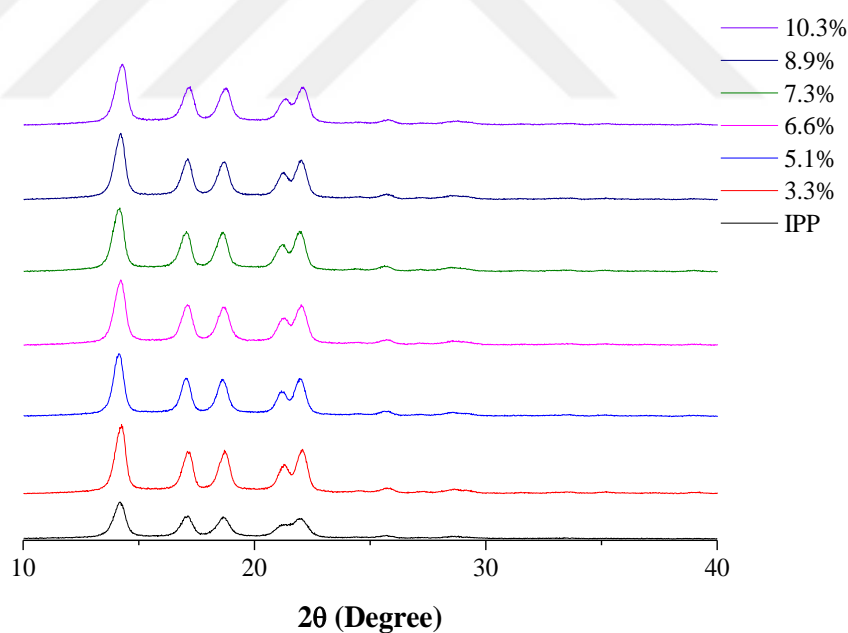


Figure 4.56. The XRD patterns of poly(BPOCPMA)-g-IPP copolymers

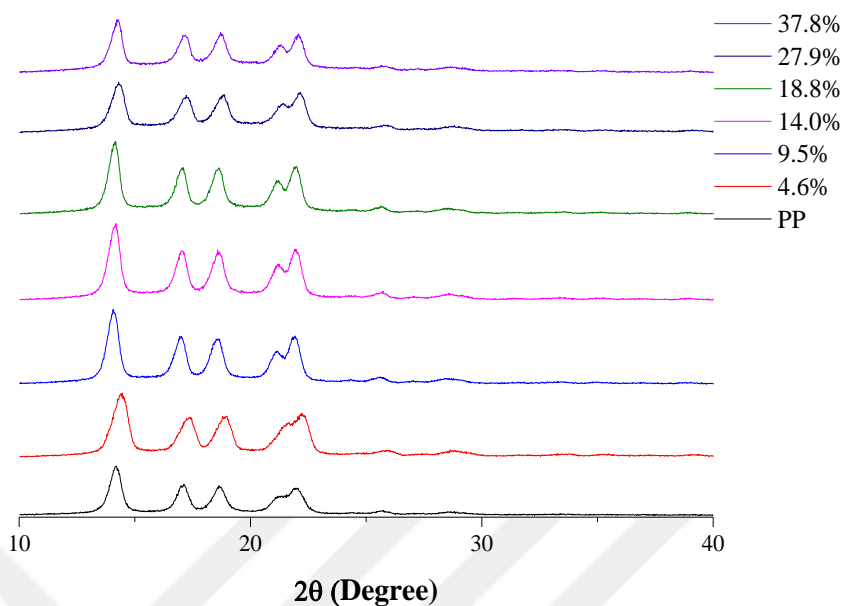


Figure 4.57. The XRD patterns of poly(BPOCPMA)-g-IPP coproducts

The lateral dimensions of the monoclinic unit cell in IPP matrices were also found to be considerably dependent on the poly(BPOCPMA) content in the products. The dependence of the unit cell parameters *a*, *b* and *c*, and the crystal sizes on the percentage of poly(BPOCPMA) in the products were given in Table 4.20 and 4.21 and the variations in the parameters were drawn in Figure 4.58 in detail. Both parameters *a* and *b* increased initially with the percentage of poly(BPOCPMA) in both copolymers and coproducts. The increases were steeper in the former. The maximum in the parameter *a*, 6.712 Å (1.2% rise comparing to virgin IPP) was recorded with 7.3% poly(BPOCPMA) in the copolymers. In the coproducts, the maximum was 6.683 Å (0.77% rise), observed at 9.5% poly(BPOCPMA). In the parameter *b*, the maxima were 20.868 Å (0.58% increase) and 20.818 Å (0.34% increase), noted at those corresponding contents as were recorded in the parameter *a*, that are, at 7.3% and 9.5% poly(BPOCPMA), respectively. Both parameters decreased after the maxima, sharply in the former and gradually in the latter, as the content increased further. It is believed that the IPP chains in the unit cells were presumably coerced apart laterally by the polar groups of graft units, thus resulting in the expansions in the lateral dimensions at low contents of poly(BPOCPMA), as commented for the products with poly(BPOCPA). The weak interactions between

polar groups of the graft units and nonpolar IPP chains were assumed to have additional effect in the expansions at those low contents. Apparently, this effect was more significant in the dimension *a*. The developed interactions between the polar side groups arising from the increases in the content of polar graft units probably gave rise to the contractions in lateral dimensions of the unit cells as the percentage of poly(BPOCPMA) increased. The relatively soft changes in the lateral dimensions in the coproducts comparing to copolymers, on the other hand, are believed to result from the interactions between the polar side groups of grafted and ungrafted poly(BPOCPMA) molecules.

Table 4.20. The dependence of the unit cell parameters *a*, *b* and *c*, and crystal size in IPP matrix on poly(BPOCPMA) content in copolymers

Sample	<i>a</i> (Å)	<i>b</i> (Å)	<i>c</i> (Å)	Crystallite size (nm)
Virgin IPP	6.632	20.748	6.549	17.62
3.3% poly(BPOCPMA)	6.657	20.798	6.468	18.68
5.1% poly(BPOCPMA)	6.683	20.820	6.466	19.04
6.6% poly(BPOCPMA)	6.688	20.828	6.461	19.20
7.3% poly(BPOCPMA)	6.712	20.868	6.461	20.03
8.9% poly(BPOCPMA)	6.665	20.796	6.457	18.56
10.3% poly(BPOCPMA)	6.645	20.760	6.454	18.00

Table 4.21. The dependence of the unit cell parameters *a*, *b* and *c*, and crystal size in IPP matrix on poly(BPOCPMA) content in coproducts

Sample	<i>a</i> (Å)	<i>b</i> (Å)	<i>c</i> (Å)	Crystallite size (nm)
Virgin IPP	6.632	20.748	6.549	17.62
4.6% poly(BPOCPMA)	6.680	20.748	6.464	17.18
9.5% poly(BPOCPMA)	6.683	20.818	6.457	17.73
14.0% poly(BPOCPMA)	6.674	20.800	6.451	18.39
18.8% poly(BPOCPMA)	6.629	20.762	6.421	18.61
27.9% poly(BPOCPMA)	6.599	20.718	6.392	16.00
37.8% poly(BPOCPMA)	6.592	20.712	6.390	15.50

The parameter *c*, in contrast to the initial increases in the other dimensions, decreased consistently with the content of poly(BPOCPMA) in both copolymers and coproducts. The α IPP crystal structure is connected with the establishment of the concept of stereoregularity and the recognition of its role as a prerequisite for polymer crystallization (Meille et al., 1994). Also, molecular weight, molecular weight distribution and chain branching affect the crystallization behavior of α IPP (Nogales et al., 2001). It seems that the voluminous and polar side groups of poly(BPOCPMA) units in the products presumably led to the decreases in the *c* dimension of the unit cells.

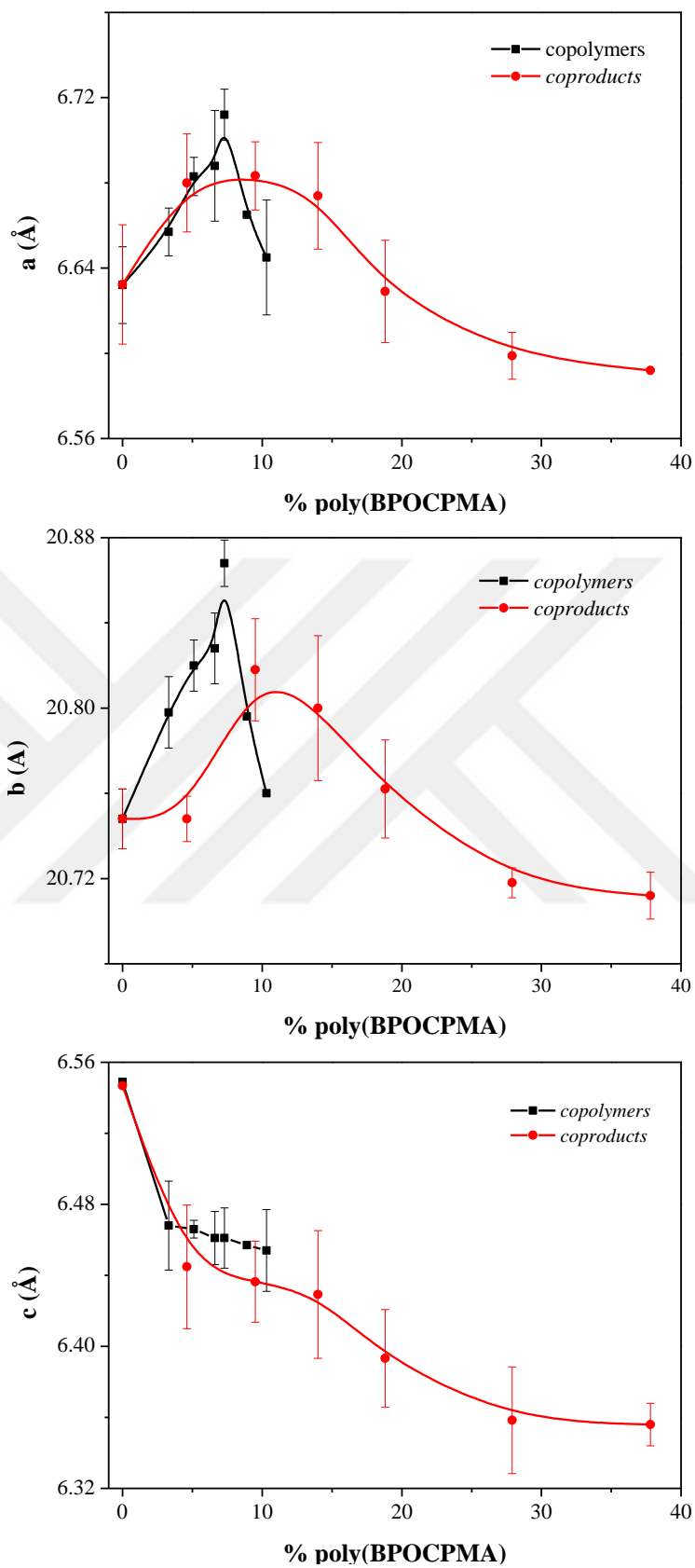


Figure 4.58. The variations of the unit cell parameters (a, b, c) in IPP matrix with poly(BPOCPMA) content, calculated from the X-ray diffraction patterns by using 110, 040 and 041 reflections

The variation of IPP crystal size with poly(BPOCPMA) content in the products were drawn in Figure 4.59. The size increased initially with the percentage of poly(BPOCPMA) in the copolymers and reached the maximum 20.03 nm (13.7% increase) with 7.3% poly(BPOCPMA). The size then decreased dramatically as the content increased further, down to the dimension of 18.00 nm at 10.3% poly(BPOCPMA), very close to the size of virgin IPP crystals. In the coproducts, however, no appreciable change was observed in the size up to the percentage of 9.5% poly(BPOCPMA). After relatively small increase (5.6%) with 18.61 nm at 18.8% poly(BPOCPMA), it reduced with the content, down to 15.50 nm (12% decrease) at 37.8% poly(BPOCPMA), in contrast to the behavior seen in the products involving poly(BPOCPA) in which all the sizes at all contents were higher comparing to virgin IPP. Apparently, crowding by α methyl group in poly(BPOCPMA) units, while leading to the small increases in crystal size in the copolymers, resulted in the comparable or smaller sizes in the coproducts. The effect of α methyl group was also observed in the thermal analysis of poly(BPOCPMA) homopolymer (section 4.1.6). The group gave rise to completely amorphous behavior in the analysis. The polar interactions between the grafted poly(BPOCPMA) units in copolymers probably conducted to more ordered packing of IPP chains and thus to the promoted growth of the crystals in the initial trend. The decrease at higher contents might be due to extensive nucleations in IPP matrix, conducted polar graft units, but with a smaller size.

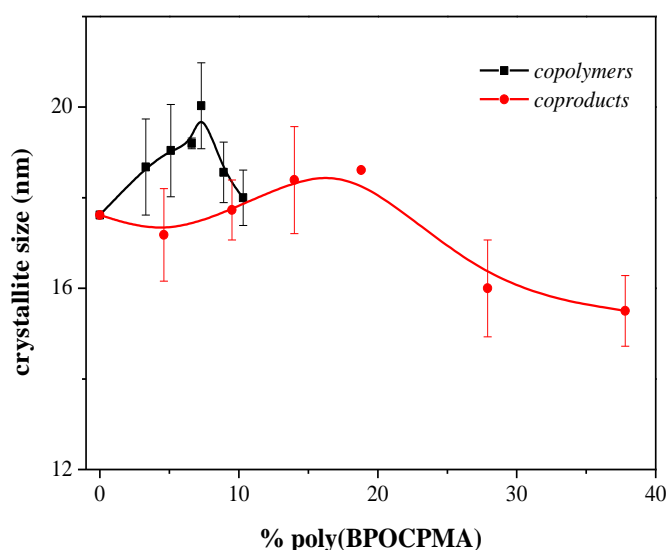


Figure 4.59. The variation of crystal size in IPP matrix with poly(BPOCPMA) content in the products

4.3.3 Mechanical Properties of The Products

The effect of graft copolymerization of BPOCPA and BPOCPMA onto IPP on the mechanical behavior of the material was also studied by analyzing the stress-strain and impact behavior of the products. The test samples in dumb-bell shape (50 mm x 76.6 mm x 2 mm) were prepared by micro-injection molding at 220°C with 8 bar injecting pressure. The processing was legitimately optimized at this fairly high temperature, comparing to the melting point of IPP, due to the difficulties in flow behavior of the melts at lower temperatures. The graft units poly(BPOCPA) and poly(BPOCPMA) with rigid and polar side groups might have caused to a restriction in chain mobility in the products, leading to an increase in the viscosity of the melts in the processing. Nevertheless, this processing temperature is well below the starting point of decomposition (245-250°) of the graft units (Sainath et al., 2000). On the other hand, while some remarkable improvements were achieved in the mechanical properties of the products involving poly(BPOCPA) at low percentages, the graft copolymerization of BPOCPMA gave rise to diminishes in all tensile and impact behaviors in consistence with the content of poly(BPOCPMA) in the products. The graft copolymerization of both monomers imparted brittleness increasing consistently with the contents to the material.

4.3.3.1 Mechanical Behavior of Poly(BPOCPA)-g-IPP Copolymers and The Coproducts

Typical stress-strain curves of the poly(BPOCPA)-g-IPP copolymers and the coproducts were presented in Figure 4.60 and 4.61, respectively. The extensive cold drawing seen in virgin IPP was not observed in any of the products even at low contents of the graft units. At low percentages, while the copolymer samples failed just after the yielding, at the onset of neck formation, the samples of coproducts failed at yielding. At the percentages of 6.2% in copolymers and 12.3% in coproducts, the failures were recorded at the beginning of plastic deformation. At further respective contents, the products then displayed elastic deformation and brittle fracture in the tests. Apparently, the rigid character of poly(BPOCPA) molecules at room temperature (with T_g value of 69°C, Sainath et al.), stemming from its large and rigid side groups with polar nature, restricts the plasticity behavior

in the products. Conclusively, the material revealed an increasing brittleness in nature with increasing graft contents.

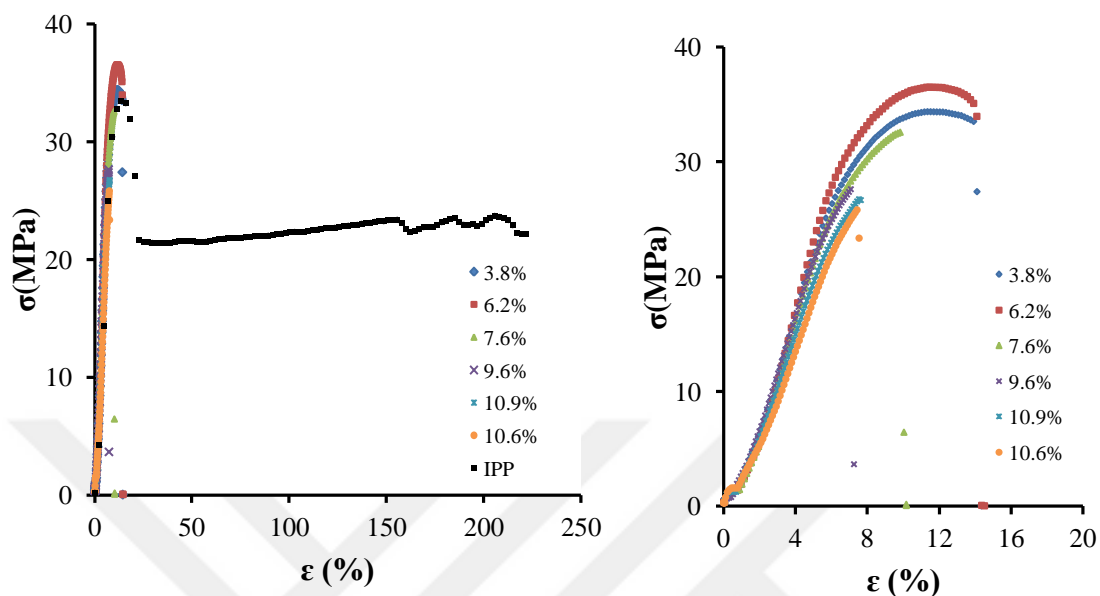


Figure 4.60. Stress-strain curves of poly(BPOCPA)-g-IPP copolymers

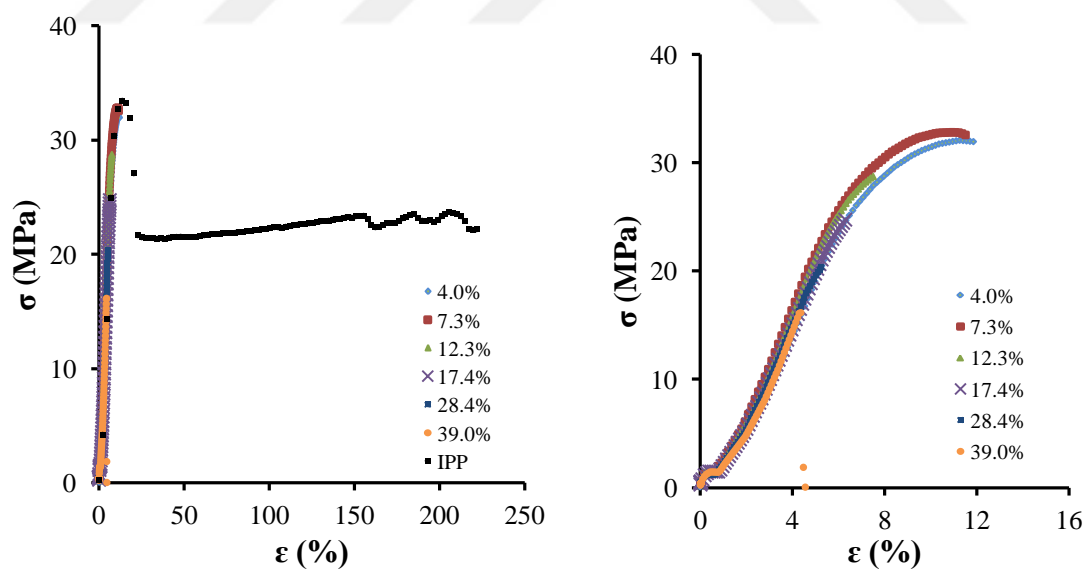


Figure 4.61. Stress-strain curves of poly(BPOCPA)-g-IPP coproducts

The results of the tensile and impact behavior measurements of the products were presented in Table 4.22 and 4.23, and their variations were drawn in Figure 4.62.a, b and c. The percentage decrease or increase in tensile strength and modulus in tables were given with respect to virgin IPP. Tensile strength increased initially

with the content in the copolymers, and reached the maximum 35.39 MPa at 6.2% poly(BPOCPA) (11.6% improvement comparing to pure IPP). The strength then weakened dramatically as the content increased, and reduced to 25.97 MPa at 10.9% poly(BPOCPA). In the coproducts, however, the initial advance in the strength was not observed. The highest values 32.46 MPa and 32.66 MPa were recorded at 4.0% and 7.3% poly(BPOCPA), respectively. The presence of the poly(BPOCPA) homopolymer molecules thus led to the strengths that lay on the values comparable with the strength of pure IPP, 31.72 MPa. As the content increased further, the strength weakened gradually in consistence with the percentage, and decreased to 17.38 MPa at 39.0% poly(BPOCPA). On the other hand, very significant improvements were recorded in Young's modulus values of the products, determined on the same samples during tensile tests. The modulus increased initially with the content in both copolymers and coproducts, and reached the maximum 749 MPa (18.9% increase) at 6.2% poly(BPOCPA) in copolymers and 754 MPa (19.7% increase) at 12.3% poly(BPOCPA) in coproducts. It diminished as the content increased further in both classes of the products, sharply in copolymers but gradually in coproducts. Nevertheless, in spite of the dramatic decreases, all the moduli lay on the values still higher comparing to pure IPP. The graft copolymerization thus gave rise to a reinforcing function in withstanding under load and in resistance to deformation. These improvements in the tensile behavior are believed to result from the developments in the ordering and orientation of IPP chains due to the constitution of side chain LCP poly(BPOCPA) molecules as graft units. The poly(BPOCPA) units with the potential of forming so regularly organized structure as nematic arrangement (Sainath et al.) probably conduced to a better ordering and orientation of IPP chains, and thus gave rise to improved tensile behaviors as mentioned above. Both the decreases in the tensile behaviors after the maxima could be explained by a low load capacity of poly(BPOCPA) molecules. Because, the polymer composed of the chains with so large and rigid side groups are very difficult to exhibit substantial withstanding under the load with respect to IPP. Consequently, relatively higher content of poly(BPOCPA) units presumably made the material less prone to resist in the tensile tests.

The variation in Izod impact strength as a function of poly(BPOCPA) content in the products were presented in Figure 4.62.c. As seen in the figure, grafted

poly(BPOCPA) units led to improvement in the strength of the copolymers at relatively low contents. The maximum 48 kJ/m² was achieved with the samples involving 3.8% poly(BPOCPA). The strength then decreased severely as the percentage increased further. The coproducts, on the other hand, had decrease trend in the strength in all samples, starting from the initial percentages and in consistence with the content.

Table 4.22. Ultimate tensile strength, Young's Modulus and impact strength of the poly(BPOCPA)-g-IPP copolymers with poly(BPOCPA) content

Specimen	Ultimate Strength (MPa)	Young's Modulus(MPa)	Impact Strenght (kJ/m ²)
Virgin IPP	31.72	631.35	40.76
3.8% poly(BPOCPA)	34.54 (+8.9%)	730.99 (+15.9%)	48.18
6.2% poly(BPOCPA)	35.39 (+11.6%)	749.84 (+18.9%)	41.72
7.6% poly(BPOCPA)	33.25 (+4.8%)	728.91 (+15.5%)	39.42
9.6% poly(BPOCPA)	27.17 (-14.3)	695.70 (+10.3%)	36.60
10.9% poly(BPOCPA)	25.97 (-18.1%)	646.96 (+2.5%)	24.50
10.6% poly(BPOCPA)	26.01 (-18%)	653.12 (+3.5%)	27.79

Table 4.23. Ultimate tensile strength, Young's Modulus and impact strength of the poly(BPOCPA)-g-IPP coproducts with poly(BPOCPA) content

Specimen	Ultimate Strength (MPa)	Young's Modulus(MPa)	Impact Strength (kJ/m ²)
Virgin IPP	31.72	631.35	40.76
4.0% poly(BPOCPA)	32.46 (+2.3%)	682.67 (+8.2%)	36.13
7.3% poly(BPOCPA)	32.66 (+2.9%)	720.79 (+14.3%)	35.95
12.3% poly(BPOCPA)	29.95 (-5.6%)	754.52 (+19.7%)	34.88
17.4% poly(BPOCPA)	27.69 (-12.7%)	741.68 (+17.6%)	30.30
28.4% poly(BPOCPA)	19.36 (-39.0%)	728.53 (+15.5%)	29.22
39.0% poly(BPOCPA)	17.38 (-45.2%)	714.22 (+13.2%)	24.86

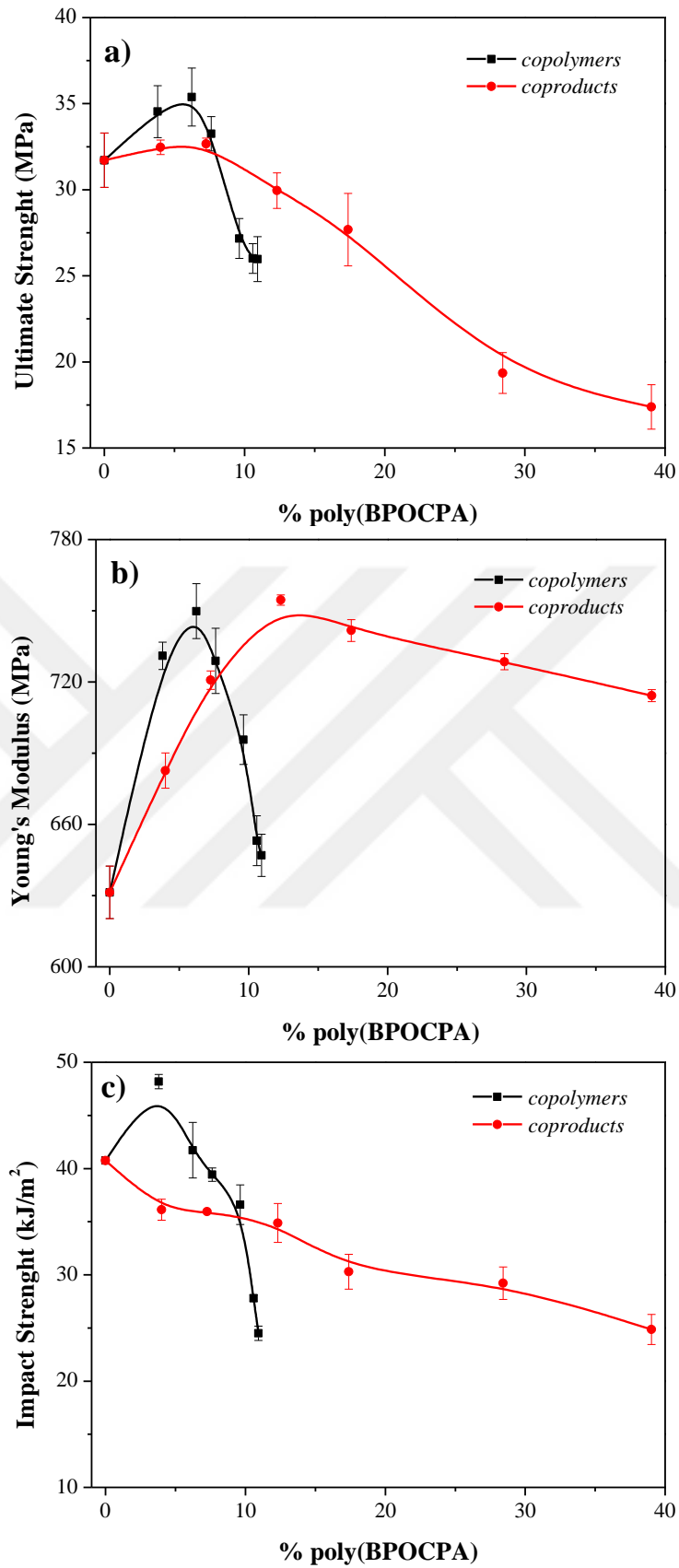


Figure 4.62. The variation of **a)** ultimate strength, **b)** Young's modulus and **c)** impact strength of the coproducts with poly(BPOCPA) content

Impact property or toughness of material is its resistance to fracture. The higher impact strength is observed due to better dissipation of the energy loaded during the test, and the more the energy is absorbed, the higher impact strength the material has. Various mechanisms may occur in (pure) polypropylene, which can lead to energy dissipation and thus to a higher toughness e.g. yielding, crazing, and phase transitions. The impact toughness is often the deciding factor in material selection because impact test measures the ability of polymer to withstand the load imposed upon being struck by an object at high velocity, thus it is a measure of energy required to propagate a crack cross the specimen. With respect to these explanations, the higher impact strength in copolymers compared to coproducts may be related to better energy dissipation in copolymers, nucleating agent properties of grafted poly(BPOCPA) content and changes in crystallinity of products. These results are consistent with DSC and XRD analysis. The percentage crystallinities were higher, whereas crystal sizes were lower in the copolymers compared to coproducts. In the study carried out by Jose et al. the increase in impact properties of PP on the addition of HDPE was related to the crystallinity changes arising due to blending. It was reported that the addition of HDPE decreases the size of PP spherulites by acting as a nucleating agent and increases impact strength of PP. Crystallinity of HDPE was higher when compared to IPP and pure HDPE has higher nucleation and growth of individual crystallites (Jose et al., 2004). Moreover, a reduction in spherulite size was reported to improve impact strength due to an increase in interfacial thickness, better interspherulitic chain mobility, and reduction of spherulitic defects. In addition, fracture toughness in semicrystalline polymers strongly depends on the number of tie molecules between the crystallinities and the disentanglement resistance of the polymer chains (tie molecules connect crystals and amorphous region) (Kersch et al., 2016).

4.3.3.2 Mechanical Behavior of Poly(BPOCPMA)-g-IPP Copolymers and The Coproducts

The typical stress-strain behavior of the poly(BPOCPMA)-g-IPP copolymers and the coproducts were illustrated in Figure 4.63 and Figure 4.64, respectively. It was observed that the extensive cold drawing observed in virgin IPP was lost in all products involving poly(BPOCPMA). At low percentages in both copolymers and coproducts the samples failed just after the yield point, at the beginning of neck formation. As the content of poly(BPOCPMA) increased, the products from both classes gained brittleness increasingly. Seemingly, the rigid character of poly(BPOCPMA) units at room temperature (with T_g value of 72°C, Sainath et al.), stemming from its large and rigid side groups with polar nature, restricted the plasticity behavior in the products. Molecular rotation and conformational freedom of IPP chains and poly(BPOCPMA) units might also be restricted due to the crowding with methyl groups, which might considerably contribute to the observed brittleness. Conclusively, the material revealed an increasing brittleness in nature with increasing graft contents as were observed in the products involving poly(BPOCPMA).

The effect of poly(BPOCPMA) content on the mechanical behavior of the material, that is, the changes in Young's modulus, tensile and impact strength as a function of poly(BPOCPMA) percentage in the products were given in Table 4.24 and 4.25, and the variations were drawn in Figure 4.65. The percentage decrease or increase in tensile strength and modulus in tables were given with respect to virgin IPP. It was revealed that the graft copolymerization of BPOCPMA onto IPP resulted in inferior performance almost in all mechanical behaviors. The higher poly(BPOCPMA) content in the products gave rise to lower ultimate tensile strength in copolymers as well as in coproducts, Figure 4.65.a. In addition, Young's modulus of the products decreased with the increment in poly(BPOCPMA) percentage, Figure 4.65.b. The methyl groups attached to every second carbon atom in IPP polymer chain restrict rotation of the chain producing a stronger but less flexible material (Salih et al., 2013). The presence of the group also on the main chain of poly(BPOCPMA) molecules might additionally contribute to the restrictions in the mobility of IPP chains and the graft units. Eventually, the restrictions probably

resulted in the observed inferior behaviors in the mechanical tests. The decrease in the properties may also be related to a reduction in the crystallization behavior of the material (Tortorella et al., 2008). Hence, the graft copolymerization of BPOCPMA molecules, while resulting in remarkably improved mechanical behaviors in the products involving HDPE (section 4.2.4), gave rise to lower performances in the properties of IPP.

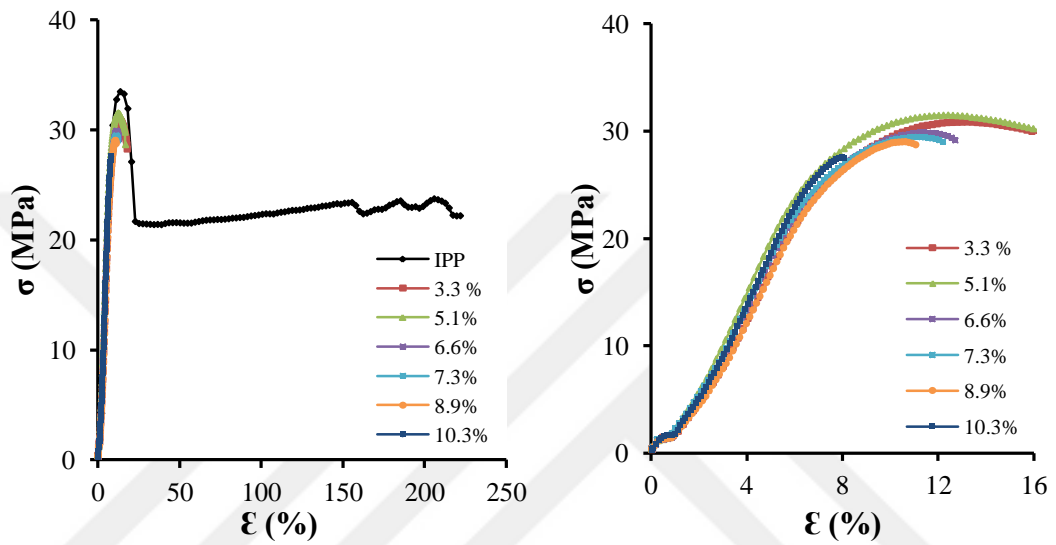


Figure 4.63. Stress-strain curves of poly(BPOCPMA)-g-IPP copolymers

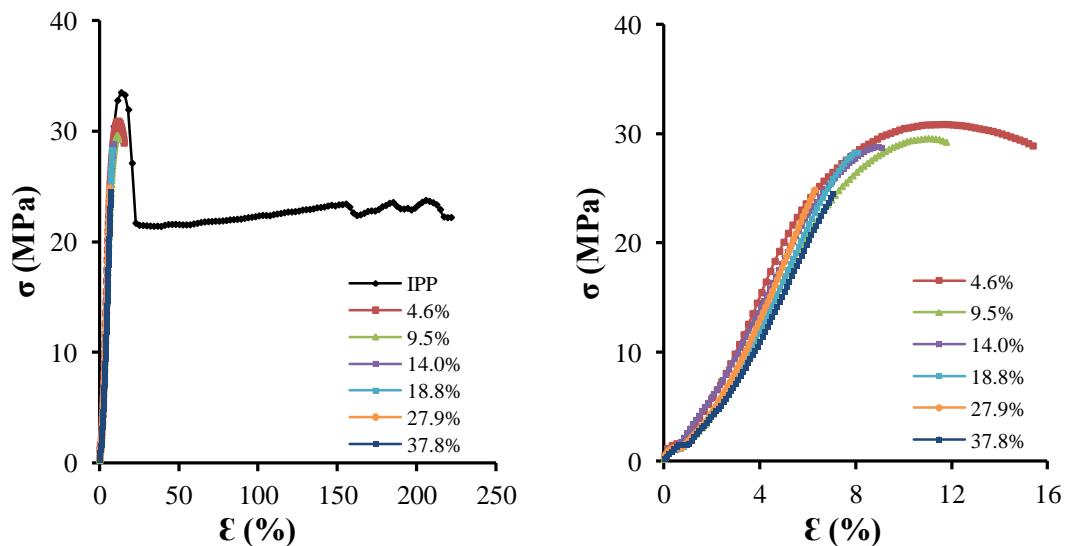


Figure 4.64. Stress-strain curves of poly(BPOCPMA)-g-IPP coproducts

Table 4.24. Ultimate tensile strength, Young's Modulus and impact strength of the poly(BPOCPMA)-g-IPP coproducts with poly(BPOCPMA) content

Specimen	Ultimate Strength (MPa)	Young's Modulus (MPa)	Impact Strength (kJ/m ²)
Neat IPP	31.72	631.35	40.76
3.3% poly(BPOCPMA)	30.58 (-3.7%)	632.46 (+0.2%)	30.33
5.1% poly(BPOCPMA)	30.25 (-4.9%)	597.49 (-5.7%)	29.22
6.6% poly(BPOCPMA)	29.72 (-6.7%)	597.25 (-5.7%)	27.27
7.3% poly(BPOCPMA)	28.78 (-10.2%)	593.68 (-6.3%)	26.10
8.9% poly(BPOCPMA)	28.8 (-10.1%)	587.48 (-7.5%)	25.59
10.3% poly(BPOCPMA)	28.49 (-11.3%)	562.50 (-12.2%)	21.51

Table 4.25. Ultimate tensile strength, Young's Modulus and impact strength of the poly(BPOCPMA)-g-IPP coproducts with poly(BPOCPMA) content

Specimen	Ultimate Strength (MPa)	Young's Modulus (MPa)	Impact Strength (kJ/m ²)
Neat IPP	31.72	631.35	40.76
4.6% poly(BPOCPMA)	29.73 (-6.7%)	638.16 (+1.1%)	29.40
9.5% poly(BPOCPMA)	29.35 (-8.1%)	621.00 (-3.1%)	27.90
14.0% poly(BPOCPMA)	28.85 (-9.9%)	612.11 (-3.1%)	26.40
18.8% poly(BPOCPMA)	28.37 (-11.8%)	603.04 (-4.7%)	15.69
27.9 % poly(BPOCPMA)	24.58 (-29.0%)	596.03 (-5.9%)	12.54
37.8 % poly(BPOCPMA)	24.67 (-28.6%)	595.51 (-6.0%)	8.10

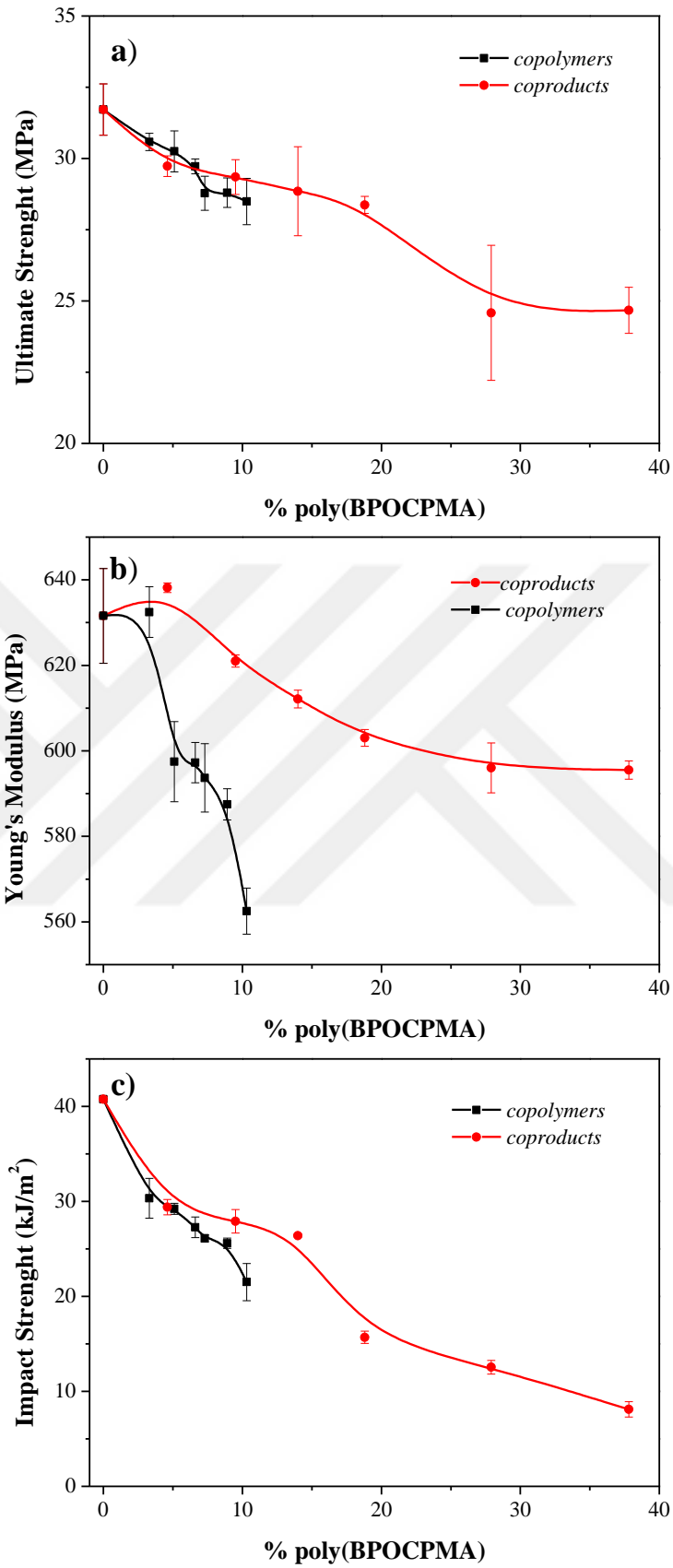


Figure 4.65. The variation of **a)** ultimate strength, **b)** Young's modulus and **c)** impact strength of the products with poly(BPOCPMA) content

The variation of Izod impact strengths of the products with poly(BPOCPMA) content were given in Figure 4.65.c. The graft copolymerization led to inferior impact strength in both copolymers and coproducts, in consistence with poly(BPOCPMA) content. That is, the dissipation of the energy loaded during the test got worse and the resistance of the material to impact thus weakened as the percentage of poly(BPOCPMA) increased. The resulting brittleness in nature was also revealed in SEM micrographs of the fracture surfaces of samples. The restricted chain mobility owing to the crowding by the methyl groups on both IPP and poly(BPOCPMA) molecules and also to the rigid and large side groups of poly(BPOCPMA) units might have substantial contribution to the observed impact behaviors, that is, to poorer dissipation of the impact energy. The weaker behaviors in the impact tests may also be related to a reduction in the crystallinity (Tortorella and Beatty, 2008). Fracture toughness in semicrystalline polymers strongly depends on the number of tie molecules between the crystallites and disentanglement resistance of polymer chains (Kersch et al., 2016). Thus, the crystallization behavior of the products, that is, the percent crystallinity and crystal size might also play role in the observed mechanical behaviors.

4.4 SEM Analysis of The Polymers

Size, size distribution of reinforcement phase and the adhesion quality of interface between matrix and the reinforcement phase are important factors for the mechanical performance of polymer blends and composites. Therefore, the tensile and impact fractured surfaces of the poly(BPOCPMA)-g-HDPE, poly(BPOCPA)-g-IPP, poly(BPOCPMA)-g-IPP copolymers and the coproducts were investigated by SEM analysis. The SEM photographs of all the fracture surfaces displayed no phase separation. The structures of the products were completely homogeneous in spite of that the graft units poly(BPOCPA) and poly(BPOCPMA) with polar side groups were essentially different in nature from apolar HDPE and IPP. This result confirmed the chemical bonding of the units, that is, graft copolymerization of BPOCPMA onto HDPE and IPP, and of BPOCPA onto IPP. Furthermore, since poly(BPOCPA) and poly(BPOCPMA) exist also as homopolymer as well as the grafted units in the coproducts, it was additionally indicated that the graft copolymers poly(BPOCPMA)-g-HDPE, poly(BPOCPA)-g-IPP and poly(BPOCPMA)-g-IPP

acted as compatibilizers providing good interfacial adhesion between the homopolymers and graft copolymers in the coproducts.

4.4.1 SEM Analysis of Poly(BPOCPMA)-g-HDPE Copolymers and The Coproducts

SEM analyses of both the copolymers and the coproducts displayed a gradual transition from ductile fracture at lower graft contents to brittle nature dominated at high percentages. The bulky and long extensions like fibrillar structure at lower contents gradually got smaller and shortened as the content increased, Figure 4.66-4.71. On the other hand, it can be stated as a general deduction that the copolymers exhibited better fibrillations and orientations at similar contents, comparing to the coproducts as revealed by the oriented structures in Figure 4.67 and 4.68 and thin extensions from the surfaces, widely observed in the copolymer samples, Figure 4.71 and 4.72. Accordingly, the better alignment and orientation in the fibrillar structure account for the better improvements in the tensile behavior of the copolymers. At high percentages in both classes the gradually shortened extensions were eventually replaced by a morphology exhibiting brittle fracture in majority, verified by the cracks and openings on the surfaces. But, the transition took place at earlier percentages in the copolymers, confirmed by the existence of small extensions even at high contents in the coproducts, Figure 4.70. On the other hand, there still existed some fibrillar extensions even at high contents in both classes. These extensions were observed in the fractographs as thin fibrils protruding from the surfaces broken in brittle nature in the copolymer samples, and in the surfaces with some small extensions in some coproduct samples, Figure 4.71-73. The thin fibrils were also seen in the impact fractograph of the coproduct sample involving 26.7% poly(BPOCPMA), besides the cracks and openings showing the brittle fracture, Figure 4.74. But, the material did not show any phase separation at all.

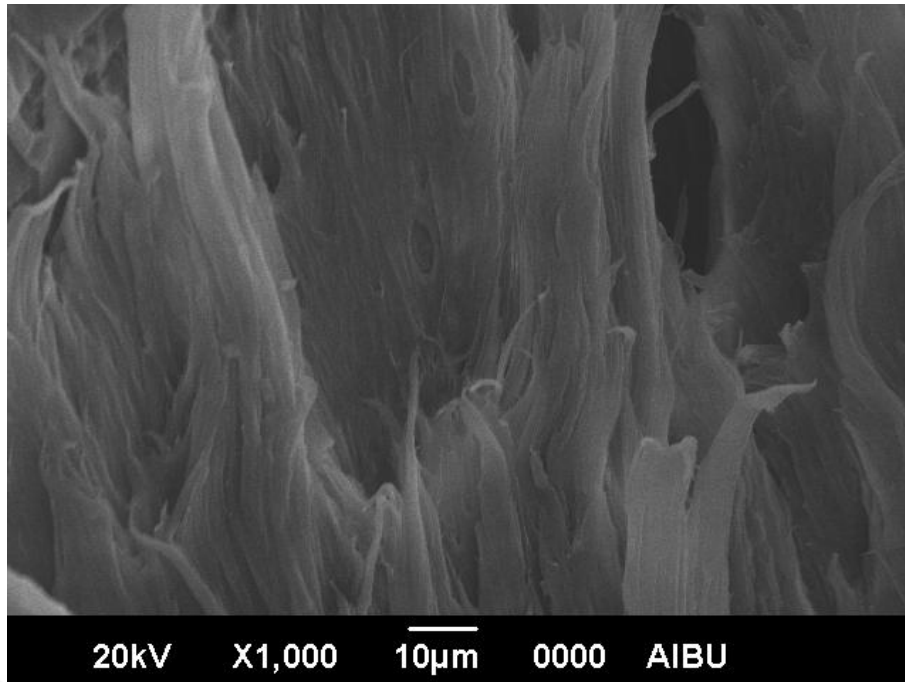


Figure 4.66. SEM micrograph of tensile fractured surface of the coproduct with 3.8% poly(BPOCPMA)-g-HDPE

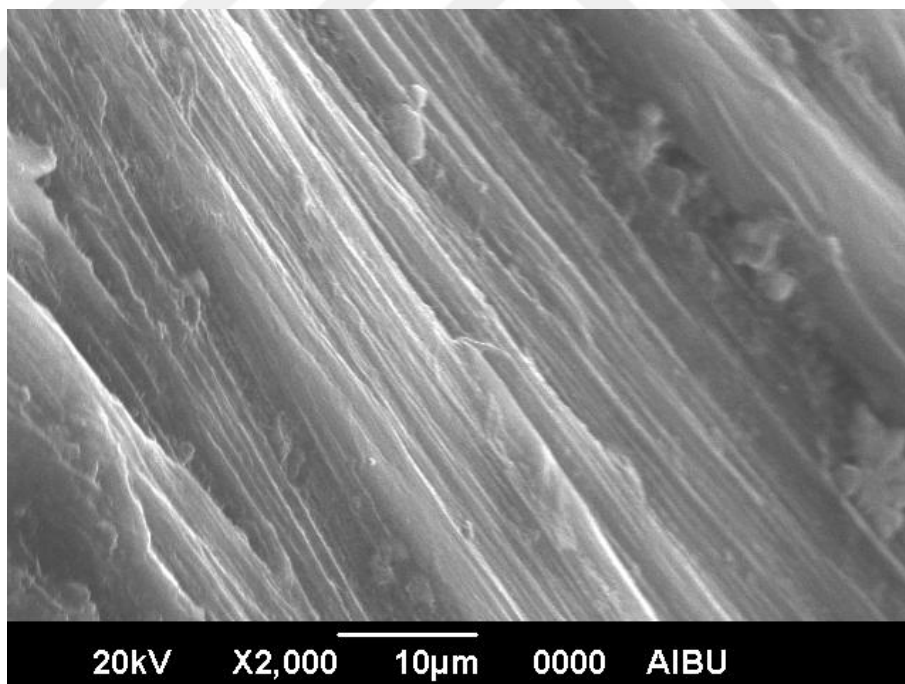


Figure 4.67. SEM micrograph of tensile fractured surface of the copolymer with 6.7% poly(BPOCPMA)-g-HDPE

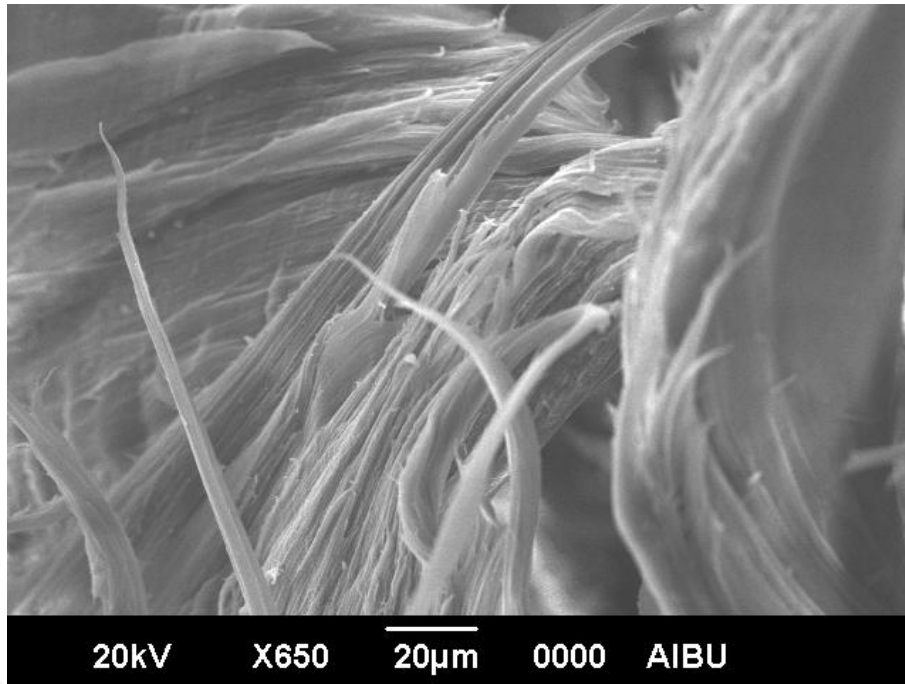


Figure 4.68. SEM micrograph of tensile fractured surface of the copolymer with 10.7% poly(BPOCPMA)-g-HDPE

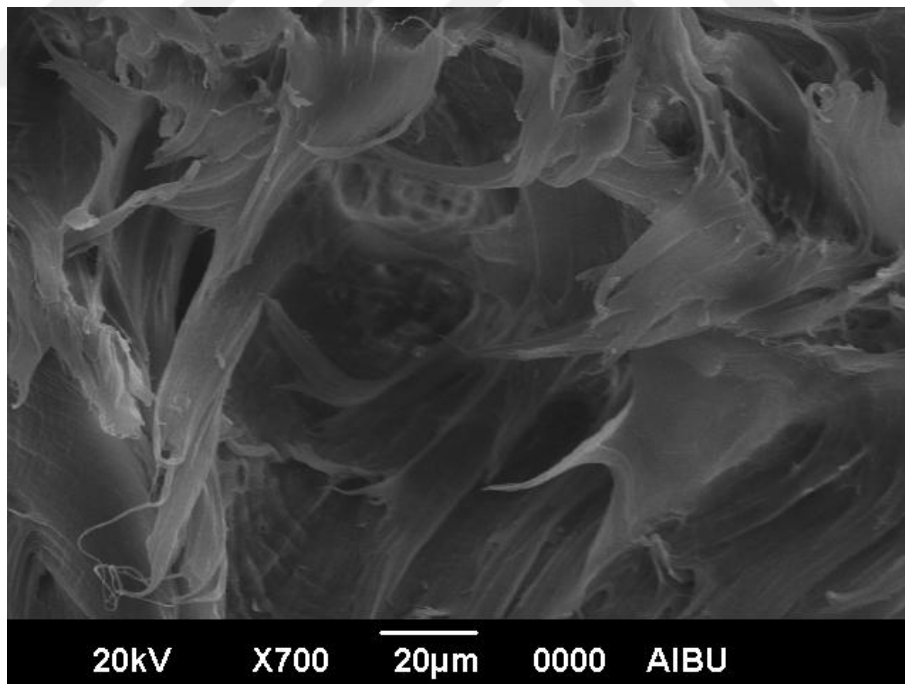


Figure 4.69. SEM micrograph of tensile fractured surface of the copolymer with 12.7% poly(BPOCPMA)-g-HDPE

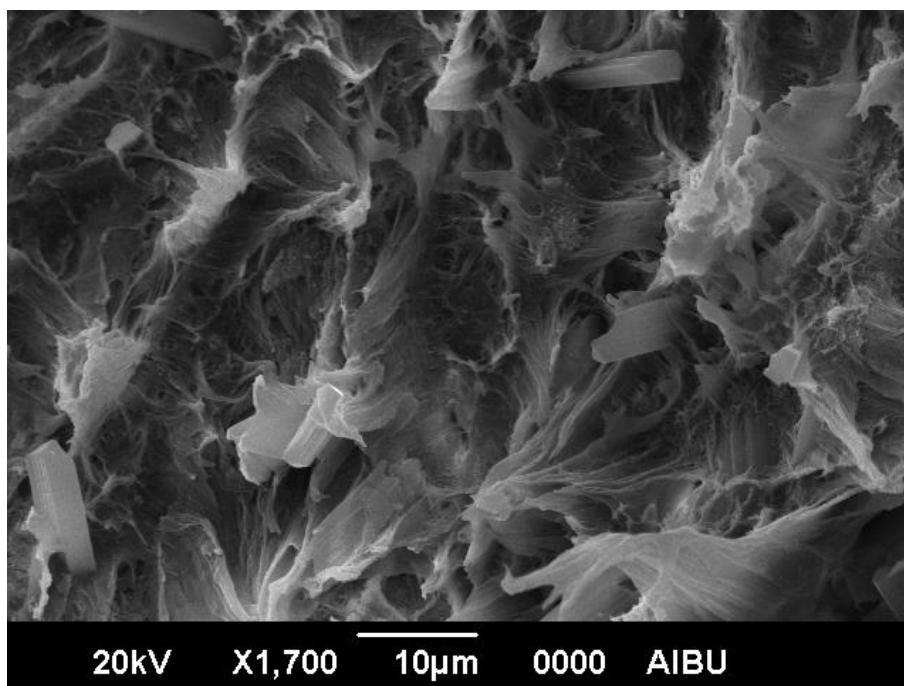


Figure 4.70. SEM micrograph of tensile fractured surface of the coproduct with 25.1% poly(BPOCPMA)-g-HDPE

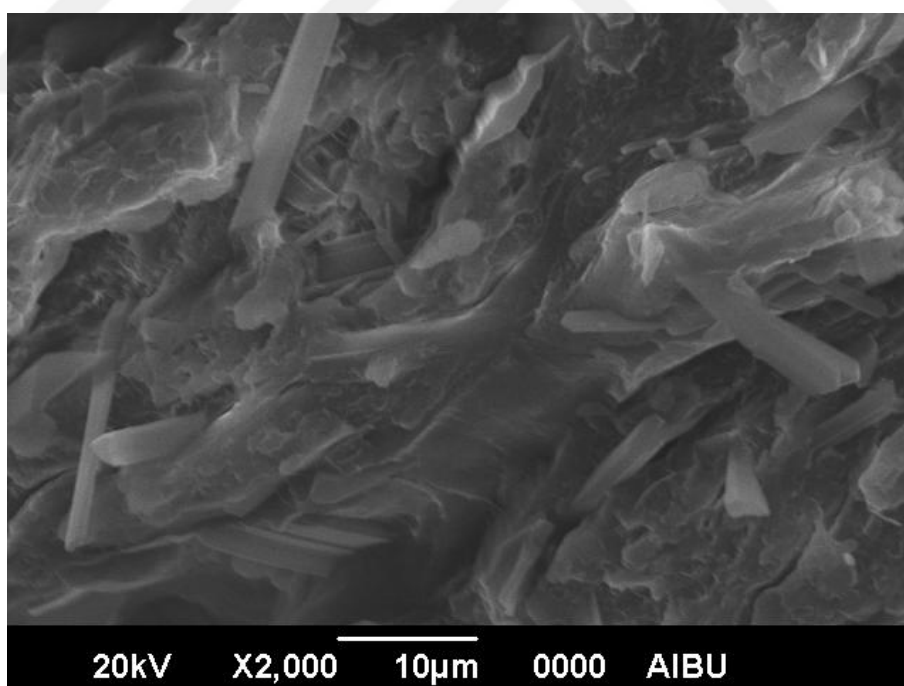


Figure 4.71. SEM micrograph of tensile fractured surface of the copolymer with 18.6% poly(BPOCPMA)-g-HDPE

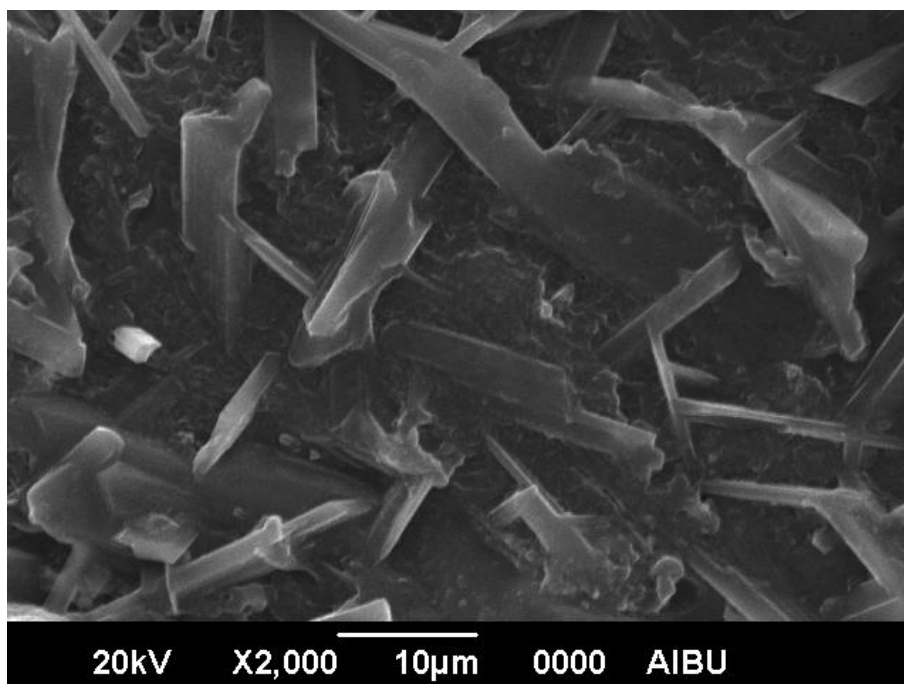


Figure 4.72. SEM micrograph of tensile fractured surface of the copolymer with 21.0% poly(BPOCPMA)

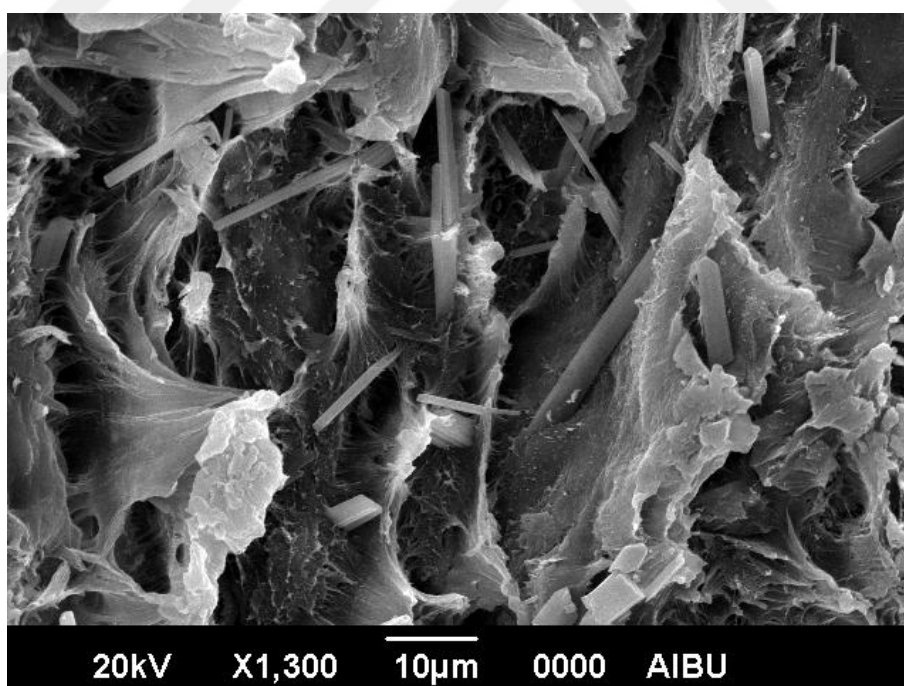


Figure 4.73. SEM micrograph of tensile fractured surface of the coproduct with 26.7% poly(BPOCPMA)-g-HDPE

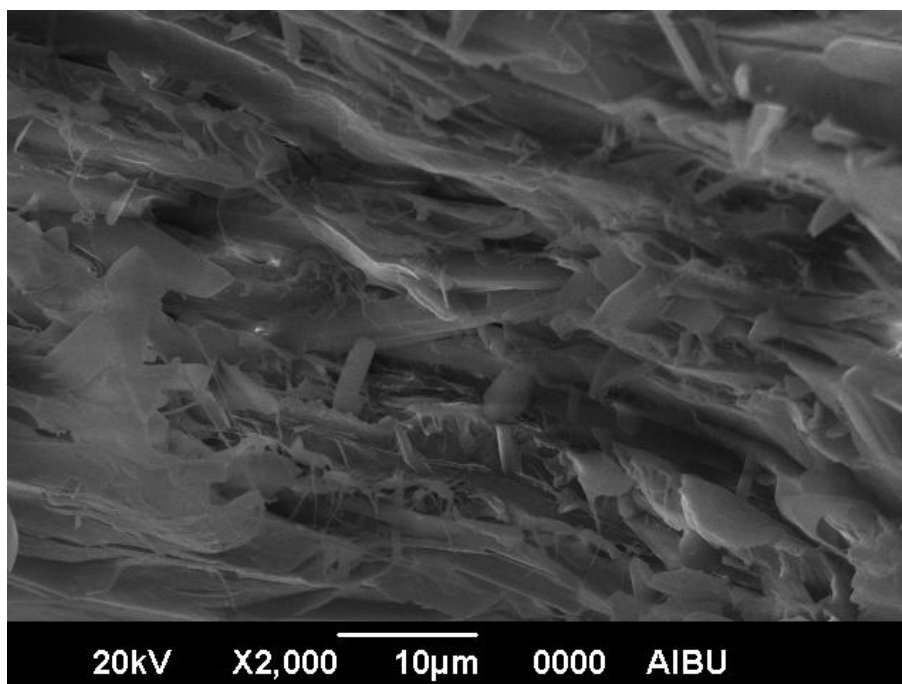


Figure 4.74. SEM micrograph of impact fractured surface of the coproduct with 26.7% poly(BPOCPMA)-g-HDPE

4.4.2 SEM Analysis of Poly(BPOCPA)-g-IPP, Poly(BPOCPMA)-g-IPP Copolymers and The Coproducts

Tensile fractographs of the poly(BPOCPA)-g-IPP copolymers and the coproducts with poly(BPOCPA) content were presented in Figure 4.75-81. The fractographs revealed that brittleness governed the fractures of the samples in general. Some extent of ductility was also detected at relatively low contents of poly(BPOCPA). We observed some short fibrillar structure broken in ductile besides the microcracks and openings showing the major fracture goes through brittle nature, Figure 4.75-78. The prominent change in the morphology was clearly seen through the fractographs given in Figure 4.75-81 at which the short fibrillar structure seen at low contents was replaced by cracks, openings and holes in the fractures. But, the photographs did not show any phase separation at all.

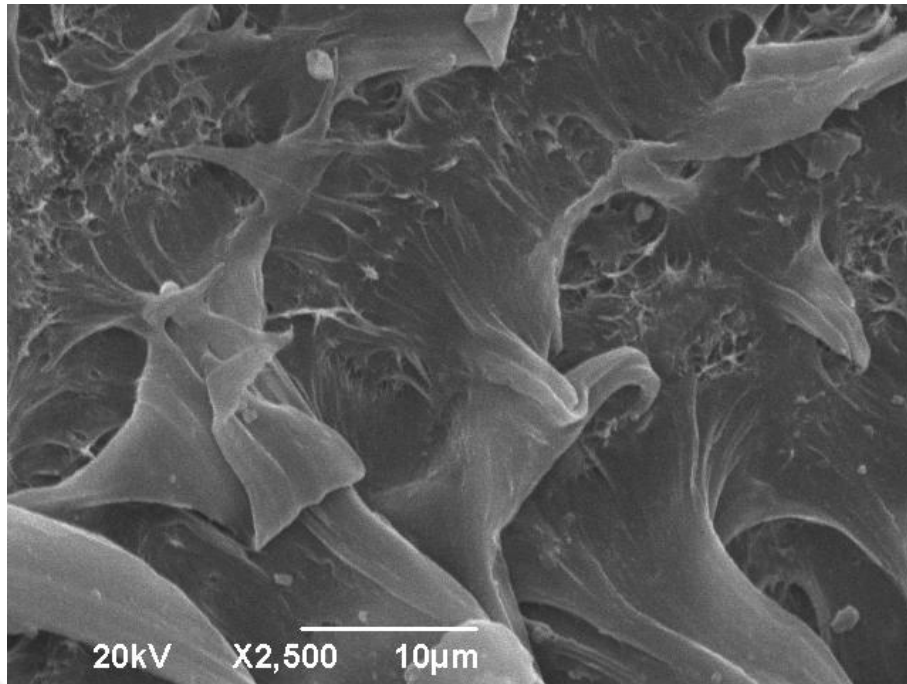


Figure 4.75. SEM micrograph of tensile fractured surface of the copolymer with 3.8% poly(BPOCPA)-g-IPP

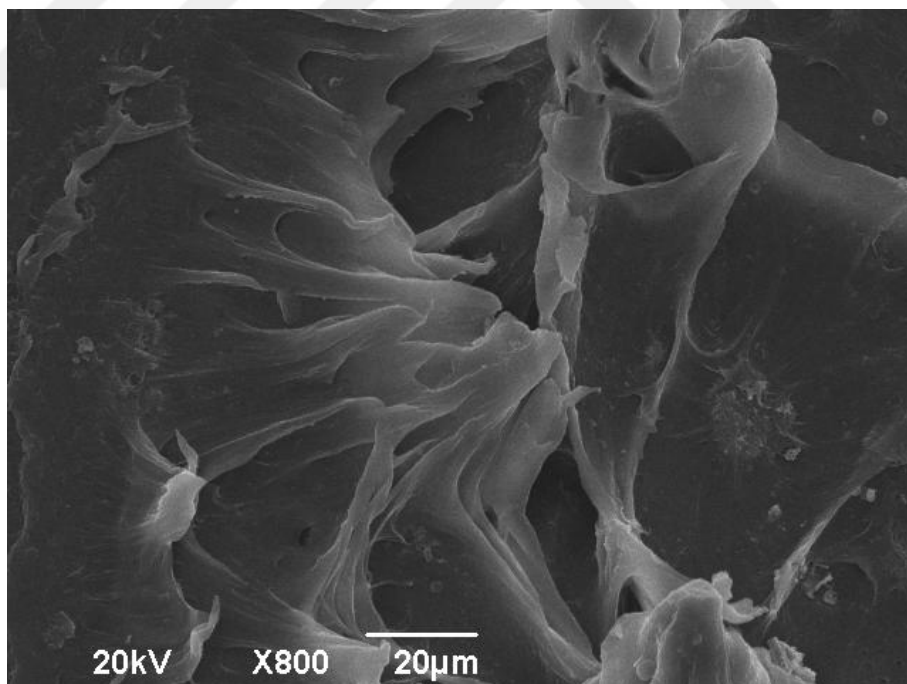


Figure 4.76. SEM micrograph of tensile fractured surface of the copolymer with 7.6% poly(BPOCPA)-g-IPP

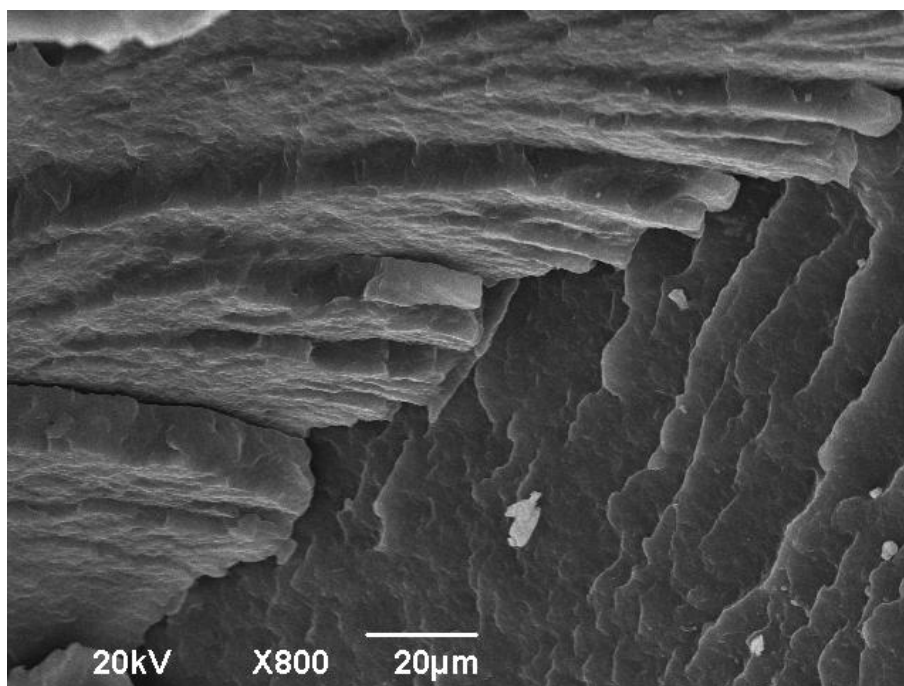


Figure 4.77. SEM micrograph of tensile fractured surface of the copolymer with 9.6% poly(BPOCPA)-g-IPP

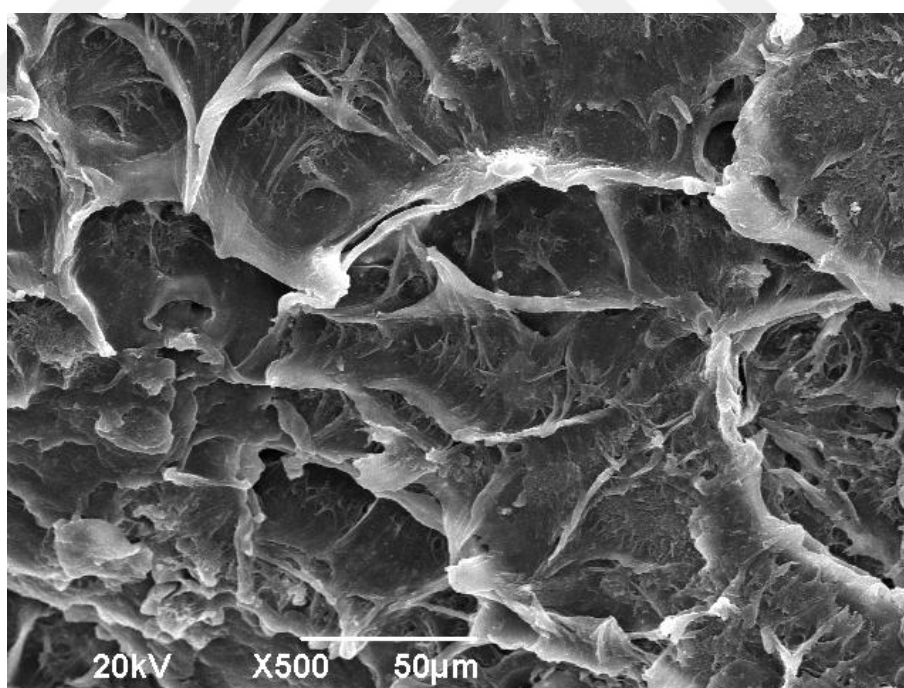


Figure 4.78. SEM micrograph of tensile fractured surface of the coproduct with 12.3% poly(BPOCPA)-g-IPP

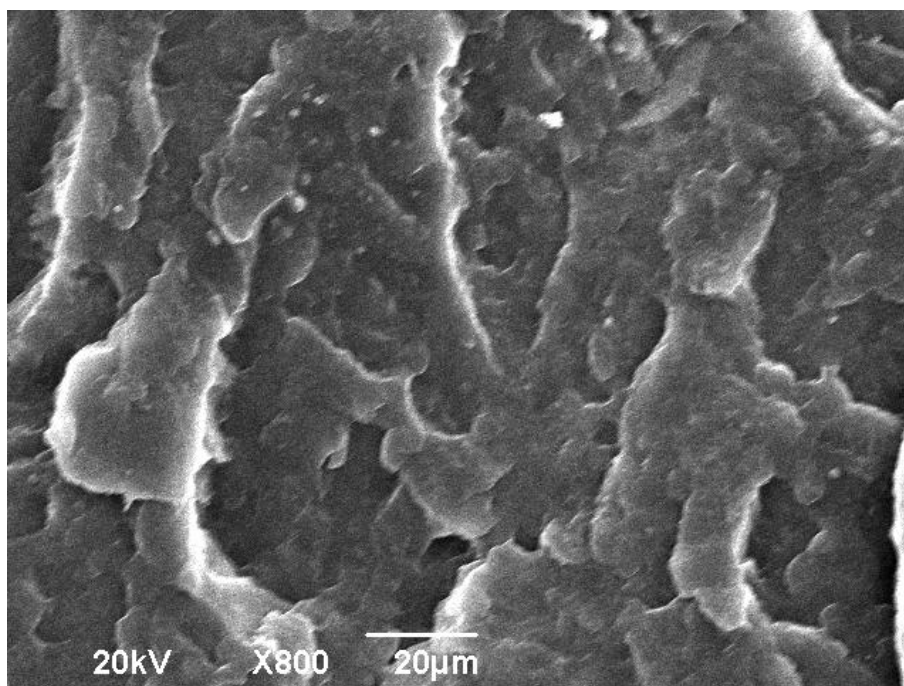


Figure 4.79. SEM micrograph of tensile fractured surface of the copolymer with 10.9% poly(BPOCPA)-g-IPP

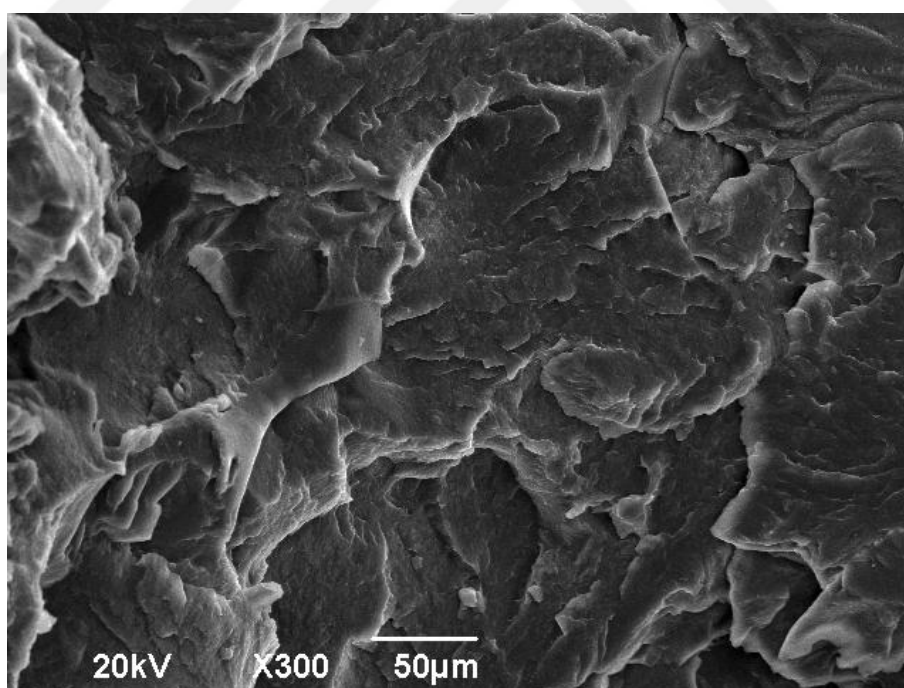


Figure 4.80. SEM micrograph of tensile fractured surface of the coproduct with 28.4% poly(BPOCPA)-g-IPP

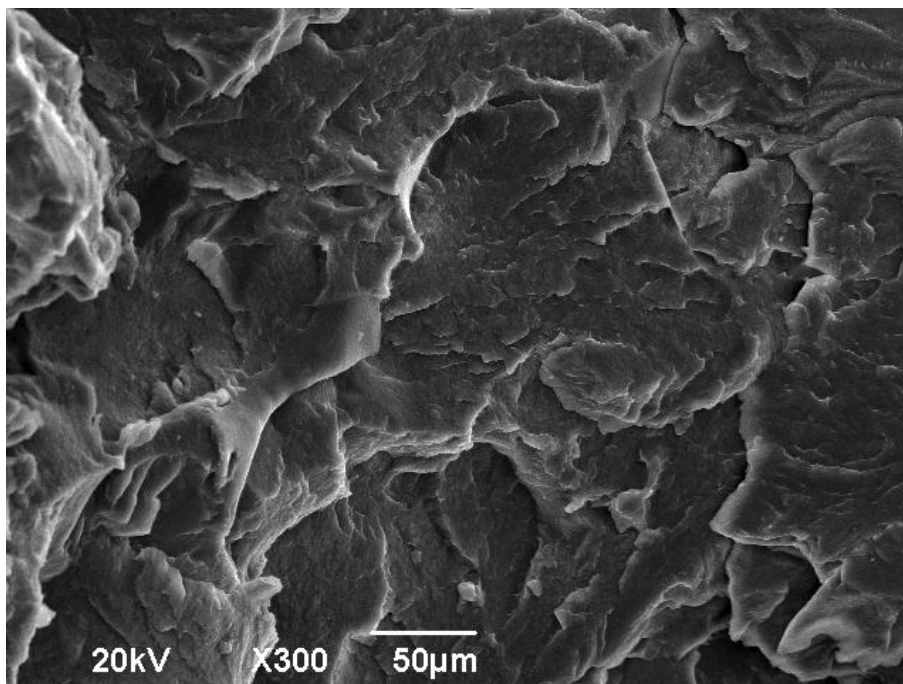


Figure 4.81. SEM micrograph of tensile fractured surface of the coproduct with 39.0% poly(BPOCPA)-g-IPP

All the micrographs of the impact fractured surfaces of the products involving poly(BPOCPA) revealed that the fractures were brittle, Figure 4.82-86. In impact testing, a force is loaded onto the certain area of the test samples in a small time scale. If the loaded impact energy is not delocalized effectively at molecular level i.e. by orientation of the macromolecules, the energy is localized in the weak regions of the structure to form cracks and voids. The fractographs given in Figure 4.82-86 illustrated how the zigzagged propagation of the cracks.

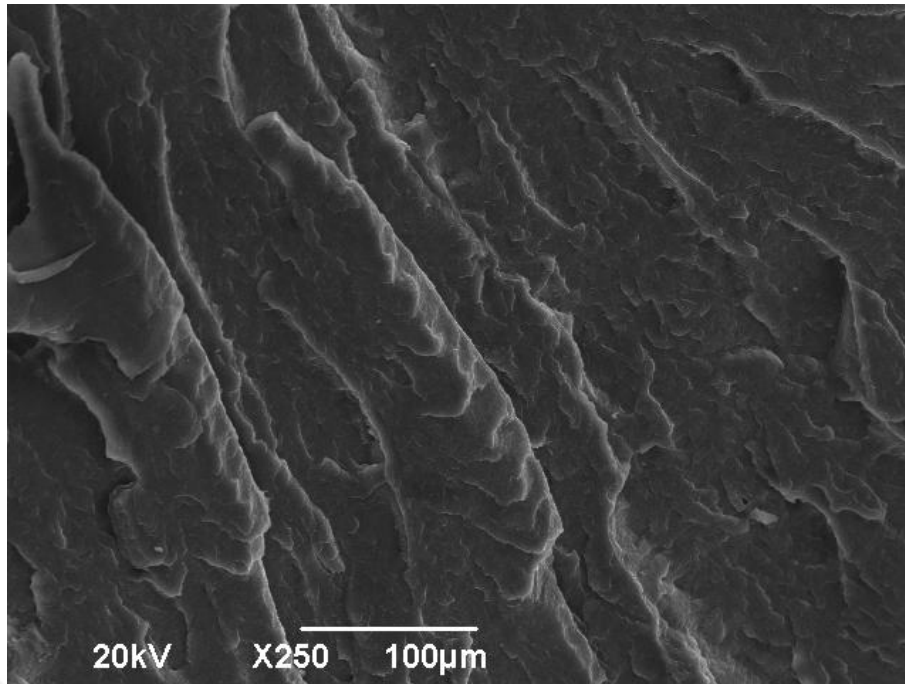


Figure 4.82. SEM micrograph of impact fractured surface of the copolymer with 7.6% poly(BPOCPA)-g-IPP

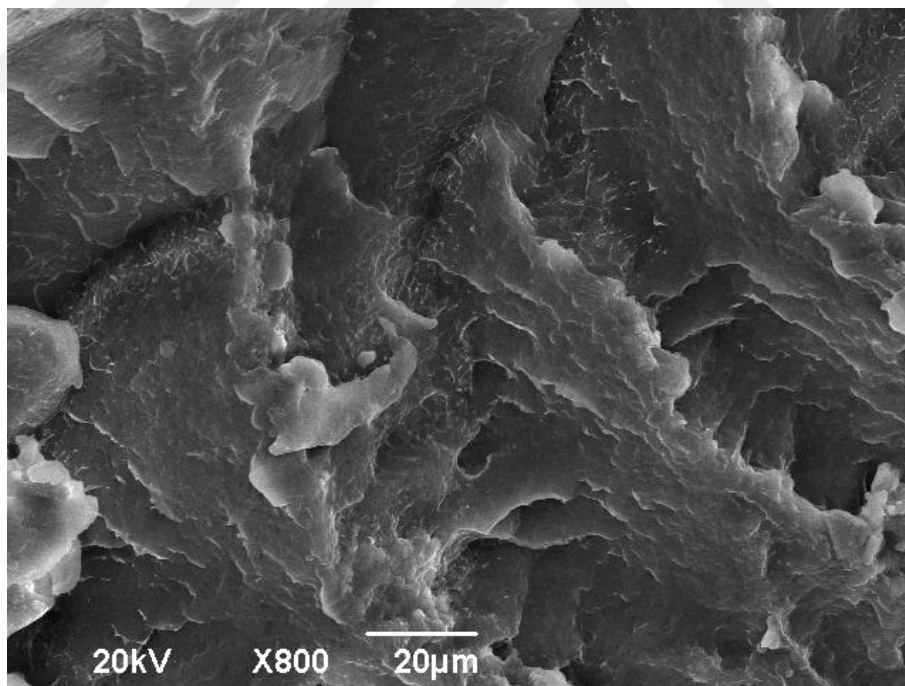


Figure 4.83. SEM micrograph of impact fractured surface of the copolymer with 10.9% poly(BPOCPA)-g-IPP

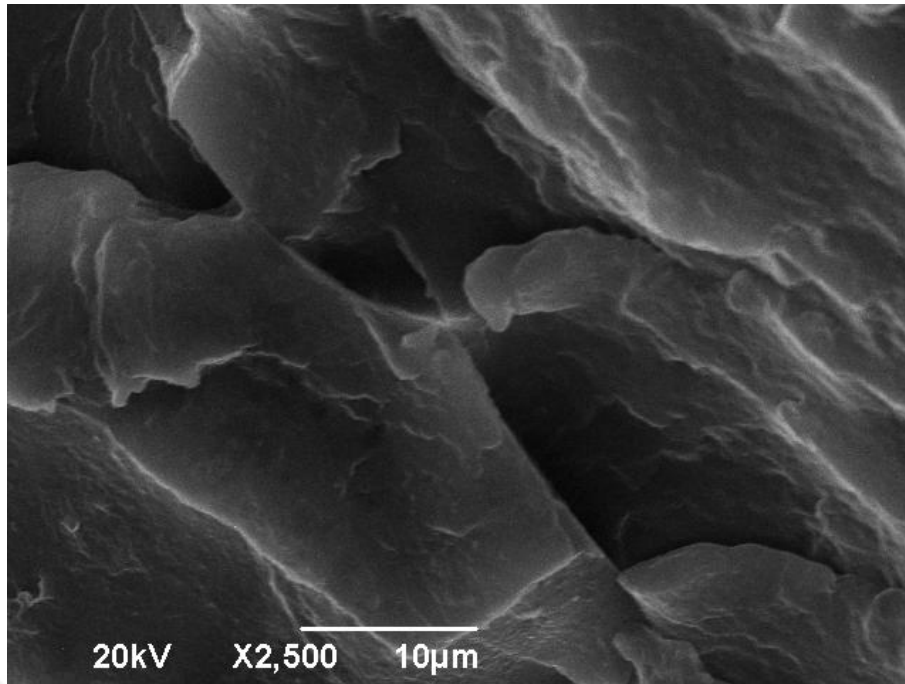


Figure 4.84. SEM micrograph of impact fractured surface of the coproduct with 4.0% poly(BPOCPA)-g-IPP

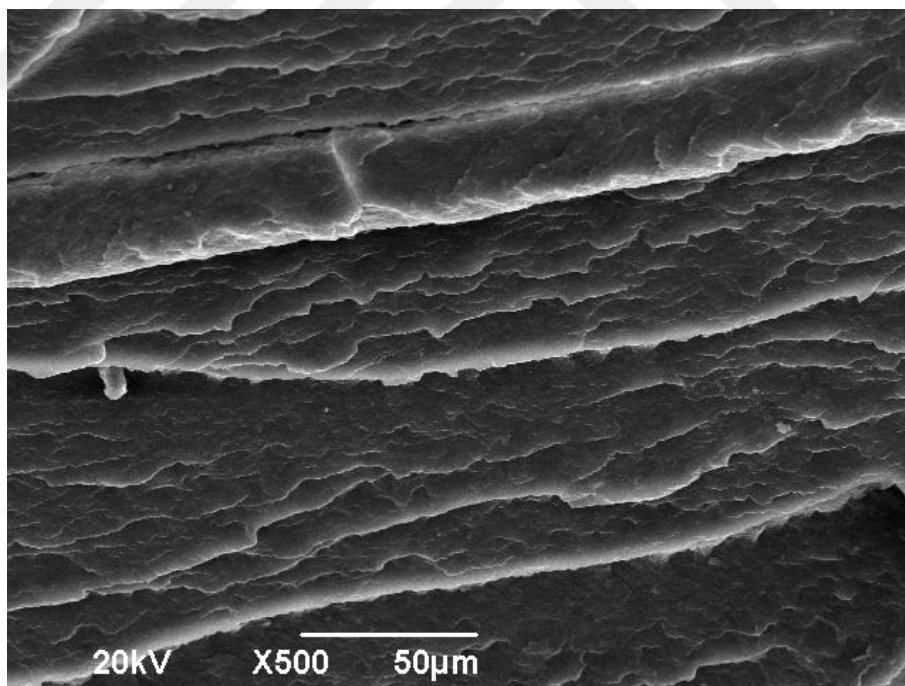


Figure 4.85. SEM micrograph of impact fractured surface of the coproduct with 12.3% poly(BPOCPA)-g-IPP

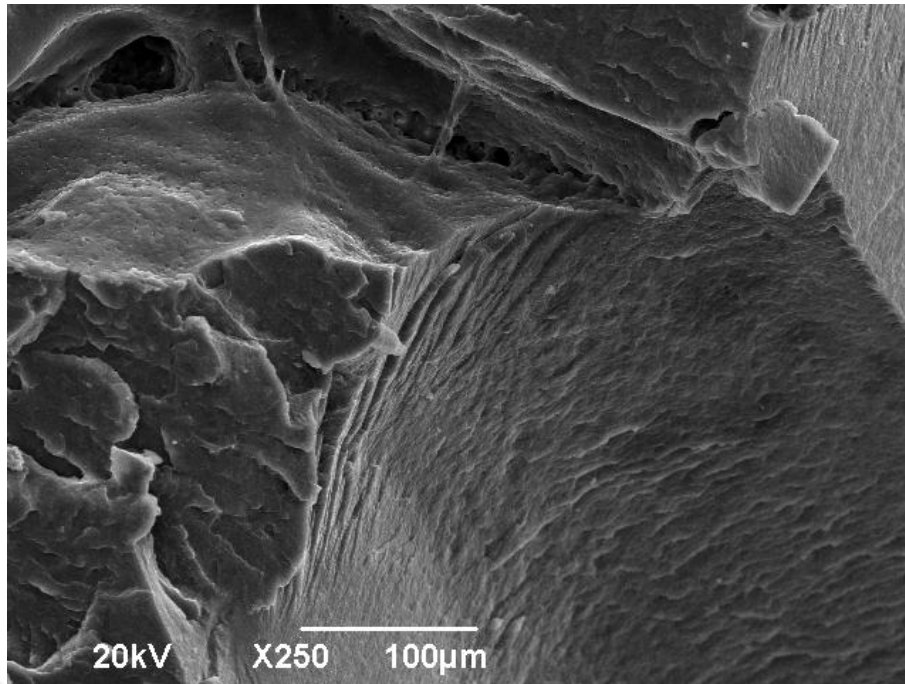


Figure 4.86. SEM micrograph of impact fractured surface of the coproduct with 39.0% poly(BPOCPA)-g-IPP

A similar morphological behavior was also observed in the products comprising poly(BPOCPMA). The tensile fractographs illustrated some extent of ductility and some short fibrillar structure broken in ductile besides the microcracks and openings, Figure 4.87-94. But, brittleness was the major in fractures and became more prominent as the content increased. This was revealed by the gradual replacement of short fibrillar structure seen at relatively low contents with cracks and openings recorded at high percentages of poly(BPOCPMA). But, there existed a small fibrillar structure even at contents, Figure 4.92-94. On the other hand, any phase separation was not detected at all.

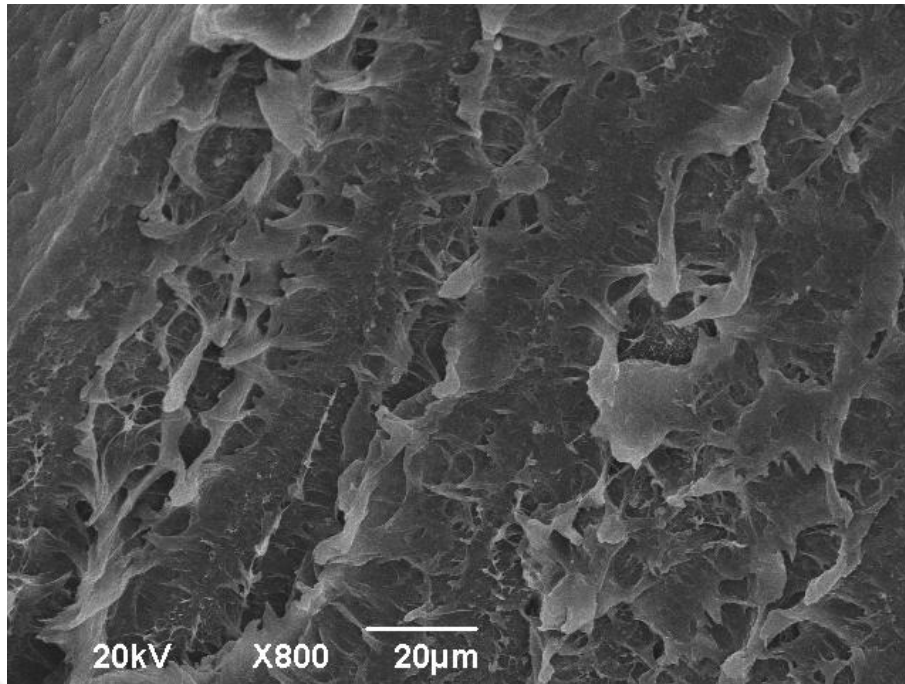


Figure 4.87. SEM micrograph of tensile fractured surface of the copolymer with 5.1% poly(BPOCPMA)-g-IPP

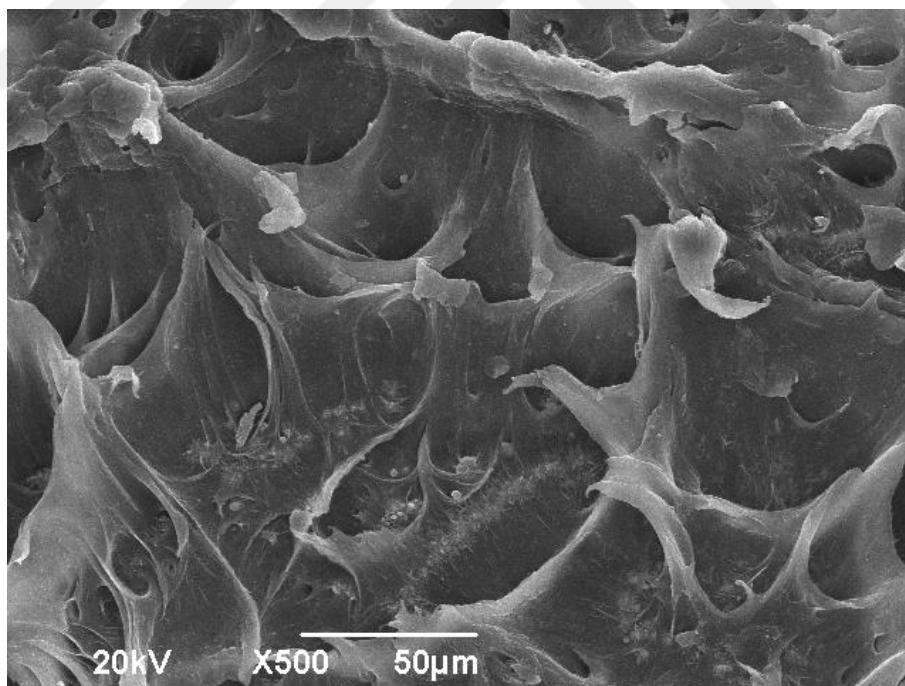


Figure 4.88. SEM micrograph of tensile fractured surface of the copolymer with 6.6% poly(BPOCPMA)-g-IPP

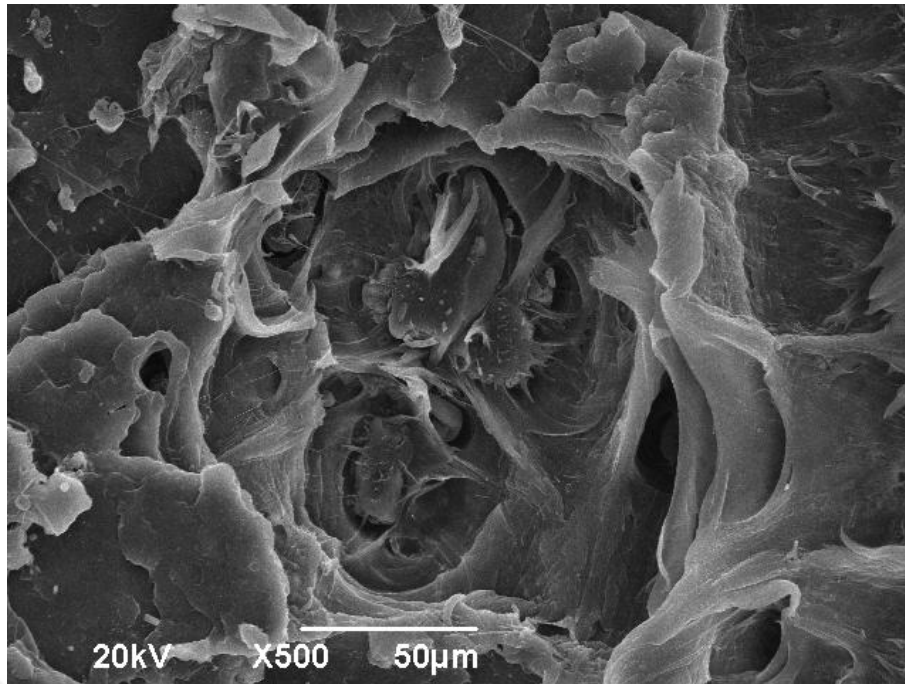


Figure 4.89. SEM micrograph of tensile fractured surface of the copolymer with 8.9% poly(BPOCPMA)-g-IPP

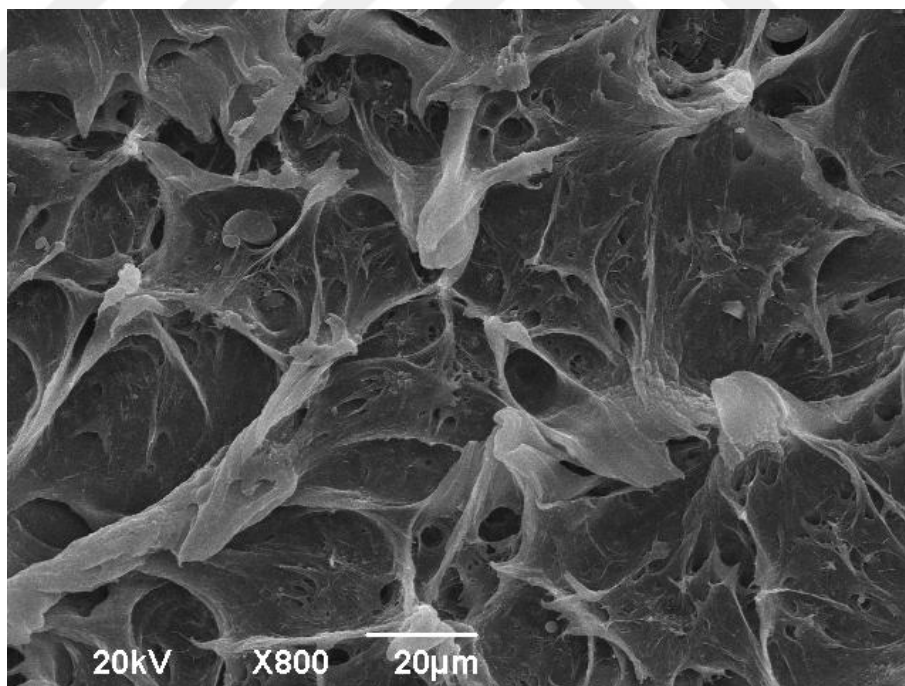


Figure 4.90. SEM micrograph of tensile fractured surface of the copolymer with 10.3% poly(BPOCPMA)-g-IPP

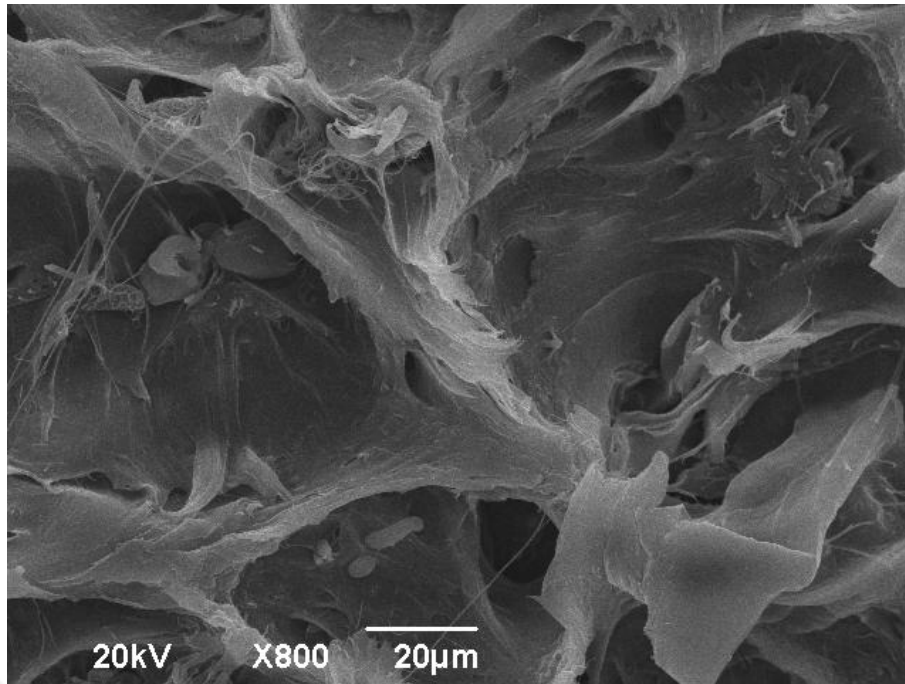


Figure 4.91. SEM micrograph of tensile fractured surface of the coproduct with 14.0% poly(BPOCPMA)-g-IPP

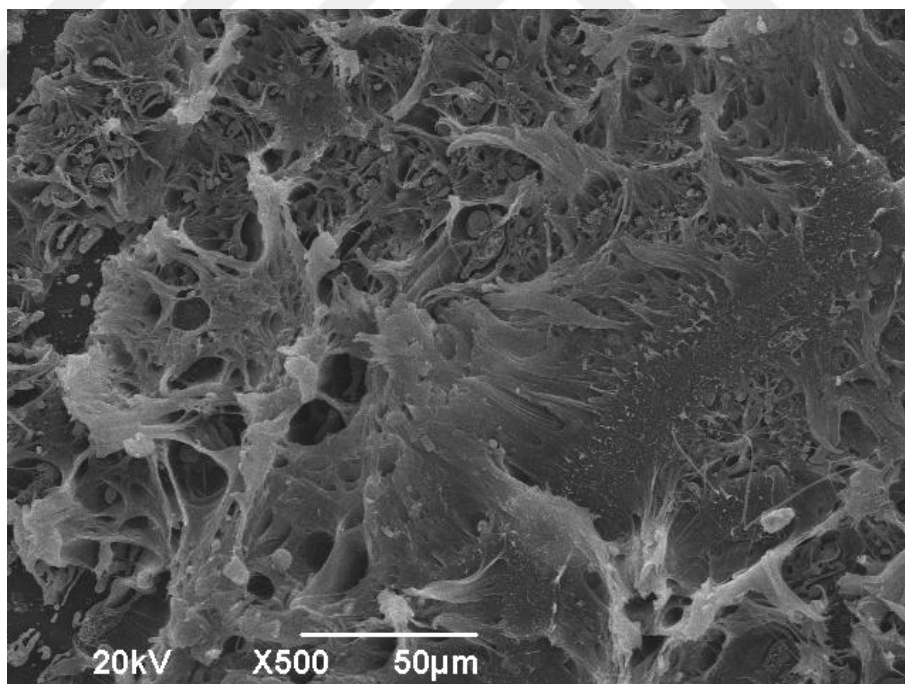


Figure 4.92. SEM micrograph of tensile fractured surface of the coproduct with 18.8% poly(BPOCPMA)-g-IPP

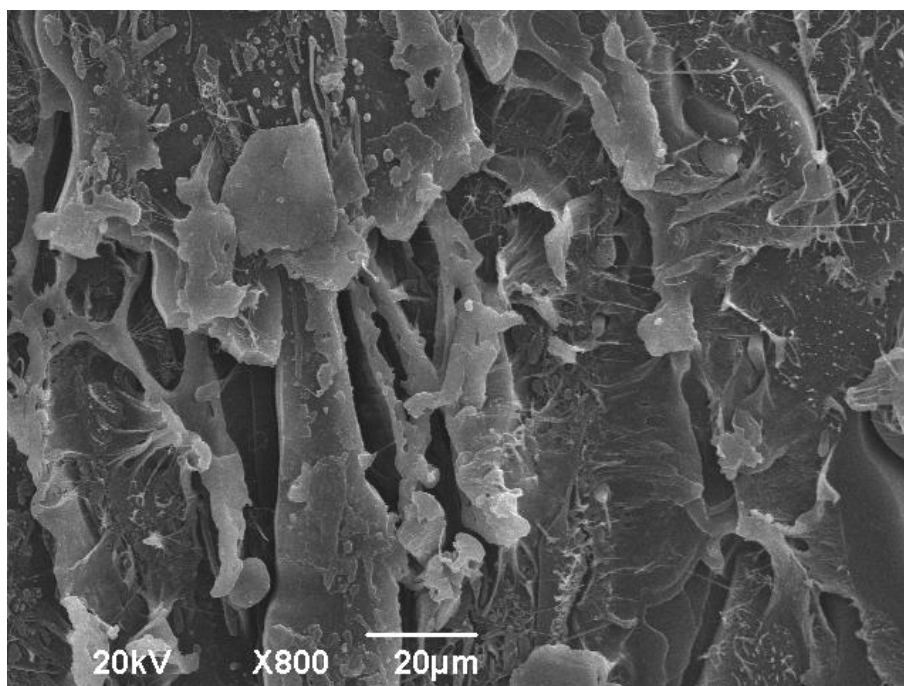


Figure 4.93. SEM micrograph of tensile fractured surface of the coproduct with 27.9% poly(BPOCPMA)-g-IPP

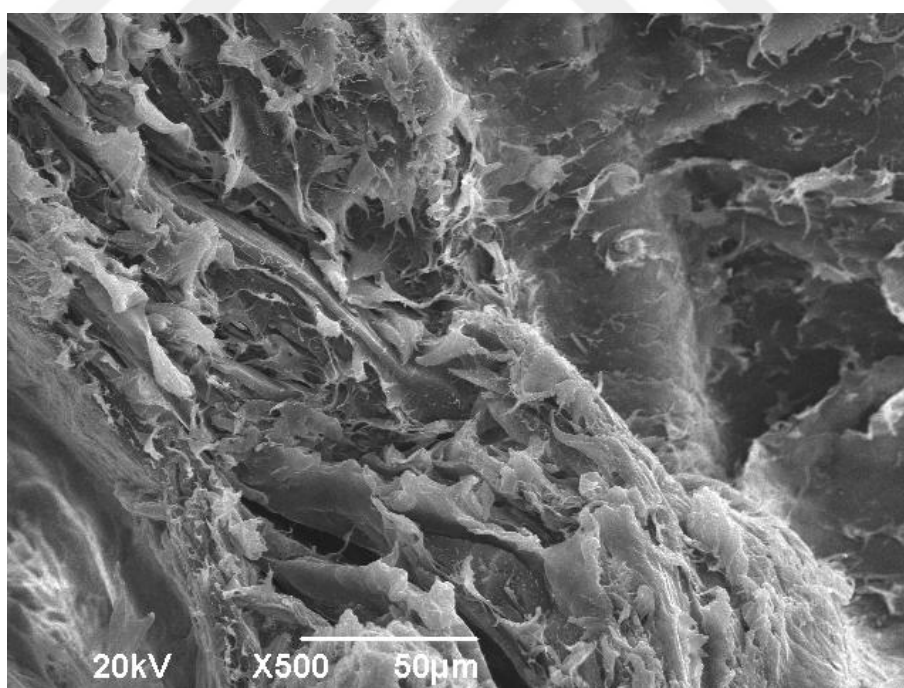


Figure 4.94. SEM micrograph of tensile fractured surface of the coproduct with 37.8% poly(BPOCPMA)-g-IPP

The brittleness in fractures was also revealed in impact fractographs of the products, Figure 4.95-98. The micrographs, however, showed some extent of ductility and fibrillar structure at low contents, Figure 4.95 and 4.96, which were replaced by zigzagged cracks and openings as the percentage of poly(BPOCPMA) increased.

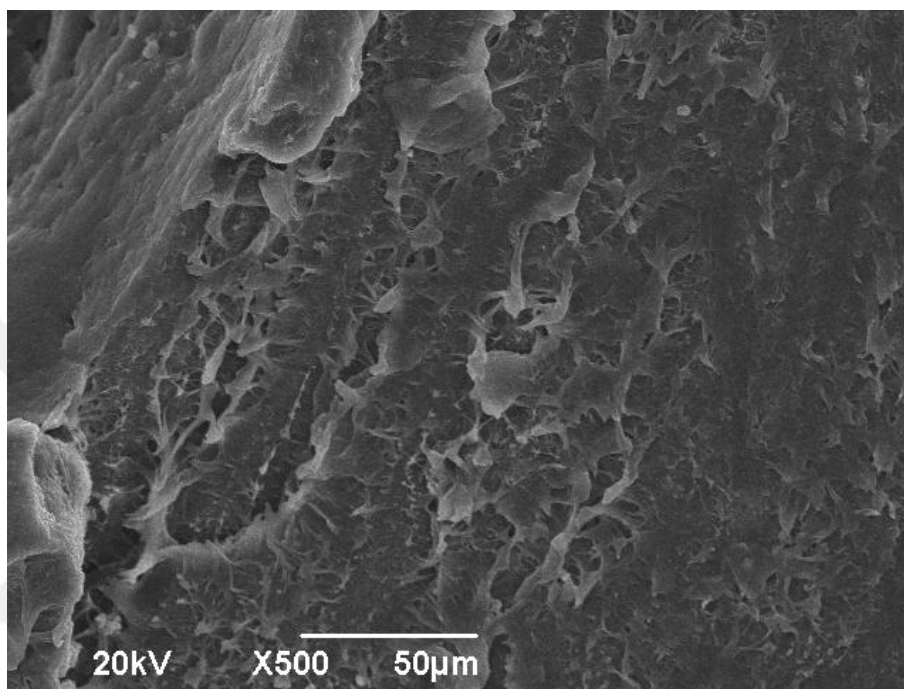


Figure 4.95. SEM micrograph of impact fractured surface of the copolymer with 5.1% poly(BPOCPMA)-g-IPP

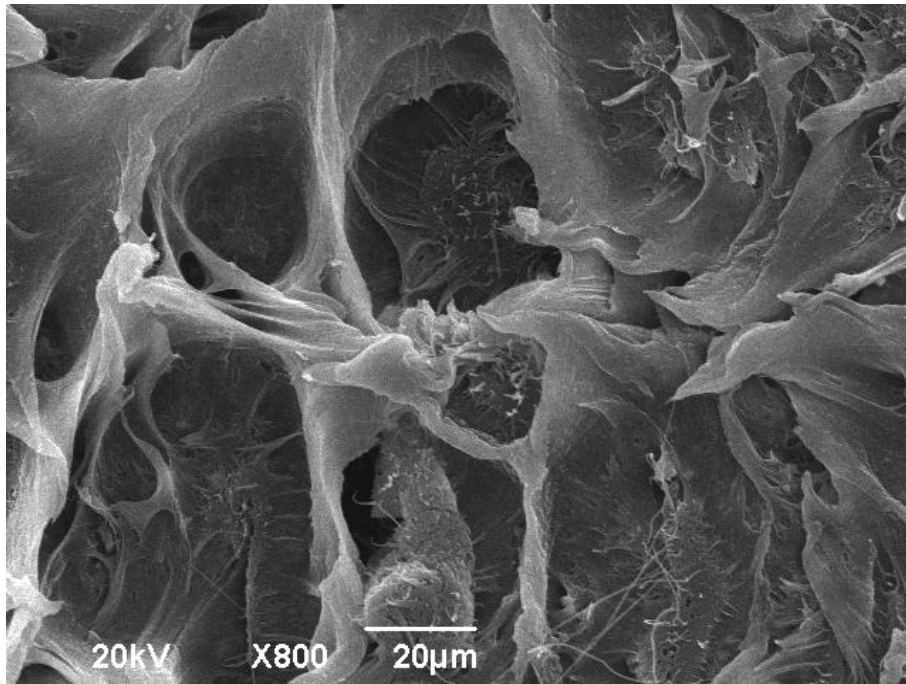


Figure 4.96. SEM micrograph of impact fractured surface of the coproduct with 9.5% poly(BPOCPMA)-g-IPP

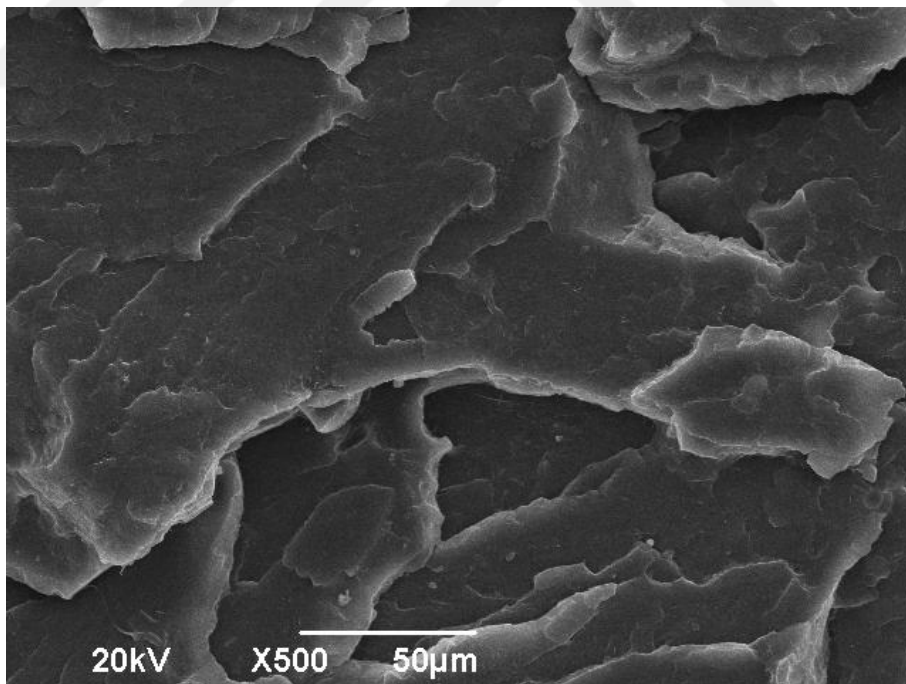


Figure 4.97. SEM micrograph of impact fractured surface of the copolymer with 10.3% poly(BPOCPMA)-g-IPP

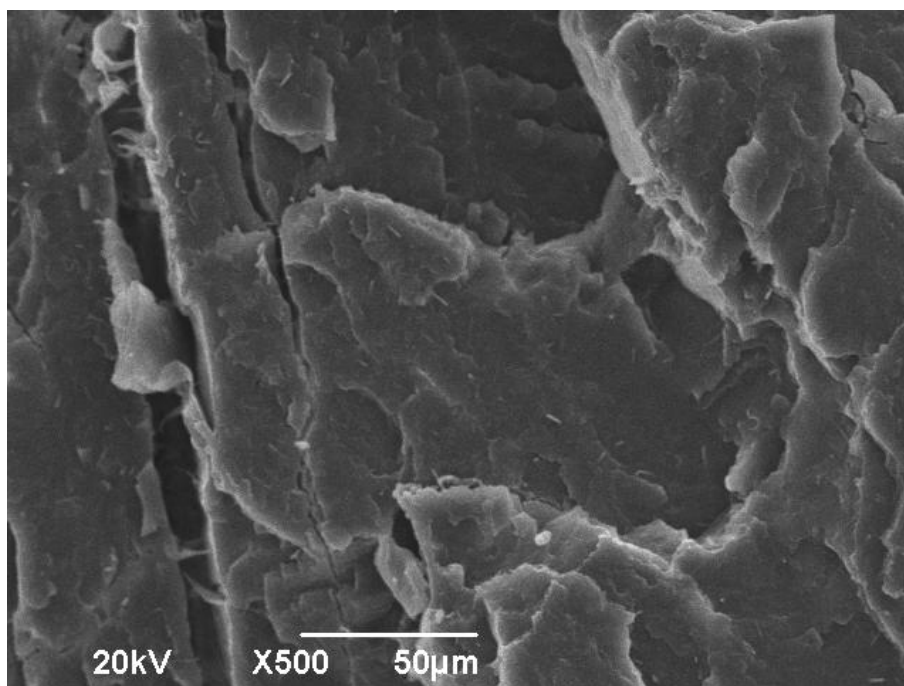


Figure 4.98. SEM micrograph of impact fractured surface of the coproduct with 27.9% poly(BPOCPMA)

5. CONCLUSIONS

✓ Thermally initiated graft copolymerization of BPOCPMA onto HDPE and of BPOCPA and BPOCPMA onto IPP were successfully carried out. Variation of grafting with the mixing ratio of the monomer and the matrix polymer (HDPE or IPP) in the reaction mixtures was investigated. The content of graft units in the products consistently increased with the percentage of the monomers in the reaction mixtures while the percent graftings reached the maximum values at relatively lower monomer concentrations, which were followed by dramatic decreases. It was presumed that the graftings took place via the radicals forming on matrix chains rather than the reactions between propagating poly(BPOCPA) and poly(BPOCPMA) radicals and the matrix macromolecules due to probable steric hindrance.

✓ The graft copolymerization of BPOCPMA led to noteworthy increases in the crystalline melting temperature of HDPE in the products. Advances in the ordered and oriented packing of HDPE chains in the crystallites due to the constitution of side chain LCP poly(BPOCPMA) molecules as graft units were believed to result in the increases.

✓ The graft copolymerizations gave rise to significant enlargements in the lateral dimensions of the unit cell (a and b parameters) of the orthorhombic structure of HDPE in consistence with the graft content. The grafted poly(BPOCPMA) molecules with rigid, voluminous and polar side groups probably forced the HDPE chains apart laterally and thus expanded the unit cell dimensions. A constant expansion in c parameter, the unit cell axis parallel with the chain axis of HDPE molecular segments, however, was recorded in all products.

✓ The lateral dimensions of the monoclinic unit cell of IPP matrix were also found to be considerably affected by poly(BPOCPA) and poly(BPOCPMA) content in the products. Both a and b parameters increased significantly at low percentages of the graft units. The IPP chains in the unit cells were probably forced apart laterally by the polar graft units, thus giving rise to expansions in the lateral dimensions at low percentages of poly(BPOCPA). The weak interactions between polar side groups

of the grafted units and nonpolar IPP chains might have an additional effect in the expansions at those low contents. This effect was more prominent in the dimension *a*. At higher contents, the developed interactions between the polar side groups probably led to the decreases in lateral dimensions of the unit cells. The parameter *c* decreased in all products in consistence with the content.

✓ The graft copolymerization of BPOCPMA gave rise to increases in the crystal size in crystalline domains of HDPE matrix with the content. The expansions in the lateral dimensions of the unit cells have seemingly resulted in the extended growth of the crystals with the dimensional enlargements. Moreover, the glassy nematic structured poly(BPOCPMA) units acting as nucleating agents during crystallizations might have conducted to more ordered packing HDPE chains and thus additionally contributed to the promoted growth of the crystals.

✓ The crystal size in the crystalline domains of IPP matrix were also found to be considerably affected by poly(BPOCPA) and poly(BPOCPMA) content in the products. The size increased initially with the percentage of poly(BPOCPA), and then had a decrease trend at higher contents. The poly(BPOCPA) units with regular structure (with the potential of forming the glassy nematic phase (Sainath et al., 2000) might have acted as nucleating agents and conducted to more ordered packing of IPP chains and thus to the promoted growth of the crystals. The decreases might have arisen mainly from the extensive nucleation resulted from the increasing poly(BPOCPA) content. The widespread nucleation might have eventually given rise to a large number of IPP crystals but with a smaller size. A similar behavior was also recorded in the copolymers involving poly(BPOCPMA). But, presence of the poly(BPOCPMA) homopolymers in the coproducts led to comparable or lower sizes detected relatively at higher contents.

✓ The grafting onto HDPE, while leading to relatively smaller increase in the free volume size at low percentage of poly(BPOCPMA), resulted in reduced volume with the increase of the content in the products. Relatively larger holes in the material at low contents presumably due to larger openings between the chains brought about by the voluminous side groups of the poly(BPOCPMA) molecules that compel the chains laterally. Moreover, the grafting resulted in dramatic decreases in the free volume fractions with the content, especially in the copolymers. The

interactions between the polar side groups, becoming more effective with the content, probably led to more compact packing of the chains in the matrix, which resulted in the reduction of the free volume fraction. The bulky side groups giving rise to the larger openings between the chains might have occupied the voids in majority with the increase of the content, owing to the preferred interactions between the polar groups and to the weak interactions between the polar units and nonpolar HDPE chains.

✓ Remarkable improvements were achieved in the mechanical properties of the poly(BPOCPMA)-g-HDPE products, particularly, in ultimate tensile strength and modulus. But, percent elongation and yield stress were lost at high contents of poly(BPOCPMA), and brittleness dominated in the mechanical characters. The mechanical behaviors were perceived to be largely governed by the free volume properties of the products. Superior tensile behaviors were recorded in the products that have lower free volume size and fraction. The larger free volumes and their greater fraction conducted to relatively extensive drawing to further elongations in the tensile direction, owing to probable reduction in resistive frictional force and higher conformational freedom of the macromolecules. Probable losses and restrictions in chain mobility at relatively higher contents, brought about by the decreases in the hole sizes and the fractions probably made the chains more resistive in sliding over each other. This effect presumably made the material superiorly withstanding under load and more resistive against deformation while leading to brittleness in the character of the material.

✓ While the graft copolymerization of BPOCPA onto IPP leading to some improvements the mechanical properties of the products at low percentages of poly(BPOCPA), the graft copolymerization of BPOCPMA gave rise to diminishes in all tensile and impact behaviors in consistence with the content of poly(BPOCPMA). Both grafting imparted brittleness increasing consistently with the contents to the material.

✓ The structures of the products were completely homogeneous in spite of that the graft units poly(BPOCPA) and poly(BPOCPMA) with polar side groups were essentially different in nature from apolar HDPE and IPP. This result confirmed the chemical bonding of the graft units, that is, graft copolymerization of BPOCPMA

onto HDPE and IPP, and of BPOCPA onto IPP. The products exhibited brittle nature with some ductility.



6. REFERENCES

- Abbe JC, Duplatre G, Maddock AG, Talamoni J and Haessler A (1981) "Correlation between Pulse Radiolysis and Positron Annihilation Techniques Data", *Journal of Inorganic and Nuclear Chemistry*, 43: 2603-2610.
- Abedi S and Abdouss M (2014) "A Review of Clay-Supported Ziegler–Natta Catalysts for Production of Polyolefin/Clay Nanocomposites through in Situ Polymerization", *Applied Catalysis A: General*, 475: 386–409.
- Almaadeed MA, Ouederni M and Khanam PN (2013) "Effect of Chain Structure on the Properties of Glass Fibre/Polyethylene Composites", *Materials & Design*, 47: 725-730.
- Avella M, Martuscelli E and Raimo M (1997) "Polypropylene Reinforced with Silicon Carbide Whiskers", *Journal Of Materials Science*, 32: 2411—2416.
- Badia A and Duplatre G (1999) "Electron Beam and Gamma Irradiation Effects on High Density Polyethylene Studied Via Positron Annihilation Lifetime Spectroscopy", *Radiation Physics and Chemistry*, 54(2): 151-158.
- Baker AME and Windle AH (2001a) "The Effects of Branching and Fibre Drawing on the Crystal Structure of Polyethylene", *Polymer*, 42: 651-665.
- Baker AME and Windle AH (2001b) "An X-Ray Diffraction and Modelling Study of Short Chain Branch Location within the Structure of Polyethylene", *Polymer*, 42: 681-698.
- Bose S, Pramanik N, Das CK, Ranjan A and Saxena AK (2010) "Synthesis and Effect of Polyphosphazenes on the Thermal, Mechanical and Morphological Properties of Poly(Etherimide)/Thermotropic Liquid Crystalline Polymer Blend", *Materials & Design*, 31(3): 1148-1155.
- Brusa RS, Naia MD, Margoni D and Zecca A (1995) "Positron Mobility in Polyethylene in the 60-400 K Temperature-Range", *Applied Physics a-Materials Science & Processing*, 60(5): 447-453.
- Bunescu A, Lee S, Li Q and Hartwig J (2017) "Catalytic Hydroxylation of Polyethylenes", *American Chemical Society*, 3: 895–903.
- Calundann GW. (1980-1981). US Patents
- Cassidy J, Nesaei S, Mctaggart R and Delfanian F (2016) "Mechanical Response of High Density Polyethylene to Gamma Radiation from a Cobalt-60 Irradiator", *Polymer Testing*, 52: 111-116.

- Cetin S and Tinçer T (2007) "Graft Copolymerization of P-Acryloyloxybenzoic Acid and P-Methacryloyloxybenzoic Acid onto Isotactic Polypropylene and Their Thermal Properties: Part I", *Journal of Applied Polymer Science*, 108: 414–422.
- Chang HS, Wu TY and Chen Y (2002) "Synthesis and Properties of Tlcps with 2,6-Naphthalene-Based Mesogen, Polymethylene Spacer and Non-Linear 4,4'-Thiodiphenyl Links", *Journal of Applied Polymer Science*, 83: 1536–1546.
- Chen BR, Ysay SY and Chen CY (2005) "Synthesis and Properties of Liquid Crystalline Polymers with Low T_m and Broad Mesophase Temperature Ranges", *Journal of Polymer*, 46: 8624-8633.
- Chiou YP, Chiou KC and Chang FC (1996) "In Situ Compatibilized Polypropylene/Liquid Crystalline Polymer Blends", *Polymer*, 37(18): 4099-4106.
- Chung T (2002) "Synthesis of Functional Polyolefin Copolymers with Graft and Block Structures", *Progress in Polymer Science*, 27: 39-85.
- Collyer A (1989) "Thermotropic Liquid-Crystal Polymers for Engineering Applications", *Journal of Materials Processing Technology*, 5: 309-322.
- Costa HM, Ramos VD and Oliveira MG (2007) "Degradation of Polypropylene (Pp) During Multiple Extrusions: Thermal Analysis, Mechanical Properties and Analysis of Variance", *Polym. Test.*, 26: 676–684.
- Dai YQ, Wang B, Wang SJ, Jiang T and Cheng SY (2003) "Study on the Microstructure and Miscibility of Dynamically Vulcanized Epdm/Pp Blend by Positron Annihilation", *Radiation Physics and Chemistry*, 68(3-4): 493-496.
- Djourelou N, He C, Suzuki T, Shantarovich VP, Ito Y, Kondo K and Ito Y (2003) "Positron Annihilation in Polypropylene Studied by Lifetime and Coincidence Doppler-Broadening Spectroscopy", *Radiation Physics and Chemistry*, 68(5): 689-695.
- Donald AM and Windle AH (1992) *Liquid Crystalline Polymers*. Cambridge: Cambridge University Press.
- Dong X, Mcdowell DL, Kalidindi SR and Jacob KI (2014) "Dependence of Mechanical Properties on Crystal Orientation of Semi-Crystalline Polyethylene Structures", *Polymer*, 55(16): 4248-4257.
- Duplatre G, Didierjean F and Abbe JC (1990). "Influence of Electron Beam Irradiation on Polyethylene: A Lifetime Spectroscopy Study Involving Dose and Temperature", Paper presented at the In Third International Workshop on Positron and Positronium Chemistry Singapore.

- Duplatre G and Jonah CD (1985) "Reactions of Electrons in High-Concentration Water Solutions-a Comparison between Pulse-Radiolysis and Positron Annihilation Lifetime Spectroscopy Data ", *Radiation Chemistry and Physics*, 24: 557-565.
- Ecevit ST (2012). "Synthesis and Characterization of Polypropylene Based Ion-Exchange Resin", Middle East Technical University.
- Edward P and Moore J (1996) *Polypropylene Handbook*. Inc., Cincinnati: Hanser/Gardner Publications.
- El-Nashar D, Gomaa E and Abd-El-Messieh S (2009) "Study of Electrical, Mechanical, and Nanoscale Free-Volume Properties of Nbr and Epdm Rubber Reinforced by Bentonite or Kaolin", *Journal of Polymer Science: Part B: Polymer Physics*, 47: 1825–1838.
- Eldrup M, Lightbody D and Sherwood JN (1981) "The Temperature-Dependence of Positron Lifetimes in Solid Pivalic Acid", *Chemical Physics*, 63: 51-58.
- Elsmer G, Rickel C and Zachmann HG (1985), *Advances in Polymer Science*, 65: 1.
- Faiz S, Anis A, Luqman M and Al Zahrani SM (2016) "Studies on Thermal, Mechanical, Morphological, and Viscoelastic Properties of Polybenzimidazole Fiber Reinforced High Density Polyethylene Composites", *Polymer Composites*, 37(1): 5-13.
- Faker M, Razavi Aghjeh MK, Ghaffari M and Seyyedi SA (2008) "Rheology, Morphology and Mechanical Properties of Polyethylene/Ethylene Vinyl Acetate Copolymer (Pe/Eva) Blends", *European Polymer Journal*, 44: 1834–1842.
- Feng J, Zhang RY, Wu JJ, Yang W, Yang MB and Feng JM (2014) "Largely Enhanced Molecular Orientation and Mechanical Property of Injection-Molded High-Density Polyethylene Parts Via the Synergistic Effect of Polyamide 6 in Situ Microfibrillar and Intense Shear Flow", *Colloid and Polymer Science*, 292(11): 3033-3044.
- Fereidoon A, Ahangari MG and Saedodin S (2009) "Thermal and Structural Behaviors of Polypropylene Nanocomposites Reinforced with Single-Walled Carbon Nanotubes by Melt Processing Method", *Journal of Macromolecular Science Part B: Polymer Physics*, 48: 196–211.
- Gomaa E, Mostafa N, Mohsen M and Mohammed M (2003) "Correlation between Free-Volume Parameters and Physical Properties of Polyethylene-Nitrile Rubber Blend", *Journal of Materials Engineering and Performance*, 13: 583-587.
- Grala M and Bartczak Z (2015) "Morphology and Mechanical Properties of High Density Polyethylene-Poss Hybrid Nanocomposites Obtained by Reactive Blending", *Polymer Engineering and Science*, 55(9): 2058-2072.

- Guerra G, Petraccone V, Corradini P, De Rosa C, Napolitano R and Pirazzi B (1984) "Crystalline Order and Melting Behavior of Isotactic Polypropylene (A Form)", *Journal of Polymer Science Part B Polymer Physics*, 22: 1029-1039.
- Hatui G, Sahoo S, Das CK, Saxena AK, Basu T and Yue CY (2012) "Effect of Nanosilica and Polyphosphazene Elastomer on the in Situ Fibrillation of Liquid Crystalline Polymer (Lcp) and Thermo-Mechanical Properties of Polybutylene Terephthalate (Pbt)/Lcp Blend System", *Materials & Design*, 42: 184-191.
- Hirade T (2003) "Positronium Formation in Low Temperature Polymers", *Radiation Physics and Chemistry*, 68: 375-379.
- Hirade T and Kumada T (2001) "The Effect of Γ -Irradiation on Positronium Formation in Polyethylene", 60: 541-544.
- Hirade T, Maurer FHJ and Eldrup M (2000) "Positronium Formation at Low Temperatures: The Role of Trapped Electrons", *Radiation Physics and Chemistry*, 58(5-6): 465-471.
- Howard PR and Crist B (1989) "Unit-Cell Dimensions in Model Ethylene Butene-1 Copolymers", *J Polym Sci B: Polym. Phys.*, 27: 2269-2282.
- Hsieh TT, Tiu C, Hsieh KH and Simon GP (2000) "Characterization of Thermotropic Liquid Crystalline Polyester/Polycarbonate Blends: Miscibility, Rheology, and Free Volume Behavior", *Journal of Applied Polymer Science*, 77(10): 2319-2330.
- Hu J, Wang ZW, Yan SM, Gao XQ, Deng C, Zhang J and Shen KZ (2012) "The Morphology and Tensile Strength of High Density Polyethylene/Nano-Calcium Carbonate Composites Prepared by Dynamic Packing Injection Molding", *Polymer-Plastics Technology and Engineering*, 51(11): 1127-1132.
- Jang SH and Kim BS (1994) "Mechanical Properties and Morphology of Liquid Crystalline Copolyester-Amide and Amorphous Polyamide Blends", *Journal of Polymer Engineering & Science*, 34: 847-856.
- Jose S, Aprem AS, Francis B, Chandy MC, Werner P, Alstaedt V and Thomas S (2004) "Phase Morphology, Crystallisation Behaviour and Mechanical Properties of Isotactic Polypropylene/High Density Polyethylene Blends", *European Polymer Journal*, 40(9): 2105-2115.
- Joshi M, Butola BS, Simon GP and Kukaleva N (2006) "Rheological and Viscoelastic Behavior of Hdpe/Octamethyl-Poss Nanocomposites", *Macromolecules*, 39(5): 1839-1849.
- Kenig S (1987) "Orientability of Liquid Crystal Polymers in Elongational Flow", *Polymer Engineering and Science*, 27(12): 887-892.

- Kersch M, Schmidt HW and Altstadt V (2016) "Influence of Different Beta-Nucleating Agents on the Morphology of Isotactic Polypropylene and Their Toughening Effectiveness", *Polymer*, 98: 320-326.
- Kindl P and Reiter G (1987) "Investigations on the Low-Temperature Transitions and Time Effects of Branched Polyethylene by the Positron Lifetime Technique", *Physica Status Solidi a-Applied Research*, 104: 707-713.
- Kirkegaard P, Eldrup M, Mogensen OE and Pedersen NJ (1981) "Program System for Analyzing Positron Lifetime Spectra and Angular-Correlation Curves", *Computer Physics Communications*, 23(3): 307-335.
- Kobayashi Y, Zheng W, Hirata K and Suzuki T (1997) "Electric Field Effect on Positronium Formation in Gamma-irradiated Polypropylene and Polyethylene", *Radiation Physics and Chemistry*, 50: 589-593.
- Kobayashi Y, Zheng W, Meyer EF, Mcgervey JD, Jamieson AM and Simha R (1989) "Free Volume and Physical Aging of Poly(Vinyl Acetate) Studied by Positron Annihilation", *Macromolecules*, 22: 2302-2306.
- Kumar SV, Ghadei B, Chaudhuri SK, Krishna JBM, Das D and Saha A (2008) "Chemical Transformations and Changes in Free Volume Holes in High-Energy Proton Irradiated Low-Density Polyethylene (Ldpe)", *Radiation Physics and Chemistry*, 77(6): 751-756.
- Lee MW, Hu X, Yue CY, Li L and Tam KC (2003) "Effect of Fillers on the Structure and Mechanical Properties of Lcp/Pp/Sio₂ in-Situ Hybrid Nanocomposites", *Composites Science and Technology*, 63(3-4): 339-346.
- Levay B, Lalovic M and Ache HJ (1989) "Solid-Solid Phase Transitions and Molecular Motions in Long-Chain Paraffins Studied by Positron Annihilation Techniques", *Journal of Chemistry and Physics*, 90: 3282-3291.
- Lewis DL and Fellers JF (1988) *High Modulus Polymers*: Marcel Dekker Inc.
- Lin X, Caton-Rose F, Ren DY, Wang KS and Coates P (2013) "Shear-Induced Crystallization Morphology and Mechanical Property of High Density Polyethylene in Micro-Injection Molding", *Journal of Polymer Research*, 20(4): 122-134.
- Liu Y, Hu Y, Liu T, Ding JL and Zhong WH (2015) "Mechanical Behavior of High Density Polyethylene and Its Carbon Nanocomposites under Quasi-Static and Dynamic Compressive and Tensile Loadings", *Polymer Testing*, 41: 106-116.
- Lu B, Zheng GQ, Dai K, Liu CT, Chen JB and Shen CY (2015) "Enhanced Mechanical Properties of Polyethylene Composites with Low Content of Electrospun Nylon-66 Nanofibers", *Materials Letters*, 140: 131-134.
- Mandal PK, Bandyopadhyay D and Chakrabarty D (2003) "Studies on Morphology, Mechanical, Thermal, and Rheological Behavior of Extrusion-Blended

- Polypropylene and Thermotropic Liquid Crystalline Polymer", *Journal of Applied Polymer Science*, 88: 767–774.
- Mayer S and Zentel R (2002) "Liquid Crystalline Polymers and Elastomers", *Journal of Current Opinion in Solid State & Material Science*, 6: 545-551.
- Meille SV, Ferro DR, Bruckner S, Lovinger A and Padden F (1994) "Structure of Beta-Isotactic Polypropylene", *Macromolecules*, 27: 2615-2622.
- Menon ARR, Sudha JD, Brahmakumar M, Pillai CKS and Kuriakose AP (2000) "Studies on Blends of Melt-Processable Liquid Crystalline Polymers and Thermoplastics. I. Blend of Polyesteramide with Polyethylene", *Journal of Applied Polymer Science*, 78(10): 1811-1817.
- Mogensen OE (1974), *J. Chem. Phys.*, 60: 998–1004.
- Mostafa N, Ali EH and Mohsen M (2009) "Dynamic Study of Free Volume Properties in Polyethylene/Styrene Butadiene Rubber Blends by Positron Annihilation Lifetime Method", *Journal of Applied Polymer Science*, 113(5): 3228-3235.
- Nahid F, Zhang JD, Yu TF, Ling CC, Fung S and Beling CD (2011) "Thermal and Optical Excitation of Trapped Electrons in High-Density Polyethylene (Hdpe) Studied through Positron Annihilation", *Radiation Physics and Chemistry*, 80(4): 529-534.
- Nakanishi H and Jean YC (1990) *Positron and Positronium Chemistry*. Amsterdam: Elsevier (Chapter 5).
- Nakanishi H, S W and Jean YC (1988). "Positron Annihilation Studies of Fluids", Paper presented at the Word Scientific Singapore.
- Nogales A, Hsiao BS, Somani RH, Srinivas S, Tsou AH, Balta-Calleja FJ and Ezquerro TA (2001) "Shear-Induced Crystallization of Isotactic Polypropylene with Different Molecular Weight Distributions: In Situ Small- and Wide-Angle X-Ray Scattering Studies", *Polymer*, 42: 5247-5256.
- O'donnell HJ and Baird DG (1995) "In Situ Reinforcement of Polypropylene with Liquid-Crystalline Polymers: Effect of Maleic Anhydride-Grafted Polypropylene", *Journal of Polymer*, 36: 3113-3226.
- P RGK (1990) "Positron Lifetime Investigations on Linear Polyethylene Compared to Branched Polyethylene", *Phys Status Solidi*, (A)118: 161-168.
- Pae KD and Sauer JA (1968) "Effects of Thermal History on Isotactic Polypropylene", *Journal of Applied Polymer Science*, 12: 1901-1919.
- Peacock A (2000) *Handbook of Polyethylene*. New York Marcel Dekker Inc.

- Pokharel P, Bae H, Lim JG, Lee KY and Choi S (2015) "Effects of Titanate Treatment on Morphology and Mechanical Properties of Graphene Nanoplatelets/High Density Polyethylene Nanocomposites", *Journal of Applied Polymer Science*, 132(23).
- Ponnamma D, Ramachandran R, Hussain S, Rajaraman R, Amarendra G, Varughese K and Thomas S (2015) "Free-Volume Correlation with Mechanical and Dielectric Properties of Natural Rubber/Multi Walled Carbon Nanotubes Composites", *Composites: Part A* 77: 164–171.
- Qi CZ, Wei W, Wu YJ, Zhang SH, Wang HJ, Li HM, . . . Yan FY (2000) "Effect of Polymer Polarity on the Positronium Formation", *Journal of Polymer Science Part B-Polymer Physics*, 38(3): 435-442.
- Qi N, Chen ZQ and Uedono A (2015) "Molecular Motion and Relaxation Below Glass Transition Temperature in Poly (Methyl Methacrylate) Studied by Positron Annihilation", *Radiation Physics and Chemistry*, 108: 81-86.
- Ratzsch M, Arnold M, Borsig E, Bucka H and Reichelt N (2002) "Radical Reactions on Polypropylene in the Solid State", *Journal of Progress in Polymer Science*, 27: 1195-1282.
- Reiter G and Kindle P (1990) "Positron Lifetime Investigations on Linear Polyethylene Compared to Branched Polyethylene", *Physica Status Solidi A-Applied Research*, 118(1): 161-168.
- Saengsuwan S, Bualek-Limcharoen S, Mitchell GR and Olley RH (2003) "Thermotropic Liquid Crystalline Polymer (Rodrun Lc5000)/Polypropylene in Situ Composite Films: Rheology, Morphology, Molecular Orientation and Tensile Properties", *Polymer*, 44(11): 3407-3415.
- Sainath AVS, Rao AK and Reddy AVR (2000) "Synthesis, Characterization and Liquid Crystalline Properties of Polyacrylates and Polymethacrylates Containing Aryl Ester Pendant Unit", *Journal Applied Polymer Science*, 75: 465-474.
- Salih SE, Hamood AF and Alsalam AHA (2013) "Comparison of the Characteristics of Ldpe : Pp and Hdpe : Pp Polymer Blends", *Modern Applied Science*, 7: 33-42.
- Shantarovich VP, Suzuki T, He C and Gustov VW (2003) "Inhibition of Positronium Formation by Polar Groups in Polymers - Relation with Tsl Experiments", *Radiation Physics and Chemistry*, 67(1): 15-23.
- Shin BY and Chung IJ (1990) "Polymer Blend Containing a Thermotropic Polyester with Long Flexible Spacer in the Main Chain", *Journal of Polymer Engineering & Science*, 30: 22-29.

- Souza JPD and Baird DG (1996) "In Situ Composites Based on Blends of a Poly(Ether Imide) and Thermotropic Liquid Crystalline Polymers under Injection Moulding Conditions", *Polymer*, 37: 1985-1997.
- Soykan U (2013). "Graft Copolymerization of P-Benzophenoneoxycarbonylphenyl Acrylate onto High Density Polyethylene", (MSc Thesis), Abant İzzet Baysal University, Bolu.
- Srinivasa RGS, Choudhary MS, Naqvi MK and Rao KV (1996) "Functionalization of isotactic Polypropylene with Acrylic Acid in the Melt: Synthesis, Characterization and Evaluation of Thermomechanical Properties", *European Polymer Journal*, 32: 695-700.
- Sun T, Lin YG, Winter HH and Porter RS (1989) "Phase Transitions of Poly(Ethylene Terephthalate-Co-P-Hydroxybenzoic Acid) Liquid Crystal by Dynamic Mechanical Analysis", *Journal of Polymer*, 30: 1257-1261.
- Suzuki T, Oki Y, Numajiri M, Miura T, Kondo K and Ito Y (1992) "Positron Annihilation in Irradiated and Unirradiated Polyethylenes", *Journal of Polymer Science B30*: 517-525.
- Suzuki T, Oki Y, Numajiri M, Miura T, Kondo K, Shiomi Y and Ito Y (1993) "Effects of Aging and Oxidation on Positronium Formation in Polyethylenes", *Radiation Physics and Chemistry*, 43: 557-562.
- Suzuki T, Ito Y, Kondo K, Hamada E and Ito Y (2000) "Radiation Effect on Positronium Formation in Low-Temperature Polyethylene", *Radiation Physics and Chemistry*, 58(5-6): 485-489.
- Suzuki T, Kondo K, Hamada E, Chen Z and Ito Y (2001) "Temperature and Radiation Effects on Positronium Formation", *Radiation Physics and Chemistry*, 60: 535-540.
- Suzuki T, Miura T, Oki Y, Numajiri M, Kondo K and Ito Y (1995) "Positron Irradiation Effects on Polypropylene and Polyethylene Studied by Positron-Annihilation", *Radiation Physics and Chemistry*, 45(4): 657-663.
- Suzuki T, Oki Y, Numajiri M, Miura T and Kondo K (1996) "Radiation Effect on Polypropylene Studied by the Relaxational Behaviour at Low Temperature Using Positron Annihilation", *Polymer*, 37: 5521-5524.
- Tang YH, Gao P, Ye L and Zhao CB (2010) "Organoclay-Modified Thermotropic Liquid Crystalline Polymers as Viscosity Reduction Agents for High Molecular Mass Polyethylene", *Journal of Materials Science*, 45(19): 5353-5363.
- Terlemezyan L, Mokreva P, Tsocheva D, Peneva S, Berovsky K and Troev T (2008) "Detection of Free Volumes in Polyaniline Complexes with Various Acids by Using Positron Lifetime Spectroscopy", *Radiation Physics and Chemistry*, 77(5): 591-596.

- Tokita M, Osada K and Watanabe J (1998) "Thermotropic Liquid Crystals of Main Chain Polyesters Having a Mesogenic 4,4'-Biphenyldicarboxylate Unit. Xi. Smectic Liquid Crystalline Glass", *Journal of Polymer*, 30: 589–595.
- Tortorella N and Beatty CL (2008) "Morphology and Mechanical Properties of Impact Modified Polypropylene Blends", *Polymer Engineering And Science*, 48(11): 2099-2110.
- Turner-Jones A, Aizlewood JM and Beckett DR (1964) "Crystalline Forms of Isotactic Polypropylene", *Macromolecular Chemistry and Physics*, 75: 134-158.
- Uedono A, Kawano T, Tanigawa S, Ban M, Kyoto M and Uozumi T (1997) "Transition and Relaxation Processes of Polyethylene, Polypropylene, and Polystyrene Studied by Positron Annihilation", *Journal of Polymer Science Part B-Polymer Physics*, 35(10): 1601-1609.
- Wang CL, Hirade T, Maurer FHJ, Eldrup M and Pedersen NJ (1998) "Free-Volume Distribution and Positronium Formation in Amorphous Polymers: Temperature and Positron-Irradiation-Time Dependence", *Journal of Chemical Physics*, 108(11): 4654-4661.
- Wang YQ, Wu YP, Zhang HF, Zhang LQ, Wang B and Wang ZF (2004) "Free Volume of Montmorillonite/Styrene-Butadiene Rubber Nanocomposites Estimated by Positron Annihilation Lifetime Spectroscopy", *Macromolecule Rapid Communications*, 25: 1973–1978.
- Whitehouse C, Lu XH, Gao P and Chai CK (1997) "The Viscosity Reducing Effects of Very Low Concentrations of a Thermotropic Copolyester in a Matrix of Hdpe", *Polymer Engineering and Science*, 37(12): 1944-1958.
- Xiang D, Harkin-Jones E, Linton D and Martin P (2015) "Structure, Mechanical, and Electrical Properties of High-Density Polyethylene/Multi-Walled Carbon Nanotube Composites Processed by Compression Molding and Blown Film Extrusion", *Journal of Applied Polymer Science*, 132(42): 665-679.
- Xu SB, Akchurin A, Liu T, Wood W, Tangpong XW, Akhatov IS and Zhong WH (2015) "Mechanical Properties, Tribological Behavior, and Biocompatibility of High-Density Polyethylene/Carbon Nanofibers Nanocomposites", *Journal of Composite Materials*, 49(12): 1503-1512.
- Yang BX, Shi JH, Pramoda KP and Hong GS (2008) "Enhancement of the Mechanical Properties of Polypropylene Using Polypropylene-Grafted Multiwalled Carbon Nanotubes", *Composite Science Technology*, 68 2490–2497.
- Yang Y (2011). "Positron Annihilation Lifetime Spectroscopy Studies of Amorphous and Crystalline Molecular Materials", (PhD. Thesis), Martin-Luther-Universität Halle-Wittenberg.

- Yılmaz ŞS (2011). "Preparation and Characterization of Organoclaypolypropylene Nanocomposites with Maleic Anhydride Grafted Polypropylene Compatibilizer", (MSc Thesis), Middle East Technical University.
- Yoon HN, Charbonneau LF and Calundann GW (1992) "Synthesis, Processing and Properties of Thermotropic Liquid-Crystal Polymers", *Journal of Advanced Materials*, 4: 206–214.
- Yu RS, Suzuki T, Djourelou N, Ito Y and Kondo K (2006) "Study of Irradiation Effect on Positronium Formation in Polypropylene", *Radiation Physics and Chemistry*, 75(2): 247-252.
- Zhang Z and Ito Y (1991) "Micro-Structures of Gamma-Ray Irradiated Polyethylenes Studied by Positron Annihilation", *Radiation Physics and Chemistry*, 38: 221-225.
- Zheng RQ, Chen EQ, Cheng SZD, Xie FC, Yan DH and He TB (1999) "Phase identification in a Series of Liquid Crystalline Tpp Polyethers and Copolyethers Having Highly Ordered Mesophase Structures, Phase Structures in a Series of Copolyethers Containing Odd and Even Numbers of Methylene Units of Different Compositions ", *Journal of Macromolecules*, 32: 6981–6988.
- Zhou J and Yan F (2004) "Mechanical and Tribological Behavior of Compatibilized Ultra High Molecular Weight Polyethylene/Liquidcrystalline Polymer Composites", *Polymer Testing*, 23: 827–833.



APPENDICES

7. APPENDICES



8. CURRICULUM VITAE

Name SURNAME : Behiye ÖZTÜRK ŞEN

Place and Date of Birth : Çorlu, 28.10.1987

Universities :

Bachelor's Degree :Balıkesir University, Faculty of Arts and Sciences, Chemistry Department, **2005-2009**

MSc Degree :Dokuz Eylül University, Graduate School of Natural and Applied Sciences, Chemistry Department, **2009-2011**

e-mail :behiye.sen@altinbas.edu.tr

List of Publications :

Soykan U, Cetin S, Ozturk B, Karaboga F, Zalaoglu Y, Dogruer M, Yildirim G, Terzioglu C (2013). “Synthesis And Characterization Of P-Benzophenoneoxycarbonylphenyl Acrylate By Means Of Experimental Measurements And Theoretical Approaches, And Bulk Melt Polymerization” *Journal of Molecular Structure*, 1049: 479–487.

Karaboga F, Soykan U, Dogruer M, Ozturk B, Yildirim G, Cetin S, Terzioglu C (2013). “Experimental And Theoretical Approaches For Identification Of P-Benzophenoneoxycarbonylphenyl Acrylate” *Spectrochimica Acta Part A: Molecular and Biomolecular Spectroscopy*, 113: 80–91.

Çetin S, Ozturk Sen B, Soykan U, Yildirim G (2015). “Experimental And Theoretical Approaches On Structural And Mechanical Properties Of Novel Side Chain Lcp-Pp Graft Coproducts”. *Turkish Journal of Chemistry*.

Ozturk Sen B, Yahsi U, Tav C, Cetin S, Yener MY, Soykan U. (2017).”Free Volume Properties of

Side Chain LCP-HDPE Graft Coproducts Probed by Positron Annihilation Lifetime Spectroscopy” The International Joint Science Congress of Materials and Polymers (ISCMP)

Ozturk Sen B, Soykan U, Cetin S. (2016). “Thermal mechanical microstructural and morphological properties of side chain LCP HDPE graft coproducts”. 46th IUPAC World Polymer Congress (MACRO 2016)

Çetin S, Soykan U, Ozturk Sen B, Eker G, Yildirim G. (2015). “Experimental and theoretical approaches for identification of 3,3,4,4,5,5,6,6,7,7,8,8,8-dodecafluoro-5-methyloctyl-4-acryloyloxy benzoate”. 9th International Physics Conference of the Balkan Physical Union BPU9.

Ozturk Sen B, Altinişik A, Yurdakoç K. (2011). “Synthesis Of Ion Imprinting Chitosan Pva Crosslinked Membrane For Selective Removal Of Ag(I)” Controlled/Living Polymerization: From synthesis to applications (CLP11).

Ozturk Sen B, Soykan U, Firat E.E, Çetin S, (2015). “p-Bifeniloksikarbonilfenil Akrilat ve p-Bifeniloksikarbonilfenil Metakrilatin İzotaktikpolipropilen Üzerine Aşı Kopolimerleşmesi”. 27. Ulusal Kimya Kongresi

Soykan U, Ozturk Sen B, Çetin S, (2014). “Aşı Polimerleşmeyle Yüksek Yoğunluklu Polietilenin Yan Zincir Sivi Kristal Polimer İlegüçlendirilmesi”. V. Ulusal Polimer Bilim ve Teknolojisi Kongresi

Hobbies (Optional)

:Ride a bike, Read a book and newspaper and Discover new places and Travel abroad